Connecting the speed-accuracy trade-offs in sensorimotor control and neurophysiology reveals diversity sweet spots in layered control architectures

Thesis by
Yorie Nakahira

In Partial Fulfillment of the Requirements for the
Degree of
Doctor of Philosophy

CALIFORNIA INSTITUTE OF TECHNOLOGY
Pasadena, California

2019
Defended May 13th, 2019

Yorie Nakahira
ORCID: 0000-0003-3324-4602

ACKNOWLEDGEMENTS

I would like to express my deepest gratitude and respect to my advisor, John Doyle. John gave me the greatest support for my research and career. His advice on my research totally changed how I find and tackle problems. His patience allowed me to try out new and uncertain research projects, planned for the long term. He let me choose research topics and collaborate freely. I feel deeply grateful to his thoughtful advising style, which largely fostered my skills to find new problems and thrive in an unstructured environment. My advisor also has a charming and caring personality, which made my Ph.D. life full of enjoyment and excitement. I would also like to express my gratitude toward the students and postdocs in Doyle laboratory, particularly Yoke Peng Leong and Quanying Liu, who I grow up together with in my Ph.D. program.

I would like to express my gratitude to Terry Sejnowski, Joel Burdick, and Simon Laughlin for their great support and advice in my main doctoral research project on neuroscience. Terry shared with me lots of great ideas and insights. Joel suggested me to look into Fitts' law, which turned out to have many interesting issues to be studied. Simon worked with me to establish the mathematical model for the neural signaling speed-accuracy tradeoffs. Their advice and support largely helped improve this thesis.

I would like to express my gratitude to Adam Wierman for being a great mentor of mine. Adam gave me much encouragement and advice in uncertain times. I also much enjoyed our collaboration.

I would like to express my gratitude to Yilin Mo. Yilin advised me on my first conference and journal papers in my Ph.D. program. What I learned from him largely helped my research to be on the track later.

I would like to express my gratitude to Lijun Chen, who gave me many pieces of advice on research and career planning.

I would like to express my gratitude to the faculties, friends, and collaborators around me: Richard Murray, Steven Low, Victoria Kostina, Niangjun Chen, Nakano Takayo, Haruka Ebisu, Ahkeel Mohideen, Dimitar Ho, Natalie Bernat, Andres Ferragut, Nikolai Matni, Ye Yuan, Seungil You, Emily Jenson, Adam Dai, Sunghoon Choi, Angelina Pan.

Finally, I feel grateful for the unconditional care and support of my family members.

ABSTRACT

Nervous systems sense, communicate, compute, and actuate movement using distributed components with trade-offs in speed, accuracy, sparsity, noise, and saturation. Nevertheless, the resulting control can achieve remarkably fast, accurate, and robust performance due to a highly effective layered control architecture. However, this architecture has received little attention from the existing research. This is in part because of the lack of theory that connects speed-accuracy trade-offs (SATs) in the components neurophysiology with system-level sensorimotor control and characterizes the overall system performance when different layers (planning vs. reflex layer) act work jointly. In thesis, we present a theoretical framework that provides a synthetic perspective of both levels and layers. We then use this framework to clarify the properties of effective layered architectures and explain why there exists extreme diversity across layers (planning vs. reflex layers) and within levels (sensorimotor versus neural/muscle hardware levels). The framework characterizes how the sensorimotor SATs are constrained by the component SATs of neurons communicating with spikes and their sensory and muscle endpoints, in both stochastic and deterministic models. The theoretical predictions are also verified using driving experiments. Our results lead to a novel concept, termed "diversity sweet spots (DSSs)": the appropriate diversity in the properties of neurons and muscles across layers and within levels help create systems that are *both* fast and accurate despite being built from components that are individually slow or inaccurate. At the component level, this concept explains why there are extreme heterogeneities in the neural or muscle composition. At the system level, DSSs explain the benefits of layering to allow extreme heterogeneities in speed and accuracy in different sensorimotor loops. Similar issues and properties also extend down to the cellular level in biology and outward to our most advanced network technologies from smart grid to the Internet of Things. We present our initial step in expanding our framework to that area and widely-open area of research for future direction.

PUBLISHED CONTENT AND CONTRIBUTIONS

[1] John C. Doyle, Yorie Nakahira, Yoke Peng Leong, Emily Jenson, Adam Dai, Dimitar Ho, and Nikolai Matni. Teaching control theory in high school. In *2016 IEEE 55th Conference on Decision and Control (CDC)*, pages 5925–5949. IEEE, 2016. doi: 10.1109/CDC.2016.7799181. URL https://ieeexplore.ieee.org/document/7799181.
Y.N. proposed the mathematical methods used in chapter 2.

[2] Yorie Nakahira. Lq vs. ℓ_∞ in controller design for systems with delay and quantization. In *2016 IEEE 55th Conference on Decision and Control (CDC)*, pages 2382–2389. IEEE, 2016. doi: 10.1109/CDC.2016.7798619. URL https://ieeexplore.ieee.org/abstract/document/7798619.
Y.N. proposed the algorithms and performed the analysis.

[3] Yorie Nakahira and Yilin Mo. Attack-resilient h_2, h_∞, and ℓ_1 state estimator. *IEEE Transactions on Automatic Control*, 63(12):4353–4360, 2018. doi: 10.1109/TAC.2018.2819686. URL https://ieeexplore.ieee.org/abstract/document/8325450.
Y.N. performed the theoretical and empirical analysis.

[4] Yorie Nakahira and Seungil You. A linear programming framework for networked control system design. *IFAC-PapersOnLine*, 48(22):34–39, 2015. doi: 10.1016/j.ifacol.2015.10.303. URL https://www.sciencedirect.com/science/article/pii/S2405896315021941.
Y.N. proposed the algorithm, analyzed its performance, and performed the simulation.

[5] Yorie Nakahira, Quanying Liu, Natalie Bernat, Terry Sejnowski, and John C. Doyle. Theoretical foundations for layered architectures and speed-accuracy tradeoffs in sensorimotor control. *Accepted to American control conference 2019*. URL http://users.cms.caltech.edu/~ynakahir/ACC2019theory.pdf.
Y.N. identified the question being studied and developed the theory.

[6] Yorie Nakahira, Niangjun Chen, Lijun Chen, and Steven H Low. Smoothed least-laxity-first algorithm for electric vehicle charging. In *Proceedings of the 8th International Conference on Future Energy Systems*, pages 242–251. ACM, 2017. doi: 10.1145/3077839.3077864. URL https://dl.acm.org/citation.cfm?id=3077864.
Y.N. proposed the algorithms and performed the theoretical analysis.

[7] Yorie Nakahira, Andres Ferragut, and Adam Wierman. Minimal-variance distributed deadline scheduling in a stationary environment. *SIGMETRICS Perform. Eval. Rev.*, 46(3):56–61, January 2019. ISSN 0163-5999. doi:

10.1145/3308897.3308925. URL https://dl.acm.org/citation.cfm?id=3308925.

Y.N. proposed the optimization techniques and the proposed algorithms and conducted the experiments.

TABLE OF CONTENTS

Chapter 1

INTRODUCTION

Over the next decade, we will witness the development of a hyper-connected world in which infrastructure, devices, and vehicles are integrated seamlessly into the Internet of Things (IoT). The IoT will interconnect hundreds of millions of heterogeneous devices, each capable of sensing, computing, actuating, and communicating. Such networks of intelligent devices have great potential to bring greater convenience and comfort to society; at the same time, the complexity of controlling and coordinating so many smart devices raises daunting challenges. How can we sense events fast and accurately over a network of devices with potential communication delays and errors? How can we control networked systems efficiently using devices with limited computation and actuation capabilities? How can we ensure the robustness and safety of the system in case of compromised devices from cyber-attacks? Addressing these challenges has been the main motivation for my research. Interestingly, these challenges are analogous to those faced by biological systems: despite using physical components that are noisy, distributed, delayed, quantized, etc., biological systems are remarkably robust in control and homeostasis.

Human sensorimotor control can achieve extremely robust performance in complex, uncertain environments, despite being implemented in systems that are distributed, sparse, quantized, delayed, and saturated. For example, Fitts' Law predicts that, in many forms of reaching (e.g. eye gaze, hand, mouse), the time required for reaching quickly to a target of width W at a distance D scales as $log_2(2D/W)$ [60, 202]. The logarithmic relation between the reaching time and target width allows faster speed to be achieved with a small decrement in accuracy. In another example of riding a mountain bike down a twisting, bumpy trail, though a trade-off exists between traveling fast and accurately following the trail, a human can often stay on the trail without crashing. On the other hand, the speed-accuracy tradeoffs (SATs) of the hardware implementing control can be much more severe. Improving either speed or accuracy in nerve signaling or muscle actuation requires profligate biological resources [185]; as a consequence, only a few types of nerves and muscles are built to be both fast and accurate [140]. Such apparent discrepancy between the speed-accuracy tradeoffs in sensorimotor control and neurophysiology poses the question: how nature de-constrains neurophysiological hardware constraints in sensorimotor

control?

We hypothesize that effective layered control architectures are the critical enablers for achieving such remarkable speed and accuracy in sensorimotor control using nerves or muscles with severe SATs (see [49] and reference therein for explanations on architectures). Biological systems have layered control architectures distributed across multiple levels, with spinal reflexes at the first level, and many well-engineered technological systems are naturally layered. The effectiveness of layered architectures can be observed in many sensorimotor control tasks. One example is the reaction to stepping on a thumbtack with bare feet. Our reaction is mainly controlled by three diverse feedback loops [16]: upon sensing, the foot is first lifted up by a fast reflexive control loop involving the spinal cord, then a control loop involving the vestibular system works on balancing our body, and finally a slow loop involving the higher cortical decisions determines the next action. These loops have diverse speeds: the reflexive loop acts in a spinal arc, taking action generated by the spinal cord within tens of milliseconds, before the vestibular and cortical loops even sense the event hundreds of milliseconds to seconds later [52, 101]. They also have diverse capabilities to convey information: the first loop only needs to transmit binary information about whether to lift up the foot, but the second and third loops can provide increasingly complex instructions. By appropriately layering these loops, we can achieve a fast and accurate system response despite using parts that are not.

Another example of effective layered architectures is the control loops involving riding a mountain bike down a twisting, bumpy trail. Vision is used to obtain an advanced warning on future uncertainties in the trail ahead when planning a route. Even large variations/disturbances in the trail can be navigated with small error provided there is enough advanced warning relative to the speed of the bike. At the same time, the bumps in the path, the bike, and the rider's body dynamics are handled by a separate reflex layer that is entirely unconscious and reacts with unavoidable delays. Without a quick reaction, even small disturbances can result in catastrophically large errors and crashes. With enough advanced warning and resources, we can be almost perfectly robust, and, at the opposite extreme with delays and uncertain dynamics, nearly infinitely fragile. An effective layered architecture allows the sensorimotor control to achieve the former while avoiding the latter.

Similar laws and architectures extend downward to the cellular level and outward to our most advanced technologies. Though based on entirely different components, such systems face similar constraints and tradeoffs (laws) in dimensions such as effi-

ciency, robustness, security, speed, flexibility, and evolvability. And the successful design of such systems shares remarkable universals in architecture, including the use of layering and diversity for managing these tradeoffs effectively.

Despite the importance of understanding successful architectures, the study of architectures have traditionally been the among the areas of engineering least guided by theory, and there is nothing remotely resembling a 'science' of system architecture. Moreover, we have little understanding of what makes an architecture effective of our brain. Understanding effective layered architectures requires connecting component constraints and trade-offs to the resulting hard limits on sensorimotor performance from a multilayer perspective. However, the component SATs in neural signaling [153, 154, 185, 210] and the system SATs in sensorimotor control [60, 135, 191, 192] have been studied separately mainly because there are few theoretical tools that can integrate both levels.

In this thesis, we develop a mathematical theory that characterizes how the component speed-accuracy constraints and trade-offs impact SATs at the system level. Using this theory, we show that *diversity* between layers and within layers can be exploited to achieve *both* fast *and* accurate performance despite being implemented using slow or inaccurate hardware. We call these synergies "diversity sweet spots". At the component level, this concept explains why there are extreme heterogeneities in the characteristics of neural components [146, 153, 154]. At the system level, DSSs explain the benefits of extreme heterogeneities in speed and accuracy in different sensorimotor loops [97, 110].[1]

1.1 Contribution of this thesis

Fundamental theory: To understand the fundamental limitations in control under communication constraints, we characterize the preformation limitations and control algorithms for systems that are delayed, quantized, and sampled, distributed, and/or saturated. We show closed-form performance bounds, including analytic bounds for a general class of nonlinear system under directed information constraints, which had previously remained open due to the technical complexity of tracking the dynamic evolution of probability density functions. For safety-critical systems, we create a state estimator with a provable estimation error bound, the first to have $\mathcal{H}_\infty$

[1] Throughout this thesis, we refer to "layers" when discussing different architectural parts (*e.g.* planning layer, reflex layer) and "levels" when referring to different levels of abstraction (*e.g.* neural hardware level, sensorimotor control level).

resilience.[2] When applied to human sensorimotor control or biomolecular control within a single cell, these theories empower us to integrate the previous findings from the system and component levels and to obtain a holistic understanding of both levels.

Insights into biological systems:

We study the speed-accuracy tradeoffs (SATs), which are ubiquitous in both neurophysiology and sensorimotor control. We clarify how the component SATs in spiking neuron communication and their sensory and muscle endpoints constrain the system SATs using both theory and experiments. The manual to set up our experimental platform and the code can be found here [112]. Moreover, we characterize how the structural constraints of biomolecular control impose fundamental limits in cell homeostasis. These results suggest that optimal layering creates "diversity sweet spots" (DSSs). DSSs show that diversity between layers (planning versus reflexive layers) and within levels (nerves and muscles) can be exploited to achieve fast *and* accurate performance using slow or inaccurate hardware. This notion explains why there is extreme heterogeneity in nerve and muscle compositions. Moreover, DSSs also show that diverse nerves/muscles lead to the logarithmic SATs, as experimentally observed in Fitts' Law. This provides a new perspective on the long history of Fitts' Law study in Human-Computer Interaction by establishing a connection between the Fitts' Law and existing muscle diversity.

Scalable algorithms for technological systems:

Many modern schedulers in smart grids and computing systems can dynamically adjust their service capacity to match the incoming workload. At the same time, however, unpredictability and instability in service capacity often incur undesirable operational and infrastructural costs. Using a deterministic framework, we develop scalable distributed scheduling policies with performance guarantees by establishing a connection between the scheduling algorithms and the utility maximization problem. In a stochastic framework, we derive the optimal solution for a deadline scheduling problem that maximizes service capacity predictability, stability, or both, subject to combinations of strict/soft demand/deadline requirements. Exact solutions for these problems were previously unknown owing to the difficulty of dealing with the discreteness in the state. When tested on the Caltech and Google electric

[2] If the estimation error is 2-norm bounded given 2-norm bounded disturbance and sparse unbounded sensory attacks, we say that the system is $\mathcal{H}_\infty$ resilient.

vehicle charging testbed, the costs of the proposed algorithms perform equally well with the optimal offline algorithm for more than 80% of days and no worse than existing centralized online algorithms. We also show an interesting connection between the resulting optimal algorithms and the optimal offline algorithm (YDS algorithm) [205], which may help inspire the transformation of other offline algorithms into online distributed algorithms.

Rethinking the fundamentals (outreach):

Despite the broad applicability of control theory for many practical problems, the impact of control theory is largely stunted by its technical accessibility. To lower the learning barriers of the theory, we are rethinking its fundamentals [48]. Specifically, we reproduce the basic results of control theory using high school-level mathematics. We have implemented the simplified theory in Caltech's control course curriculum and also taught it to the high school student who then helped conduct our experiments.

1.2 Related work

Control and information theory

Control under communication constraints has been extensively studied. The comprehensive surveys [5, 9, 54, 138] cover important issues in the field of networked control. The necessary and sufficient data rate through the feedback loop in order to achieve system stability in linear stochastic control is studied in [137, 189, 207]. The optimal controller structure, separation principles, performance bounds are studied in [13, 31, 63, 93, 174, 175, 188, 190, 208]. Some of the important results include separation principle between the controller design and communication protocols [58, 65, 190], and the relation between optimal cost and the causal rate-distortion function [25, 32, 45, 72, 93, 159].

Relevant to control information-theoretic quantities include mutual information [39, 190], anytime capacity [163], and directed information [124, 188], among others. In the classical setting of information theory, the source and channel codes can be designed separately without loss of optimality in the limit of infinite coding delay [171]. However, if the allowable delay is limited, as is the case in zero-delay coding for control, then separating the design of source and channel can perform strictly worse compared with designing them jointly [88].

1.3 Control and security

For the secure estimation problem in static systems, robust estimators are extensively studied in the literature. Common robust estimators include the M-estimator, L-estimator, and R-estimator [81, 87, 123], and they are used to account for sensor integrity attacks in [130]. For the secure estimation problem in dynamical systems, robust control provides tools to deal with noise in estimation and control [40, 47]. Although robust control typically assumes that system disturbances are bounded or follow well-defined distributions, such assumptions may not be valid for sensor faults caused by intelligent attackers [41, 130]. Fault detection and isolation (FDI) also provide methods for identifying and pinpointing faults in sensors [33, 70, 84, 195]. One common approach of FDI for linear dynamical systems under sensor integrity attacks is to construct *residuals* that take non-zero values only in the presence of faults (see [152] and references therein). The generation of such residuals is possible only when a fault is separable from normal disturbances and modeling uncertainties, which requires certain kinds of system observability.

When attackers can change the measurements of a limited number of sensors in large-scale systems, sensor attacks can be modeled as *sparse* but unbounded disturbances. For sparse sensor integrity attacks, recent literature has studied the fundamental limitation and achievable performance to identify the attacks and estimate the system states. Fawzi et al. show that if ρ sensors are compromised, then 2ρ-observability (*i.e.* the system remains observable after removing any set of 2ρ sensors) is necessary to guarantee perfect attack identification and accurate state estimation for noiseless systems [56]. The authors further propose to solve a ℓ_0 problem to achieve accurate state estimation under the assumption of 2ρ-observability. This work is generalized to noisy systems by Pajic et al. [148, 149]. Shoukry et al. propose to use a Satisfiability Modulo Theory (SMT) solver to harness the complexity in secure estimation [173]. However, the worst case complexity for the ℓ_0 optimization and that of the SMT solver are combinatorial. Moreover, these estimators also have delays, which may cause performance degradation when used for real-time control. To transform the problem into a convex program, Fawzi et al. and Mo et al. propose to use optimization based methods [56, 129]. To address the estimation delays, various Luenberger-like observers are proposed [38, 118, 129, 139, 172, 173]. It is worth noticing that the estimators proposed in [38, 118, 129, 148, 149, 172, 173] require the assumption of 2ρ-observability or stronger to guarantee accurate attack identification and secure state estimation.

1.4 Optimal control and scheduling

There is an extensive literature that studies the design and analysis of deadline scheduling algorithms (see [7, 26, 90, 182] and references therein). Examples of classic scheduling algorithms include Earliest Deadline First [17, 80, 94, 132, 150, 151] and Least Laxity First [80], among others [104, 156]. Beyond these classic algorithms, more modern algorithms simultaneously perform admission control and service rate control to exploit the flexibility arising from soft demand or deadline requirements, *e.g.* [30, 121, 157].

The trade-offs between service quality and costs associated with variability have become a focus only recently [21, 44, 57], motivated by applications such as cloud computing and power distribution systems. In the context of cloud computing, algorithms have been proposed to control the variability of power usage in data centers using deferrable jobs (see [2, 3, 37, 68, 69, 95, 109, 115, 133, 193, 197, 211] and references therein). In the context of power distribution systems, algorithms have been designed to control the variability of energy supply using deferrable loads (see [18, 34, 66, 143, 186] and references therein).

Interesting optimality results have been obtained in some limited settings, such as deterministic worst-case settings [11, 205], single server systems [17, 150, 151], and/or heavy traffic settings [74, 105]. For example, in heavy traffic settings, the dynamic behavior of discrete queueing systems can be approximated by a continuous-state process involving Brownian motion, for which there exist established tools to optimize [74, 105]. On the other hand, optimizing queueing systems without continuous-state approximations remains to be a hard problem. Particularly, the problem of designing *optimal* algorithms that minimize service capacity variability while achieving high service quality has remained open. Solving this problem is a challenging task due to the heterogeneity of jobs (diversity in demands and deadlines) and the size of the state and decision space (of possible configurations on existing job profiles and the set of feasible scheduling policies).

The existing EV charging algorithms can be categorized into either offline or online. The *offline* algorithms require complete information on all EVs to decide on the charging rates [35, 66, 119, 160, 186, 187]. However, information on future EV arrivals may not be available or very costly to obtain, which motivates *online* algorithms [29, 36, 67, 75, 92, 169, 184, 186, 186, 206, 206]. The performance of the online algorithm is generally analyzed for the worst-case [36, 92] or average-case [67, 206]. Other desirable properties of charging algorithms are low complexity

in computation and memory usage, which can be achieved by sorting or bisection based methods, such as earliest-deadline-first, least-laxity-first [182], Whittle's index policy [200, 206], among others.

The *multi-processor deadline scheduling problem* [43, 46, 111] considers the scheduling of jobs on multiple processors. We can view the EV charging problem as a deadline scheduling problem by considering chargers as processors, and EVs with certain energy demand as jobs. Resource augmentation is a prominent analysis framework [82, 83, 86, 155] for analyzing the performance of online algorithms for multi-processor scheduling, we apply this framework to the EV charging problem. The main difference is that in our setting the power limit is time-varying, the maximum rates are heterogeneous, and the power limit may not necessarily be integer multiplication of the maximum rate.

1.5 Preliminary

In this section, we summarize the existing control theory and its notation used in this thesis.

Notations

For a continuous time process $\{X(t)\}_{t\in\mathbb{R}_+}$, abbreviated as $X(t)$, we use the notations $X^T \triangleq \{X(t) : t \le T\}$, $X^{T-} \triangleq \{X(t) : t < T\}$, and $X_{t_2}^{t_1} \triangleq \{X(t) : t_1 \le t \le t_2\}$. The expected value and the variance of $X(t)$ at time t are denoted by $\mathbb{E}[X(t)]$, $\mathrm{Var}[X(t)]$ respectively; *stationary mean* and *variance* are denoted by

$$\mathbb{E}[X] \triangleq \lim_{t\to\infty} \mathbb{E}[X(t)], \tag{1.1}$$

$$\mathrm{Var}[X] \triangleq \lim_{t\to\infty} \mathrm{Var}[X(t)], \tag{1.2}$$

provided that the said limits exist. For a discrete time process $\{X[k]\}_{k\in\mathbb{Z}_+}$, abbreviated as $X[k]$, we use the notations $X^n \triangleq \{X[k] : k \le n\}$ and $X_{k_2}^{k_1} \triangleq \{X[k] : k_1 \le t \le k_2\}$. The stationary mean and variance are defined analogously to (1.1) and (1.2).

Systems and norms

A discrete-time linear time-invariant (LTI) system can be written in the form

$$x(t+1) = Ax(t) + Bw(t), \qquad y(t) = Cx(t) + Dw(t), \tag{1.3}$$

with the initial condition $x(0) = 0$, system state $x(t) \in \mathbb{R}^n$, system input $w(t) \in \mathbb{R}^l$, and system output $y(t) \in \mathbb{R}^m$. The transfer matrix of the system is

$$G = \left[\begin{array}{c|c} A & B \\ \hline C & D \end{array}\right].$$

The transfer function of the system is $\hat{G}(z) = B(zI - A)^{-1}C + D$. For ℓ_p system input and ℓ_q system output, the system norm (namely, *induced norm*) is given by

$$\|G\|_{p\to q} \triangleq \sup_{\|w\|_p \neq 0} \frac{\|y\|_q}{\|w\|_p}. \tag{1.4}$$

In particular, the induced-norms for $(p, q) = (2, 2), (2, \infty), (\infty, \infty)$ are given by $\mathcal{H}_\infty$, $\mathcal{H}_2$, and $\mathcal{L}_1$ norms, respectively. These induced-norms are bounded when A is strictly stable (*i.e.* all the eigenvalues of A is in the open unit circle). See [40, 47] for further details.

In particular, the induced-norms for $(p, q) = (2, 2), (2, \infty), (\infty, \infty)$ are respectively $\mathcal{H}_\infty$, $\mathcal{H}_2$, and $\mathcal{L}_1$ norms, which are defined as

$$\|G\|_{2\to\infty} = \|G\|_2 = \int_{-\pi}^{\pi} tr(\hat{G}(e^{i\theta})\hat{G}^T(e^{-i\theta}))d\theta/2\pi \tag{1.5}$$

$$\|G\|_{2\to 2} = \|G\|_\infty = \operatorname{ess\,sup}_{e^{i\theta}} \sigma_{\max}\hat{G}(e^{i\theta}) \tag{1.6}$$

$$\|G\|_{\infty\to\infty} = \|G\|_1 = \max_{1\le i\le n} \sum_{j=1}^{l}\sum_{t=0}^{\infty} |h_{ij}(t)|, \tag{1.7}$$

where h_{ij} is the impulse response from $w_j(t)$ to $y_i(t)$. These induced-norms are bounded when A is strictly stable (*i.e.* all the eigenvalues of A is in the open unit circle). See [40] for further details.

Quantizers

A quantizer partitions the input space into disjoint sets, and maps each set onto its representative point. We considers uniform quantizers.

Definition 1.5.1. *An uniform quantizer with $L \in \mathbb{N}^n$ level and saturation $X \in \mathbb{R}^n_+$ is a mapping $\mathbb{Q}_{L_x,X} : x \in \mathbb{R}^n \to y \in \mathbb{R}^n$ defined as following: for $X < \infty$,*

$$y_i = \begin{cases} -X_i + \frac{X_i}{L_i} & \text{if } x_i \in \left[-\infty, -X_i + 2\frac{X_i}{L_i}\right) \\ -X_i + 3\frac{X_i}{L_i} & \text{if } x_i \in \left[-X_i + 2\frac{X_i}{L_i}, -X_i + 4\frac{X_i}{L_i}\right) \\ \qquad\vdots & \\ X_i - \frac{X_i}{L_i} & \text{if } x_i \in \left[X_i - 2\frac{X_i}{L_i}, \infty\right] \end{cases},$$

and for $X = \infty$, $\mathbb{Q}_{\cdot,\infty}$ is a identify map, i.e. $x = \mathbb{Q}_{\cdot,\infty}\, x$.

This type of uniform quantizer $\mathbb{Q}_{L_x,X}$ has a useful property that greatly simplifies the analysis: if $|x_i| \le X_i$, then $|x_i - Q_{L_x,X} x_i| \le X_i/L_i$. Let invdiag$(L)$ denote an $n \times n$ square matrix

$$\text{invdiag}(L)_{ij} = \begin{cases} L_i^{-1} & i = j \\ 0 & i \neq j. \end{cases}$$

This property has an alternative expression:

$$\text{if } |x| \ge_+ X, \text{ then } |x - y| \ge_+ \text{invdiag}(L)X.$$

Estimators

To construct a linear state estimator with bounded estimation errors, the LTI system (1.3) is required to be detectable, *i.e.* there exist some matrix K such that $A + KC$ is stable. Given the matrix K such that $A + KC$ is strictly stable, we can construct a linear estimator

$$\hat{x}(t+1) = A\hat{x}(t) - K(y(t) - C\hat{x}(t)),\ \hat{x}(0) = 0. \tag{1.8}$$

We define its estimation error e and residual vector r as

$$e(t) \triangleq x(t) - \hat{x}(t), \qquad r(t) \triangleq y(t) - C\hat{x}(t),$$

respectively. The signals e and r satisfy the following dynamics

$$\begin{aligned} e(t+1) &= (A + KC)e(t) + (B + KD)w(t), \qquad e(0) = 0 \\ r(t) &= Ce(t) + Dw(t). \end{aligned}$$

Thus, the LTI system from w to e, $E(K)$, and the LTI system from w to r, $F(K)$, are respectively given by

$$E(K) = \left[\begin{array}{c|c} A + KC & B + KD \\ \hline I & 0 \end{array}\right] \tag{1.9}$$

$$F(K) = \left[\begin{array}{c|c} A + KC & B + KD \\ \hline C & D \end{array}\right]. \tag{1.10}$$

Because $A + KC$ is strictly stable, both $E(K)$ and $F(K)$ have bounded induced-norms. The induced-norms upper-bound the values of $\|e\|_q$ and $\|r\|_q$ as follows.

Lemma 1.5.1. *If $\|w\|_p \le 1$, then the estimation error e and residual vector r satisfy*

$$\|e\|_q \le \|E(K)\|_{p\to q}, \qquad \|r\|_q \le \|F(K)\|_{p\to q}. \tag{1.11}$$

Chapter 2

COMPONENT SPEED-ACCURACY TRADEOFFS (SATS) IN NEUROPHYSIOLOGY

There exist trade-offs between neural signaling speed and accuracy arising from the fixed spatial and metabolic cost to build and maintain nerves or muscles. Specifically, nerves with the same cross-sectional area can either contain many small axons or a few large axons (Fig. 2.1b), which inevitably leads to SATs in neural signaling [153, 154, 185]. The specific forms of SATs depend on how the nerves encode information (*e.g.* spike-based, rate-based, and spike-interval-based encoding). In this section, we derive the SATs for nerve signaling and muscle actuation.

2.1 Spike-based nerve signaling

In a spike-based encoding scheme, information is encoded in the presence or absence of a spike within each time interval, analogous to digital packet-switching networks [164, 180]. This encoding method requires spikes to be generated with sufficient timing accuracy, which has been experimentally verified in many types of neurons [61, 122]. To quantify the bundle of axons in certain nerves that can sometimes have complex size distributions, we can classify axons into m distinct types, where each type corresponds to axons of identical size. We index each type by $k \in \{1, 2, \cdots, m\}$ and model type k axons as a communication channel with signaling delay T_k and signaling rate R_k (*e.g.* the total amount of information in bits that can be transmitted per unit time). Let n_k, ρ_k, s_k denote the number, radius, and total space used by type k axons, respectively. When the signaling is precise and noiseless, a type k axon with achievable firing rate ϕ_k can transmit

$$C_s = \phi_k \tag{2.1}$$

bits of information per unit time. For sufficiently large myelinated axons, the propagation speed $1/T_k$ and firing rate ϕ_k of action potentials are both approximately proportional to the axon radius ρ_k [185]:

$$T_k = \alpha/\rho_k \qquad\qquad \phi_k = \beta\rho_k, \tag{2.2}$$

where α and β are proportionality constants. Moreover, the space and metabolic cost of nerves is proportional to their volume [185], and given a fixed nerve length, these

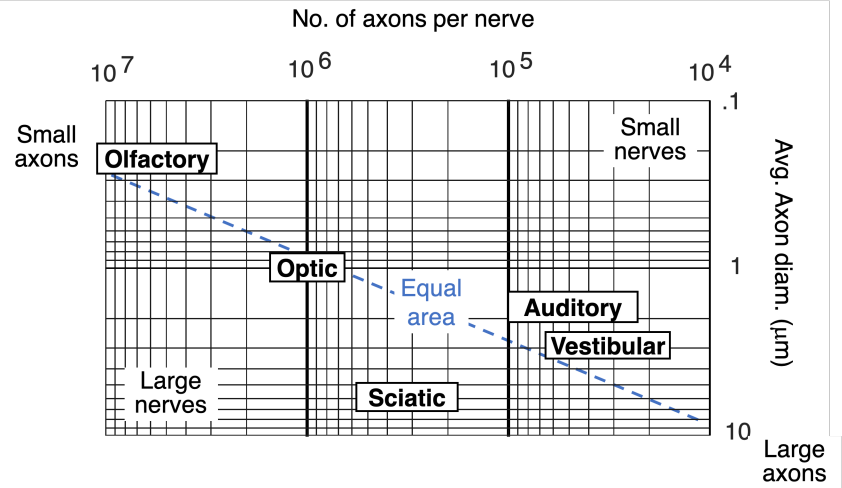

(a) Cartoon diagram showing how nerve size and number trade-offs result in its signaling SATs. The region above the dashed line represents the achievable speed and accuracy given a fixed total cross-sectional area, which is proportional to λ.

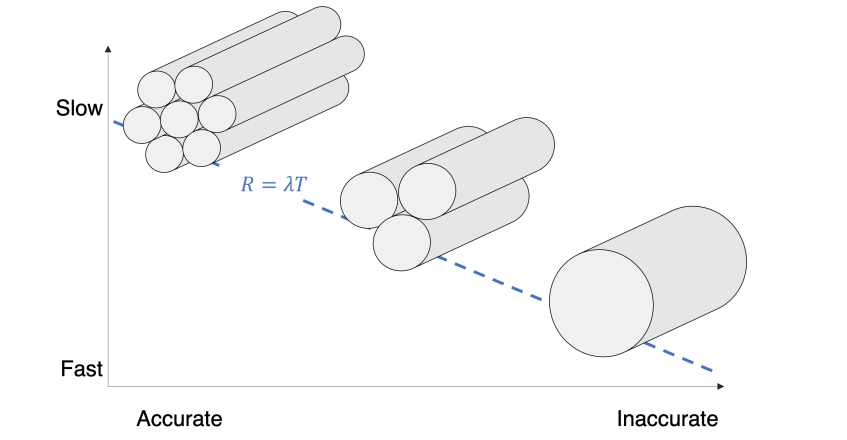

(b) Cartoon diagram showing how nerve size and number trade-offs result in its signaling SATs. The region above the dashed line represents the achievable speed and accuracy given a fixed total cross-sectional area, which is proportional to λ.

Figure 2.1: Component-level speed-accuracy trade-off (SAT) in nerves [142].

costs are proportional to the nerve's total cross-sectional area s. These properties lead to

$$R_k = \lambda_k T_k \tag{2.3}$$

$$\sum_{k=1}^{m} \lambda_k = \lambda, \tag{2.4}$$

where $\lambda_k = s_k \beta / \pi \alpha > 0$ is a constant associated with the total resource use (*i.e.* space available to build the axons). A special case of (2.3) is when all axons have the same size. In such cases, we can model the bundle of axons as a single communication channel with signaling delay $T_s = T_k$ and signaling delay $R = \sum_{i=1}^{m} R_k$ satisfying

$$R = \lambda T_s, \tag{2.5}$$

where $\lambda = s\beta / \pi\alpha$.

2.2 Rate-based encoding

In rate-based encoding scheme, the information is encoded in the rate of spiking instead of individual spikes [183]. We can model this process as a Poisson-type communication channel whose input is the spike rate $\gamma(t)$ and the output is the spike timing $M(t)$. We assume that the spike timing is a non-homogeneous Poisson point process with rate (intensity) $\gamma = \{\gamma(t) \geq 0 : t \in \mathbb{R}_+\}$, denoted by $\mathcal{P}_t(\gamma)$.[1] The communication channel is then given by

$$M(t) = \mathcal{P}_t(\gamma), \tag{2.7}$$

where the spike rate is bounded by

$$\gamma(t) \leq \phi \qquad\qquad t \in \mathbb{R}_+, \tag{2.8}$$

for some $\phi > 0$. The information capacity of communication channel (2.8) is defined to be

$$C_r = \sup \lim_{T \to \infty} \frac{1}{T} I(\gamma^T; M^T). \tag{2.9}$$

[1] The process $\mathcal{P}_t(\gamma)$ has the transition probability

$$\mathbb{P}[\mathcal{P}_{t+h}(\gamma) - \mathcal{P}_t(\gamma) = n] = \frac{1}{n!} \Lambda(t,h)^n e^{-\Lambda}, \tag{2.6}$$

where $\Lambda(t,h)$ is the time integral of rate γ, *i.e.* $\Lambda(t,h) \triangleq \int_t^{t+h} \gamma(t) dt$.

where the supremum is taken over all distributions of the input process $\mathcal{P}_{\gamma(t)}$ satisfying (2.8). Kabanov has shown in [42] that C_r is upper-bounded by

$$C_r = \frac{(\phi+1)^{1+\phi^{-1}}}{2} - \left(1+\frac{1}{\phi}\right)\log(\phi+1) \tag{2.10}$$

So for sufficiently large ϕ,

$$C_r \to \phi/2 \text{ as } \phi \to \infty. \tag{2.11}$$

Replacing (2.1) with (2.11) in the argument of (2.2)–(2.4), for the case of diverse axons, we obtain

$$R_k = \lambda'_k T_k \tag{2.12}$$

$$\sum_{k=1}^{m} \lambda'_k = \lambda', \tag{2.13}$$

where $\lambda' = s\beta/2\pi\alpha > 0$. Similarly, for the case of uniform axons, we have

$$R = \lambda' T \tag{2.14}$$

for the case of uniform axons, where

$$\lambda' = s\beta/2\pi\alpha > 0. \tag{2.15}$$

Remark 2.2.1. *There are a few alternative assumptions, which lead to different tradeoffs. For example, with an additional constraint in the input mean, i.e.* $\mathbb{E}[\gamma] = n$*, the capacity equals* $n\log(\phi/n)$ *[42]. When the constraints are on the input mean and variance, i.e.* $\mathbb{E}[\gamma] = n$ *and* $\mathrm{Var}[\gamma] = \sigma^2$*, the information capacity equals* $n\log(\sigma^2/n^2)$ *[108].*

2.3 Spike-interval-based nerve signaling

Alternatively, the information can also be encoded in the inter-arrival durations. One possible model for this type of neural signaling process is to use an Exponential-type communication channel, *i.e.*

$$M_i = \gamma_i + v_i, \qquad i \in \mathbb{N}, \tag{2.16}$$

where the sequence $\gamma_i (\geq 0)$ is the channel input, and the sequence M_i is the channel output, the sequence v_i is the error in spike timing (spike timing jitter). The spike timing error v_i is generated from *i.i.d.* exponential distribution with

$$\mathbb{E}[v_i] = b, \qquad \mathrm{Var}[v_i] = b^2. \tag{2.17}$$

We model v_i as an exponential random variable because spike intervals are observed to be close to exponential or Gamma distribution [176]. We assume that the input sequence is below the achievable spike rate ϕ, *i.e.*

$$\sum_{i=1}^{n} \gamma_i / n \leq 1/\phi. \tag{2.18}$$

The capacity of the communication channel from input $\gamma(t)$ and output $M(t)$ is defined as

$$C_d = \sup \lim_{n\to\infty} \frac{1}{n} I(\gamma^n; M^n), \tag{2.19}$$

where the supremum is taken over all distributions P_γ of the input process $\{\gamma_i\}_{i\in\mathbb{N}_+}$ satisfying (2.17). In [196], Verdu showed that

$$C_d = \log\left(1 + \frac{1}{b\phi}\right) \tag{2.20}$$

We consider two different assumptions: when $\mathbb{E}[v_i] = b$ is inversely proportional to the axon cross-sectional area, and when $\mathrm{Var}[v_i] = b^2$ is inversely proportional the axon membrane area. In the former case, we have

$$b = \frac{1}{r\rho} \tag{2.21}$$

for some proportionality constant $r > 0$. Substituting (2.21) into (2.20), we obtain

$$C_d = \log\left(1 + \frac{\sqrt{r\pi}}{\beta}\right). \tag{2.22}$$

By the same argument with Section 2.1, for the case of diverse axons, we obtain

$$\begin{aligned} R_k &= n_k \phi_k C_d && (2.23)\\ &= \frac{s_k \beta}{\pi \rho_k} \log\left(1 + \frac{\sqrt{r\pi}}{\beta}\right) && (2.24)\\ &= \lambda T_s, && (2.25) \end{aligned}$$

where $\lambda_k'' = \lambda \log\left(1 + \frac{\sqrt{r\pi}}{\beta}\right)$. For the case of uniform axons, we have

$$R = \lambda T_s, \tag{2.26}$$

where $\lambda_k'' = \lambda \log\left(1 + \frac{\sqrt{r\pi}}{\beta}\right)$. In the latter case, we have

$$b^2 = \frac{1}{2r\rho\pi} \tag{2.27}$$

for some proportionality constant $r > 0$. Substituting (2.27) into (2.20), we obtain

$$C_d = \log\left(1 + \frac{\sqrt{r\pi\rho}}{\phi}\right) \tag{2.28}$$

for some constraint $\gamma > 0$. By the same argument with Section 2.1, for the case of diverse axons, we obtain

$$R_k = n_k \phi_k C_d \tag{2.29}$$

$$= \frac{s_k \beta}{\pi \rho_k} \log\left(1 + \sqrt{\frac{r\pi T_s}{\alpha\beta^2}}\right) \tag{2.30}$$

$$= \lambda T_s \log\left(1 + \sqrt{\frac{r\pi T_s}{\alpha\beta^2}}\right), \tag{2.31}$$

where $\lambda_k'' = \frac{s_k\beta}{\pi\alpha}$. For the case of uniform axons, we have

$$R = \lambda T_s \log\left(1 + \sqrt{\frac{r\pi T_s}{\alpha\beta^2}}\right). \tag{2.32}$$

2.4 Summary of nerve signaling SATs

Rate-based encoding was believed to be the most standard encoding schemes because it was unclear if spikes can be generated with enough timing precision to carry information in individual spikes. However, there is growing evidence that nerves are able to use encoding schemes that requires high spike timing precision [183]: nerves are capable of spiking with highly precise timing [19, 61, 122]; and a few experiments also observe that spike timing carries behaviorally relevant information [19, 180]. The SATs we derive support this view by showing that spike-based encoding or spike-interval-based encoding allows more information to be transmitted per spike than rate-based encoding given a fixed maximum spike rate ϕ. However, interestingly, the SATs under all three types encodings may have qualitatively similar SATs: under certain assumptions, the achievable data rate is roughly proportional to delay.

2.5 Muscle actuation SATs

The actuation components, muscle, also have tradeoffs in terms of the reaction speed, accuracy in strength level, strength, and ease of fatigue. Moreover, most muscles carry diverse muscle fibers, *e.g.* striated muscles typically have both large fast twitch fibers and many more smaller slow twitch muscles (Fig. 2.2a). In particular, its SATs can be modeled using a simplified muscle model that includes m motor

	Bits per spike	SATs
Spike-based	1	$R = \lambda T$
Rate-based	$1/2$	$R = (\lambda/2)T$
Spike-interval-based	$\log\left(1 + \sqrt{r\pi}/\beta\right)$	$R = \lambda \log\left(1 + \sqrt{r\pi}/\beta\right) T_s$

Table 2.1: Efficiency of different neural signaling schemes. The SATs can take different forms than above, depending on the assumptions. See Section 2.1-2.3 for the assumptions made.

units, indexed by $i \in \{1, 2, \cdots, m\}$, each associated with a reaction speed and a strength. We use F_i to denote its strength and assume without loss of generality that $F_1 \leq F_2 \leq \cdots \leq F_m$. According to Henneman's size principle [78], motor units in the spinal cord are recruited in ascending order of F_i, so a muscle (at non-transient time) can only generate $m + 1$ discrete strength levels:

$$\sum_{i=1}^{n} F_i, \qquad n \in \{0, 1, \cdots, m\}. \tag{2.33}$$

Given a fixed length, the maximum strength of a muscle $\ell = \sum_{i=1}^{m} F_i$ is known to be proportional to its cross-sectional area [71]. This implies that, given a fixed space to build a muscle, its maximum strength does not depend on the specific composition of motor units. Constrained on the maximum strength, a muscle can be built from many motor units with small strengths or a few motor units with large strengths. In the former case, the muscle has better resolution but slow reaction speed, while in the latter case, the muscle has fast reaction speed but coarser resolution. This SAT can be quantified using the following formula (see Fig. 2.2b):

$$\begin{aligned} \dot{a}_i(t) &= \alpha f_i^p(t)(1 - a_i(t)) - \beta a_i(t) \\ a_i^q(t) &= c_i(t), \end{aligned} \tag{2.34}$$

where $\alpha = 1, \beta = 1, p = 1, q = 3$ are fixed constants [23]. If a motor unit is recruited at time $t = 0$, then its strength $c_i(t)$ rises according to (2.34) with

$$f_i(t) = 1(t)/((1/F_i)^{1/q} - 1), \tag{2.35}$$

where $1(t)$ is a unit step function. Similarly, when a recruited motor unit is released at time $t = \tau$, its contraction rate falls according to (2.34) with

$$f_i(t) = 1(-t + \tau)/((1/F_i)^{1/q} - 1). \tag{2.36}$$

From (2.34), the reaction speed of a muscle is an increasing function of F_i, and the time required for a muscle to reach to $c_i(t) = F_i$ from $c_i(0) = 0$ is decreasing in F_i. Thus, better resolution (having small F_i) can only be achieved with decreased reaction speed.

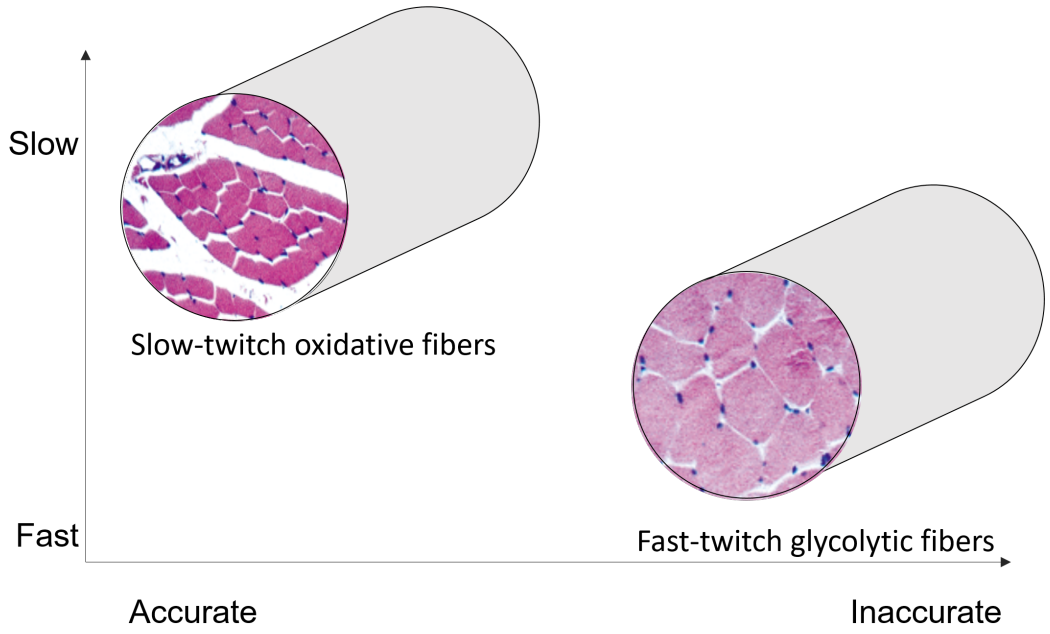

(a) Diagram showing the speed-accuracy trade-offs (SAT) in muscles. Different types of muscle fibers and their resulting actuation SATs. The one with a smaller diameter and darker color (due to larger amounts of myoglobin, numerous mitochondria, and extensive capillary blood supply) are the oxidative fibers, and the other is the glycolytic fibers. Oxidative fibers are slower but more accurate, whereas glycolytic fibers are faster but less accurate.

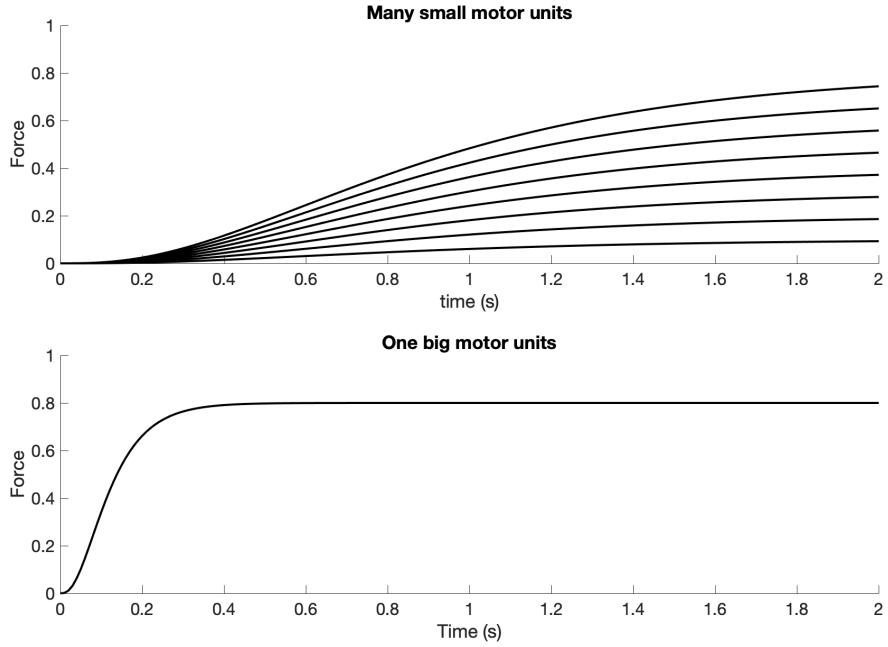

(b) Forces generated by different types of motor units. The total force of a sum of many small motor units versus one large motor unit, generated from (2.34).

Figure 2.2: Muscle speed-accuracy trade-offs

Chapter 3

SYSTEM SPEED-ACCURACY TRADEOFFS (SATS): FUNDAMENTAL LIMITS

An example of effective layered control architectures is the oculomotor system that stabilizes the eye on a moving target while you are bouncing down a trail (Fig. 5.7). Neurons in the visual cortex responding to target motion on the retina drive the actuators to pursue the target after a delay of 100 milliseconds. In contrast, fast head motions are compensated by control systems in the brainstem in the millisecond range. Together, they allow you to maintain fixation on a distant moving target despite severe bumps. In trail following (Fig. 5.9), higher-level cortical control systems in the cortex and basal ganglia provide advanced warning for planning actions to avoid trees and other obstacles. This is accompanied by a fast feedback system in the spinal cord that maintains steady tracking.

To study how these control systems are coordinated, we will introduce a task in which the subjects aim to follow desired trajectory in the presence of uncertainty and noise. The diagram of the control architectures used in the task is shown in Fig. 5.1 for reaching, Fig. 5.7 for visual tracking, and Fig. 5.9 for tracking a trail. We define the error dynamics $x(t)$ from the system evolution of the rider or eye movement that must track a reference trail or trajectory with small error despite uncertainty:

$$x(t+1) = ax(t) + w(t) + u(t), \tag{3.1}$$

which relates the future error $x(t+1)$ with the previous error $x(t)$, the uncertainty $w(t)$ (trajectory changes, bumps, trail changes, etc.), and the control action $u(t)$. The control action $u(t)$ is generated using a feedback controller, which uses sensing components such as eyes, muscle sensors, and the inner ear; communication components such as nerves; computing components such as the cortex in the central nervous system; and actuation components such as eye and arm muscles. Here, T_s captures the signaling delay in feedback due to the latency in nerve signaling, and T_i captures other internal delays in the feedback loop. The advanced warning of the uncertainty T_a models situations such as when vision informs the rider about the trail ahead by T_a time steps (a form of advanced warning, which depends on the rider's speed and the trail's features), and when the muscle tone changes before an expected

Parameter	Description
$x(t)$	Error at time step t
$\mathcal{K}$	Controller
$T_s \geq 0$	Signaling delay
$T_i \geq 0$	Internal delay
$T = T_s + T_i$	Total delay
T_t	Time to reach target
R	Information rate (bits per unit time)
λ	Cost associated with the resource use

Table S1: Parameters in the basic model.

perturbation [20, 125]. We additionally assume that the feedback loop has limited data rate R, which accounts for the limitations in nerve signaling. In this chapter, we derive the hardware tradeoffs for system (3.1) with delay only, quantization only, and both delay and quantization.

3.1 The impact of delay

We consider the system (error) dynamics (3.1) with zero initial condition, *i.e.* $x(0) = 0$. The controller $\mathcal{K}$ generates the control action $u(t)$ using the full information on the histories of the state, disturbance, and control input with delay $T_u \geq 0$, *i.e.*

$$u(t + T_u) = \mathcal{K}(x(0 : t), w(0 : t - 1), u(0 : t + T_u - 1)). \tag{3.2}$$

The sensorimotor control in risk-aware setting motivates the use of L_1 optimal control, and as such, our goal is to solve the following robust control problem:

$$\inf_{\mathcal{K}} \sup_{\|w\|_\infty \leq 1} \|x\|_\infty \tag{3.3}$$

subject to (3.1) and (3.2). This problem admits a simple and intuitive solution. In particular, the optimal cost is given by

$$\inf_{\mathcal{K}} \sup_{\|w\|_\infty \leq 1} \|x\|_\infty = \sum_{i=0}^{T_u} |a^i|. \tag{3.4}$$

This optimal cost is achieved by the control policy

$$u(t) = -a^{T_u+1} w(t - 1 - T_u). \tag{3.5}$$

To prove (3.4) and (3.5), we first first derive a lower bound for the optimal cost, and we then find a controller that achieves the lower bound. The lower bound is obtained

by noticing that the delay T_u in the control loop introduces an initial uncontrollable window in the closed loop response of the system. So we have

$$\begin{aligned}\max_{\|w\|_\infty \le 1} \|x\|_\infty &\ge \max_{\|w\|_\infty \le 1} |x(T_u+1)| \\ &\ge \max_{\|w\|_\infty \le 1} |a^{T_u} w(0) + a^{T_u-1} w(1) + \cdots + w(T_u)| \\ &= \textstyle\sum_{i=0}^{T_u} |a^i|.\end{aligned}$$

This lower bound can also be realized by the control policy (3.5), which yields the following closed loop behavior

$$x(t+1) = a^{T_u} w(t-T_u) + a^{T_u-1} w(t-T_u+1) + \cdots + w(t).$$

From (3.1), we observe that the worst-case disturbance is

$$\begin{aligned} w(t-T_u) &= \operatorname{sign}(a^{T_u}) \\ w(t-T_u+1) &= \operatorname{sign}(a^{T_u-1}) \\ &\vdots \\ w(t) &= 1, \end{aligned}$$

which attains the optimal cost in (3.4).

3.2 The impact of quantization

Quantization is the process of converting a continuous signal to a discrete one. It can arise in many biological systems where sensing, computation, and actuation components are not co-located. We consider the error dynamics (3.1) and a quantized controller

$$u(t) = \mathcal{K}(x(0:t), w(0:t-1), u(0:t-1)). \tag{3.6}$$

We also assume zero initial condition, *i.e.* $x(0) = 0$. The desired control action $u(t)$ is generated using full information on the histories of state, disturbance, and control input, but the feedback loop can only transmit R bits of information per unit time. In all of what follows, we assume that the data rate is above the minimum stabilizing rate, *i.e.* $R > \log_2 |a|$ [138]. This problem also admits an analytic formula

$$\inf_{\mathcal{K}} \sup_{\|w\|_\infty \le 1} \|x\|_\infty = \frac{1}{2^R - |a|} + 1, \tag{3.7}$$

which can be attained by the control policy

$$u(t) = \bar{Q}_{R,\Psi}(-ax(t)), \tag{3.8}$$

where $\Psi = 2^R|a|/(2^R - |a|)$, and the map $Q_{R,\Psi}$ is defined to be a uniform quantizer of rate R on domain $[-\Psi, \Psi]$.

Similarly, (3.7) and (3.8) can be proved by first lower-bounding the optimal cost and then find a controller that achieves the bound. A lower bound can be obtained using the problem of estimating $w(\tau)$ at time t:

$$H(t,\tau) = \inf_{Q} \quad \sup_{|w(\tau)|\le 1} |w(\tau) - \hat{w}(\tau)| \tag{3.9}$$

$$\text{s.t.} \quad \hat{w}(\tau) = Q(w(\tau)) \tag{3.10}$$

$$Q \text{ is a quantizer with data rate } (t-\tau)R. \tag{3.11}$$

Because $w(\tau)$ can take any values in the interval $[-1, 1]$, and the output of $Q(w(\tau))$ can take at most $2^{(t-\tau)R}$ discrete values, the estimation error is lower-bounded by $H(t,\tau) \ge 2^{-(t-\tau)R}$. On the other hand, the above lower bound can also be attained using a uniform quantizer on domain $[-1, 1]$. It then follows that

$$H(t,\tau) = \begin{cases} 2^{-(t-\tau)R} & t \ge \tau + 1 \\ 1 & t < \tau + 1. \end{cases} \tag{3.12}$$

The problem $H(t,\tau)$ can be used to lower-bound the value of $|x(t+1)|$. The state can be decomposed into terms due to past disturbance and a term due to past control action:

$$x(t+1) = a^t w(0) + a^{t-1} w(1) + \cdots + w(t) + U'(t), \tag{3.13}$$

where $U(t) = \sum_{\tau=0}^{t} a^\tau u(t-\tau)$. We define an auxiliary state x' and its control action U' as follows:

$$x'(t+1) = a^t w(0) + a^{t-1} w(1) + \cdots + w(t) + U(t) \tag{3.14}$$

$$U'(t) = -(a^t \hat{w}(0) + a^{t-1}\hat{w}(1) + \cdots + \hat{w}(t)), \tag{3.15}$$

where $\hat{w}(\tau)$ is the optimal solution of the estimation problem $H(t,\tau)$. The worst-case absolute value of $x'(t+1)$ can be easily computed as

$$\sup_{\|w\|_\infty \le 1} |x'(t+1)| \tag{3.16}$$

$$= \sup_{\|w\|_\infty \le 1} |a^t(w(0) - \hat{w}(0)) + a^{t-1}(w(1) - \hat{w}(1)) + \cdots + (w(t) - \hat{w}(t))| \tag{3.17}$$

$$= \sup_{\|w\|_\infty \le 1} |a^t(w(0) - \hat{w}(0))| + |a^{t-1}(w(1) - \hat{w}(1))| + \cdots + |w(t) - \hat{w}(t)| \tag{3.18}$$

$$= |a^t| H(t,0) + |a^{t-1}| H(t,1) + \cdots + H(t,t) \tag{3.19}$$

$$= \frac{1 - (|a|/2^R)^{t+1}}{1 - |a|/2^R}. \tag{3.20}$$

This value monotonically increases as time t grows. Under the assumption $R > \log_2 |a|$, we have

$$\lim_{t\to\infty} \frac{1-(a/2^R)^t}{1-(a/2^R)} = \frac{2^R}{2^R-|a|}, \tag{3.21}$$

where the convergence of the infinite series is due to the assumption on minimum stabilizing data rate, *i.e.* $|a|/2^R < 1$. Meanwhile, the disturbance $w(\tau)$ can take any values from $[-1, 1]$, and at most $2^{(t-\tau)R}$ bits of information can be used to transmit the information on $w(\tau)$ during the time interval $[\tau, t]$. Therefore, the control action $U(t)$ for $x(t+1)$ cannot perform better than $U'(t)$ for $x'(t+1)$, *i.e.*

$$\sup_{\|w\|_\infty \le 1} |x(t+1)| \ge \sup_{\|w\|_\infty \le 1} |x'(t+1)|. \tag{3.22}$$

Combining (3.16)–(3.22), we obtain the following lower bound on the achievable cost:

$$\sup_{\|w\|_\infty \le 1} \|x\|_\infty \ge \lim_{t\to\infty} \sup_{\|w\|_\infty \le 1} |x(t+1)| \ge \lim_{t\to\infty} \sup_{\|w\|_\infty \le 1} |x'(t+1)| = \frac{2^R}{2^R-|a|}. \tag{3.23}$$

Next, we show that the control policy (3.8) achieves the optimal cost (3.7). Let $u^*(t)$ be the input to the quantizer, and $x_q(t+1) = \bar{Q}_{R,\Psi}(u^*(t)) - u(t)$ be the quantization error. Observe that $x(t) = w(t-1) + x_q(t)$. Using mathematical induction, it can be shown that there exists a control and communication policy that achieves

$$\sup_{\|w\|_\infty \le 1} \|x_q\|_\infty \le \frac{|a|}{2^R-|a|}. \tag{3.24}$$

Condition in (3.24) holds at time $t = 0$. Now we assume that condition in (3.24) holds at time t. It then follows that

$$|u^*(t)| = |-ax(t)| = |-a(x_q(t) + w(t-1))| \le \frac{2^R|a|}{2^R-|a|} = \Psi. \tag{3.25}$$

Since the quantizer output $\bar{Q}_{R,\Psi}(u(t))$ can take at most 2^R discrete values, the value of $x_q(t+1)$ can be bounded by

$$|x_q(t+1)| = |\bar{Q}_{R,\Psi}(u^*(t)) - u^*(t)| \tag{3.26}$$

$$\le 2^{-R}\Psi \tag{3.27}$$

$$= \frac{|a|}{2^R-|a|}. \tag{3.28}$$

Thus, condition (3.24) also holds at time $t+1$, and this finishes the proof of (3.24). Combining (3.23) with (3.24) yields

$$\sup_{\|w\|_\infty \le 1} \|x\|_\infty = \sup_{\|w\|_\infty \le 1} \|x_q + w\|_\infty \le \frac{|a|}{2^R-|a|} + 1.$$

3.3 The impact of delay and quantization in reaching tasks

The above analysis tool can be used to study the fundamental limits in a reaching task and derive a formula similar to Fitts' law [60]. We model this setting by error dynamics (3.1) with $w(t) = d\delta(t)$ in (3.1), where $d \in [-D, D]$ is the distance between the initial position and the target position, and $\delta(t)$ is the Kronecker delta function, which is defined as follows: $\delta(t) = 1$ if $t = 0$, and $\delta(t) = 0$ otherwise. The error is controlled by a delayed and quantized controller:

$$u(t+T) = \mathcal{K}(x(0:t), w(0:t-1), u(0:t+T-1)) \tag{3.29}$$

where $x(t) \in \mathbb{R}$ is the system state, $u(t) \in \mathbb{R}$ is the control action, and $w(t) \in \mathbb{R}$ is the disturbance. We also assume zero initial condition, *i.e.* $x(0) = 0$. The desired control action $u(t)$ is then generated by the controller $\mathcal{K}$, which can transmit R bits per unit time with a delay of T, using full information on the histories of the state, disturbance and control input. The setting of Reaching tasks described in Section B.1 in the main text can be recovered by setting $T := T_s + T_i - T_a$. The reaching time T_{ent} can be formally defined as

$$T_{\text{ent}} = \inf\{t : |x(t)| \le W/2 \text{ for any } |w| \le D\}. \tag{3.30}$$

Similar to the case in Section 3.2, we define the problem of estimating $w(0)$ at time t as follows:

$$H(t,0) = \inf_{Q} \quad \sup_{|w(0)| \le D} |w(0) - \hat{w}(0)| \tag{3.31}$$

$$\text{s.t.} \quad \hat{w}(0) = Q(w(0)) \tag{3.32}$$

$$Q \text{ is a quantizer with data rate } (t-T)R. \tag{3.33}$$

The value of $H(t,0)$ can be computed to be

$$H(t,0) = \frac{1}{2^{(t-T)R}} D. \tag{3.34}$$

The minimum worst-case reaching time is lower-bounded by

$$T_{\text{ent}} \ge \min\{t : H(t,0) \le W\} \tag{3.35}$$

$$\ge T + R^{-1} \log_2 \left(\frac{2D}{W} \right). \tag{3.36}$$

3.4 The impact of delay and quantization in driving tasks

We consider the system dynamics (3.1) with delayed and quantized controller

$$u(t+T_u) = \mathcal{K}(x(0:t), w(0:t+T_a-1), u(0:t+T_u-1)), \tag{3.37}$$

where $x(t) \in \mathbb{R}$ is the system state, $u(t) \in \mathbb{R}$ is the control action, and $w(t) \in \mathbb{R}$ is the disturbance. We also assume zero initial condition, *i.e.* $x(0) = 0$. The controller $\mathcal{K}$ receives advanced warning on disturbance T_a ahead of time.The desired control action $u(t)$ is then generated by the controller $\mathcal{K}$ using full information on the histories of the state, disturbance and control input. The actual control action is delayed by T_u and quantized by $\mathcal{R}$ with data rate R, where R is minimum stabilizing, *i.e.* $R > \log_2 |a|$. This problem also admits a simple and intuitive solution. In particular, the optimal cost is given by

$$\min_{\mathcal{K}} \max_{\|w\|_\infty \le 1} \|x\|_\infty = \begin{cases} \sum_{i=0}^{T} |a^i| + |a^{T+1}| \left(2^R - |a|\right)^{-1} & \text{if } T > 0 \\ \left(2^R - |a|\right)^{-1} & \text{if } T \le 0, \end{cases} \tag{3.38}$$

where $T := T_u - T_a$ is the net delay from the disturbance to the control action. The optimal cost only depends on $T_u - T_a$ but not individual values of T_u and T_a because systems with constant $T_u - T_a = T$ can all be reduced to systems with either $(T_a, T_u) = (-T, 0)$ for $T \le 0$ or $(T_a, T_u) = (0, T)$ for $T > 0$. Therefore, the proof for optimal cost and optimal control policy in the case of $T < 0$ is given in (3.8). On the other hand, the optimal control policy for $T > 0$ is

$$\begin{aligned} x_q(t) &= u(t-1) - u^*(t-1) \\ u^*(t) &= -a^{T+1} w(t-T-1) - a x_q(t) \\ u(t) &= \bar{Q}_{R,\Psi}(u^*(t)), \end{aligned} \tag{3.39}$$

where $\Psi = 2^R |a^{T+1}| / (2^R - |a|)$.

Similar to previous cases, we prove (3.38) and (3.39) by first deriving a lower bound of the optimal cost and then finding a control achieving the lower bound. To obtain the lower bound, we decompose the state $x(t)$ into the term due to delayed control $x_d(t)$ and the term due to quantized control $x_q(t)$ as follows:

$$x(t) = x_d(t) + x_q(t). \tag{3.40}$$

Because this information about the disturbance $w(t-T:t)$ is not available to the controller when generating the control signal $u(t)$, its effect on $x(t+1)$ cannot be

controlled. It then follows that the effects of $w(t-T:t)$ on $x(t+1)$ is

$$x_d(t+1) = a^T w(t-T) + a^{T-1} w(t-T+1) + \cdots + w(t). \tag{3.41}$$

Given the term $x_d(t+1)$, we can then define

$$x_q(t+1) = x(t+1) - x_d(t+1), \tag{3.42}$$

which is a function of $w(0:t-T-1)$ and $u(0:t)$, but not $x_d(t+1)$. Here, disjoint subsets of the disturbance affect the term due to delay $x_d(t+1)$ and the term due to quantization $x_q(t+1)$, and the value of $x_d(t+1)$ is not impacted by the chosen control policy. Therefore, the optimal cost can also be decomposed into

$$\inf_{\mathcal{K}} \sup_{\|w\|_\infty \le 1} \|x\|_\infty = \sup_{\|w\|_\infty \le 1} \|x_d\|_\infty + \inf_{\mathcal{K}} \sup_{\|w\|_\infty \le 1} \|x_q\|_\infty, \tag{3.43}$$

where the infima on both sides are subject to the system dynamics (3.1). From (3.41), the first term satisfies

$$\sup_{\|w\|_\infty \le 1} \|x_d\|_\infty = \sum_{i=0}^{T} |a^i|. \tag{3.44}$$

We will show below that the second term satisfies

$$\inf_{\mathcal{K}} \sup_{\|w\|_\infty \le 1} \|x_q\|_\infty \ge \frac{|a^T|}{2^R - |a|}. \tag{3.45}$$

Similar to the case in Section 3.2, we define the problem of estimating $w(0)$ at time t as follows:

$$\begin{aligned} H(t,\tau) = \inf_{Q} \quad & \sup_{|w(\tau)| \le 1} |w(\tau) - \hat{w}(\tau)| \\ \text{s.t.} \quad & \hat{w}(\tau) = Q(w(\tau)) \\ & Q \text{ is a quantizer with data rate } (t-T-\tau)R. \end{aligned} \tag{3.46}$$

Now we use the estimation problem $H(t,\tau)$ to lower-bound the value of $|x_q(t+1)|$. The term $x_q(t+1)$ can also be decomposed into

$$x_q(t+1) = a^t w(0) + a^{t-1} w(1) + \cdots + a^{T+1} w(t-T-1) + U(t), \tag{3.47}$$

where $U(t) = \sum_{\tau=0}^{t-T} a^\tau u(t-T-\tau)$. We define an auxiliary state x' and its control action U' as follows:

$$x'_q(t+1) = a^t w(0) + a^{t-1} w(1) + \cdots + a^{T+1} w(t-T-1) + U(t) \tag{3.48}$$

$$U'(t) = -(a^t \hat{w}(0) + a^{t-1} \hat{w}(1) + \cdots + a^{T+1} \hat{w}(t-T-1)), \tag{3.49}$$

where $\hat{w}(\tau)$ is the optimal solution of the estimation problem $H(t,\tau)$. The worst-case absolute value of $x'_q(t+1)$ can be bounded by

$$\begin{aligned}
&\sup_{\|w\|_\infty \le 1} |x'_q(t+1)| \\
=&\sup_{\|w\|_\infty \le 1} |a^t(w(0)-\hat{w}(0))| + |a^{t-1}(w(1)-\hat{w}(1))| + \cdots && (3.50)\\
&+ |a^{T+1}(w(t-T-1)-\hat{w}(t-T-1))| && (3.51)\\
=&|a^t|H(t,0) + |a^{t-1}|H(t,1) + \cdots + |a^{T+1}|H(t,t-T-1) && (3.52)\\
=&\frac{|a^{T+1}|}{2^R}\frac{1-(|a|/2^R)^{t-T}}{1-(|a|/2^R)}. && (3.53)
\end{aligned}$$

From the same argument with Section 3.2, the control action $U(t)$ for $x_q(t+1)$ cannot perform better than $U'(t)$ for $x'_q(t+1)$, *i.e.*

$$\sup_{\|w\|_\infty \le 1} |x_q(t+1)| \ge \sup_{\|w\|_\infty \le 1} |x'_q(t+1)|. \tag{3.54}$$

The lower-bound on $\sup_{\|w\|_\infty \le 1} |x'_q(t+1)|$ monotonically increases as time t grows. Taking $t \to \infty$, we obtain that

$$\begin{aligned}
\sup_{\|w\|_\infty \le 1} \|x_q\|_\infty &\ge \lim_{t\to\infty} \sup_{\|w\|_\infty \le 1} |x_q(t+1)| && (3.55)\\
&\ge \lim_{t\to\infty} \sup_{\|w\|_\infty \le 1} |x'_q(t+1)| && (3.56)\\
&\ge \frac{|a^{T+1}|}{2^R - |a|}, && (3.57)
\end{aligned}$$

where the infinite series in (3.57) converges because the data rate is assumed to be minimum stabilizing, *i.e.* $|a|/2^R < 1$. Combining (3.44) and (3.45), we obtain the following lower bound on the optimal cost

$$\|x\|_\infty \ge \sum_{i=1}^{T} |a^{i-1}| + \frac{|a^{T+1}|}{2^R - |a|}. \tag{3.58}$$

Next, we find a control policy that achieves the lower bound (3.38). We follow the same procedure with Section 3.2 to show that the controller (3.39) achieves

$$\sup_{\|w\|_\infty \le 1} |x_q(t)| \le \frac{|a^{T+1}|}{2^R - |a|}. \tag{3.59}$$

Condition in (3.59) holds for $t = 0$. Now we assume that condition in (3.59) holds for time t. It then follows that

$$|u^*(t-T)| = |-ax_q(t) - a^{T+1}w(t-T-1)| \le |a^{T+1}|\left(1 + \frac{|a|}{2^R - |a|}\right) = \Psi. \tag{3.60}$$

It then follows that the value of $x_q(t+1)$ is bounded by

$$|x_q(t+1)| = \frac{|a^{T+1}|}{2^R - |a|}. \tag{3.61}$$

Thus, condition (3.59) holds at time $t+1$. Combining (3.44) and (3.59) yields

$$\max_{\|w\|_\infty \le 1} \|x\|_\infty \le \sum_{i=0}^{T} |a^i| + \frac{|a^{T+1}|}{2^R - |a|}.$$

3.5 Impact of layering diversity on system SATs

We consider the layered system with two feedback loops

$$\begin{aligned} x(t+1) &= ax(t) + u(t) + w(t) + r(t - T_a) \\ u(t) &= u_L(t) + u_H(t) \\ u_L(t) &= \mathcal{L}(x(0:t), w(0:t-1)) \\ u_H(t) &= \mathcal{H}(x(0:t), r(0:t-1))). \end{aligned} \tag{3.62}$$

The disturbance is now composed of two terms: a component $r(t - T_a)$ that is observed with advance warning $T_a \ge 0$ and a component $w(t)$ that can be observed only through its impact on system performance. We assume that the two disturbances are bounded by

$$\|r\|_\infty \le 1, \quad \|w\|_\infty \le \delta. \tag{3.63}$$

The control action is generated by two nominally independent feedback loops, each having their own sensing, computation, and communication components. Both feedback loops, $\mathcal{L}, \mathcal{H}$ act through a motor nerve pathway with data rates R_L, R_H and delays T_L, T_H, respectively. The optimal cost in worst-case ℓ_∞ norm of this problem is

$$\inf_{\mathcal{H}, \mathcal{L}} \sup_{\|w\|_\infty \le \delta, \|r\|_\infty \le 1} \|x\|_\infty = \left\{ \sum_{i=0}^{T_L} |a^i| + \frac{|a^{T_L+1}|}{2^{R_L} - |a|} \right\} \delta + \frac{1}{2^{R_H} - |a|}. \tag{3.64}$$

To begin, we decompose (3.62) into

$$\begin{aligned} x_L(t+1) &= ax_L(t) + u_L(t) + w(t), \quad x_L(0) = 0 \\ u_L(t) &= \mathcal{L}(x(0:t), w(0:t-1)) \end{aligned} \tag{3.65}$$

and

$$\begin{aligned} x_H(t+1) &= ax_H(t) + u_H(t) + r(t - T_a), \quad x_H(0) = 0 \\ u_H(t) &= \mathcal{H}(x(0:t), r(0:t-1)). \end{aligned} \tag{3.66}$$

From linearity, the state of (3.62) is the sum of the two sub-systems' states, *i.e.*

$$x(t) = x_L(t) + x_H(t). \tag{3.67}$$

Because the disturbances that steer the dynamics of $x_L(t)$ and $x_H(t)$ are disjoint, the optimal cost can also be decomposed into

$$\inf_{\mathcal{L},\mathcal{H}} \sup_{\|w\|_\infty \le 1} \|x\|_\infty = \inf_{\mathcal{L}} \sup_{\|w\|_\infty \le 1} \|x_L\|_\infty + \inf_{\mathcal{H}} \sup_{\|w\|_\infty \le 1} \|x_H\|_\infty \tag{3.68}$$

$$= \left\{ \sum_{i=0}^{T_L} |a^i| + \frac{|a^{T_L+1}|}{2^{R_L} - |a|} \right\} \delta + \frac{1}{2^{R_H} - |a|}. \tag{3.69}$$

In the last equality, we applied the results from Section 3.5 on both sub-systems.

3.6 Impact of axonal diversity on system SATs

We consider the system dynamics (3.1) with the feedback controller $\mathcal{K}$ of the form

$$[s_1(t), s_2(t), \cdots, s_m(t)] = K_t(x(0:t), w(0:t+T_a), s(0:t-1)) \tag{3.70}$$

$$u(t) = \sum_{i=1}^{m} Q_{t,i}(s_i(t - T_i - T_c)), \tag{3.71}$$

where $x(t) \in \mathbb{R}$ is the state, $w(t) \in \mathbb{R}$ is the disturbance, $u(t) \in \mathbb{R}$ is the control action. We assume that the disturbance is ∞-norm bound and, without loss of generality, $\|w\|_\infty \le 1$.

Recall from (3.46) that $H(t, \tau)$ is defined to be the problem of estimating $w(\tau)$ at time t. Its worst-case estimation error can be computed by

$$H(t, \tau) = \frac{1}{2^{\mathcal{R}(h)}}, \tag{3.72}$$

where $\mathcal{R} : \mathbb{Z}_+ \to \mathbb{R}_+$ is defined to be

$$\mathcal{R}(h) := \sum_{i=1}^{m} \max\{0, h - T_i - T_c + T_a\} R_i. \tag{3.73}$$

Adapting same procedure with Section 3.4, we obtain that the worst-case error is bounded by

$$\min_{\mathcal{K}} \max_{\|w\|_\infty \le 1} \|x\|_\infty \ge \sum_{h=1}^{\infty} |a^{h-1}| \frac{1}{2^{\mathcal{R}(h)}}, \tag{3.74}$$

yielding Formula [19].

Next, we construct a control policy that achieves the equality of (6.2). To begin, without loss of generality, we assume that $T_1 < T_2 < \cdots < T_m$ and $R_i > 0$ for $i \in \{1, 2, \cdots, m\}$. We define the following terms recursively.

$$\begin{aligned}
\hat{w}(t, i, \tau) =& 0 \text{ for } t - \tau \le T_1 \\
\hat{w}(t, i+1|\tau) =& \bar{Q}_{R_{i+1}, \ell_{t-\tau,i+1}}(w(\tau) - \hat{w}(t, i|\tau)) + \hat{w}(t, i|\tau) \\
& \text{for } i \in \{1, 2, \cdots, k-1\} \text{ and } T_1 < t - \tau \le T_{k+1} \\
\hat{w}(t+1, 1|\tau) =& \bar{Q}_{R_1, \ell_{t-\tau+1,1}}(w(\tau) - \hat{w}(t, i|\tau)) + \hat{w}(t, m|\tau) \\
& \text{for } i = k,
\end{aligned} \tag{3.75}$$

where ℓ is recursively defined by

$$\ell_{T_1,1} = 1 \tag{3.76}$$

$$\ell_{t-\tau,i+1} = \ell_{t-\tau,i}/2^{-R_i} \text{ for } i \in \{1, 2, \cdots, k\} \qquad \text{if } T_1 < t - \tau \le T_{k+1} \tag{3.77}$$

$$\ell_{t-\tau+1,1} = \ell_{t-\tau,i}/2^{-R_i} \text{ for } i = k \qquad \text{if } T_1 < t - \tau \le T_{k+1}. \tag{3.78}$$

We define the scaled estimation errors to be

$$e(t, i|\tau) = a^{t-\tau}(w(t) - \hat{w}(t, i|\tau)). \tag{3.79}$$

Let $Q_{t,i} = \bar{Q}_{R_i, \Psi_{t,i}}$ be a uniform quantizer with the quantization interval $[-\Psi_{t,i}, \Psi_{t,i}]$ defined from

$$\Psi_{t,i} = \sum_{\tau=0}^{t} \sum_{i: t-\tau > T_i} \ell_{t-\tau,i+1}. \tag{3.80}$$

We consider the control policy

$$u(t) = Q_{t,i}\left(\sum_{\tau=0}^{t} \sum_{i: t-\tau > T_i} e(t, i|\tau) \right), \tag{3.81}$$

where $Q_{t,i}$ is a uniform quantizer on domain x. Let us define the the quantization error $x_q(t)$ to be the sum of the errors from all quantizers $Q_{t,i}, i = \{1, 2, \cdots, m\}$, and the remaining errors in $x(t)$ to be the delay error $x_d(t)$. Observe that the delay error and the quantization error can be computed as follows:

$$x_d(t+1) = a^{T_i} w(t - T_i) + a^{T_i - 1} w(t - T_i + 1) + \cdots + w(t) \tag{3.82}$$

$$x_q(t+1) = u(t) - \sum_{\tau=0}^{t} \sum_{i: t-\tau > T_i} e(t, i|\tau). \tag{3.83}$$

Moreover, it can be shown that they are respectively bounded by

$$\mathbb{E}[x_d(t+1)] \leq \sum_{h=1}^{T_1} |a^{h-1}|/2^{\mathcal{R}(h)} \tag{3.84}$$

$$\mathbb{E}[x_q(t+1)] \leq \sum_{h=T_1+1}^{\infty} |a^{h-1}|/2^{\mathcal{R}(h)}. \tag{3.85}$$

Therefore, the control policy (3.81) achieves the equality of (6.2).

Chapter 4

SYSTEM SPEED-ACCURACY TRADEOFFS (SATS): ACHIEVABLE PERFORMANCE AND OPTIMAL CONTROLLERS

In the design of cyber-physical systems, it is essential to account for a broad range of uncertainties such as disturbances due to environmental changes and control errors due to delays and quantizations in feedback loops. Two approaches are typically used to handle uncertainties: deterministic or stochastic. In the deterministic approach, uncertain input or parameters are assumed to be in an uncertainty set, and the design goal is to optimize the worst-case performance over the uncertainty set. In the stochastic approach, uncertain input or parameter is assumed to have a certain distribution, and the design goal is to optimize the average performance. It is obvious that the applicability of each approach depends on the characterization of uncertainty. However, it is not clear which approach incurs less complexity in time and space (i.e., memory). In this chapter, we investigate some of the related issues in controller design for linear systems with delay and quantization.

Specifically, we consider a linear dynamical system with delay and rate constrained communications between the observer and the controller; see Fig. 4.1 for a schematic. Previous work [138, 140] takes the deterministic approach of ℓ_∞ control, *i.e.* to design an optimal controller that minimizes the worst-case infinity-norm of the system output under infinity-norm bounded disturbances. The resulting controller uses static memoryless quantizers and therefore has low time and space complexity. However, the efficacy of this approach partly depends on how "tight" the uncertainty set is in covering all possible disturbances, and the assumption of bounded uncertainty set will necessarily leave out large disturbance that may occasionally occur.

In contrast, this chapter, we take a stochastic approach that can better handle (occasional) large disturbances and study the linear-quadratic (LQ) control problem with costs (i.e., performance) in both the state and the control action. Building upon controller design methods for the quantized system [12], we design a controller for the delayed and quantized system. We further derive a lower bound on the optimal performance and compare the performance of the proposed LQ controller against

it. The comparison shows that the LQ controller can reject large disturbance while achieving near-optimal performance. However, the LQ controller needs to store the whole distribution of the system state, which incurs a much higher time and space complexity than the optimal ℓ_∞ controller.

The above optimal/near-optimal controllers based on the two approaches have different advantages and limitations regarding robustness to uncertainty and complexity in time and space. An interesting question that arises from these differences is if it is possible to design a controller that has the advantages of both the above controllers. In this chapter, we take a hybrid approach to create such a controller. Specifically, we assume that the *typical* disturbance is relatively small and covered by a bounded set, while the large disturbance (outside of the bounded set) is *rare* event that has a (tail) Gaussian distribution. Under this assumption, we construct a hybrid controller that interpolates between the ℓ_∞ controller and the LQ controller. Using both theoretical bounds and numerical examples, we show that the hybrid controller can achieve a sweet spot in the robustness-complexity tradeoff, *i.e.* reject occasional large disturbance while operating with low complexity most of the time.

Related work

There is a large literature on the topics studied in this chapter. Here we briefly review only those that are directly relevant. Applications of the model studied in this chapter range from cyber-physical systems [5, 9, 54, 138, 168, 209] to neuroscience [140] and cell biology [108, 141, 194]. Motivated by these applications, there exists a large literature on control under communication constraints, based on either the deterministic approach or the stochastic approach. For the former, stability conditions are known for a broad class of linear systems with quantization or data rate constraints [136, 203], and optimal controllers for systems with delay and quantization are given in [138, 140]. For the latter, stability conditions are known for linear systems with quantization or data rate constraints [137, 189, 207], and performance bounds are given in [13, 31, 58, 63, 65, 93, 174, 175, 188, 190, 208]. The relation between the optimal cost and the causal rate-distortion function is studied in [25, 32, 45, 72, 93, 159]. The information-theoretic quantities used to model communication constraints include mutual information [39, 190], anytime capacity [163], and directed information [124, 188], among others. The optimal controllers are studied for quantized systems [12]. In contrast, in this chapter, we study optimal controller design for delayed and quantized systems, and further, we take a hybrid deterministic-stochastic approach.

4.1 System model

Consider a feedback dynamical system with delay and rate constrained communications between the observer and the controller. The plant follows the discrete-time dynamics:

$$x_{t+1} = Ax_t + u_t + w_t, \tag{4.1}$$

where $x_t \in \mathbb{R}$ is the state, $w_t \in \mathbb{R}$ is the disturbance, and $u_t \in \mathbb{R}$ is the control action at time t. Without loss of generality, assume the initial condition $x_0 = 0$ and $w_t = 0$ for $t < 0$.

The communication channel between the observer and the controller is characterized by delay d and bandwidth R, with $R > \log_2 |A|$ to ensure stability [137]. Associated with the observer is an encoder that at time t is defined by a mapping E_t from the available information $\mathcal{I}_t = \{\{x_\tau\}_{\tau=0,\dots,t}, \{w_\tau\}_{\tau=0,\dots,t-1}\}$ to a proper codeword s_t, *i.e.*

$$s_t = E_t(\mathcal{I}_t) \in S, \tag{4.2}$$

where the set S of codewords has cardinality of at most 2^R. Associated with the controller is an decoder that at time t recovers the information on state and disturbance upon the received (delayed) information $\mathcal{J}_{t-d} = \{s_\tau\}_{\tau=0,\dots,t-d}$, based on which the controller will decide the control action u_t. The encoder and controller can be jointly defined by a mapping D_t:

$$u_t = D_t(\mathcal{J}_{t-d}) \in \mathbb{R}. \tag{4.3}$$

We may loosely refer to D_t as decoder, controller or decoder-encoder, whichever is more convenient in the relevant context.

Let $K := \{(E_0, D_0), (E_1, D_1), \cdots, (E_t, D_t), \cdots\}$, which we also broadly call the controller, and denote by $\mathcal{K}(R, d)$ the space of such controllers with delay d and bandwidth R. The design goal for the controller is to achieve a good performance (small state deviation under disturbance) with small control effort (small actuation, small computation time, and low memory usage), which can be quantified in terms of $\|x\|$, $\|u\|$ for certain norm $\|\cdot\|$ and by the functional form of (E_t, D_t).

4.2 The ℓ_∞ controller

In this section, we summarize the existing robust control theory for the ℓ_∞ system with delay and quantization [138, 140], where the design objective is to minimize

$\max_w \|x\|_\infty$. For disturbance with bounded support $\|w\|_\infty \leq L$ and stabilizing bandwidth $R > \log_2 |A|$, the optimal performance is given by:

$$\max_{\|w\|_\infty \leq L} \|x\|_\infty = \left\{ \sum_{i=0}^{d} |A^i| + \frac{|A^{d+1}|}{(2^R - |A|)^{-1}} \right\} L. \tag{4.4}$$

Let $\Psi(L) := \left\{ |A^{d+2}|(2^R - |A|)^{-1} + |A^{d+1}| \right\} L$. The optimal performance is achieved by the ℓ_∞ controller as shown in Algorithm 1. In Algorithm 1, $Q_\ell : \mathbb{R} \to S_R$ denotes a uniform quantizer of rate R (i.e., with 2^R levels) over the interval $[-\ell, \ell]$, and $|S_R| = 2^R$.

Algorithm 1 The ℓ_∞ controller.

Encoder:
$$q_t = Q^{-1}_{\Psi(L)}(s_{t-d-1}) - u^*_{t-1}$$
$$z_t = A^d w_{t-d-1} + q_t$$
$$u^*_t = -A z_t$$
$$s_{t-d} = Q_{\Psi(L)}(u^*_t)$$

Decoder:
$$u_t = Q^{-1}_{\Psi(L)}(s_{t-d})$$

The advantage of this controller is that it requires little computation and storage: the encoder only needs to store the last codeword and perform minimum computation, and the decoder is static and memoryless. In addition, this controller requires minimum actuation effort when $|A| \geq 1$: the stabilizing control law that minimizes $\max_{\|w\|_\infty \leq 1} \|u\|_\infty$ is identical to the above control law, which minimizes $\max_{\|w\|_\infty \leq 1} \|x\|_\infty$. However, the low complexity of the ℓ_∞ controller does not come for free. For a disturbance with unbounded support, the fixed quantizer in Algorithm 1 is not stabilizing because there is always a nonzero probability that the quantizer saturates. In next section, we will consider the LQ controller that can better handle large disturbance.

4.3 The linear quadratic controller

In this section, we study the robust control problem for the linear quadratic (LQ) system with delay and quantization. The disturbance w_t, $t \geq 0$ is assumed to be *i.i.d.* Gaussian with zero mean and variance σ^2, i.e., $w_t \overset{i.i.d.}{\sim} \mathcal{N}(0, \sigma^2)$ for $t \geq 0$. The control objective is to minimize an average cost subject to the plant dynamics

(4.1):[1]

$$\underset{K\in\mathcal{K}(R,d)}{\text{minimize}} \quad \lim_{t\to\infty} \mathbb{E}[x_t' P x_t + u_t' Q u_t], \tag{4.5}$$

where $P \geq 0$ and $Q \geq 0$ balance the cost of state deviation and control action. The following result gives a lower bound on the theoretically opimal LQ cost.

Theorem 4.3.1. *The optimal performance of the robust control problem (4.5) is bounded below as follows:*

$$\begin{aligned} &\lim_{t\to\infty} \mathbb{E}[x_t' P x_t + u_t' Q u_t] \\ &\geq P \sum_{i=0}^{d-1} A^{2i}\sigma^2 + P^\star A^{2d}\sigma^2 + G^\star A^{2d} \frac{\sigma^2}{2^{2R} - A^2}, \end{aligned} \tag{4.6}$$

where $P^\star$ and $G^\star$ are the unique solution to the equations:

$$\begin{aligned} P^\star &= A' \left[P^\star + P - P^\star (Q + P^\star)^{-1} P^\star \right] A, \\ G^\star &= A' P^\star A + P - P^\star. \end{aligned} \tag{4.7}$$

The first and second terms in the lower bound (4.6), $P \sum_{i=0}^{d-1} A^{2i}\sigma^2 + P^\star A^{2d}\sigma^2$, are due to delay in control action, while the third term $G^\star A^{2d} \frac{\sigma^2}{2^{2R}-A^2}$ is mainly due to limited data rate. The lower bound is derived using the following lemma, which characterizes the structure of the optimal controller to (4.5) and holds generally for multiple-input-multiple-output (MIMO) systems.

We first describe a result that will be used later.

Lemma 4.3.1 ([93, 190])**.** *Consider a scalar Gauss-Markov sequence $\{y_t\}$ satisfying*

$$y_{t+1} = A y_t + v_t, \quad y_0 = 0, \tag{4.8}$$

where $A \in \mathbb{R}$, $y_t \in \mathbb{R}$, and $v_t \overset{i.i.d.}{\sim} \mathcal{N}(0, \sigma^2)$. Assume that at each time t, only $R(> \log_2 |A|)$ bits of information about y^t can be transmitted to $s_t \in S$, where $|S| = 2^R$ and s_t is a function of (y^t, s^{t-1}). Let $\hat{y}_t$ be an estimate of y_t using only the information of s^t. Then, the following inequality holds:

$$\lim_{t\to\infty} \frac{1}{N} \mathbb{E}\left[\sum_{t=1}^{N} (y_t - \hat{y}_t)^2 \right] \geq \frac{\sigma^2}{2^{2R} - A^2}. \tag{4.9}$$

[1] In this section, we consider the scalar system (4.1), except for Lemma 4.3.2 which is for the vector system (4.27). But notice that we treat a scalar as a vector or matrix (of dimension one) in many equations.

With Lemmas 4.3.2 and 4.3.1, we are ready to prove Theorem 4.3.1.

Proof. (Theorem 4.3.1) By (4.39),

$$\lim_{t\to\infty} \mathbb{E}[x_t' P x_t + u_t' Q u_t] \tag{4.10}$$

$$= \lim_{N\to\infty} \frac{1}{N}\, \mathbb{E}\left[x_N' P x_N + \sum_{t=0}^{N-1} x_t' P x_t + u_t' Q u_t \right] \tag{4.11}$$

$$= \lim_{N\to\infty} \frac{1}{N} \mathbb{E}[J_1] \tag{4.12}$$

$$= \lim_{N\to\infty} \frac{1}{N} \mathbb{E}[J_d(s^0)] \tag{4.13}$$

$$= \lim_{N\to\infty} \frac{1}{N} \mathbb{E}\left[\mathbb{E}\left[\hat{z}_d P_d \hat{z}_d | s^0 \right] + \alpha_d(s^0) \right] \tag{4.14}$$

$$= \lim_{N\to\infty} \frac{1}{N} \mathbb{E}\left[\alpha_d(s^0) \right]. \tag{4.15}$$

With a slight abuse of notation, we use J_1 without the conditioning of the sequence s_t because it is purely determined from the initial condition.

Next we observe that $\mathbb{E}[\alpha_t]$ satisfies the relation

$$\mathbb{E}[\alpha_k(s^{k-d})] \tag{4.16}$$

$$= \mathbb{E}[\mathbb{E}[\alpha_{k+1}(s^{k-d+1}) + e_k' P e_k + w_{k-d}'(A^d)' P_{k+1} A^d w_{k-d} \tag{4.17}$$

$$+ \tilde{z}_k'(A' P_{k+1} A + P)\tilde{z}_k' - \tilde{z}_{k+1}' P_{k+1} \tilde{z}_{k+1} | s^{k-d}]] \tag{4.18}$$

$$= \mathbb{E}[\alpha_{k+1}(s^{k-d+1})] + \mathbb{E}[e_k' P e_k + w_{k-d}'(A^d)' P_{k+1} A^d w_{k-d} \tag{4.19}$$

$$+ \tilde{z}_k'(A' P_{k+1} A + P)\tilde{z}_k' - \tilde{z}_{k+1}' P_{k+1} \tilde{z}_{k+1}] \tag{4.20}$$

$$= \mathbb{E}[\alpha_N(s^{N-d})] + \sum_{\tau=k}^{N-1} \mathbb{E}[e_\tau' P e_\tau + w_{\tau-d}'(A^d)' P_{\tau+1} A^d w_{\tau-d} \tag{4.21}$$

$$+ \tilde{z}_\tau'(A' P_{\tau+1} A + P)\tilde{z}_\tau' - \tilde{z}_{\tau+1}' P_{\tau+1} \tilde{z}_{\tau+1}]. \tag{4.22}$$

Because the system is controllable, the Riccati difference (4.7) has a unique solution $P^\star$, and $\lim_{N\to\infty} P_k = P^\star$. Therefore, we have

$$\lim_{N\to\infty} \frac{1}{N} \sum_{\tau=d}^{N-1} \mathbb{E}[w_{\tau-d}'(A^d)' P_{\tau+1} A^d w_{\tau-d}] = P^\star A^{2d} \sigma^2 \tag{4.23}$$

and

$$\lim_{N\to\infty} \frac{1}{N} \sum_{\tau=d}^{N-1} \mathbb{E}[\tilde{z}_t'(A' P_{k+1} A + P - P_{k+1})\tilde{z}_t] \tag{4.24}$$

$$= \lim_{N\to\infty} \frac{1}{N} \sum_{t=1}^{N-1} \mathbb{E}[\tilde{z}_t'(A' P^\star A + P - P^\star)\tilde{z}_t]. \tag{4.25}$$

Combining (4.16)–(4.22) and (4.23)–(4.25), we obtain that

$$\begin{aligned}
&\lim_{N\to\infty}\frac{1}{N}\mathbb{E}[\alpha_d(s^0)]\\
&= P(1+A^2+A^4+\cdots+A^{2(d-1)})\sigma^2 + P^\star A^{2d}\sigma^2\\
&\quad+\lim_{N\to\infty}\frac{1}{N}\sum_{t=1}^{N-1}\mathbb{E}[\tilde{z}_t'(A'P_{k+1}A+P-P_{k+1})\tilde{z}_t]\\
&= P\sum_{i=0}^{d-1}A^{2i}\sigma^2 + P^\star A^{2d}\sigma^2\\
&\quad+\lim_{N\to\infty}\frac{1}{N}\sum_{t=1}^{N-1}\mathbb{E}[\tilde{z}_t'(A'P^\star A+P-P^\star)\tilde{z}_t].
\end{aligned}$$

When $x_t \in \mathbb{R}$, from Lemma 4.3.1, the second term is lower bounded by

$$\mathbb{E}[(\bar{z}_t - \mathbb{E}[\bar{z}_t|\bar{s}^{t-d}])'G^\star(\bar{z}_t - \mathbb{E}[\bar{z}_t|\bar{s}^{t-d}])] \geq G^\star A^{2d}\frac{\sigma^2}{2^{2R}-A^2}. \tag{4.26}$$

Therefore, we have obtained (4.28). □

Lemma 4.3.2. *Consider a MIMO system*

$$x_{t+1} = Ax_t + Bu_t + w_t \tag{4.27}$$

with $x_t \in \mathbb{R}^m$, $u_t \in \mathbb{R}^n$, $w_t \in \mathbb{R}^m$ and $w_t \overset{i.i.d}{\sim} \mathcal{N}(0,\Sigma)$ with covariance matrix $\Sigma \geq 0$, and the corresponding robust control problem

$$\min_{K\in\mathcal{K}(R,d)}\lim_{N\to\infty}\ \mathbb{E}\left[x_N'Px_N + \sum_{t=0}^{N-1}\left(x_t'Px_t + u_t'Qu_t\right)\right] \tag{4.28}$$

with $P \geq 0$, $Q \geq 0$. Given any encoding scheme $\{E_t\}$, the optimal decoder-controller D_t has the following structure:

$$u_t = L_t\ \mathbb{E}[z_t|s^{t-d}], \tag{4.29}$$

where z_t is defined by the recursion

$$z_{t+1} = Az_t + A^d w_{t-d} + B_t u_t, \quad z_0 = 0, \tag{4.30}$$

and

$$L_t = -(Q + B'P_{t+1}B)^{-1}B'P_{t+1}A, \tag{4.31}$$

with P_t defined by the recursion

$$\begin{aligned}
&P_N = P,\\
&P_t = A'\left[P_{t+1} + P - P_{t+1}B(Q+B'P_{t+1}B)^{-1}B'P_{t+1}\right]A.
\end{aligned} \tag{4.32}$$

Next, we present the steps to prove Lemma 4.3.2. Define

$$e_t = w_{t-1} + Aw_{t-2} + \cdots + A^{d-1}w_{t-d}, \tag{4.33}$$

$$z_t = x_t - e_t, \tag{4.34}$$

where e_t captures the component in the state x_t that results from the disturbance w_{t-d}^{t-1} and cannot be mitigated due to the delay in control, while z_t depends on the information of w_0^{t-d-1} and the control action in response to it. Obviously, z_t and e_t are *independent*. Moreover, $\mathbb{E}[e_t] = 0$, and z_t satisfies (4.30), restated below:

$$z_{t+1} = Az_t + A^d w_{t-d} + Bu_t, \quad z_0 = 0.$$

In order to decompose the effects of control action and disturbance, we define $\bar{z}_t$ to be the state z_t that would be generated at time t when the system (4.27) has zero control $u_t \equiv 0$. Setting $u_t = 0$ in the above equation, we obtain

$$\bar{z}_{t+1} = A\bar{z}_t + A^d w_{t-d}, \quad \bar{z}_0 = 0. \tag{4.35}$$

Recall that $\{s_t\}$ is the codewords generated by $\{z_t\}$. We introduce an auxiliary encoder

$$f(\bar{s}_{t-d}|\bar{z}^t, \bar{s}^{t-d-1}) = f(s_{t-d}|\bar{z}^t, s^{t-d-1}) \tag{4.36}$$

to generate another sequence of codewords $\{\bar{s}_t\}$.

Lemma 4.3.3. *The following relation holds:*

$$z_t - \mathbb{E}[z_t|s^{t-d}] = \bar{z}_t - \mathbb{E}[\bar{z}_t|\bar{s}^{t-d}].$$

Proof. (Lemma 4.3.3) We first use mathematical induction to show

$$f(s^{t-d}, \bar{z}^t) = f(\bar{s}^{t-d}, \bar{z}^t). \tag{4.37}$$

Obviously, (4.37) holds at $t = 0$. If (4.37) holds until t, then (4.37) also holds for $t + 1$ because

$$\begin{aligned}
&f(\bar{s}^{t-d+1}, \bar{z}^{t+1}) \\
=&f(\bar{s}^{t-d}, \bar{z}^t) f(\bar{z}_{t+1}|\bar{s}^{t-d}, \bar{z}^t) f(\bar{s}_{t-d+1}|\bar{s}^{t-d}, \bar{z}^{t+1}) \\
=&f(s^{t-d}, \bar{z}^t) f(\bar{z}_{t+1}|s^{t-d}, \bar{z}^t) f(s_{t-d+1}|s^{t-d}, \bar{z}^{t+1}) \\
=&f(s^{t-d+1}, \bar{z}^{t+1}),
\end{aligned}$$

where the second equality is due to construction (4.36), the induction hypothesis (4.37), and the fact that $f(\bar{z}_{t+1}|\bar{s}^{t-d}, \bar{z}^t) = f(\bar{z}_{t+1}|\bar{z}^t) = f(\bar{z}_{t+1}|s^{t-d}, \bar{z}^t)$. By (4.37), we obtain

$$\begin{aligned}\mathbb{E}[z_t|s^{t-d}] &= \mathbb{E}[\bar{z}_t + \sum_{k=1}^{t} A^{k-1}Bu_{t-k}|s^{t-d}] \\ &= \mathbb{E}[\bar{z}_t|s^{t-d}] + \sum_{k=1}^{t} A^{k-1}Bu_{t-k} \\ &= \mathbb{E}[\bar{z}_t|\bar{s}^{t-d}] + \sum_{k=1}^{t} A^{k-1}Bu_{t-k},\end{aligned}$$

and thus

$$\begin{aligned}&z_t - \mathbb{E}[z_t|s^{t-d}] \\ =&\bar{z}_t + \sum_{k=1}^{t} A^{k-1}Bu_{t-k} - \left(\mathbb{E}[\bar{z}_t|\bar{s}^{t-d}] + \sum_{k=1}^{t} A^{k-1}Bu_{t-k}\right) \\ =&\bar{z}_t - \mathbb{E}[\bar{z}_t|\bar{s}^{t-d}].\end{aligned}$$

□

Lemma 4.3.3 implies that we can negate all the effect of the control action to obtain $\bar{z}_t$. Intuitively, this is because u_0^t is generated from s^{t-d}. This separation allows us to prove Lemma 4.3.2.

Proof. (Lemma 4.3.2) Consider the cost-to-go:

$$J_t(s^{t-d}) = \mathbb{E}\left[x_N' P x_N + \sum_{\tau=t}^{N-1} x_\tau' P x_\tau + u_\tau' Q u_\tau \Big| s^{t-d}\right] \tag{4.38}$$

for any $k < N$ and $J_N = \mathbb{E}[x_N' P x_N]$. We use mathematical induction to show the following properties:

(i) The optimal cost-to-go satisfies

$$J_t(s^{t-d}) = \mathbb{E}\left[\hat{z}_t' P_t \hat{z}_t | s^{t-d}\right] + \alpha_t(s^{t-d}), \tag{4.39}$$

where $\hat{z}_t = \mathbb{E}[z_t|s^{t-d}]$ and $\alpha_t(s^{t-d})$ is a function of s^{t-d} whose expected value does not depend on the choice of control action, *i.e.*

$$\mathbb{E}\left[\alpha_t(s^{t-d})\right] = \mathbb{E}\left[\alpha_t(\bar{s}^{t-d})\right]. \tag{4.40}$$

(ii) The optimal controller admits the form (4.29).

At $t = N$, the cost-to-go satisfies

$$\begin{aligned} J_N &= \mathbb{E}[x_N' P x_N | s^{N-d}] \\ &= \mathbb{E}[(\hat{z}_N + \tilde{z}_N + e_N)' P (\hat{z}_N + \tilde{z}_N + e_N) | s^{N-d}] \\ &= \mathbb{E}[\hat{z}_N' P \hat{z}_N | s^{N-d}] + \mathbb{E}[\tilde{z}_N' P \tilde{z}_N | s^{N-d}] + \mathbb{E}[e_N' P e_N], \end{aligned}$$

where $\tilde{z}_t := z_t - \hat{z}_t$, and the last equality holds because e_N, $\hat{z}_N$ and $\tilde{z}_N$ are uncorrelated and e_N is independent of s^{N-d}. By Lemma 4.3.3, $\mathbb{E}[\tilde{z}_N' P \tilde{z}_N | s^{N-d}]$ does not depend on the choice of control action. Letting $\alpha_N = \mathbb{E}[\tilde{z}_N' P \tilde{z}_N | s^{N-d}] + \mathbb{E}[e_N' P_N e_N]$ yields (4.39) for $t = N$.

Assume now that (4.39) holds for $t = k + 1$. The optimal cost-to-go at time $t = k$ can be derived as follows:

$$\begin{aligned} & J_k(s^{k-d}) \\ & = \min_{u_k} \mathbb{E}[x_k' P x_k + u_k' Q u_k + J_{k+1} | s^{k-d}] \qquad (4.41) \\ & = \min_{u_k} \mathbb{E}[x_k' P x_k + u_k' Q u_k \\ & \qquad + \mathbb{E}\left[\hat{z}_{k+1}' P_{k+1} \hat{z}_{k+1} | s^{k-d+1}\right] + \alpha_{k+1} | s^{k-d}] \\ & = \min_{u_k} \mathbb{E}[\hat{z}_k' (P + A' P_{k+1} A) \hat{z}_k + u_k' (Q + B' P_{k+1} B) u_k \\ & \qquad + u_k' B' P_{k+1} A \hat{z}_k + \hat{z}_k' A' P_{k+1} B u_k | s^{k-d}] \qquad (4.42) \\ & \qquad + \mathbb{E}[e_k' P e_k + \hat{w}_k' P_{k+1} \hat{w}_k + \tilde{z}_k' P \tilde{z}_k | s^{k-d}] \\ & \qquad + \mathbb{E}[\alpha_{k+1}(s^{k-d+1}) | s^{k-d}], \end{aligned}$$

where $\hat{w}_k = \mathbb{E}[A^d w_{k-d} + A \tilde{z}_k | s^{k-d+1}]$, and by induction hypothesis the second equality holds. By Lemma 4.3.3 and induction hypothesis, $e_k' P e_k + \hat{w}_k' P_{k+1} \hat{w}_k + \tilde{z}_k' P \tilde{z}_k$ does not depend on the control action u_t. Therefore, we can just consider minimizing the first term (4.42). The control action that minimizes this term is given by (4.29), *i.e.*

$$u_k = -(Q + B' P_{k+1} B)^{-1} B' P_{k+1} A \, \hat{z}_k, \qquad (4.43)$$

where

$$P_k = A' \left[P_{k+1} + P - P_{k+1} B (Q + B' P_{k+1} B)^{-1} B' P_{k+1} \right] A.$$

Substituting this control action u_k into J_k, we obtain the optimal cost-to-go

$$J_k(s^{k-d}) = \mathbb{E}\left[\hat{z}_k' P_k \hat{z}_k | s^{k-d}\right] + \alpha_k(s^{k-d}) \qquad (4.44)$$

with

$$\begin{aligned}\alpha_k(s^{k-d}) &= \mathbb{E}[e_k' P e_k + \hat{w}_k' P_{k+1} \hat{w}_k + \tilde{z}_k' P \tilde{z}_k + \alpha_{k+1} | s^{k-d}] \\ &= \mathbb{E}[e_k' P e_k + \tilde{z}_t' A' P_{k+1} A \tilde{z}_t + w_{t-d}' (A^d)' P_{k+1} A^d w_{t-d} \\ &\quad - \tilde{z}_{t+1}' P_{k+1} \tilde{z}_{t+1} + \tilde{z}_k' P \tilde{z}_k + \alpha_{k+1}(s^{k-d+1}) | s^{k-d}], \end{aligned} \tag{4.45}$$

where the second equality is obtained as follows. Given s^{k-d}, the random variable $\hat{w}_k$ is the estimate of $A^d w_{k-d} + A\tilde{z}_k$ given s_{k-d+1}, and the random variable $\tilde{z}_{k+1}$ is the resulting estimation error, *i.e.*

$$\hat{w}_k + \tilde{z}_{k+1}' = A^d w_{k-d} + A\tilde{z}_k. \tag{4.46}$$

Therefore, the weighted covariance of the estimation target equals the sum of the weighted estimation error covariance and the weighted estimation covariance

$$\begin{aligned}&\mathbb{E}[(A^d w_{k-d} + A\tilde{z}_k)' P_{k+1} (A^d w_{k-d} + A\tilde{z}_k) | s^{k-d}] \\ &= \mathbb{E}[\tilde{z}_{k+1}' \tilde{z}_{k+1} | s^{k-d}] + \mathbb{E}[\hat{w}_k' P_{k+1} \hat{w}_k | s^{k-d}].\end{aligned}$$

Combining above with

$$\begin{aligned}&\mathbb{E}[(A^d w_{k-d} + A\tilde{z}_k)' P_{k+1} (A^d w_{k-d} + A\tilde{z}_k) | s^{k-d}] \\ &= \mathbb{E}[\tilde{z}_t' A' P_{k+1} A \tilde{z}_t + w_{k-d}' (A^d)' P_{k+1} A^d w_{k-d} | s^{k-d}]\end{aligned}$$

yields (4.45). By Lemma 4.3.3 and the induction hypothesis $\mathbb{E}[\alpha_{k+1} | s^{k-d}] = \mathbb{E}[\alpha_{k+1} | \bar{s}^{k-d}]$, α_k does not depend on the choice of control action. So, (4.39) holds for $t = k$. □

From the proof of lemma, we can observe that, given any encoder, the optimal decoder are essentially the optimal LQ controller for the sequence $\hat{z}_t$, which evolves according to the dynamics

$$\hat{z}_{t+1} = A\hat{z}_t + Bu_t + \hat{w}_t. \tag{4.47}$$

In other words, the optimal decoder are the certainty equivalent controller for the sequence z_t, the estimation target of $\hat{z}_t$. When there is no delay in the control action, *i.e.* $d = 0$, then this optimal decoder reduces to the certainty equivalent controller for x_t, as is given by [190].

Notice that Lemma 4.3.2 does not specify what an optimal encoder is. Also, seen from the proof of Theorem 4.3.1, the first two terms in the lower bound (4.6) of the optimal performance are tight for any delay d if the decoder-controller has the structure (4.29).

Remark 4.3.1 (Certainty equivalence)**.** *The definition of certainty equivalence and its extension to quantized systems are given in [13, 190]. The optimal controller structure in Lemma 4.3.2 is an extension of certainty equivalence to systems with delay and quantization. The auxiliary sequence* $\{z_t\}$ *and Lemma 4.3.2 together allow us to bound the objective value by studying an estimation problem of a Gauss-Markov source and an LQ control problem of a fully observed system. The sequence* $\{z_t\}$ *also plays an important role in Section 4.4.*

Based on the optimal decoder-controller structure characterized in Lemma 4.3.2, we propose a controller, referred to as *the LQ controller*, in Algorithm 2. The encoder and decoder in Algorithm 2 use an adaptive quantizer generated by the Lloyd algorithm [12, 51, 116] and estimate z_t using recursive Bayesian estimation. The encoder computes the prior density function[2]

$$\begin{aligned} f(z_t|s^{t-d-1}) &= \int_{-\infty}^{\infty} f(z_t, z_{t-1}|s^{t-d-1}) dz_{t-1} \\ &= \int_{-\infty}^{\infty} f(z_t|z_{t-1}, s^{t-d-1}) f(z_{t-1}|s^{t-d-1}) dz_{t-1}, \end{aligned} \tag{4.48}$$

where $f(z_t|z_{t-1}, s^{t-d-1})$ can be computed by

$$\begin{aligned} f(z_t|z_{t-1}, s^{t-d-1}) &= f(z_t|z_{t-1}) \\ &= f(Az_{t-1} + A^d w_{t-d-1} + u_{t-1}|z_{t-1}). \end{aligned}$$

Then, $f(z_t|s^{t-d-1})$ is used to run the Lloyd algorithm [12, 51, 116] to find a quantizer Q_t that maps z_t to s_t. Given the received codeword s_{t-d} at the decoder, the update process computes the posterior density function

$$\begin{aligned} f(z_t|s^{t-d}) &= \frac{f(z_t, s_{t-d}|s^{t-d-1})}{f(s_{t-d}|s^{t-d-1})} \\ &= \frac{f(z_t|s^{t-d-1}) f(s_{t-d}|z_t, s^{t-d-1})}{f(s_{t-d}|s^{t-d-1})} \\ &\propto f(z_t|s^{t-d-1}) f(s_{t-d}|z_t, s^{t-d-1}), \end{aligned} \tag{4.49}$$

where $f(z_t|s^{t-d-1})$ is the prior density function computed in (4.48), and $f(s_{t-d}|z_t, s^{t-d-1})$ is determined by the quantizer Q_t. Finally, $f(z_t|s^{t-d})$ is used to generate an estimate of z_t as follows:

$$\hat{z}_t \quad = \quad \mathbb{E}[z_t|s^{t-d}] = \int_{-\infty}^{\infty} z_t f(z_t|s^{t-d}) dz_t. \tag{4.50}$$

Algorithm 2 The LQ controller

Initialize:

1. Compute $f(z_d|s^0) = \mathcal{N}(0, \sigma^2)$.
2. Set $z_d = 0, u_0 = 0$.

Encoder: At time t, the encoder performs the following procedures:

1. Update the auxiliary variable (4.30).
2. Generate the prior density function by (4.48).
3. Run the Lloyd algorithm to obtain Q_t.
4. Send the codeword $s_t = Q_t(z_t)$ to the decoder.
5. Generate the posterior density function by (4.49).

Decoder: At time t, the decoder receives the codeword s_{t-d} that was generated d sampling intervals before, and performs the following procedures:

1. Compute the prior density function by (4.48).
2. Run the Lloyd algorithm to recover Q_t.
3. Use the delayed codeword s_{t-d} to generate the posterior density function by (4.49).
4. Calculate the estimate $\hat{z}_t$ of z_t by (4.50).
5. Compute the control action:

$$u_t = -(Q + P^*)^{-1} P^* A\, \hat{z}_t. \tag{4.51}$$

The proposed LQ controller may not be optimal, but can be shown to achieve near optimal performance by comparing with the lower bound (4.6) of the optimal performance. As mentioned in the above, the first two terms of the lower bound are tight for any delay d if the decoder-controller has the structure (4.29), which is the case for the LQ controller. Thus, the performance gap to the lower bound reduces mostly to the difference between the achievable $(z_t - \hat{z}_t)G^*(z_t - \hat{z}_t)$ and the lower bound of $\mathbb{E}[(z_t - \hat{z}_t)G^*(z_t - \hat{z}_t)]$.

[2] With a slight abuse of notation, we use $f(x|y)$ to denote both the probability density function of a random variable x conditioned on another random variable y and the function that is computed by the controller to approximate the actual density function.

Compared with the the ℓ_∞ controller that can only handle bounded disturbance, the Gaussian distribution has infinite support, *i.e.* the LQ controller can handle large disturbance. However, the LQ controller is demanding in both computation and memory, due to the use of an adaptive quantizer that is necessary for stabilizing an unstable system if the disturbance has an infinite support [136].

4.4 A hybrid controller

We have seen from the previous sections that the ℓ_∞ controller has low time and space complexity but can only handle bounded disturbance, while the LQ controller can reject arbitrarily large disturbance but incurs much higher time and space complexity. An interesting question that arises from these differences is if it is possible to design a controller that has the advantages of both controllers. In this section, we take a hybrid approach to design such a controller.

Specifically, we assume that the *typical* disturbance is relatively small and covered by a bounded set, while the large disturbance (outside of the bounded set) is a *rare* event that has a (tail) Gaussian distribution. Under this assumption, we construct a hybrid controller that interpolates between the ℓ_∞ controller and the LQ controller. Using both theoretical bounds and numerical simulations, we show that the hybrid controller can achieve a sweet spot in the robustnes-complexity tradeoff, *i.e.* reject occasional large disturbance while operate with low complexity most of the time.

We consider the setting when the LQ cost function has no control cost, *i.e.* $Q = 0$ in (4.5). This condition yields the optimal LQ controller

$$u_t = -A\hat{z}_t \tag{4.52}$$

to replace (4.51) in Algorithm 2. This simplification allows the ℓ_∞ and LQ controllers to be considered in an unified framework.

The proposed hybrid controller has two modes: *normal mode* that runs the ℓ_∞ controller (Algorithm 1) and *acute mode* that runs the LQ controller (Algorithm 2). We now explain the switching policy between the ℓ_∞ and LQ controllers using a bridging variable z_t and a design parameter L. Notice that the sequences $\{z_t\}$ in the ℓ_∞ and LQ controllers have identical role (storing the sum of the quantization error from past control action and the scaled disturbance $A^d w_{t-d-1}$), and thus can serve as a bridging variable to connect the two controllers. Re-define the sequence $\{q_t\}$ as

$$q_{t+1} = Aq_t + u_t + A^{d+1} w_{t-d-1} \tag{4.53}$$

with $w_t = 0$ for $t < 0$. The definition (4.53) does not rely on the particular realization of the controller, so q_t is well-defined in both Algorithms 1 and 2. Using q_t, z_t can be written as

$$z_t = A^d w_{t-d-1} + q_t \tag{4.54}$$

with the $z_t = 0$ for $t \leq d$. Thus, z_t in Algorithm 2 satisfies

$$\begin{aligned} z_{t+1} &= Az_t + A^d w_{t-d} + u_t \\ &= A^d w_{t-d} + Aq_t + u_t + A^{d+1} w_{t-d-1} \\ &= A^d w_{t-d} + q_{t+1}, \end{aligned} \tag{4.55}$$

where the first equality follows form (4.30), the second equality from (4.54), and the third equality from (4.53). Therefore, z_t takes the same value in both Algorithms 1 and 2. The proposed controller sets a threshold on the absolute value of z_t to determine whether the ℓ_∞ controller or the LQ controller should be used.

Let the design parameter $L \in \mathbb{R}$ be the size of the disturbance up to which the controller stays in normal mode, *i.e.* normal mode when $\|w\|_\infty \leq L$. Since $\|w_0^{t-d-1}\|_\infty \leq L$ implies $|z_t| \leq \Psi(L)/A$, equivalently $|z_t| > \Psi(L)/A$ implies $|w_\tau| \geq L$ for some $\tau \leq t - d - 1$. Thus, the condition

$$|z_t| > \Psi(L)/A \tag{4.56}$$

is a sufficient condition for $\|w_0^{t-d-1}\|_\infty > L$. We use this sufficient condition to define the switching policy as follows:

$$mode = \begin{cases} `normal' & |z_t| \leq \Psi(L)/A, \\ `acute' & |z_t| > \Psi(L)/A. \end{cases} \tag{4.57}$$

The proposed hybrid controller is described in Algorithm 3.

The design parameter L impacts the system performance and controller complexity, and there exists a tradeoff between the two. We will next discuss its choice and the resulting performance and complexity tradeoff.

4.5 Performance analysis of the proposed hybrid controller

In this section, we analyze the behavior of the hybrid controller using the switching time from normal to acute mode and the recovery time from acute to normal mode.

Algorithm 3 The hybrid controller

Initialize: $mode \leftarrow$ '$normal$'
$\Psi(L) \leftarrow \{|A^{d+2}|(2^R - |A|)^{-1} + |A^{d+1}|\}L$
for $t \in \mathbb{N}$ **do**
  if mode = 'acute' **then**
    Perform the LQ controller (Algorithm 2)
    if $|z_t| \leq \Psi(L)/A$ **then**
      $mode \leftarrow$ '$normal$'
    end if
  else if mode = 'normal' **then**
    Perform the ℓ_∞ controller (Algorithm 1)
    if $|z_t| > \Psi(L)/A$ **then**
      $mode \leftarrow$ '$acute$'
    end if
  end if
end for

We denote the set of times at which the controller switches from normal to acute mode as

$$\mathcal{T}_s = \{t \in \mathbb{N} : |z_t| > \Psi(L)/A \ \ \& \ \ |z_{t-1}| \leq \Psi(L)/A\},$$

and the set of time at which the controller switches from acute to normal mode as

$$\mathcal{T}_r = \{t \in \mathbb{N} : |z_t| \leq \Psi(L)/A \ \ \& \ \ |z_{t-1}| > \Psi(L)/A\}.$$

Let $t_r \in \{0\} \cup \mathcal{T}_r$ be the beginning of a normal mode, the switching time T_s is defined as

$$LT_s(t_r) = \min\{t > t_r : |z_t| > \Psi(L)/A\} - t_r. \tag{4.58}$$

Let $t_s \in \mathcal{T}_s$ be the beginning of an acute mode, the recovery time T_r is similarly defined as

$$LT_r(t_s) = \min\{t > t_s : |z_t| \leq \Psi(L)/A\} - t_s. \tag{4.59}$$

Long switching time and short recovery time imply that the controller stays in normal mode most of the time, and thus requires less computation and memory. Therefore, the controller complexity can be roughly characterized by the time of operating in acute mode.

Let a random variable w be drawn from the same distribution with the disturbance w_t, *i.e.* $w, w_t \overset{i.i.d.}{\sim} \mathcal{N}(0, \sigma)$. The following result characterizes the relation between the design parameter L and the expected switching time $\mathbb{E}[T_s(t_r)]$.

Theorem 4.5.1. *Define a mappng* $\hat{T}_s : \mathbb{R} \to \mathbb{R}_+$

$$\hat{T}_s(t_r) = \begin{cases} d + \mathbb{P}(|w| > L)^{-1} & t_r = 0, \\ \mathbb{P}(|w| > L)^{-1} & t_r \in \mathcal{T}_r. \end{cases}$$

The expected switching time $T_s(t_r)$ *is lower bounded by*

$$\mathbb{E}[T_s(t_r)] \geq \hat{T}_s(t_r), \tag{4.60}$$

and the lower bound becomes tight as the bandwidth $R \to \infty$.

The proof of Theorem 4.5.1 uses the concept of *majorization* to approximate the switching time by *geometric distribution*. Theorem 4.5.1 suggests that the expected switching time can be approximated by $\mathbb{E}[T_s(t_r)] \approx \hat{T}_s(t_r)$.

Proof. (Theorem 4.5.1) We first prove the lower bound for $\tau = 0$. Let $\{E_k\}$ be the event that the controller switches at time k, *i.e.*

$$\mathbb{R}E_k = \{|z_t| \leq \Psi(L)/A \text{ for all } t < k \text{ and } |z_k| > \Psi(L)/A\}. \tag{4.61}$$

Notice that $\{E_k\}$ a sequence of a mutually exclusive set of events, and that $\mathbb{P}(E_k) = 0$ for $k \leq d$ (since $z_t = 0$ for $t \leq d$ by definition). Let $\{F_k\}$ be the event that the disturbance first exceeds L in amplitude at time k, *i.e.*

$$F_k = \{|w_t| \leq L \text{ for all } t < k \text{ and } |w_k| > L\}. \tag{4.62}$$

The sequence $\{E_k\}$ is a mutually exclusive set of events, and $\lim_{\tau\to\infty} \sum_{i=0}^{\tau} \mathbb{P}(E_i) = 1$. Same holds for $\{F_k\}$, *i.e.* $\lim_{\tau\to\infty} \sum_{i=0}^{\tau} \mathbb{P}(F_i) = 1$. From $\cup_{i\geq k} E_i \subset \cup_{i\geq k} F_i$, we obtain

$$\sum_{i=k-d-1}^{\infty} \mathbb{P}(F_i) \leq \sum_{i=k}^{\infty} \mathbb{P}(E_i) \tag{4.63}$$

for any $k \in \mathbb{N}$. Using (4.63), the expected switching time can be bounded below by

$$\begin{aligned}
\mathbb{E}[T_s(\tau)] &= \sum_{k=0}^{\infty} k\ \mathbb{P}(E_k) \\
&= \sum_{k=0}^{\infty} k\ \mathbb{P}(E_k) - \sum_{k=0}^{\infty} k\ \mathbb{P}(E_{k+d}) + \sum_{k=0}^{\infty} k\ \mathbb{P}(E_{k+d}) \\
&= d + \sum_{k=0}^{\infty} k\ \mathbb{P}(E_{k+d}) \\
&= d + \sum_{k=1}^{\infty} \sum_{i=k}^{\infty}\ \mathbb{P}(E_{i+d}) \\
&\geq d + \sum_{k=1}^{\infty} \sum_{i=k}^{\infty}\ \mathbb{P}(F_{i-1}) \\
&= d + \sum_{k=1}^{\infty} k\ \mathbb{P}(F_{k-1}) \\
&= d + \sum_{k=1}^{\infty} k\ \left(1 - \mathbb{P}(|w| > L)\right)^{k-1} \mathbb{P}(|w| > L) \\
&= d + \mathbb{P}(|w| > L)^{-1},
\end{aligned}$$

where the last equality can be interpreted as computing the mean of a geometric distribution with failure probability $\mathbb{P}(|w| > L)$.

Next, notice that $|z_t| \leq \Psi(L)/A$ and $|w_{t-d}| \leq L$ implies $|z_{t+1}| \leq \Psi(L)/A$. Thus, we can apply the argument in $\tau = 0$ to obtain the lower bound for $\tau \in \mathcal{T}$:

$$\mathbb{E}[T_s(\tau)] \leq \mathbb{P}(|w| > L)^{-1}.$$

Next, we prove the convergence for $\tau = 0$, *i.e.* $\mathbb{E}[T_s(0)] \overset{R\to\infty}{\to} d + \mathbb{P}(|w| > L)^{-1}$. Since $d + \sum_{k=1}^{\infty} \sum_{i=k}^{\infty} \mathbb{P}(E_{i+d}) \geq d + \sum_{k=1}^{\infty} \sum_{i=k}^{\infty}\ \mathbb{P}(F_{i-1})$ is the only inequality from the above analysis, it is suffice to show that $\left|\sum_{k=1}^{\infty} \sum_{i=k}^{\infty}\ \mathbb{P}(E_{i+d}) - \sum_{k=1}^{\infty} \sum_{i=k}^{\infty}\ \mathbb{P}(F_{i-1})\right| \to 0$. By $\|q\|_\infty \overset{R\to\infty}{\to} 0$ and $z_t \to A^d w_{t-d-1}$, $\mathbb{P}(F_{t-d-1}) \to \mathbb{P}(E_t)$. This implies that

$$\begin{aligned}
&\left| \sum_{i=k-1}^{\infty} \mathbb{P}(F_{i-1}) - \sum_{i=k}^{\infty} \mathbb{P}(E_{i+d}) \right| \\
&= \left| \left(1 - \sum_{i=0}^{k-2} \mathbb{P}(F_i)\right) - \left(1 - \sum_{i=0}^{k-1} \mathbb{P}(E_{i+d})\right) \right| \\
&\to 0 \text{ as } R \to \infty
\end{aligned}$$

holds for any $k \in \mathbb{N}$. Since both $\sum_{k=1}^{\infty}\sum_{i=k}^{\infty}\mathbb{P}(E_{i+d})$ and $\sum_{k=1}^{\infty}\sum_{i=k}^{\infty}\mathbb{P}(F_{i-1})$ are bounded, for any $\epsilon > 0$ there exits a sufficiently large T such that $\tau > T$ implies

$$\sum_{k=\tau}^{\infty}\sum_{i=k}^{\infty}\mathbb{P}(E_{i+d}) \leq \epsilon/4 \quad \text{and} \quad \sum_{k=\tau}^{\infty}\sum_{i=k}^{\infty}\mathbb{P}(F_{i-1}) \leq \epsilon/4,$$

and sufficiently large $\bar{R}$ such that $R > \bar{R}$ implies

$$\sum_{k=1}^{\tau}\sum_{i=k}^{\infty}\mathbb{P}(E_{i+d}) \leq \epsilon/4 \quad \text{and} \quad \sum_{k=1}^{\tau}\sum_{i=k}^{\infty}\mathbb{P}(F_{i-1}) \leq \epsilon/4,$$

which jointly yields

$$\left|\sum_{k=1}^{\infty}\sum_{i=k}^{\infty}\mathbb{P}(E_{i+d}) - \sum_{k=1}^{\infty}\sum_{i=k}^{\infty}\mathbb{P}(F_{i-1})\right| \leq \epsilon. \tag{4.64}$$

The case for $\tau \in \mathcal{T}$ follows the same argument and is omitted here. □

Similarly, the expected recovery time $T_r(\cdot)$ can be approximated by

$$\mathbb{E}[T_r(\cdot)] \approx \hat{T}_r = \mathbb{P}(|w| \leq L)^{-1}. \tag{4.65}$$

Recall from (4.55) that the evolution of z_t follows $z_{t+1} = A^d w_{t-d} + q_{t+1}$ where q_{t+1} is a function of z_t. Assuming the quantizer (defined from the encoder and decoder) is near-optimal, a large z_{t_s} at the beginning of the an acute mode is approximately reduced by rate $|A|2^{-R}$ per unit time and by $|A^\tau|2^{-\tau R}$ after τ times. Thus, for sufficiently large $|A|2^{-R}$, the term $A^d w_{t-d}$ in (4.55) dominates. In this situation, observing a small disturbance, *i.e.* $|w_{t-d}| \leq L$, is enough to lessen the value of z_t below $\Psi(L)/A$. This explains why the recovery time can be approximated by a geometric distribution with success probability $\mathbb{P}(|w_t| \leq L)$.

Fig. 4.1 shows a comparison between the empirical value of the expected switching time $T_s(0)$ and the theoretical approximation $\hat{T}_s(0)$ and between the empirical value of the expected recovery time $T_r(\cdot)$ and the theoretical approximation $\hat{T}_r$. We see that the approximation becomes tight when the bandwidth R is large enough.

4.6 Tradeoffs between performance versus complexity

We now take a look at the performance of the proposed controllers (Algorithms 1-3) under the mixed disturbance:

$$w_t = v_t + r_t \tag{4.66}$$

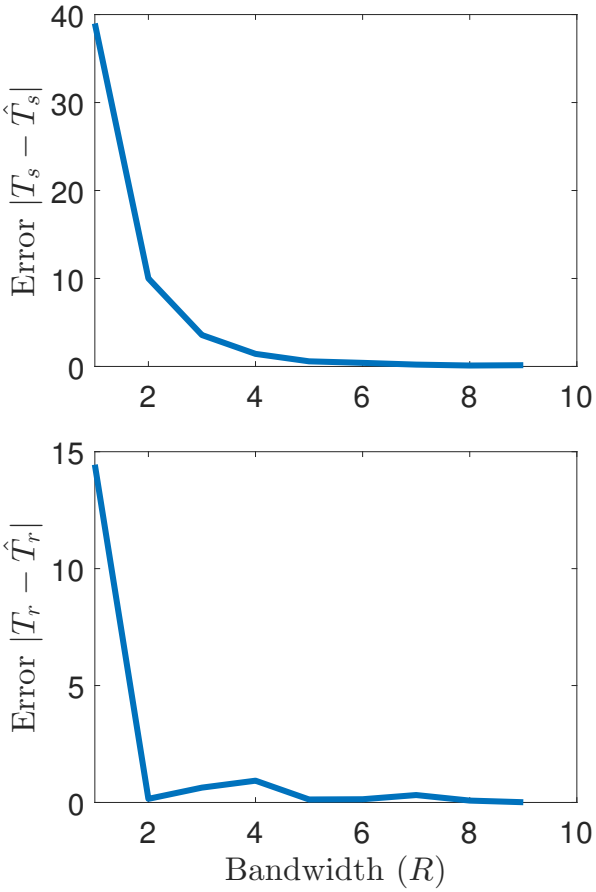

Figure 4.1: The accuracy of the theoretical approximations (4.60) of the switching time and (4.65) of the recovery time for a system with $A = 1$ and $d = 1$. The empirical values of T_s and T_r are first generated by averaging 100 trials for different values of $L \in [0.1, 2]$ and $R \in \{1, 2, \cdots, 9\}$. Then, the approximation errors $|T_s - \hat{T}_s|$ and $|T_r - \hat{T}_r|$ are averaged over all L, and their mean values are plotted for different values of R.

with $v_t \overset{i.i.d.}{\sim} \mathcal{N}(0, \sigma_v^2)$ and $\|r\|_\infty \leq 1$. We use this type of structured disturbance to model the common situation where the system experiences bounded disturbance most of the time and large disturbance occasionally (*i.e.* with small probability).

For a feedback system with perfect communications, the optimal ℓ_∞ controller and LQ controller for the scalar system (4.1) are identical when the control cost is not considered. However, with communication constraints, the optimal ℓ_∞ controller and LQ controller are radically different, and the mixed disturbance poses significant challenge in encoding/decoding strategies as the system state can be defined neither in a worst-case framework nor in a stochastic framework.

The ℓ_∞ controller cannot stabilize such systems because there is a non-zero prob-

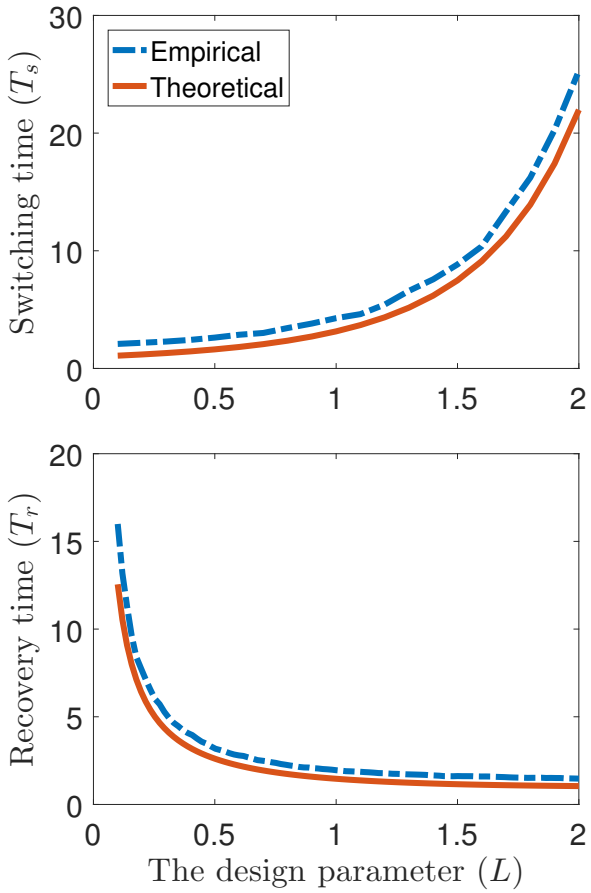

Figure 4.2: The switching and recovery times as a function of L for a system with $A = 1$, $d = 1$, and $R = 6$. The averages over 100 trials are plotted for the empirical values.

ability for the fixed quantizer to saturate. The performance of the LQ controller and the proposed hybrid controller is compared in Fig. 4.4. The LQ controller has degraded performance when there exists an additional disturbance r that cannot be well-defined using probability density function. However, the proposed hybrid controller consistently achieves robust performance under such disturbance. By exploiting the additional dimension in the controller design space, the right integration of stochastic (LQ) and worst-case (ℓ_∞) enables a robust controller under communication constraints.

The above theoretical approximations suggest that, for sufficiently large bandwidth ($|A|2^{-R} \ll 1$), a greater L implies larger switching time (from $T_s(t_r) \approx \hat{T}_s(t_r) = \mathbb{P}(|w_t| > L)^{-1}$) and smaller recovery time (from $T_r(t_s) \approx \hat{T}_r(t_s) = \mathbb{P}(|w_t| \leq L)^{-1}$). This can be empirically verified; see, e.g., Fig. 4.2. Since the switching (recovery) time is an increasing (decreasing) function of L, the complexity of the hybrid

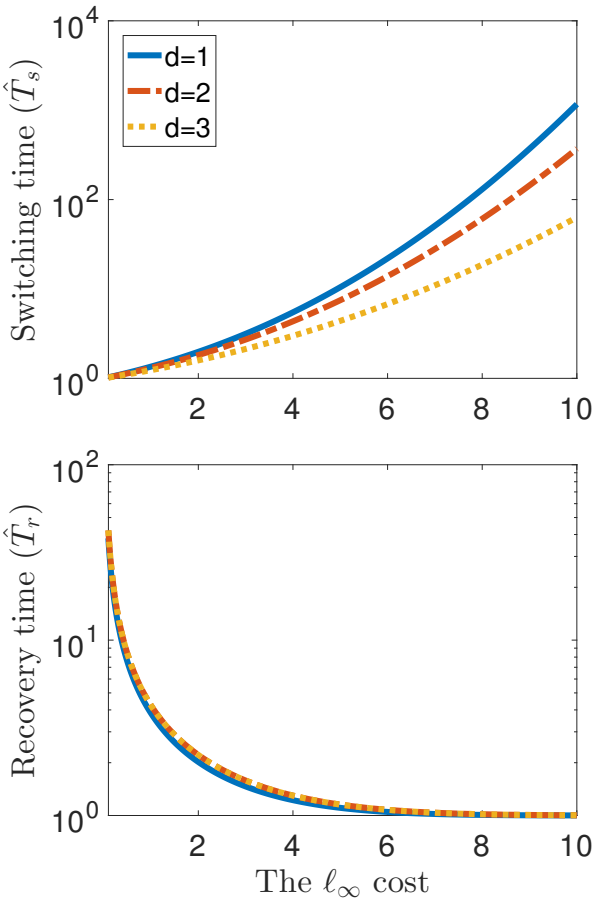

Figure 4.3: The tradeoff between complexity (as implied by the switching time and the recovery time) and performance (as represented by the worst-case ℓ_∞ cost in normal mode) for a system with $A = 1$ and $(d, R) = \{(1, 1), (2, 2), (3, 3)\}$.

controller decreases as L increases.

One the other hand, the decrease in controller complexity comes with cost of degraded performance because a larger L also implies a coarser quantizer in Algorithm 1 (and thus larger quantization error). Specifically, in normal mode,

$$|x_t| \leq \left(\sum_{i=0}^{d} |A^i| + |A^{d+1}|(2^R - |A|)^{-1} \right) L. \tag{4.67}$$

So, the worst-case ℓ_∞ cost in normal model is an increasing function of L, and a smaller L leads to better performance. This tradeoff between performance and complexity is as shown in Fig. 4.3. It is noteworthy that a significant increase (decrease) in switching (recovery) time can be achieved with small performance degradation (notice that the vertical axes are in log-scale).

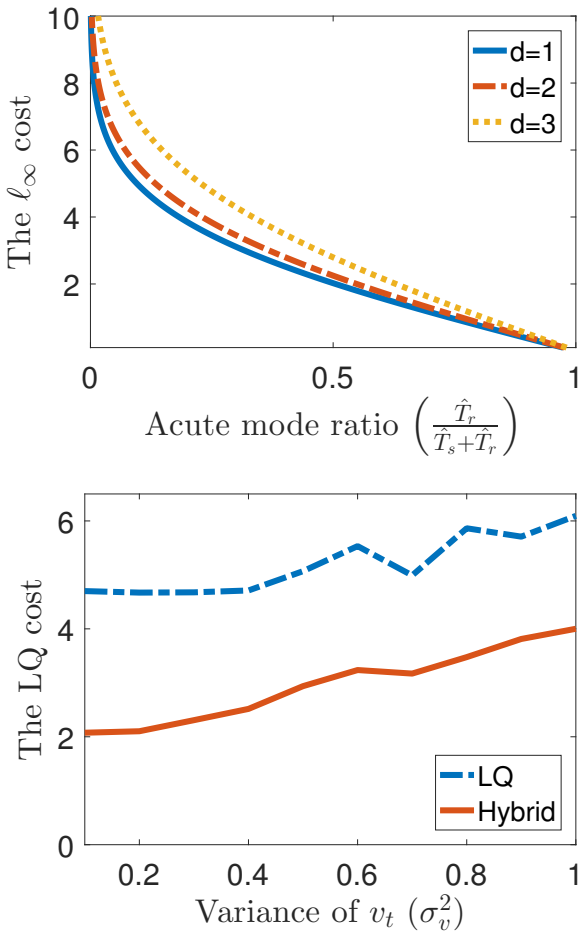

Figure 4.4: Performance of the hybrid controller. The figure on the top shows the tradeoff between the normal mode performance (in the ℓ_∞ cost) and the approximated acute mode ratio $\hat{T}_s/(\hat{T}_r + \hat{T}_s)$ for a system with $A = 1$ and $(d, R) = \{(1, 1), (2, 2), (3, 3)\}$. The figure on the bottom shows the performance (in the LQ cost) for a system with $A = 1$, $d = 1$, $R = 3$ and under the mixed disturbance with different variances σ_v^2. The averaged LQ costs for 100 trials are plotted.

In summary, we have considered robust control design for linear systems with delayed and rate constrained communications between the observer and the controller. We first take a stochastic approach and propose an LQ controller that can handle arbitrarily large disturbance but has large complexity in time and space. This is different from the ℓ_∞ control (a deterministic approach) that previous work have shown to have low time/space complexity but can only handle bounded disturbance. The differences in robustness and complexity of the LQ and ℓ_∞ controllers motivate the design of a hybrid controller that interpolates between the ℓ_∞ and LQ controllers. Using both theoretical bounds and numerical examples, we show that the hybrid

controller can achieve a sweet spot in the robustness-complexity tradeoff, *i.e.* reject occasional large disturbance while operating with low complexity most of the time.

Chapter 5

CONNECTING THE COMPONENT AND SYSTEM SATS IN SENSORIMOTOR CONTROL

In this chapter, we build upon the results of Chapter 2 and Chapter 3 to study how the hardware SATs impact the system SATs for different types of sensorimotor tasks. We first consider reaching tasks in two different regimens: when nerve signaling is the bottle neck (Section 5.1), and when muscle actuation is the bottleneck (Section 5.2). Then, we study riding a mountain bike (Section 5.4) and visual tracking of a moving object (Section 5.5).

5.1 Reaching tasks with bottleneck in nerve signaling

In a reaching task, the subjects' goal is to move their hand or cursor to a target as rapidly and accurately as possible. The control loop involved in a reaching task is shown in Fig. 5.1. There exist tradeoffs between the reaching speed and accuracy, where the speed of reaching is quantified by the reaching time T_r (*i.e.* time taken to reach the target area), and the accuracy is quantified by the radius of the target W. Such tradeoffs have been extensively studied in the context of Fitts' law [60], which states that the reaching time follows

$$T_r = p + q \log_2(2D/W), \tag{5.1}$$

where D is the distance of the target, p and q are fixed constants, and

$$F = \log_2(2D/W) \tag{5.2}$$

is the Fitts' index of difficulty. It shall be noted that the logarithmic relation between D/W and T_r allows faster speed to be achieved with a small decrement in accuracy.

Next, we show how the reaching speed and accuracy is achieved despite slow or inaccurate hardware when nerve signaling is the bottleneck in control. We model this setting using the feedback control system in Section 3.3, in which the controller is assumed to have delay T and data rate R. From Section 3.3, the reaching time T_r is lower-bounded as follows:

$$\sup_{|d| \le D} T_r \ge T + F/R, \tag{5.3}$$

which recovers Fitts' law. Interestingly, the lower bound decomposes into two terms: the first term T is only a function of the total delay and thus can be considered as the delay cost; the second term F/R is only a function of the signaling rate and thus can be considered as the rate cost. Intuitively, this formula can be seen as follows: identifying a target of width W in the area $[-D, D]$ requires F bits of information, and transmitting F bits of information requires F/R time steps with additional T time steps of (transmission) delay in the feedback loop.

By combining the component-level SATs in (2.5) and the system-level SATs in (5.3), we can predict how the SATs in neural signaling impact sensorimotor control in Fig. 5.2a. Fig. 5.2 suggest that axon compositions that minimize either the signaling delay or the rate alone suffer from large delay or rate costs, rendering the system suboptimal. Conversely, the minimum reaching time is achieved when both the signaling delay and rate are chosen to be moderate levels, leading to a minimum delay plus rate costs.

From Fig. 5.2a, we observe that the signaling delay T_s affects the reaching time T_r in a linear manner, and the delay cost of T_r increases as T_s grow. On the other hand, the signaling rate R affects T_r in an inversely proportional manner, and the rate cost of T_r decreases as $T_s \propto R$ grow. Thus, T_r takes a minimum value when both the delay cost and rate cost are controlled to a moderate level. This theoretical prediction is then verified using reaching experiments. During the experiments, the subjects are asked to control a steering wheel with added delays, quantization, and both, and their reaching times for each case are shown in Fig. 5.2b (see Section 5.3 for the experimental setting).

5.2 Reaching tasks with bottleneck in muscle actuation

Formula (5.3) assumes that the SATs in nerve signaling are the bottleneck in the reaching task. Although this assumption is valid for certain eye movements or small-distance reaching, in many other types of reaching tasks, muscle actuation SATs is the major limiting factors in the reaching SATs. To understand how the muscle SATs impact the reaching SATs, we model the sensorimotor system by (3.1) with limited muscle actuation SATs. The muscle SATs is obtained from (2.34) for cases with either uniform or diverse motor units. We compare these two cases and their resulting reaching SATs in Fig. 5.3a. It can be observed that muscles of uniform motor units give rise to a linear SAT, which is not consistent with the logarithmic form of Fitts' law. On the contrary, a bundle of motor units with *diverse* sizes yields

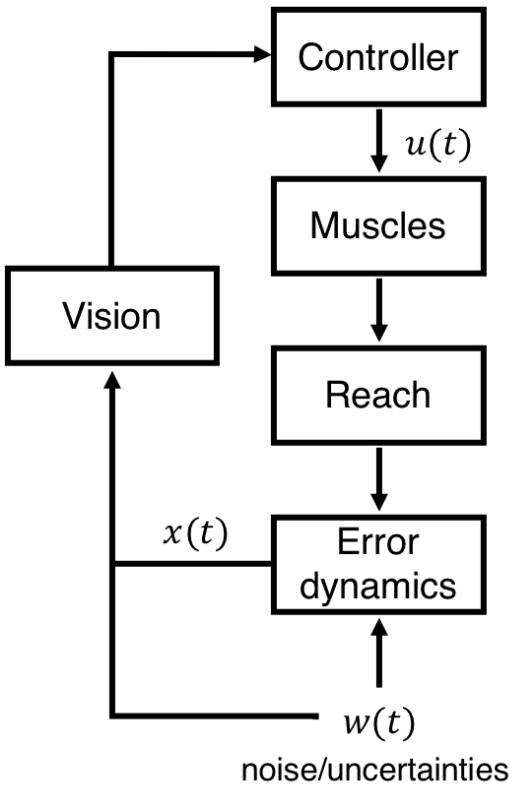

Figure 5.1: Block diagram of the sensorimotor control model that simulates the reaching task. Each box is a component in the model that communicates (vision), computes (controller), or actuates (muscles) with potentially limited speed and accuracy.

a DSS alike Fitts' formula, in which fast reaching can be performed accurately.

We confirmed the benefit of diversity using reaching experiments. In the experiments, subjects were asked to move to a target of fixed width as fast as possible under two settings: using uniform speed or diverse speeds (see Section 5.3 for the experimental setting). Fig. 5.3b compares their reaching SATs when only one level of speed was allowed versus when two levels of speed were allowed versus. The performance under diverse speed largely outperforms that under uniform speed. Moreover, a uniform speed gave rise to a linear SAT which is not consistent with the logarithmic form of Fitts' law, while the flexibility to use diverse speeds yielded a DSS like Fitts' law, in which fast reaching can be performed accurately. Although the logarithmic form of Fitts' law has been confirmed in many experiments and explained using various models (see [59, 76, 96, 120, 202] and references therein), our results reveal that Fitts' law arises from DSSs, in which the hardware diversity is key for achieving fast and accurate performance using slow or inaccurate hardware.

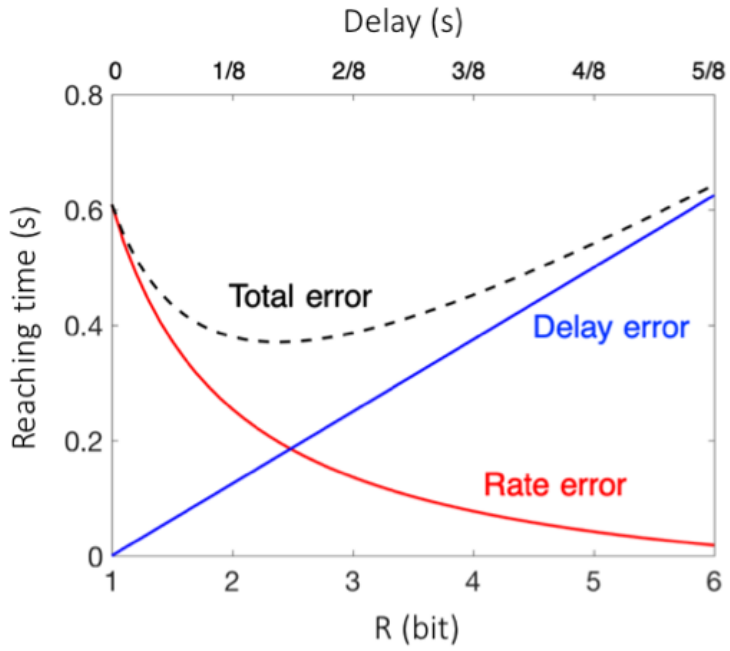

(a) Theoretical SAT in reaching. Theoretical SATs in the reaching task. The delay cost (blue line), rate cost (red line), and the total cost (dashed black line) in (5.3) are shown with varying component SAT $T = (R - 1)/8$.

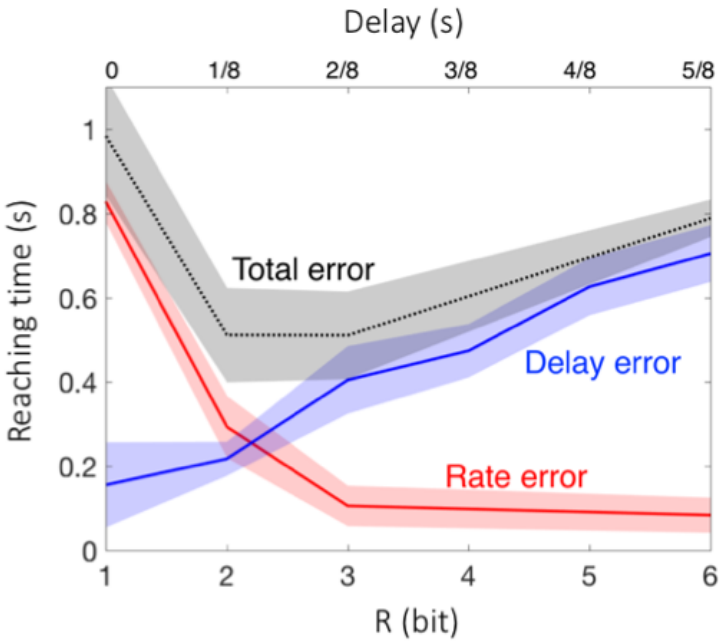

(b) Empirical SAT in reaching. Data obtained from 4 subjects who performed the task over a range of time delays and quantization rate errors ((See Fig. S1 for data from individual subjects). The blue line shows the performance with added actuation delay T; the red line shows the performance with added quantization with the rate R; and the black line shows the performance with added delay and quantization subject to the SAT $T = (R - 1)/8$. The shaded region around the lines is standard errors.

Figure 5.2: Reaching SATs imposed by nerve signaling SATs.

This relation of DSSs and logarithmic laws potentially provide new insights into other logarithmic laws observed.

5.3 Reaching experiments: materials and methods

We verified the theory using reaching task experiments (Fig. 5.4). Subjects are asked to steer a wheel to reach and stay in the gray zone (target) as quickly as possible. The target randomly appears on one side of the screen with varying center positions across trials. We externally constrained the delay and date rate of the feedback loop by manipulating the gray zone in Fig. 5.4b.

Setting for Fig. 5.2b. To test the effect of having a delay and limited data rate in the feedback loop, we conducted two types of experiments: 1) reaching with added delay, and 2) reaching with added data rate limitation. In 1) reaching with added delay, the visual display was delayed for $1, 1/8, \cdots, 5/8$ seconds. To be noted, this delay did not influence subjects motion execution, and subjects even did not notice the visual delay. In 2) reaching with added data rate limitation, we added the data rate of 1, 2, 3 and 6 bits per $T_{interval}$ ($T_{interval} = 350ms$). For example, in the setting of $R = 1$, the initial width of gray zone is $W = W_{screen}/2^1$, where W_{screen} is the width of screen ($W_{screen} = 20$ for our test). After a time interval of $T_{interval}$, a new data package arrives and the width of the gray zone reduces to $W = W_{screen}/2^2$. We repeat this procedure until $W = W_{screen}/2^6$. We tested 50 trials for each setting and measured the reaching time. The subject-specific internal delay was estimated for each subject by the minimal time to reach the target area with no external delay and with the maximum rate (mean = 1.17s, ste = 0.06). The internal delay was subtracted for the following analysis. Plots of the mean movement time from a representative subject are shown in Fig. 5.2b , and the average of all four subjects is shown in Fig. 5.5b.

Setting for Fig. 5.3b. To test the effects of diverse muscles on system performance with experiment, we considered two types of muscles: uniform muscle with a uniform actuation speed $V_0 = 2.5$, and diverse muscles realized by two actuation speeds $V_0 = 2.5$ and $V_1 = 5$. We set the target distance to be $D = 12$ and varied the target width W. The performance from both cases is compared in Fig. 5.3b.

5.4 Tracking tasks

In a driving task, the subjects' goal is to follow desired trajectory in the presence of uncertainty and noise. We define the error dynamics $x(t)$ from the system evolution of the rider or eye movement that must track a reference trail or trajectory with small

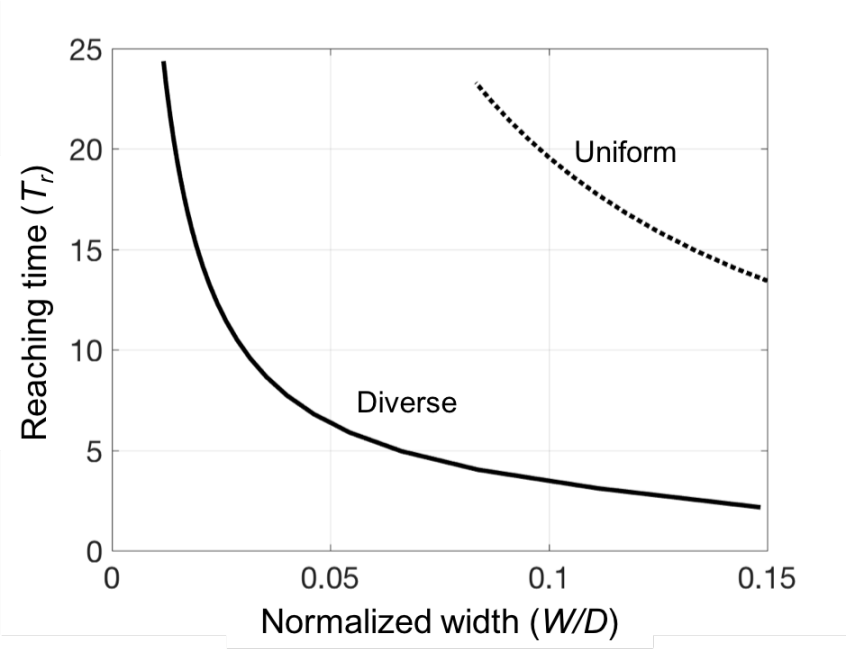

(a) Theoretical DSSs in reaching. The SAT is compared for systems implemented by a muscle with uniform or diverse motor units.

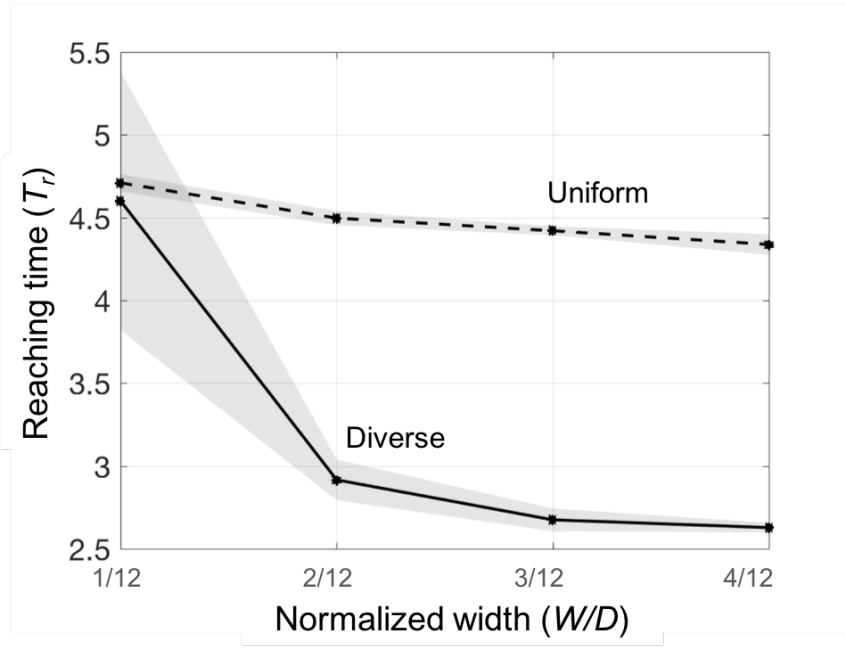

(b) Empirical DSSs in reaching. The plot shows the performance of a subject who performed the reaching task with uniform or diverse speeds, which is designed to mimic the case of uniform or diverse muscles, respectively.

Figure 5.3: Diversity Sweet Spots (DSSs) in reaching.

(a) Photo of a subject performing the reaching task.

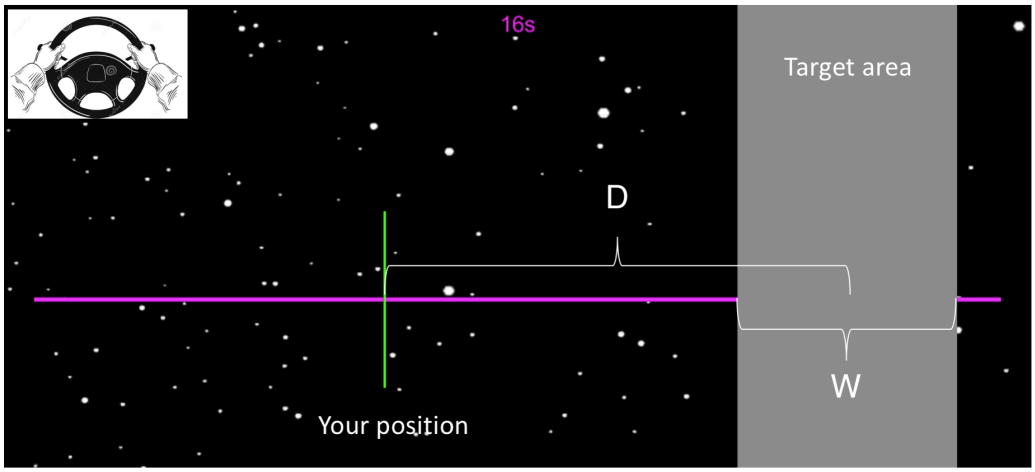

(b) Monitor display of the reaching task.

Figure 5.4: The experimental setting of the reaching task. The green line indicates the player's position and the gray zone is the desired position. The subjects' goal is to steer the wheel to reach and stay in the gray zone as fast as possible.

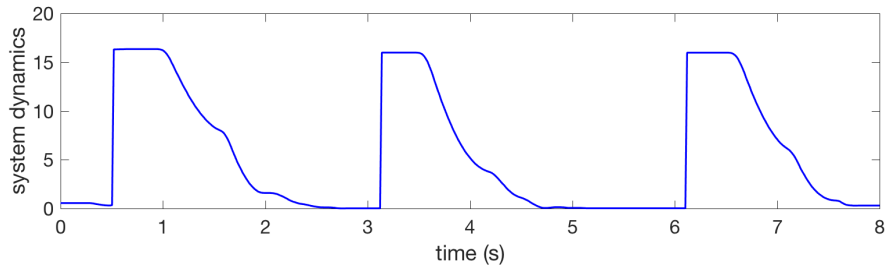

(a) An example of error dynamics measured in an experiment. The error $x(t)$ is defined as the difference between the player's position and the mid-point of the desired position.

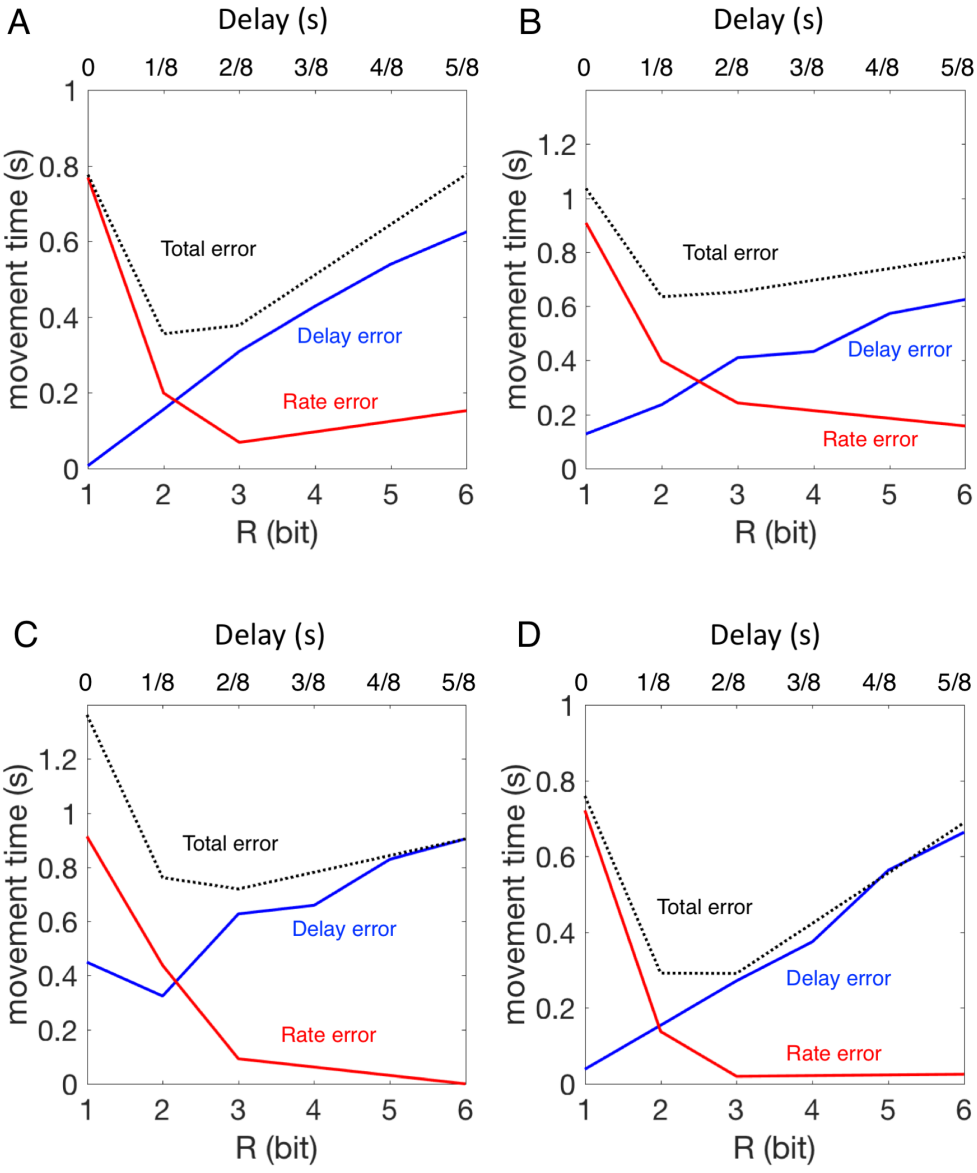

(b) Empirical SAT in the reaching task. The blue line shows the error in a delayed system with perfect communication for varying T; the red line shows the error in a quantized system with no delay but varying information rate R; and the black line shows the error in a delayed and quantized system with the component SAT $T = (R-1)/8$.

Figure 5.5: Additional experimental results

error despite unseen bumps/disturbances. We model the setting by the system in Section 3.4. The worst-case error $\max_{\|w\|_\infty \le 1} \|x\|_\infty$ is lower-bounded by

$$\max(0, T+1) + \left(2^R - 1\right)^{-1}, \tag{5.4}$$

where $T := T_s + T_i - T_a$ is the total delay from the disturbance to the control action, and R is the data rate. The worst-case framework models risk-averse sensorimotor behaviors, such as riding a mountain bike on a cliff/trail, in which staying on the cliff is necessary for survival even in the presence of the worst possible uncertainty [134, 166, 167, 201]. Alternatively, we can also consider the average-case framework, which models risk-neutral sensorimotor behaviors, such as riding a mountain bike across a broad field, in which there is no fatal risk of leaving the field [185]. In this case, the mean squared error $\lim_{n\to\infty}(1/n)\sum_{t=1}^{n}\mathbb{E}[x(t)^2]$ is lower-bounded by

$$\max(0, T+1) + \left(2^{2R} - 1\right)^{-1}. \tag{5.5}$$

The proof of (5.5) and the performance bound for a more general case of $a \neq 1$ are given in Section 4.3. The performance bounds in both settings ((5.4)–(5.5)) are qualitatively similar: both bounds decompose into two terms. The shared first term, $\max(0, T+1)$, is only a function of the total delay and thus can be considered as the cost due to delay. The second terms, $(2^R - 1)^{-1}$ and $(2^{2R} - 1)^{-1}$, are only functions of the signaling rate and can be considered as the cost due to rate limits.

By combining the component SATs in (2.5) and the system SATs in (5.4), we can predict the influence of the neural signaling constraints on sensorimotor control, shown in Fig. 5.6b. The prediction is also verified using driving game experiments (see Materials and Methods for more details). The subjects played the driving game under three different cases: with added delay, with added quantization, and with added delay and quantization. Their trajectories are measured for each case, and the errors are computed and shown in Fig. 5.6B. In both theory and experiment, increasing delay in the feedback loop rises the delay errors, while increasing rate leads to a large decrease in the rate errors. The errors for the cases of added delayed and quantization also sum up to the error in the case of added delay and quantization, as predicted by the theory. From Fig. 5.6, we see that delays can cause small disturbances to escalate into larger errors [106], and the familiar notion that bits are powerful in the context of control. Furthermore, the minimum reaching time or the minimum error is achieved when the deleterious effects of the signaling delay and inaccuracy are both controlled within a moderate range. Consequently, constrained by component SAT (2.5), the optimal axon composition is achieved

at a sweet spot of intermediate levels of signaling delay and rate. Conversely, minimizing either the signaling delay or the rate leads to suboptimal performance, suggesting the importance of studying neurophysiology and sensorimotor control from a holistic perspective.

5.5 Visual tracking of a moving object

In this section, we study the effective layered architecture of the oculomotor system. The oculomotor system has two major feedback loops: a VOR feedback loop that compensates for head motion, and a visual feedback loop through the visual cortex that tracks a moving object (Fig. 5.7). From a control perspective, an important difference of the two loops is their levels of advanced warning. VOR feedback reacts after head moves, while the visual environment is highly correlated over time and is thus predictable. We refer to the regime of VOR feedback as *delayed reaction*, in which $T_i - T_a > 0$, and the uncertainty $w(t)$ becomes accessible to the controller *after* $w(t)$ affects the error dynamics. We refer to the regime of visual feedback *advanced planning* in which $T_a - T_1 \geq 0$, and the uncertainty $w(t)$ becomes accessible to the controller *before* $w(t)$ affects the error dynamics. These two regimes are qualitatively different in their optimal choice of T_s and R for achieving optimal robust performance, as shown in Fig. 5.8 and summarized below.

(i) Delayed reaction: When the net delay $T_i - T_a > 0$ is large or the system is unstable ($|a| > 1$), the total error can be much larger than the size of the uncertainty $\|w\|_\infty$ and goes to infinity as $T_i \to \infty$. This large error amplification is consistent with the all-too-familiar observation that even a small bump on a trail can cause a cyclist to lose control of the bike and crash. As $T_i (> 0)$ increases, the delay error increasingly dominates the total error. Since the delay error largely contributes to the total error, the total error is minimized when T_s is set to be small in return for small R. Therefore, a feedback loop in this regime performs better when it is built from a few large axons. Interestingly, the flat optimal delay/rate within the delayed reaction regime suggests that optimal performance can be achieved using one type of nerve composition for a broad range of advanced warnings. This property is beneficial because the net delay (defined from advanced warning) differs across different sensorimotor tasks.

(ii) Advanced planning: When the net warning $T_a - T_s > 0$ is large, the total error approaches zero as $R \to \infty$. This large disturbance attenuation is consistent with the observation that a cyclist can avoid obstacles given enough time to plan a response,

e.g. route a path around them or brace against their impact. Given sufficiently large advanced warning T_a, the rate error increasingly dominates the total error because the growth in T_s incurs no additional delay error. Since the rate error contributes largely to the total error, the total error is minimized when the signaling rate R is set to be large at the expense of large signaling delay T_s. Therefore, a feedback loop in this regime performs better when it is built from many small axons.

This optimal nerve signaling speed or accuracy is also qualitatively consistent with the anatomy of the human oculomotor system (Fig. 2.1a). The vestibular nerve, which transmits motion information from the inner ear to the vestibular nucleus in the brainstem, has $20,000$ axons with mean diameter $3\,\mu m$ and coefficient of variation $0.4\,\mu m$. In contrast, the optic nerve carrying visual signals from the retina has approximately 1 million axons with mean diameter $0.6\,\mu m$ and coefficient of variation $0.5\,\mu m$, significantly smaller but more numerous and with greater variability [185]. As a consequence, the visual feedback is slower (approximately 100 ms delay) but more accurate than the VOR feedback (approximately 10 ms delay) [19]. This diversity in control performance can also be observed in two simple tests: moving one's hand left and right across the visual field with increasing frequency while holding the head still (Test 1); and shaking the head back and forth (in a 'no' pattern) at increasing frequency while holding the hand still (Test 2). In Test 1, the hand starts to blur at around 1-2 Hertz due to delays in tracking. In Test 2, blurring due to the inability to compensate for fast head motion occurs at a much higher frequency. This difference illustrates that the visual cortex feedback responsible for Test 1 (object tracking) has lower levels of tolerable delays than the VOR feedback responsible for Test 2 (head motion compensation). However, though slower, the visual cortex feedback is more accurate than the VOR feedback. This explains why standing on one leg with closed eyes is more difficult than with eyes open.

5.6 Riding a mountain bike to follow a trail

We simulate the task of riding a mountain bike using the driving game experiments. The control system associated with the task is shown in Fig. 5.9. Specifically, the error dynamics is given by

$$x(t+1) = ax(t) + u_L(t) + u_H(t) + w(t) + r(t - T_a), \tag{5.6}$$

where $w(t)$ captures the disturbance due to trail bumps and $r(t)$ captures the curvature of the desired trajectory. There are two major feedback loops that act to

control the error $x(t)$: a reflex feedback loop that compensates for bumps, and a planning feedback loop that determines which trajectory to follow. These feedback controllers can be written as

$$\begin{aligned} u_h(t) &= H(r(0:t-T_h+T_a), u(0:t-1)) \\ u_\ell(t) &= L(w(0:t-T_\ell-T_c), u(0:t-1)) \\ u(t) &= Q_m(Q_\ell(u_\ell(0:t)), Q_h(u_h(0:t))). \end{aligned} \tag{5.7}$$

Here H is a high-layer planner and L is a lower-layer disturbance compensator. The object position $r(t)$ is accessible to the controller with advanced warning T_a, which models the predictability of the object's motion.

The accuracy constraint of each controller is modeled by quantizers Q_ℓ/Q_h with signaling rates R_ℓ/R_h. The commands from both controllers are put into action by the cyclist's muscles, the accuracy of which is modeled by a quantizer Q_m with signaling rate R_m. Let $\bar{R}_\ell$ and $\bar{R}_h$ be defined by $\bar{T}_\ell := T_\ell + T_c$, $\bar{R}_\ell := \min(R_\ell, R_m)$, $\bar{T}_h := T_h - T_a$, and $\bar{R}_h := \min(R_h, R_m)$. In our driving task experiments where $a = 1$ with sufficiently large advanced warning T_a, the state-deviation $\sup_{\|w\|_\infty \le \epsilon, \|r\|_\infty \le 1} \|x\|_\infty$ achievable by the controller (5.7) is lower-bounded by

$$\left\{ \bar{T}_\ell + \frac{1}{2^{\bar{R}_\ell} - 1} \right\} \delta + \frac{1}{2^{R_h} - 1}. \tag{5.8}$$

Intuitively, this result follows from the decomposition of the problem described in (5.8) into two independent sub-problems, one for each of the feedback loops involving H and L. (See the Supplementary Information for a more general case of $a \neq 1$.)

To confirm the errors from each loop sum up to be the the total error, we designed three types of driving experiments: with bump only, with trail only, and with both bump and trail. The sum of errors from the bump-only and trail-only showed no significant difference when compared to that of both-bump-and-trail (paired t-test, t=0.21, p=0.83). The experimental results are shown in Fig 5.10. The results confirm that the two feedback loops can be analyzed separately.[1] These results, together with those of Fig. 5.6, validate (5.8).

The separation of (5.8) into the individual errors caused by two sub-systems allow us to analyze the optimal nerve compositions of the two feedback loops as follows. The reflex feedback typically operates in the regime of delayed reaction, as reflexes

[1] Such separation of different feedback loops is common in many processes, *e.g.* [91].

often sense bumps only after the bike has hit them. The planning feedback typically works in the regime of advanced planning, as the bike's trajectory can often be seen in advance. Similar to the case of the oculomotor system, the reflex feedback has better performance when it is designed to have a small signaling delay at the expense of a low signaling rate; in contrast, the planning feedback is constructed to have a large signaling rate at the expense of a large signaling delay [126, 161].

5.7 Driving experiments: materials and methods

We developed a driving game platform that simulates riding a mountain bike [112]. The platform is cheap to build and easy to implement. The code and manual to build our platform are distributed in `https://github.com/Doyle-Lab/WheelCon`https://github.com/Doyle-Lab/WheelCon.

In the experiments, subjects look at a PC monitor and steer a wheel to follow the desired trajectory (Fig 5.6b. The trajectory has a constant velocity for each segment but abruptly switched between right and left segments.

Setting for Fig 5.6b. The effects of delay or quantization were studied by inserting additional delay or quantizer between the wheel (control input) and the actual position (target of control). The delays were set to be $-4, -3, \cdots, 2$ sampling intervals, respectively, where each sampling interval is 16.67 ms. Here, negative delays are realized by added advance warning in vision input, while the positive delays by adding an external delay in actuation. The signaling rates of the quantizer were set to be $1, 2, ..., 7$ bits per unit time. Each set of parameters lasted for 30 seconds before switching to a new set of parameters. Within the 30 seconds, we removed the first 10 seconds from the performance measure in order to eliminate the switching and learning effects. Before each experiment, subjects were trained until their performance stabilized. Plots of the mean squared error between the road (the desired position) and the current position of the player are shown in Fig. 5.6b. Additionally, we tested SAT for the deterministic settings with the component-level SAT $T = (R - 5)/20$, shown in Fig 5.12.

Setting for Fig 5.6b. To study how the high-layer planning and the low-layer disturbance rejection combines, we studied the setting involving bump and trail changes. We studied three settings: with bump disturbance, with trail changes, and both. In last setting, we generated the bump disturbance and trail changes independently. The bumps were generated by pushing the steering wheel at a constant torque of 0.5 second. Our experimental results are shown in Fig. 5.10.

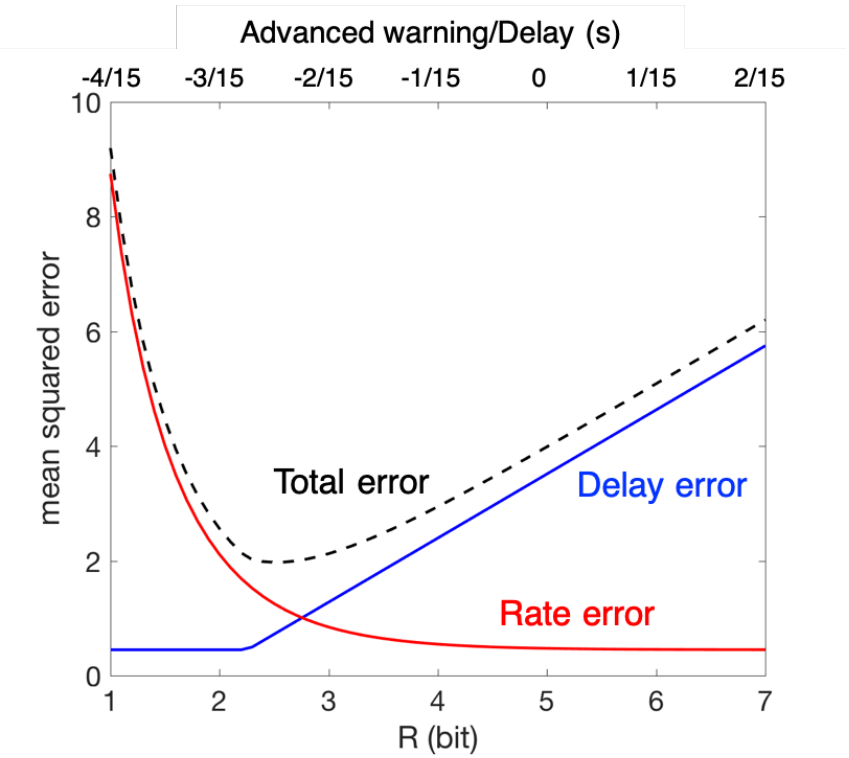

(a) Theoretical SATs in the tracking (driving) task. The delay error (blue), rate error (red), and the total error (black) in (5.5) are shown with varying component SAT $T = (R-5)/15$.

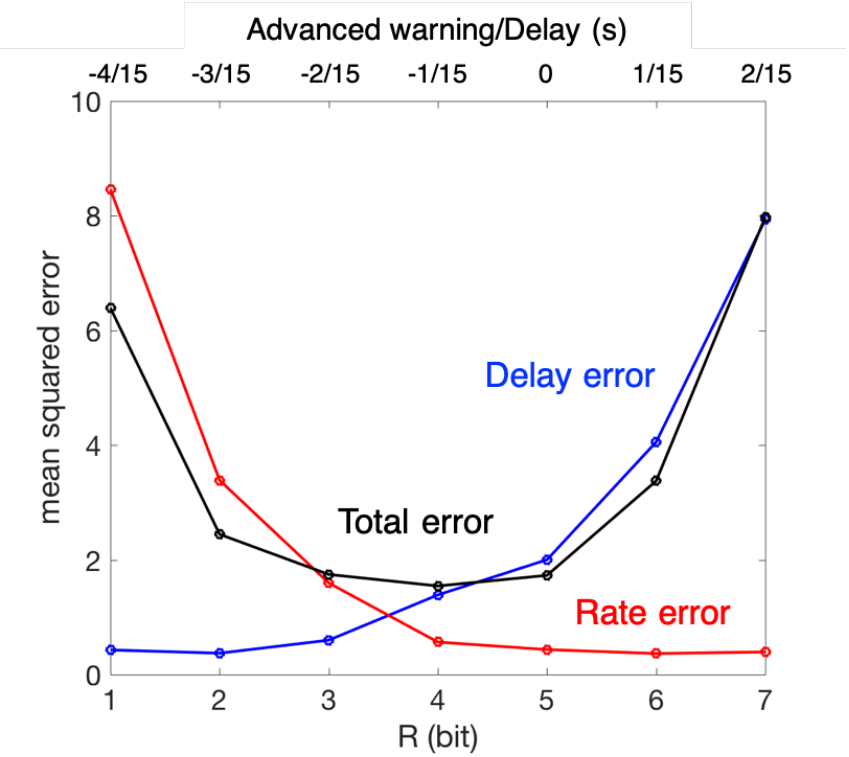

(b) Empirical SATs in the tracking (driving) task. The blue line shows the error in a delayed system with perfect communication varying only T; the red line shows the error in a quantized system with no delay but varying signaling rate R; and the black line shows the error in a delayed and quantized system with the component SAT $T = (R-5)/15$. Also see Fig. 5.12 for the deterministic setting.

Figure 5.6: System SATs in sensorimotor control

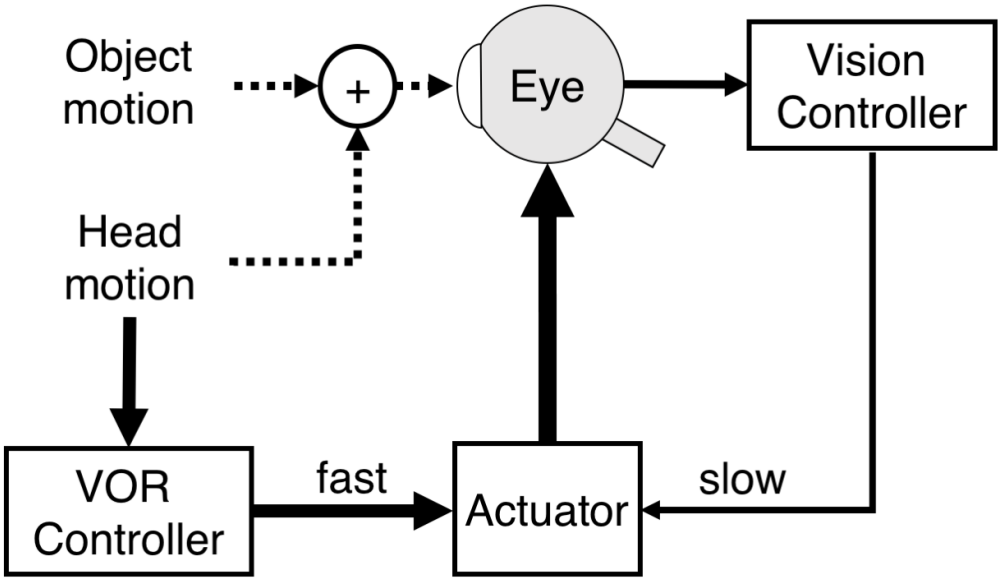

Figure 5.7: Cartoon diagram of two major feedback loops involved in the eye movement: visual cortex feedback and vestibular-ocular reflex (VOR) feedback. Objects are tracked using the slow visual cortex feedback, while head motion is compensated for by the much faster VOR feedback.

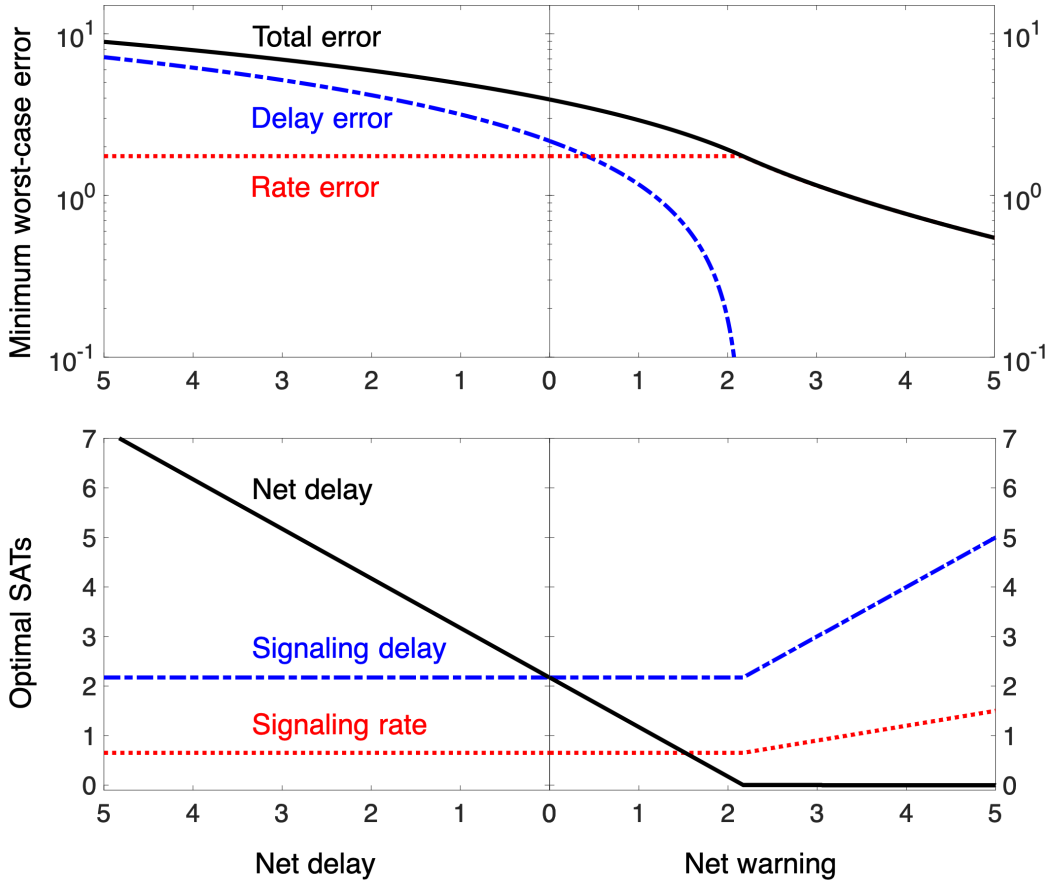

Figure 5.8: Delayed reaction vs. advanced planning. Comparison between the regime of advanced warning and that of delayed reaction. The top figure shows the minimum total error (5.4) (the delay error plus the rate error) given a fixed resource level λ. The bottom figure shows the optimal signaling delay T_s, total delay $T = T_s + T_i - T_a$, and rate $R = \lambda T_s$ for varying net delay $T_i - T_a$. In both figures, the horizontal axes denote the net delay $T_i - T_a \geq 0$ or the net warning $T_a - T_i > 0$.

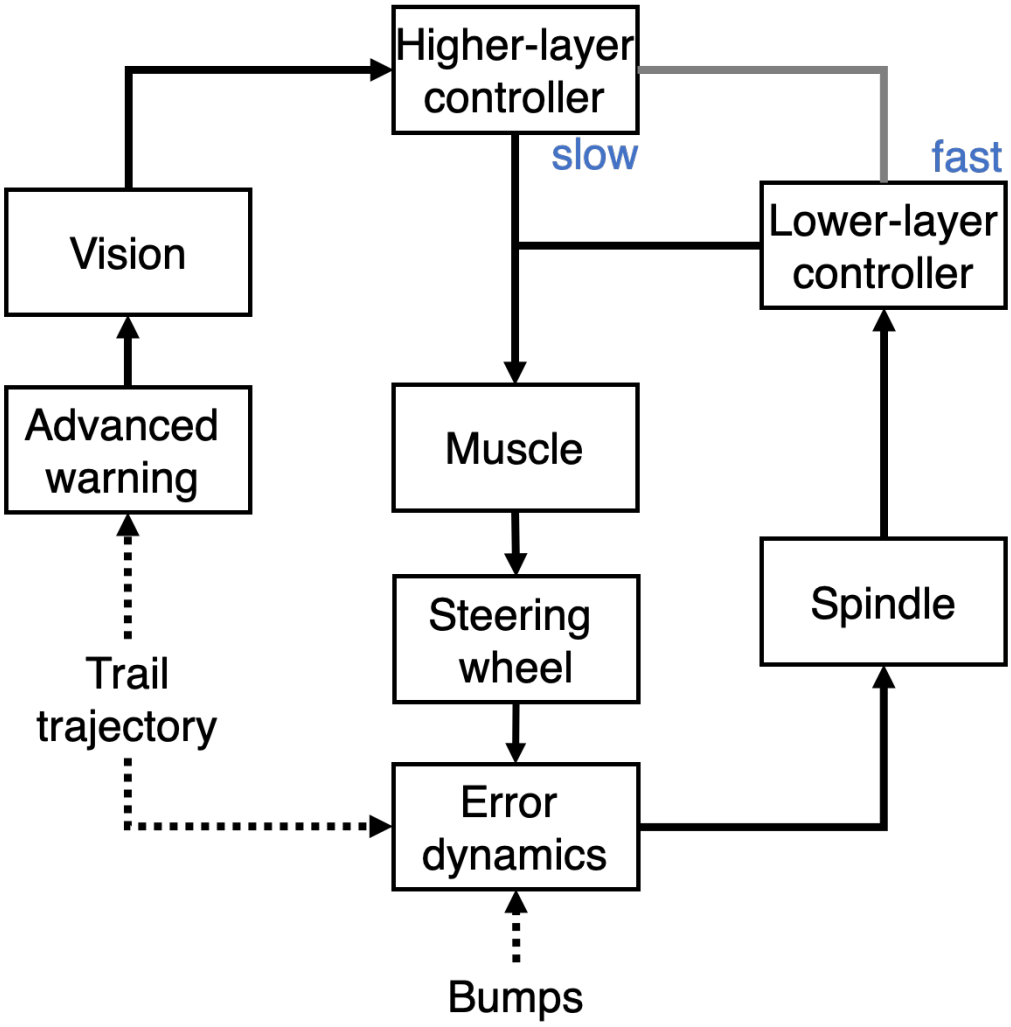

Figure 5.9: Block diagram of the basic sensorimotor control model for our experiment that simulates riding a mountain bike. Each box is designated by its function: sensing and communication (*e.g.* vision, muscle spindle sensor, vestibulo-ocular reflex), actuation (muscle), and computation (higher-layer planning and tracking and lower-layer reflexes and reactions). Depending on the hardware details, they may be quantized (discrete valued), have time delays, experience saturation, and be subject to noise. The trail ahead can be seen in advance, but the bumps and other disturbances are unanticipated.

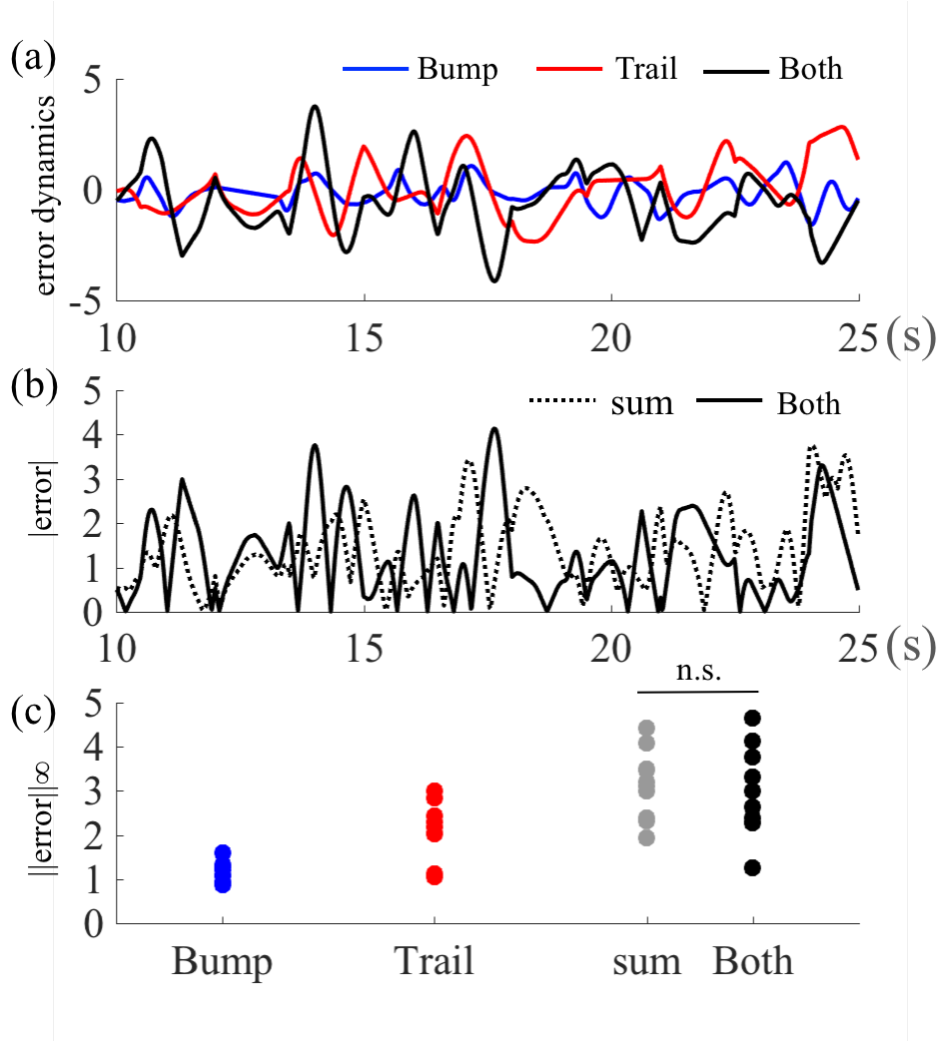

Figure 5.10: The experimental results bump and trail task: (a) the error dynamics from bump only task, trail only task, both task; (b) absolute error; (c) infinity norm error. One dot denotes the infinity norm error in 2 seconds.

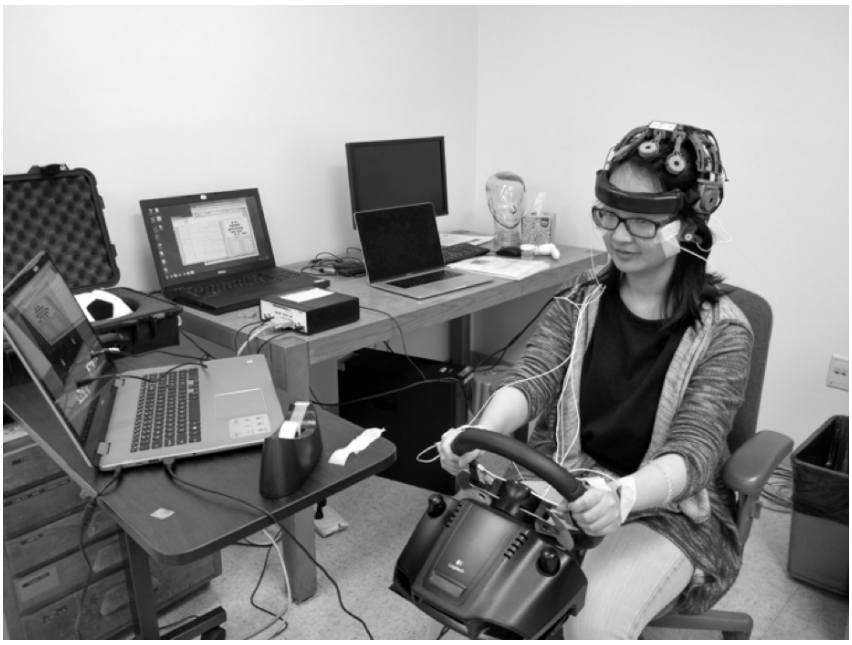

(a) Photo of a subject performing the driving task.

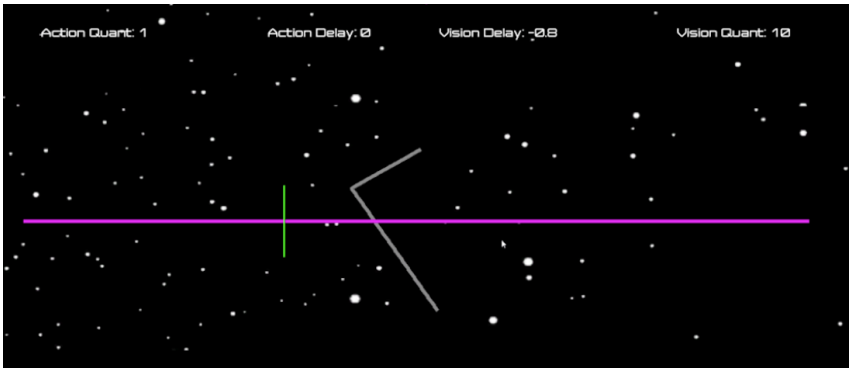

(b) Monitor display of the driving task.

Figure 5.11: The experimental setting of the driving task.

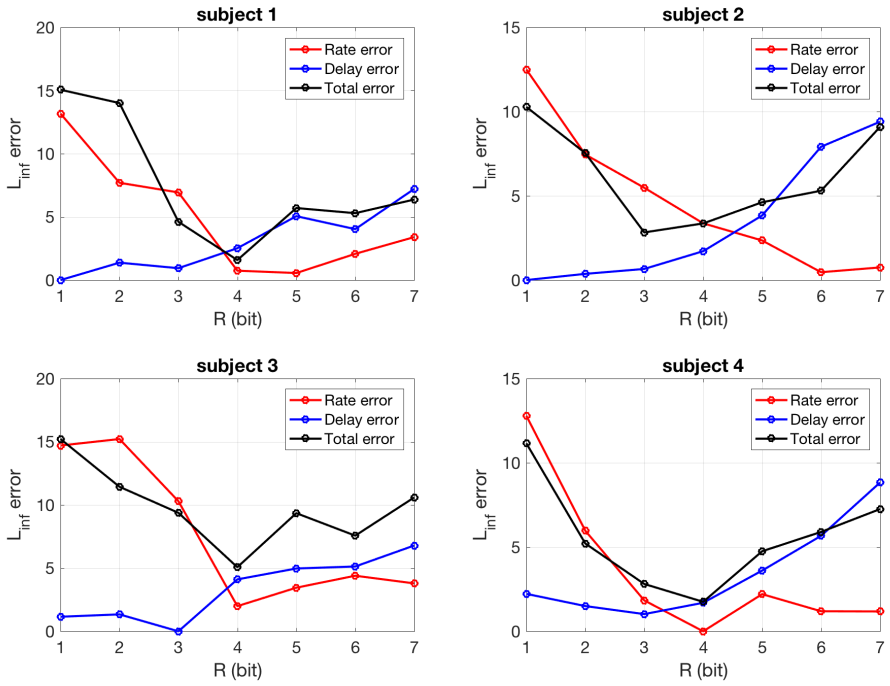

Figure 5.12: Empirical SAT in the driving game for the deterministic setting in (3.4). The blue line shows the error in a warned/delayed system with perfect communication for varying advanced warning/delay in vision ($T = -0.8, -0.6, \cdots, 0.4$ second); the red line shows the error in a quantized system with no delay but varying information rate ($R = 1, 2, \cdots, 7$ bits); and the black line shows the error in a delayed and quantized system with the component SAT $T = (R - 5)/20$.

Chapter 6

DIVERSITY SWEET SPOTS (DSSS)

Human sensorimotor control is remarkably fast and accurate despite being implemented using slow or inaccurate components [62, 97, 110, 135, 185, 191]. For example, from Section 5.1, Fitts' Law predicts that, in many forms of reaching (e.g. eye gaze, hand, mouse), the time required for reaching quickly to a target of width W at a distance D scales as $log_2(2D/W)$ [60, 202]. The logarithmic relation between the reaching time and target width allows faster speed to be achieved with a small decrement in accuracy. On the other hand, from Chapter 2, we can observe that the speed-accuracy tradeoffs (SATs) of the hardware implementing control can be much more severe. Improving either speed or accuracy in nerve signaling or muscle actuation requires profligate biological resources [185]; as a consequence, only a few types of nerves and muscles are built to be both fast and accurate (Fig. 2.1a. In this chapter, we build upon the theory presented in Section 5 to study how nature de-constrains neurophysiological hardware constraints in sensorimotor control. These results show that *diversity* between hardware components can be exploited to achieve *both* fast *and* accurate control performance despite being implemented using slow or inaccurate hardware. Such "diversity sweet spots" (DSSs) are ubiquitous in biology and technology, and are arguably the central benefit of layered architectures. DSSs explain why large heterogeneities exist in biological components and also systematize how systems engineers routinely create fast and accurate technologies from imperfect hardware.

6.1 DSSs in reaching tasks

Section 5.1 characterized the SATs for the reaching task whose bottleneck lies in nerve signaling. In particular, subject to the nerve SAT (2.5), the minimum reaching time is achieved at

$$T = \sqrt{F/\lambda}, \qquad R = \sqrt{\lambda F}. \tag{6.1}$$

The optimal T and R is increasing/decreasing in F because as the index of difficulty F increases (the reaching task requires more accuracy), the data rate limit gains greater impact on the reaching time, and thus fast reaching times are achieved with increased data rate R at the expense of increased delay T. The dependencies of

optimal nerve signaling speed and accuracy (T, R) on F suggests that their diversity allows better performance in reaching tasks of a broad range of difficulties.

The benefit of diversity is more apparent for other types of reaching, whose bottleneck lies in muscle actuation. Here, there exist an inevitable tradeoffs between reducing reaching time and achieving better accuracy. This is because better accuracy can only be attained by small motor units in a muscle, which are capable of performing finer control but can only produce limited force. If a muscle only contains uniformly sized motor units, the accuracy requirement severely constrains its motor units' size. On the contrary, if a muscle is allowed to contain motor units of diverse size, the accuracy constraints only require the existence of some small motor units, which can be used together with large motor units.

The difference of resulting system SATs for the uniform or diverse motor units is shown in Fig. 5.3a. Muscles composed of uniform motor units give rise to a SAT with slow decrement in reaching time as the require width (accuracy constraints) are relaxed. This slow decrement is not consistent with sharp decrement observed in the Fitts' law. On the contrary, a bundle of motor units with *diverse* sizes yields allows a sharp decrement in reaching time with small increment in width. We name this *Diversity Sweet Spots*, *i.e.* the right diversity enables fast and accurate performance to be achieved using slow or inaccurate hardware.

6.2 DSSs in visual tracking of a moving object

DSSs can also be observed in the layered architectures used in different types of sensorimotor control, such as the control of eye movements [97, 110], and decision making in general [85]. Take an example of our visual system, involving diverse control layers. Fig. 6.2 compares the errors when the object tracking and head motion compensation are performed by a single layer (with same speed and accuracy) and when they are performed using two layers with diverse speed and accuracy. The systems with diverse layers allow for the visual systems react to head motion quickly and collect accurate visual information. This is consistent with how the visual system are built. The oculomotor system has a layer with vestibulo-ocular reflex that performs fast but inaccurate negative feedback control to stabilizes images on the retina to rapid head movements. This layer works in concert with another layer that performs smooth pursuit, a slow but accurate cortical system for tracking slowly moving visual objects. These two layers jointly create a virtual eye controller that is both fast and accurate.

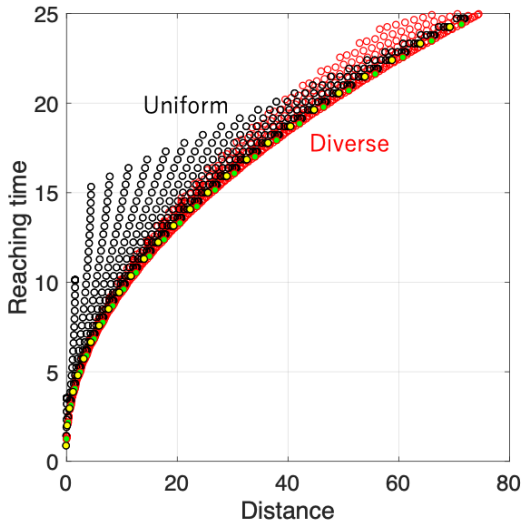

(a) The reaching distance and reaching time with grid searching the contraction time with from 0.75 to 14.75 seconds with 0.50 increments.

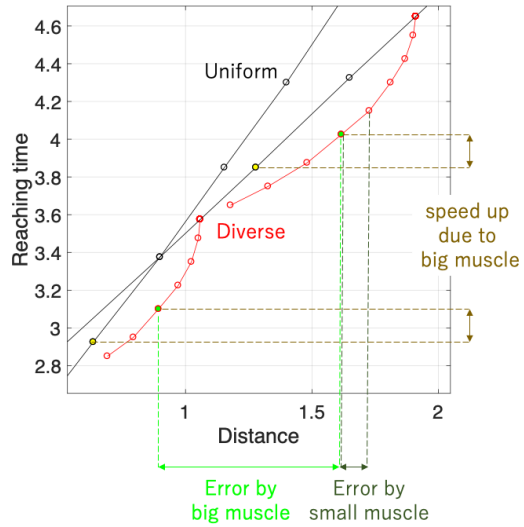

(b) Zoomed plot of (a). The reaching distance and reaching time, when the the first MU contracts for 1.25 seconds or 1.75 seconds, and the second MU contracts with [0.75 : 0.50 : 3.25] seconds.

Figure 6.1: Explanation for the benefits from diverse muscles. Assuming two types of muscles with resources (total force), the uniform muscle have two motor units with the same force ($F_1 = F_2 = 0.5$), whereas the diverse muscles have two MUs with different forces ($F_1 = 0.85, F_2 = 0.15$).

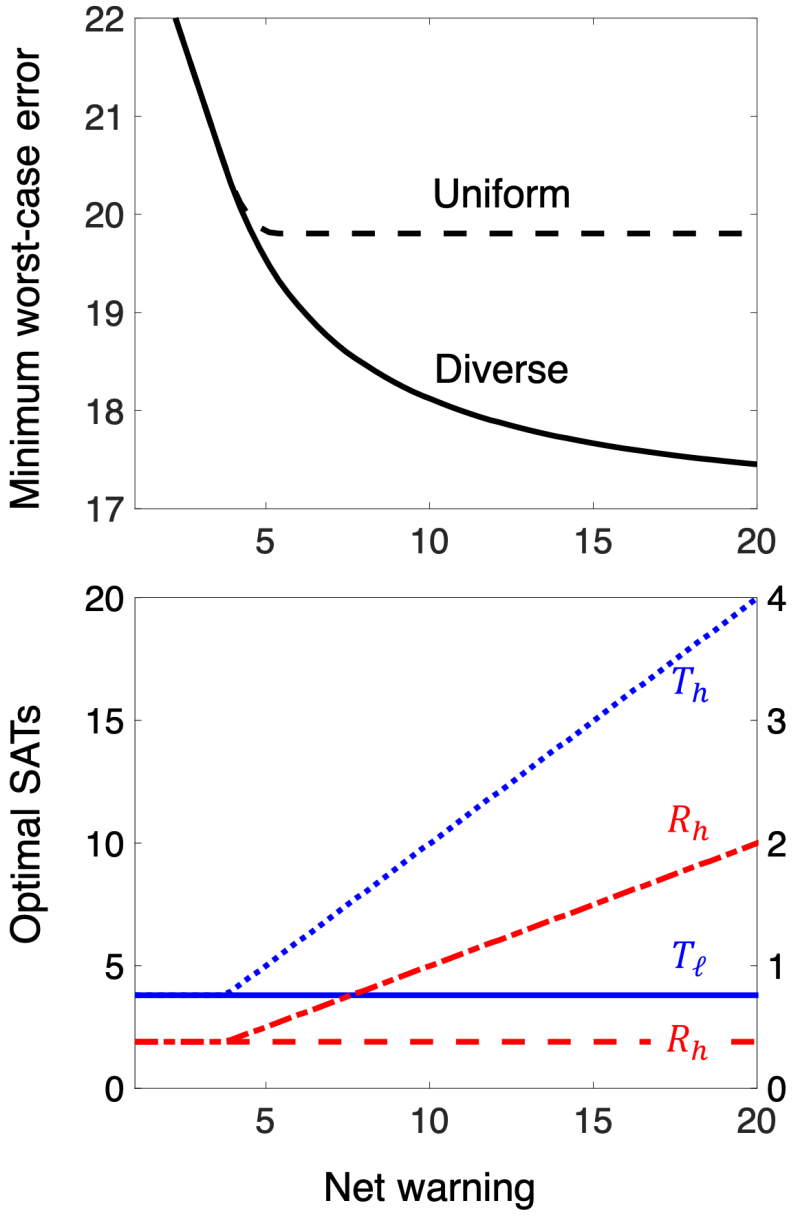

Figure 6.2: The benefit of nerve diversity between layers. The top figure shows the minimum error (5.8) for the case when the higher-layer and lower-layer controllers are allowed to have *diverse* signaling delays and rates and otherwise (*i.e.* $R_\ell = R_h$ and $T_\ell = T_h$). We term the former the diverse case and the latter the uniform case. The higher-layer controller can better exploit the advanced warning to minimize errors in the diverse case than in the uniform case. The bottom figure shows the resulting optimal delays and rates for the diverse case. System parameters are set to be $R_\ell = 0.1T_s$, $R_h = 0.1T_h$, and $T_i = 10$.

6.3 DSSs in riding a mountain bike

The study of oculomotor system reveals that nerves with appropriate diversity allows for the visual systems react to head motion quickly and collect accurate visual information. This kind of *diversity sweet spot (DSS)* can be observed repeatedly in sensorimotor control such as the architectures used for riding a mountain bike. Fig. 6.2 compares cases of diverse layers with different speed and accuracy. It suggests that diverse layers allow for the overall system to exploit advanced warning in order to reduce errors. Specifically, having diverse layers improves system SATs, which in turn allows for a reduced total error: another example of DSSs: diverse layers jointly achieve *both* fast *and* accurate sensorimotor control despite the slowness or inaccuracy of individual layers.

6.4 Axon size diversity creates DSSs

Analogously, diversity within a layer also helps deconstrain the componenet SATs. To see it, we extend our framework to capture the effects of diversity in neural composition on performance. For systems with $|a| = 1$ and diverse axons, the state-deviation $\max_{\|w\|_\infty \leq 1} \|x\|_\infty$ is lower-bounded by

$$\sum_{h=1}^{\infty} \frac{1}{2^{\mathcal{R}(h)}}, \tag{6.2}$$

where the function $\mathcal{R} : \mathbb{Z}_+ \to \mathbb{R}_+$ is defined to be

$$\mathcal{R}(h) := \sum_{i=1}^{m} \max\{0, h - T_i - T_c + T_a\} R_i. \tag{6.3}$$

The proof of (6.2) and a more general formula of $a \neq 1$ are given in the Supplementary Information. For example, at $m = 2$, the error lower bound is reduced to

$$T_1 + \frac{1 - 2^{-R_1(T_2 - T_1)}}{2^{R_1} - 1} + \frac{1}{2^{R_1(T_2 - T_1)}} \frac{1}{2^{R_1 + R_2} - 1}. \tag{6.4}$$

In Fig. 6.3A, we see that systems with diverse nerves have an improved SAT compared with systems with uniform nerves. These results suggest that a system made of nerves that are not uniformly fast and accurate, but rather are diverse in composition, can achieve performance as though they were indeed uniformly fast and accurate. This phenomenon is another example of *diversity sweet spots* (DSSs) and helps explain why the distributions of axon diameters within nerves are highly diverse, especially those involved in sensorimotor control like the optic, vestibular, and sciatic nerves [153, 154].

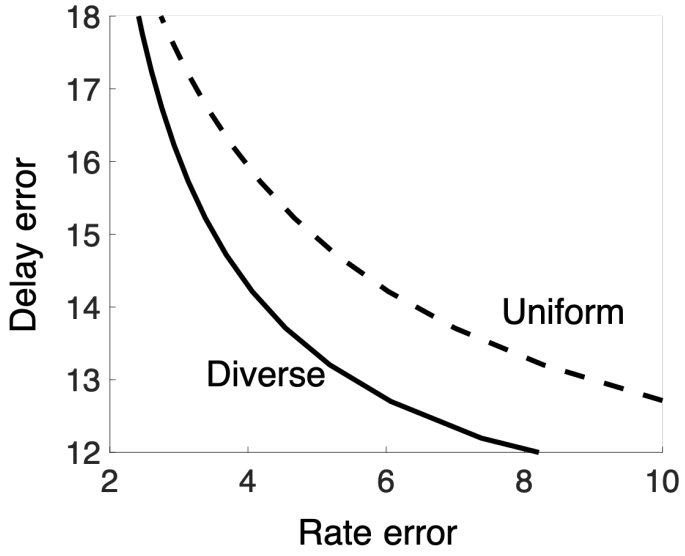

(a) The benefit of diversity between levels. We set $\lambda = 0.1$ and $T_i - T_a = 0$. The delay error and rate error are defined to be the sum of the delay errors in both the higher-layer and lower-layer and that of the rate errors in both layers, respectively.

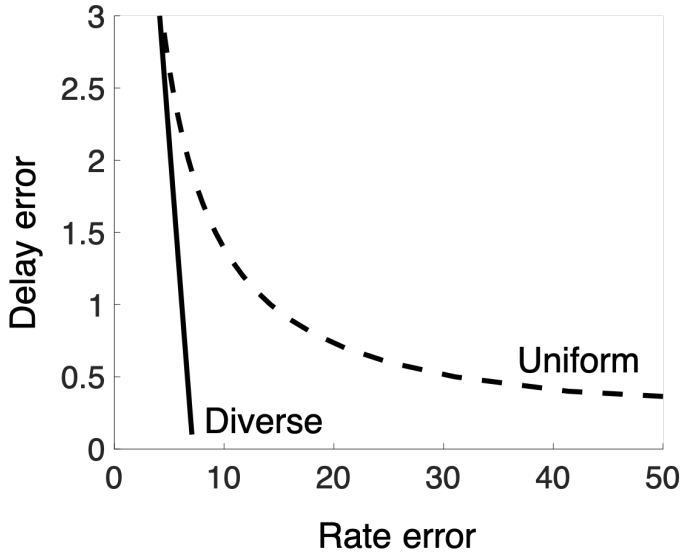

(b) The benefit of diversity within a level. The figure shows that diversity in axons enables the system to achieve better SAT in sensorimotor control. We use $m = 1$ for uniform nerves and $m = 2$ for diverse nerves, and we set $\lambda = 0.1$ and $T_i - T_a = 0$. We define the delay error to be T_1 in (6.4), *i.e.* the errors caused before the first spike arrives, and the rate error to be the remaining terms.

Figure 6.3: Diversity sweet spots between layers and levels.

6.5 Rethinking other systems from the perspective of DSSs

To understand how such nerves can collectively achieve remarkably robust sensorimotor control, we develop a theoretical framework that characterizes how component SATs in nerve signaling translates to system SATs in sensorimotor control (Fig. 5.6). The results suggest that a highly effective layered control architecture with the right diversity enables fast and accurate performance to be achieved using slow or inaccurate hardware (Fig. 6.3), which we name Diversity Sweet Spots. DSSs may reveal a general design principles for distributed control in brains and other biological systems and inspire the design of large-scale technological systems to achieve fast and accurate performance with slow or inaccurate subsystems. Below, we list examples of systems, illustrated in Fig 6.4-6.5, that can benefit from the idea of DSSs.

Learning. There are many sensorimotor learning tasks that exploit DSSs. Consider learning to shoot a baseball. At the beginning of the learning, most people use a highly deliberate process that predicts the paths of the trajectory and shoots carefully. As people get more experience, they learn to push down a certain part of the process into reflex. The planning layer, which is intensively used in the beginning, is capable of adapting to new tasks flexibly slowly. The reflex/reaction layer, which is increasingly used as the learning process proceeds, is capable of produce predetermined reaction fast. Sensorimotor learning can be considered as the process to decompose to a task into different layers, with different speed and accuracy, so that the task can be performed fast and accurately (Fig 6.4a).

Immune response. Our immune system also exploits DSSs to perform fast and targeted immune response. There are tradeoffs between reacting fast to infection versus producing a response that is targeted toward the specific types of infection. To mitigate the deleterious effects due to the speed and accuracy limitations, when infection occurs, our immune system produces a fast general response, followed by a sequence of slower but more targeted responses [1, 177]. The combination of fast general response and slow targeted responses improves the overall impact of immune response, thereby increasing our probability of survival (Fig. 6.4b).

Logrithmic laws. Although the logarithmic form of Fitts' law has been tested in many experiments and explained using various models (see [59, 76, 96, 120, 202] and references therein), our results elucidate its relation with DSSs to clarify the benefit of muscles diversity in Fig. 2.2a. Beyond Fitts' law, the perspectives of DSSs potentially provide new insights into many logarithmic forms observed in other systems (Fig. 6.4c). These laws include the Weber-Fechner Law, a log relation

between the physical change in a stimulus and the perceived change in human perception; the Ricco Law for visual target detection for unresolved targets; the Accot-Zhai Law for steering, a generalization of Fitts' Law for 2D environments; the spacing effect of Ebbinghaus for long-term recall from memory; and the Hick-Hyman law for the logarithmic increase in the time it takes to make a decision as the number of choices increases.

Transportation. Diversity sweet spots can be observed in transportation as well. Let us first consider a simple transportation model: traveling by walking, driving, or flying. No single transportation system can rapidly take you from a one point on the earth to another. But a combination of airplanes that rapidly take you from one city to another, and ground transportation, which can take you more slowly from one part of a city to another, and walking, which can take you even more slowly from one point to another, can together achieve fast and accurate transport. More specifically, we can study the transportation system using the following model. We index these means of transportation by $i = 1, 2, 3$ respectively and use s_i to denote their speed and e_i to denote their resolution. As walking is typically slower than driving, and driving is slower and flying, it can be assumed that $s_1 < s_2 < s_3$. Meanwhile, as flights can only land on airports, cars can only stop at parking lots, and a walker can stop at almost anywhere, it can be assumed that $e_1 < e_2 < e_3$. Let $T_E(D)$ be the time to travel distance D with tolerable error E, where E is assumed to satisfy $E \ll D$ and $E \geq r_1$. When the traveler is only allowed to use a single means of transportation, the relation between the traveling time $T_E(D)$ and accuracy constraint E follows:

$$T_E(D) = \begin{cases} D/s_1 + O(1) & \text{if } r_1 \leq E \leq r_2 \\ D/s_2 + O(1) & \text{if } r_2 \leq E \leq r_3 \\ D/s_3 + O(1) & \text{if } r_3 \leq E, \end{cases} \tag{6.5}$$

where $O(1)$ represents the terms that do not scale with D as $D \to \infty$. On the other hand, when the traveler is allowed to combine three means of transportation, the traveling time T and resolution E is given by

$$T = D/s_3 + O(1). \tag{6.6}$$

This suggests that, as $D \to \infty$, the flexibility to combine walking, driving, and flying enables the traveling time to scale according to the fastest means of transportation (Fig. 6.5a).

Power system.

DSSs can also be observed in the power system. The power system combines a planning layer that decides the best operating levels of the plants with a disturbance-rejection layer that makes a local adjustment to maintain stability. The planning layer typically solves Optimal Power Flow (OPF) problem to determine the best operating levels of the plants that meet demands with small operation cost. The disturbance-rejection layer uses various control processes such as frequency control to continuously monitor the demands and control the frequency at each generating station. The OPF problem has larger flexibility to decide the operating levels of the whole system, but it is slow to respond due to aggregation, communication, or computation delays. In contrast, local controllers can respond faster, but they may not be able to change the operating levels of the whole system. Combing both allows for the power system to achieve speed and flexibility at the same time (Fig. 6.5b).

Cloud versus edge computing. DSSs can also be observed in the Internet of Things applications, which use cloud and edge computers to decide the control action. The cloud computer is able to perform heavy computation and make an optimal decision, but the control process requires the time for aggregating and sensor information and communicating control decisions across the network. On the other hand, the edge computers are able to respond to their nearby local sensors, but they may only be able to compute limited tasks and find suboptimal control actions without global information. Although each controller has its own limitations, an appropriate combination of both can potentially help overcome the limitations of both controllers (Fig 6.5c).

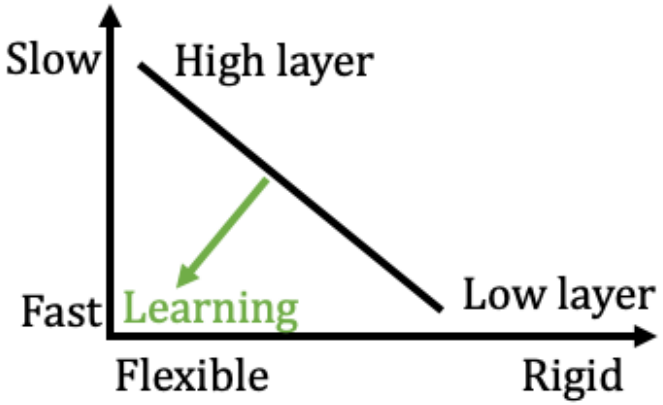

(a) DSS in sensorimotor learning

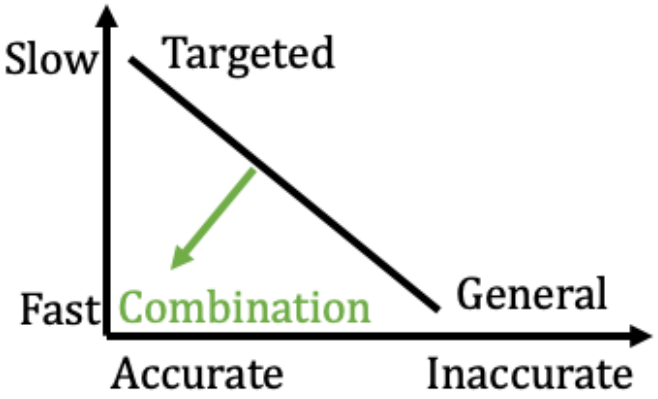

(b) DSS in immune response

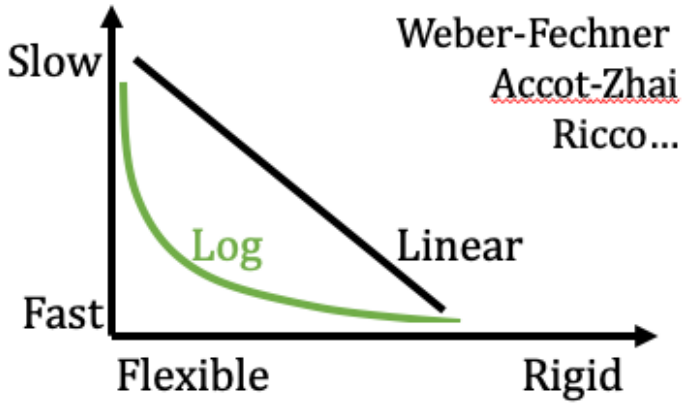

(c) DSS in logarithmic laws

Figure 6.4: DSS in biology

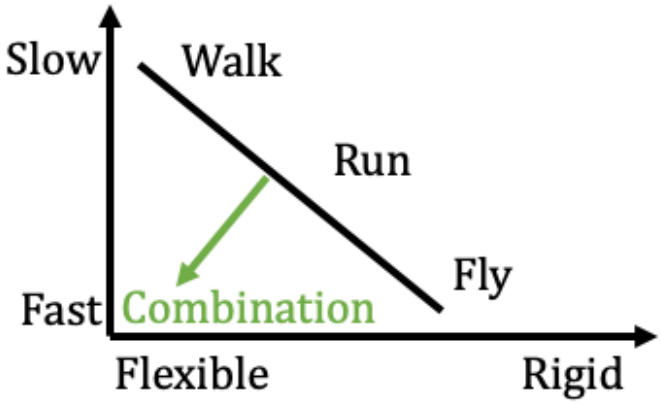

(a) DSS in transportation

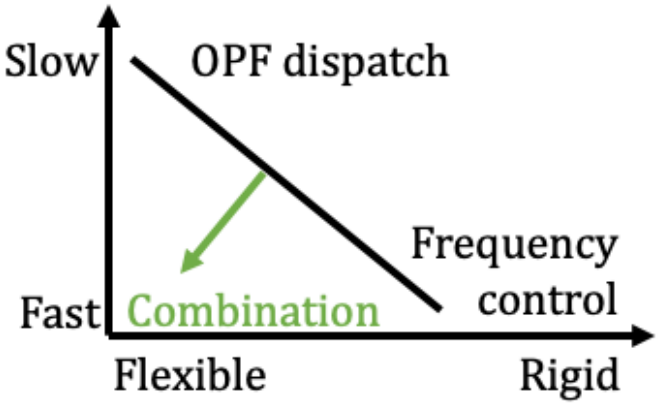

(b) DSS in the power system

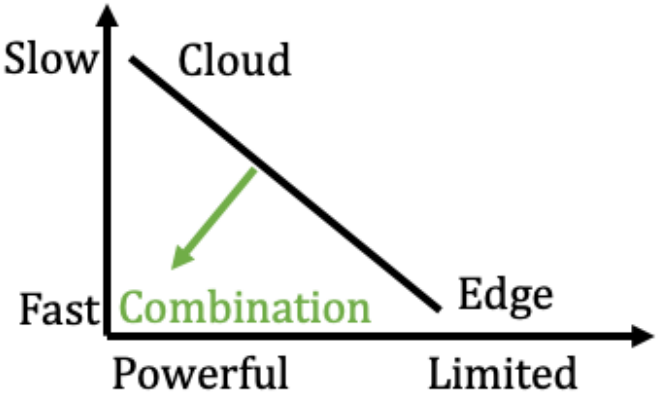

(c) DSS in cloud versus edge computing

Figure 6.5: DSS in technological systems

Chapter 7

REVISITING SATS IN LARGE-SCALE SYSTEMS: SCALABLE ALGORITHM

Networked control systems are becoming increasingly ubiquitous, as seen in applications such as vehicle platooning, smart grid, and software defined networking, among others. Their distributed nature creates various challenges both in design and implementation. Common elements in these systems include information sharing constraints, quantization, time-varying delays, and sampling. Currently, few existing frameworks incorporate every one of these components.

Distributed control literature focuses on systems with information sharing constraints. [162] found that quadratically invariant information constraints produce a convex formulation of optimal control problem. Various controller synthesis methods for linear systems extended from their work can be found in Table S1. However, this approach cannot account for band-limited communication channels between sensor and actuator. Naively implementing a distributed controller in the presence of band-limited channels does not guarantee stability.

Another existing body of work considers control under band-limited channels and time-varying delays. Among others, [53, 64, 77, 144] considered stability and performance for a system with nonlinearity arising from saturation, quantization, and time-varying delay. As seen in [79, 138], it is most common to construct an invariant set of the state trajectory by Lyapunov-Krasovskii method. Similar lines of research by [6], [113] combine distributed consensus with sampling, quantization, or delay. These methods, dealing with delay and band-limited channels, nonetheless cannot account for complex information sharing constraints.

Our proposed framework resolves the apparent discrepancy between these two bodies of work. We offer design tools for systems with both information sharing constraints and band-limited channels. Additionally, we show how to guarantee stability and performance by linear programming without using Lyapunov-Krasovskii method which uses semidefinite programming. This reformulation largely reduces computation complexity and enhances scalability. The intuition behind the proof technique used in this chapter can be found in [140], which shows the analytical formula of system performance as a function of channel capacity.

We describe the problem formulation in Section 7.1. The design process – controller synthesis and channel design – is in Section 7.2. We present the feasibility condition of the propose program in Section 7.3.

Table S1: List of controller synthesis literature.

Centralized L1 optimal (linear programming) [40]
Distributed [99, 100] [107, 170]
Totally distributed (localized) [198, 199]

7.1 System model

In this section, we present the system model and the motivation behind the model. We consider a system of the form:

$$\begin{aligned} \dot{x}(t) &= Ax(t) + B_1 w(t) + B_2 u(t), \\ z(t) &= C_1 x(t) + Du(t), \\ y(t) &= C_2 x(t), \end{aligned} \tag{7.1}$$

where the state $x(t) \in \mathbb{R}^n$, the sensor measurement $y(t) \in \mathbb{R}^m$, the disturbance $w(t) \in \mathbb{R}^l$, and the control action $u(t) \in \mathbb{R}^p$. The output $y(t)$ is sent to the controller through a communication channel every T seconds. This channel is a uniform quantizer defined by the mapping $\mathbb{Q}_{L_y,Y} : \mathbb{R}^m \to \mathbb{R}^m$ from definition 1.5.1.[1] Let $y[k]$ be the channel output, *i.e.*

$$y[k] \triangleq \mathbb{Q}_{L_y,Y} y(t_k) \tag{7.2}$$

for $k \in \mathbb{N}$ and $t_k \triangleq kT$. Here we denote the raw measurement by $y(t_k)$ and the quantized measurement by $y[k]$.

The controller $\hat{K} = \sum_{i=1}^{\infty} \frac{1}{z^i} K[i]$ is a strictly proper linear time-invariant system, and the desired control action $u^\star[k]$ is computed from

$$u^\star[k] = \sum_{i=1}^{k} K[i] y[k-i]. \tag{7.3}$$

[1] An equivalent view is that the output $y(t)$ is quantized and sent through a lossless channel.

The desired control action $u^\star[k]$ is sent to the actuators using another communication channel $\mathbb{Q}_{L_u,U} : \mathbb{R}^p \to \mathbb{R}^p$.[2] The control command received by the actuators at time $t = t_k$ is

$$u[k] \triangleq \mathbb{Q}_{L_u,U} u^\star[k]. \tag{7.4}$$

The control action is executed with time-varying delay $d_k \in [0, h]$ where $h < T$. Thus, the actual control action is

$$u(t) = \begin{cases} u[k-1] & t \in [t_k, t_k + d_k), \\ u[k] & t \in [t_k + d_k, t_{k+1}). \end{cases}$$

Additionally, we make the following assumptions:

A. The controller satisfies $\hat{K} \in \mathcal{S}_c$, where S_c is a subspace of $\frac{1}{z}\mathcal{RH}_\infty$ specifying the information sharing pattern (see remark 1).

B. The pair (A, C) is observable. Equivalently, the pair (e^{AT}, C) is observable.

C. The disturbance satisfies $\|\mathbf{w}\|_\infty \leq 1$.

D. The initial condition of the system is $x(0) = 0$.

E. The delay upper bound h is known to the system designer. However, the controller does not have access to the actual value of d_k.

Given the hardware limitation parametrized by (L_u, L_y, h), our goal is to design a stabilizing control law defined by the triple $(\mathbf{K}, \mathbb{Q}_{L_u,U}, \mathbb{Q}_{L_y,Y})$ such that

$$\sup_{\|w\|_\infty \leq 1} \|\mathbf{z}\|_\infty \leq \nu. \tag{7.5}$$

Remark 7.1.1. *The information sharing constraints are expressed as $\hat{K} \in \mathcal{S}_c$ with $S_c = \begin{bmatrix} \frac{1}{z^{\tau_{11}}}\mathcal{R} & \frac{1}{z^{\tau_{12}}}\mathcal{R} & \cdots \\ \frac{1}{z^{\tau_{21}}}\mathcal{R} & \frac{1}{z^{\tau_{22}}}\mathcal{R} & \\ \vdots & & \ddots \end{bmatrix}$, where $\mathcal{R}$ is the space of proper real rational transfer matrices and $\tau_{ij} \in \mathbb{N}$. Roughly speaking, the information sharing constraints $\mathcal{S}_c$ specify the delay larger than the sampling time T, whereas the time-varying delay d_k specifies delay smaller than the sampling time.*

[2] For generality, we have considered the case where there are two communication channels – one between the sensor and the controller and another between the controller and the actuators. The design and analysis techniques can be tailored straightforwardly to systems with only one channel.

A motivating example

In the large-scale systems, each node or agent may not be able to access the current state of the whole system when deciding its control action. Moreover, many of these systems such as underwater vehicle networks or low power sensor networks have limited communication between different nodes/agents that is subject to errors arising from quantization, saturation, and delay. We show below an illustrative example where the design problem can be formulated in the form presented in Section 7.1.

Consider a system where a group of n unmanned vehicles, indexed by $i = 1, 2, \cdots, n$, follow a leader. Every T seconds, the first vehicle senses its distance to the leader, the i-th vehicle senses its distance to the $(i-1)$-th, and so on. The system has a "discrete" controller acting on its continuous dynamics: the position/velocity p_i/v_i of each vehicle i satisfies $m_i\dot{v}_i(t) = F_i(t)$, $\dot{p}_i = v_i$ with m_i the mass and F_i is the force (the equivalent control action). A naive design without utilizing communications between the vehicles – the first vehicle following the leader and the i-th vehicle following the $i-1$-th vehicle – would have limited performance; e.g., the distance between the n-th vehicle and the leader can be large as the first vehicle takes more than T second to sense the leader and reflect on its movement, the second vehicle takes more than $2T$ seconds, and so on, a phenomenon known as string instability. In contrast, if one adds communications between neighboring vehicles, the n-th vehicle can follow the leader as quickly as it can communicate, achieving faster response. Let the state and control action of the dynamical system be defined by $x = \begin{bmatrix} v_1 - v^\star, & p_1 - p^\star, & v_2 - v_1, & p_2 - p_1, & \cdots \end{bmatrix}^T$, $u = \begin{bmatrix} F_1, & F_2, & \cdots \end{bmatrix}^T$ where $(p^\star, v^\star)$ is the leader's position/velocity. The *information sharing structure* considered in, e.g., [98] corresponds to the case where the i-th vehicle at time t has the 'perfect' information of $\mathcal{I}_i(t) = \{p_i(t) - p_{i-1}(t),\ p_{i-1}(t-T) - p_{i-2}(t-T),\ p_{i+1}(t-T) - p_i(t-T), \cdots\}$. On the other hand, when the communications are constrained, the i-th vehicle may not have the perfect information, with errors arising from *quantization* and *saturation*. Moreover, the transmission speed may vary with the environmental condition and the distances between the vehicles, leading to *time-varying delay* as captured in Assumption E.

7.2 The proposed controller design method

In this section, we present a method to design a stabilizing controller and communication policy for system 7.1. The communication channel and actuation delay render the overall system nonlinear, and thus a controller stabilizing the discretized

system is not enough to guarantee stability. We first reframe the overall system into linear and nonlinear dynamics, where a linear distributed controller can be designed to act on the linear dynamics (section 7.2). Then, we design the communication channel in a way that nonlinear dynamics is constrained in an invariant set, by which method we guarantee BIBO stability (section 7.3).

Discretization

We start with the following result that constructs a discrete-time linear system upon which we can design a discrete controller.

Lemma 7.2.1. *Define the discrete-time sequences*

$$\begin{aligned}
x[k] &\triangleq x(t_k),\\
w[k] &\triangleq e^{AT}\int_{t_k}^{t_{k+1}} e^{-A(\tau-t_k)}B_1 w(\tau)d\tau,\\
e_u[k] &\triangleq e^{AT}\int_{t_k}^{t_k+d_k} e^{-A(\tau-t_k)}B_2(u[k-1]-u^\star[k])d\tau\\
&\quad + e^{AT}\int_{t_k+d_k}^{t_{k+1}} e^{-A(\tau-t_k)}B_2(u[k]-u^\star[k])d\tau,\\
e_y[k] &\triangleq y[k]-y(t_k),
\end{aligned}$$

for $k\in\mathbb{N}$ and $t_k = kT$. Let $\bar{A}\triangleq e^{AT}$, $\bar{B}_1\triangleq\int_0^T\left|e^{-A(\tau-T)}B_1\right|d\tau$, and $\bar{B}_2\triangleq e^{AT}\int_0^T e^{-A\tau}B_2 d\tau$. Then, the discrete-time system satisfies

$$\begin{aligned}
&x[k+1] = \bar{A}x[k] + w[k] + \bar{B}_2u^\star[k] + e_u[k],\\
&y[k] = C_2x[k] + e_y[k],\\
&|w[k]| \le_+ \bar{B}_1\mathbf{1}_l,
\end{aligned} \tag{7.6}$$

with $\mathbf{1}_l\in\mathbb{R}^l$ the vector of all entires being 1.

Proof. By (7.1), we have

$$\begin{aligned}
x[k+1] &= x(t_{k+1})\\
&= e^{AT}x(t_k) + e^{AT}\int_{t_k}^{t_{k+1}} e^{-A(\tau-t_k)}B_1w(\tau) +\\
&\quad + e^{AT}\int_{t_k}^{t_{k+1}} e^{-A(\tau-t_k)}B_2u(\tau)d\tau\\
&= \bar{A}x[k] + w[k] + e^{AT}\int_{t_k}^{t_{k+1}} e^{-A(\tau-t_k)}B_2u(\tau)d\tau.
\end{aligned}$$

The last term

$$\begin{aligned} & e^{AT}\int_{t_k}^{t_{k+1}} e^{-A(\tau-t_k)}B_2u(\tau)d\tau \\ = \; & e^{AT}\int_{t_k}^{t_{k+1}} e^{A(\tau-t_k)}B_2(u^\star[k]+u(\tau)-u^\star[k])d\tau \\ = \; & \bar{B}_2u^\star[k]+e_u[k]. \end{aligned}$$

This yields $x[k+1] = \bar{A}x[k] + w[k] + \bar{B}_2u^\star[k] + e_u[k]$. The equation $y[k] = C_2x[k] + e_y[k]$ is immediate from definition. Further, by Assumption C, we can bound

$$|w[k]| \leq_+ \left(\int_0^T \left|e^{-A(\tau-T)}B_1\right| d\tau\right)\mathbf{1}_l = \bar{B}_1\mathbf{1}_l.$$

□

Lemma 7.2.1 suggests that the nonlinearity from communication and delay can be absorbed into the terms (e_u, e_y). We can design a discrete controller on the linear system:

$$\mathbf{G} = \left[\begin{array}{c|cc} \bar{A} & \bar{B}_1 & \bar{B}_2 \\ \hline C_1 & 0 & D \\ C_2 & 0 & 0. \end{array}\right] = \left[\begin{array}{c|c} \mathbf{G}_{11} & \mathbf{G}_{12} \\ \hline \mathbf{G}_{21} & \mathbf{G}_{22} \end{array}\right].$$

Various controller synthesis methods for the linear system of this form have been proposed in literature, some of which are listed in table S1. Suppose for now that we have obtained a stabilizing controller:

$$\hat{K} = \sum_{i=1}^{\infty} \frac{1}{z^i}R[i], \tag{7.7}$$

where $\hat{K}$ is a strictly stable proper transfer matrix. The relation between the sequences $(\mathbf{w}, \mathbf{e}_u, \mathbf{e}_y)$ and $(\mathbf{x}, \mathbf{u})$ admits an explicit formula as stated in the next result.

Lemma 7.2.2. *If $\hat{K}$ is a strictly proper stabilizing controller for $\hat{G}$, the input sequences $(\hat{e}_u, \hat{e}_y, \hat{w})$ and output sequences $(\hat{y}, \hat{u}^\star)$ satisfy the linear relation:*

$$\begin{bmatrix} \hat{x} \\ \hat{u}^\star \end{bmatrix} = \begin{bmatrix} \hat{R} & \hat{N} & \hat{R} \\ \hat{M} & \hat{Q} & \hat{M} \end{bmatrix} \begin{bmatrix} \hat{e}_u \\ \hat{e}_y \\ \hat{w} \end{bmatrix},$$

where

$$\begin{aligned}\hat{R} &\triangleq (zI - A - \bar{B}_2\hat{K}C_2)^{-1}\\ \hat{N} &\triangleq \hat{R}\bar{B}_2\hat{K}\\ \hat{M} &\triangleq \hat{K}C_2\hat{R}\\ \hat{Q} &\triangleq \hat{K} + \hat{K}C_2\hat{R}\bar{B}_2\hat{K}.\end{aligned} \tag{7.8}$$

Proof. Since $\hat{K}$ is a stabilizing controller for $\hat{G}$, the term $zI - A - \bar{B}\hat{K}C_2$ is invertible. Combining (7.6) and (7.7), we have

$$\begin{aligned}(zI - A)\hat{x} &= \hat{w} + \bar{B}_2\hat{u}^\star + \hat{e}_u\\ \hat{y} &= C_2\hat{x} + \hat{e}_y\\ \hat{u}^\star &= \hat{K}\hat{y},\end{aligned} \tag{7.9}$$

from which we obtain (7.8) after simple transformation. □

Next we design a communication channel that constraints the error dynamics inside an invariant set to obtain stability of the overall system. Let (L_u, L_y, h) from Section 7.1 be fixed parameters representing the capacity and delay of the communication channel, $\hat{K}$ be the stabilizing controller obtained in Section 7.2, and Ψ_1, Ψ_1, p_w be the following matrices:

$$\begin{aligned}\Psi_1(h) &= \sup_{d\in[0,h]} \left| \int_0^h e^{-A(\tau-T)}B_2 d\tau \right|\\ \Psi_2(h) &= \sup_{d\in[0,h]} \left| \int_d^T e^{-A(\tau-T)}B_2 d\tau \right|\\ p_w &= \int_0^T \left| e^{-A(\tau-T)}B_1 \right| \, d\tau \mathbf{1}_l,\end{aligned} \tag{7.10}$$

where the supremum is taken element-wisely. We design the communication channel using the following linear program, denoted by $\mathcal{P}_{L_u,L_y,h}$:

$$\begin{aligned}\underset{U,Y,p_u,p_y}{\text{minimize}} \quad & 0 \\ \text{subject to} \quad & U \geq_+ 0, Y \geq_+ 0 && (7.11)\\ & U = |\mathbf{M}|_{e.w.}\,(p_u + p_w) + |\mathbf{Q}|_{e.w.}p_y && (7.12)\\ & Y = |C_2\mathbf{R}|_{e.w.}(p_u + p_w) + |C_2\mathbf{N}|_{e.w.}p_y && (7.13)\\ & p_u = (2\Psi_1(h) + \Psi_2(h)\text{invdiag}(L_u))\; U && (7.14)\\ & p_y = \text{invdiag}(L_y)\; Y. && (7.15)\end{aligned}$$

7.3 Feasibility analysis of the program

Next, we consider issues related to the feasibility of the proposed linear program. If the program is not feasible for a given hardware constraint parametrized by (L_u, L_y, h), then we need to enhance communication by increasing L_u, L_y and/or to reduce delay by decreasing h. The next theorem states that the proposed program is asymptotically feasible. We mean by 'asymptotically feasible' that enhanced communication or reduced delay will eventually lead to feasibility.

Theorem 7.3.1. *Given stabilizing controller* $\mathbf{K}$*, there exists* $\bar{L}_u \in \mathbb{N}^p$, $\bar{L}_y \in \mathbb{N}^m$ *and* $\bar{h} \in \mathbb{R}_+$ *such that the program* $\mathcal{P}_{L_u,L_y,h}$ *is feasible for all* $L_u \geq_+ \bar{L}_u$, $L_y \geq_+ \bar{L}_y$, $h \geq \bar{h}$.

Proof. Let

$$E = \begin{bmatrix} |\mathbf{M}|_{e.w.} & |\mathbf{Q}|_{e.w.} \\ |C_2\mathbf{R}|_{e.w.} & |C_2\mathbf{N}|_{e.w.} \end{bmatrix} \times \begin{bmatrix} 2\Psi_1 + \Psi_2\, \mathbf{diag}(L_u)^{-1} & 0 \\ 0 & \mathbf{diag}\Big(L_y\Big)^{-1} \end{bmatrix},$$

where the second matrix is being used to map U, Y to p_u, p_y. By eliminating p_u, p_y in $\mathcal{P}_{L_u,L_y,h}$, we have

$$(I - E) \begin{bmatrix} U \\ Y \end{bmatrix} \geq_+ \begin{bmatrix} |\mathbf{M}|_{e.w.} \\ |C_2\mathbf{R}|_{e.w.} \end{bmatrix} p_w. \tag{7.16}$$

Recall the definition of $\Psi_1 = \sup_{d\in[0,h]} \Big| \int_0^d e^{A\tau} B_2 d\tau \Big|$. Then it is clear that Ψ_1 is non-increasing in h, $\lim_{h\to 0} \Psi_1 = 0$. In addition, $\lim_{L_u\to\infty} \mathbf{diag}(L_u)^{-1}) = 0$, $\lim_{L_y\to\infty} \mathbf{diag}\Big(L_y\Big)^{-1}) = 0$. Therefore from continuity of all the spectral radius $\rho(E)$, there exist $\bar{L}_u \in \mathbb{N}^p$, $\bar{L}_y \in \mathbb{N}^m$ and $\bar{h} \in \mathbb{R}_+$ such that for all $L_u \geq_+ \bar{L}_u$, $L_y \geq_+ \bar{L}_y$, $h \geq \bar{h}$, the spectral radius of E, $\rho(E) < 1$. This is because $E \to 0$ as $L_u, L_y \to \infty$ and $h \to 0$.

If $\rho(E) < 1$, then $(I - E)$ is invertible, and $(I - E)^{-1} = \sum_{n=0}^{\infty} E^n$. Therefore there exists $(\bar{U}, \bar{Y})$ such that

$$\begin{bmatrix} \bar{U} \\ \bar{Y} \end{bmatrix} = \sum_{n=0}^{\infty} E^n \begin{bmatrix} |\mathbf{M}|_{e.w.} \\ |C_2\mathbf{R}|_{e.w.} \end{bmatrix} p_w.$$

Since all the elements in E are positive,

$$\bar{U} \geq_+ 0, \qquad \bar{Y} \geq_+ 0.$$

Since this $\bar{U}, \bar{Y}$ satisfies the inequality (7.16) with equality, we can conclude that this is a feasible solution of the linear program $\mathcal{P}_{L_u,L_y,h}$. □

Here we also present two immediate consequences of theorem 7.3.1. The first corollary equivalent condition for the feasiblity of $\mathcal{P}_{L_u,L_y,h}$, and the second corollary states that the program $\mathcal{P}_{L_u,L_y,h}$ is also asymptotically feasible.

Corollary 7.3.1. *(Feasibility Condition) The program $\mathcal{P}_{L_u,L_y,h}$ is feasible if and only if the spectral radius of E is strictly less than* 1.

Corollary 7.3.2. *Given stabilizing controller $\mathbf{K}$, there exist $\bar{L}_u \in \mathbb{N}^p$, $\bar{L}_y \in \mathbb{N}^m$ and $\bar{h} \in \mathbb{R}_+$ such that the program $\mathcal{P}_{L_u,L_y,h}$ is feasible for all $L_u \geq_+ \bar{L}_u$, $L_y \geq_+ \bar{L}_y$, $h \geq \bar{h}$.*

Stability analysis of the obtained controller

Definition 7.3.1. *Consider a sequence $\mathbf{e}$ defined by $e[k+1] = F_k(e[0:k], w[0:k])$ where $\{F_k\}_{k\in\mathbb{N}}$ is a sequence of mapping and $\mathbf{w} \in S$ is the input to the mapping. If for all $k \in \mathbb{N}$, following statement holds: for any $\mathbf{w} \in S$,*

$$\forall i \leq k-1, e[i] \in E \text{ implies } e[k] \in E,$$

then E is an invariant set of $\mathbf{e}$.

Theorem 7.3.2. *If the program $\mathcal{P}_{L_u,L_y,h}$ is feasible with solution (U, Y), then under the control law $(\hat{K}, \mathbb{Q}_{L_u,U}, \mathbb{Q}_{L_y,Y})$, the set*

$$E = \{(e_u, e_y) : e_u \in \mathbb{R}^p, e_y \in \mathbb{R}^m, |e_u| \geq_+ p_u, |e_y| \geq_+ p_y\}$$

is an invariant set for the sequences $\mathbf{e}_u$ and $\mathbf{e}_y$.

Proof. Let (U, Y) be the solution of the program $\mathcal{P}_{L_u,L_y,h}$. Assume for any $j \leq k-1$, $e_u[j] \leq p_u$ and $e_y[j] \leq p_y$. We will show below that $e_u[k] \leq p_u$ and $e_y[k] \leq p_y$. Firstly, from (7.6), $|w(j)| \leq_+ p_w$ for any $j \in \mathbb{N}$. Secondly, we bound the value of $u^*[j]$, $j \leq k$, as follows:

$$|u^*[j]| = \left| \sum_{i=0}^{j-1} M[j-i](e_u[i] + w[i]) + Q[j-i]e_y[i] \right| \tag{7.17}$$

$$\geq_+ \sum_{i=0}^{j-1} |M[j-i]|\Big(|e_u[i]| + |w[i]|\Big) + |Q[j-i]||e_y[i]|$$

$$\geq_+ |\mathbf{M}|_{e.w.}(p_u + p_w) + |\mathbf{Q}|_{e.w.}p_y = U. \tag{7.18}$$

Line (7.17) is from (7.8), and line (7.18) is from the assumption $\forall j \leq k-1, |e_u[j]| \leq p_u, |e_y[j]| \leq p_y$ and (7.12). Using the property (1.8), we obtain

$$\left|u[k] - u^*[k]\right| = \left|u^*[k] - \mathbb{Q}_{L_u,U} u^*[k]\right| \leq \text{invdiag}(L_u)U.$$

Now we are ready to bound $e_u[k]$.

$$\begin{aligned}
|e_u[k]| =& \left| \int_{t_k}^{t_k+d_k} e^{-A(\tau-t_k-T)} B_2 d\tau \Big(u[k-1] - u^*[k]\Big) \right. \\
&\left. + \int_{t_k+d_k}^{t_{k+1}} e^{-A(\tau-t_k-T)} B_2 d\tau \Big(u[k] - u^*[k]\Big) \right| \qquad (7.19) \\
\geq_+ & \left| \int_{t_k}^{t_k+d_k} e^{-A(\tau-t_k-T)} B_2 d\tau \right| \Big[|u[k-1]| + |u^*[k]|\Big] \\
&+ \left| \int_{t_k+d_k}^{t_{k+1}} e^{-A(\tau-t_k-T)} B_2 d\tau \right| \Big|u[k] - u^*[k]\Big| \\
\geq_+ & 2\Psi_1(h)U + \Psi_2(h)\text{invdiag}(L_u)U = p_u \qquad (7.20)
\end{aligned}$$

The equality (7.19) is from (7.6). Notice $|u^*[j]| \leq U$ implies $|u[j]| \leq U$. We obtain the inequality (7.20) is from (7.10) and (7.19). Similarly, combining $y(t_k) = C_2 x[k]$, (7.8) and (7.13) to have

$$\begin{aligned}
|y(t_k)| &= \left| \sum_{i=0}^{k-1} C_2 R[k-i](e_u[i] + w[i]) + C_2 N[k-i] e_y[i] \right| \\
&\geq_+ |C_2\mathbf{R}|_{e.w.}(p_u + p_w) + |C_2\mathbf{N}|_{e.w.} p_y = Y \qquad (7.21)
\end{aligned}$$

Combining the property (1.8) with (7.15) to have

$$|e_y[k]| = \Big|y(t_k) - \mathbb{Q}_{L_y,Y} y(t_k)\Big| \geq_+ \text{invdiag}(L_y)Y = p_y \qquad (7.22)$$

Therefore, the set E is an invariant set of $\mathbf{e}_u, \mathbf{e}_y$. □

Corollary 7.3.3. *If the linear program $\mathcal{P}_{L_u,L_y,h}$ is feasible with solution (U, Y), then under the control law $(\hat{K}, \mathbb{Q}_{L_u,U}, \mathbb{Q}_{L_y,Y})$, both the state* $\mathbf{x}$ *and the ouput* $\mathbf{z}$ *are bounded.*

Proof. From Theorem 7.3.3 and initial condition $x(0) = 0$ (assumption D), we obtain $\|e_u\|_\infty \leq p_u, \|e_y\|_\infty \leq p_y$. Since $\hat{K}$ is a stabilizing controller for $\hat{G}$, the transfer matrices $\hat{R}, \hat{N}, \hat{M}, \hat{Q}$ from (7.8) are stable. From $\hat{x} = \hat{R}\hat{e}_u + \hat{N}\hat{e}_y + \hat{R}w$, $\hat{u} = \hat{M}\hat{e}_u + \hat{Q}\hat{e}_y + \hat{M}w$, we obtain that the sequences $\mathbf{x}$ and $\mathbf{u}$ are bounded. Therefore, the output sequence $\mathbf{z}$ is also bounded. □

7.4 Performance analysis of the obtained controller

Next, we bound the sub-optimality gap of the system performance. Recall from (7.5) that our goal is to achieve $\sup_{\|w\|_\infty \le 1} \|\mathbf{z}\|_\infty \le \nu$. Let ν_p be the value of $\sup_{\|w\|_\infty \le 1} \|z\|_\infty$ when the distributed controller $\hat{K}$ from (7.7) is used with perfect communication and no delay, *i.e.* $y[k] = y(t_k), u^*[k] = u[k]$ and $h = 0$. Let $\nu_c = \nu - \nu_p$, the performance criteria (7.5) is equivalent with

$$\sup_w \|z(t)\|_\infty \le \nu_p + \nu_c.$$

Intuitively, ν_c captures the performance degradation due to information sharing constraints, and ν_c due to unreliable communication. We assume $\nu_c > 0$.

Theorem 7.4.1. *Let*

$$\begin{aligned}
r_u &\triangleq |C_1|\{2\Psi_1(h)|\mathbf{M}|_{e.w} + \Psi_1(T)\big(invdiag(L_u) + I\big)|\mathbf{M}|_{e.w} \\
&\qquad + |e^{A\rho}\mathbf{R}|_{e.w.}\} + |C_2\mathbf{M}|_{e.w.} \\
r_y &\triangleq |C_1|\{2\Psi_1(h)|\mathbf{Q}|_{e.w} + \Psi_1(T)\big(invdiag(L_u) + I\big)|\mathbf{Q}|_{e.w})| \\
&\qquad + |e^{A\rho}\mathbf{N}|_{e.w.}\} + |C_2\mathbf{Q}|_{e.w} \\
r_w &\triangleq |C_1|\{2\Psi_1(h) + \Psi_1(T)\big(invdiag(L_u) + I\big)\}|\mathbf{M}|_{e.w.}
\end{aligned} \tag{7.23}$$

If the linear program $\mathcal{Q}_{L_u,L_y,h}$:

$$\begin{aligned}
&\underset{U,Y,p_u,p_y}{\textit{minimize}} && 0 \\
&\textit{subject to} && (7.11) - (7.15) \\
& && \max\{r_u p_u + r_y p_y + r_w p_w\} \le \nu_p
\end{aligned} \tag{7.24}$$

is feasible, then the overall performance is bounded by

$$\sup_w \|\mathbf{z}\|_\infty \le \nu_p + \nu_c. \tag{7.25}$$

In above theorem, the constraint (7.11) – (7.15) is same with the program $\mathcal{P}_{L_u,L_y,h}$, and it guarantees system stability. The additional constraint (7.24) is used for system performance.

Proof. In order to bound the value ν_c, we decompose the discrete state $x[k]$ into two terms: the term due to the disturbance $\mathbf{x}_p$, and the term due to unreliable

communication $\mathbf{x}_c$, *i.e.*

$$x_p[k] \triangleq \sum_{i=0}^{k} R[k-i]w[i] \quad x_c[k] \triangleq x[k] - x_p[k].$$

The controller output $u[k]$ also admits the decomposition:

$$u_p[k] \triangleq \sum_{i=0}^{k} M[k-i]w[i] \quad u_c[k] \triangleq u^*[k] - u_p[k].$$

The continuous counterparts of the four terms can be defined as follows: for any $\rho \in [0, T)$, let

$$\begin{aligned}
x_p(t_k+\rho) &\triangleq e^{A\rho}x_p[k] + \int_{t_k}^{t_k+\rho} e^{-A(\tau-t_k-T)}B_1 w(\tau)d\tau \\
&\quad + \int_{t_k}^{t_k+\rho} e^{A(\tau-t_k-T)}B_2 u_p[k]d\tau \\
x_c(t_k+\rho) &\triangleq e^{A\rho}x_c[k] \\
&\quad + \int_{t_k}^{t_k+\rho} e^{-A(\tau-t_k-T)}B_2(u(\tau)-u_p[k])d\tau \\
u_p(t_k+\rho) &\triangleq u_p[k] \\
u_c(t_k+\rho) &\triangleq u(t_k+\rho) - u_p[k].
\end{aligned}$$

This formulation satisfies $x(t) = x_p(t) + x_c(t)$ and $u(t) = u_p(t) + u_c(t)$. Now we use these terms to separately bound system output:

$$\begin{aligned}
\sup_w \|z(t)\|_\infty &\leq \sup_w \|C_1 x_p(t) + Du_p(t)\|_\infty \\
&\quad + \sup_w \|C_1 x_c(t)\|_\infty + \sup_w \|Du_c(t)\|_\infty.
\end{aligned}$$

First, notice that when the system has perfect communication and no actuation delay, the term $\mathbf{x}_p, \mathbf{u}_p$ remains same while the term $\mathbf{x}_c, \mathbf{u}_c$ becomes zero. Thus, the first term on the right hand side of (7.26) is $\sup_w \|C_1 x_p(t) + Du_p(t)\|_\infty = \nu_p$. Next, we bound the second term of (7.26) as follows:

$$\begin{aligned}
|x_c(t_k+\rho)| \leq_+ \Psi_1(\min(\rho, h))\Big|u[k-1] - u_p[k]\Big| \\
+ \Psi_1(T)\Big|u[k] - u_p[k]\Big| + \Big|e^{A\rho}x_c[k]\Big|.
\end{aligned}$$

We have

$$\begin{aligned}
&\Psi_1(\min(\rho, h))\Big|u[k-1] - u_p[k]\Big| \\
&\qquad \leq_+ \Psi_1(h)\Big(|u[k-1]| + |u_p[k]|\Big) \\
&\qquad \leq_+ 2\Psi_1(h)U,
\end{aligned}$$

where the first inequality is because each element of $\Psi_1(h)$ is an increasing function of h, the second inequality comes from $|\mathbf{u}| \leq_+ U, |\mathbf{u}_p| \leq_+ U$ (see proof of Theorem 7.3.3).

$$\begin{aligned}
&\Psi_1(T)\left|u[k] - u_p[k]\right| \\
&\qquad \leq_+ \Psi_1(T)\left(\,|u[k] - u^*[k]| + |u_c[k]|\,\right) \\
&\qquad \leq_+ \Psi_1(T)(\text{invdiag}(L_u) + I)U
\end{aligned}$$

$$\left|e^{A\rho}x_c[k]\right| \leq_+ |e^{A\rho}\mathbf{R}|_{e.w.}p_u + |e^{A\rho}\mathbf{N}|_{e.w.}p_y.$$

Combining above, we obtain

$$\begin{aligned}
|C_1 x_c(t_k + \rho)| \leq_+ |C_1|\Big\{&|e^{A\rho}\mathbf{R}|_{e.w.}p_u + |e^{A\rho}\mathbf{N}|_{e.w.}p_y \\
&+ 2\Psi_1(h)U + \Psi_1(T)(\text{invdiag}(L_u) + I)U\Big\}.
\end{aligned}$$

In a similar manner, we bound the third term of (7.26) by

$$|C_2 u_c[k]| \leq_+ |C_2\mathbf{M}|_{e.w.}p_u + |C_2\mathbf{Q}|_{e.w}p_y.$$

Therefore, from definition (7.23),

$$\sup_w \|C_1 x_c(t)\|_\infty + \sup_w \|Du_c(t)\|_\infty \leq_+ r_u p_u + r_y p_y + r_w p_w,$$

which combining with (7.24) yields $\sup_w \|\mathbf{z}\|_\infty \leq \nu_p + \max\{r_u p_u + r_y p_y + r_w p_w\} \leq \nu_p + \nu_c$. □

Chapter 8

APPLICATION TO SECURITY

Fault tolerance in Cyber-physical Systems (CPSs) is of great importance [27, 28, 41, 158, 179]. For example, in the power system, false data injection can introduce errors in state estimation and provide financial gains for attackers [114, 165, 204]. In flights, autonomous vehicles, and the Internet of Things, manipulations in software and sensing can cause human injury and economic damage [55, 127, 145].

Motivated by these security issues, in this chapter, we consider the fundamental limitation and achievable performance to achieve fault-tolerant estimation. By fault-tolerant estimation, we refer to achieving bounded estimation errors. Compared with fault identification, fault-tolerant estimation requires relaxed assumptions and accounts for potentially non-detectable and non-identifiable attacks in noisy systems. We prove that a necessary condition to achieve fault-tolerant estimation under ρ compromised sensors is that the system is 2ρ-detectable (the system needs to remain detectable after removing any set of 2ρ sensors). This necessary condition suggests that, if a system has many stable modes, then the number of sensors required to achieve fault-tolerant estimation is much smaller than that to achieve fault identification. Conversely, we propose a secure state estimator that guarantees bounded estimation error under the assumption of 2ρ-detectability. The proposed state estimator is inspired by robust control and FDI: that is, it consists of the local Luenberger estimators, the local residual detectors, and a global fusion process. A preliminary version of this chapter was presented at the 2015 IEEE Conference on Decision and Control, deriving the worst-case estimation errors in the ℓ_1 system [139]. This chapter extends the result of [139] to the $\mathcal{H}_2$ system and the $\mathcal{H}_\infty$ system. To the best of our knowledge, our chapter is the first to show that a mixture of two-norm bounded and sparse-unbounded input can produce *two-norm* bounded output. Finally, numerical examples show that the proposed state estimator has relatively low estimation errors among existing algorithms and average computation time for systems with a sufficiently small number of compromised sensors.

8.1 System model

We study the secure state estimation problem in the presence of sensor attacks. Consider the discrete-time LTI system:

$$\begin{aligned} x(t+1) &= Ax(t) + Bw(t), \qquad x(0) = 0 \\ y(t) &= Cx(t) + Dw(t) + a(t), \end{aligned} \tag{8.1}$$

where $x(t) \in \mathbb{R}^n$ is the system state, $w(t) \in \mathbb{R}^l$ is the input disturbance, $y(t) \in \mathbb{R}^m$ is the output measurement, and $a(t) \in \mathbb{R}^m$ is the bias injected by the adversary (we call $a(t)$ the *attack*). The time indices $t \in \mathbb{Z}_+$ are non-negative integers and start from zero. Without loss of generality, we assume that the disturbance matrix B has full row rank (otherwise we can perform the Kalman decomposition and work on the controllable space of (A, B)). Each sensor is indexed by $i \in \{1, \cdots, m\}$ and produces measurement $y_i(t)$, which jointly comprises the measurement vector $y(t) = [y_1(t), \ldots, y_m(t)]^T$. Sensor i is said to be *compromised* if $a_i(t) \neq 0$ at some time $t \in \mathbb{Z}_+$ and is said to be *benign* otherwise. The maximum number of sensors that the attacker can compromise is ρ, *i.e.*

$$\|a\|_0 \leq \rho. \tag{8.2}$$

If $a(t)$ satisfies (8.2), then we say that it is ρ-*sparse*. Let $\mathcal{S} \triangleq \{1, \ldots, m\}$ denote the set of all sensors, $\mathcal{C} \subset \mathcal{S}$ denote the set of compromised sensors, and $\mathcal{B} \triangleq \mathcal{S} \backslash \mathcal{C}$ denote the set of benign sensors. The set $\mathcal{C}$ is assumed to be unknown.[1] A causal state estimator is an infinite sequence of functions $\{f_t\}$, where f_t is a mapping from all output measurements to a state estimate:

$$\hat{x}(t) = f_t(y(0 : t-1)). \tag{8.3}$$

The estimation error of (8.3) is defined as the difference between the system state and the state estimate:[2]

$$e(t) \triangleq x(t) - \hat{x}(t). \tag{8.4}$$

We consider the input containing a mixture of a p-norm bounded disturbance and a ρ-sparse attack and study the following worst-case estimation error in q-norm:

$$\sup_{\|w\|_p \leq 1,\, \|a\|_0 \leq \rho} \|e\|_q, \tag{8.5}$$

[1] Take the setting of [147] for example. When the system is noisy, the optimization problem $\min_{x_t \in \mathbb{R}^n} \|[y(t)^T, \cdots, y(t+n-1)^T]^T - \mathcal{O} x_t\|$ ($\mathcal{O}$ is the observability matrix) may not give correct set of compromised sensors $\{i : \exists t, a_i(t) \neq 0\}$.

[2] Although abbreviate it as $e(t)$, the estimation error is also a function of disturbance w, attack a, and the estimator $\{f_t\}$.

where

$$(p, q) = (2, 2), (2, \infty), (\infty, \infty). \tag{8.6}$$

We consider (8.5) instead of attack isolation because the attack on a noisy system may not be correctable in the sense defined in [56, 147].

Definition 8.1.1. *An causal state estimator $\{f_t\}$ is said to be ϵ-resilient to attack if its worst-case estimation error satisfies* $\sup_{\|w\|_p \le 1,\, \|a\|_0 \le \rho} \|e\|_q < \epsilon$, *where ϵ is a positive and finite scalar.*

When the estimator is ϵ-resilient for some finite $\epsilon > 0$, then we say the state estimator is resilient to attack. The goal of this chapter is to study the design problem of a resilient state estimator $\{f_t\}$. Towards that end, we first show a fundamental limitation for the existence of a resilient estimator (Section 8.2), and we then propose a resilient estimator (Section 8.3) and analyze the estimation errors (Section 8.4).

Definition 8.1.2 (Projection map)**.** *Let e_i be the i_{th} canonical basis vector of the space $\mathbb{R}^m$ and $\mathcal{I} = \{i_1, \ldots, i_{m'}\} \subseteq \mathcal{S}$ be an index set with carnality $m'(\le m)$. We define the projection map $P_{\mathcal{I}} : \mathbb{R}^m \to \mathbb{R}^{m'}$ as*

$$P_{\mathcal{I}} = \begin{bmatrix} e_{i_1} & \ldots & e_{i_{m'}} \end{bmatrix}^T \in \mathbb{R}^{m' \times m}. \tag{8.7}$$

Using $P_{\mathcal{I}}$ in (8.7), the measurements of the set of sensors $\mathcal{I} \subset \mathcal{S}$ can be written as

$$y_{\mathcal{I}}(t) \triangleq P_{\mathcal{I}} y(t) \in \mathbb{R}^{m'}.$$

Similarly, the measurement matrix and the sensor noise matrix corresponding to the set of sensors $\mathcal{I}$ can be respectively written as

$$C_{\mathcal{I}} \triangleq P_{\mathcal{I}} C, \qquad\qquad D_{\mathcal{I}} \triangleq P_{\mathcal{I}} D.$$

8.2 Necessary condition for resilience to attack

In this section, we give a fundamental limitation for achieving bounded worst-case estimation errors.

Definition 8.2.1. *The system* (8.1) *is said to be χ-detectable if $(A, C_{\mathcal{K}})$ is detectable for any set of sensors $\mathcal{K} \subset \mathcal{S}$ with cardinality $|\mathcal{K}| = m - \chi$.*

Theorem 8.2.1. *If system* (8.1) *is not 2ρ-detectable, then there is no state estimator $\{f_t\}$ that is ϵ-resilient to attack for any finite $\epsilon > 0$.*

Theorem 8.2.1 implies that the following (denote as Condition A) is necessary for the existence of a resilient state estimator:

A. The system (8.1) is 2ρ-detectable.

An intermediate step in the proof of Theorem 8.2.1 is to consider the following condition (denote as Condition B).

B. There exist two states (x, x'), two disturbances (w, w'), and two attacks (a, a') such that all of the followings are satisfied:

   a) both (x, w, a) and (x', w', a') satisfies the dynamics (8.1) and assumptions $\|a\|_0 \leq r$, and $\|w\|_p \leq 1$

   b) $y(t) = y(t)'$ at all time $t \in \mathbb{N}$

   c) the difference between the two states is unbounded, *i.e.* $\|x - x'\|_q = \infty$.

Lemma 8.2.1. *If $(A, C_{\mathcal{K}})$ is not detectable for some set $\mathcal{K} \subset \mathcal{S}$ with $|\mathcal{K}| = m - 2r$, then Condition B holds.*

Proof. (Lemma 8.2.1) We first prove that an undetectable $(A, C_{\mathcal{K}})$ implies that the linear transformation $O_t : \mathbb{R}^n \to \mathbb{R}^{t(m-2r)}$ defined by

$$O_t = \begin{bmatrix} C_{\mathcal{K}} \\ C_{\mathcal{K}} A \\ C_{\mathcal{K}} A^2 \\ \vdots \\ C_{\mathcal{K}} A^{t-1} \end{bmatrix}$$

has a non-trivial kernel (Step 1). Form the kernel space of O_t, we then find two states (x, x') that satisfy condition B (Step 2).

Step 1: If $(A, C_{\mathcal{K}})$ is not detectable for some set of sensors $\mathcal{K}$, then at least one of the following conditions holds.

(i) For some $z \in \mathbb{R}$, $\text{abs}(z) \geq 1$ and $v \in \mathbb{R}^n$, $Av = zv$ and $Cv = 0$.

(i) For some complex conjugate pairs $z, \bar{z} \in \mathbb{C}$, $\text{abs}(z) = \text{abs}(\bar{z}) \geq 1$ and $v, \bar{v} \in \mathbb{C}^n$, $Av = zv$, $A\bar{v} = \bar{z}\bar{v}$, $Cv = 0$, and $C\bar{v} = 0$.

Condition (i) implies that

$$\mathcal{O}_t v = 0, \qquad t \in \mathbb{N} \tag{8.8}$$

and Condition (i) implies that

$$\mathcal{O}_t(v + \bar{v}) = 0, \qquad t \in \mathbb{N}. \tag{8.9}$$

Step2: We construct two dynamics with the same measurement. There exists two disjoint sets of sensors $\mathcal{K}_1, \mathcal{K}_2$ that satisfy $|\mathcal{K}_1| = |\mathcal{K}_2| = r$, $\mathcal{K}_1 \cap \mathcal{K}_2 \cap \mathcal{K} = \emptyset$, and $\mathcal{K} \cup \mathcal{K}_1 \cup \mathcal{K}_2 = \mathcal{S}$. Consider first when condition (i) holds. Since B has full-rank, there exists an impulse disturbance $w(0)$ that produces

$$\begin{aligned} &x(1) = v, \\ &w(t) = 0, t \geq 1 \\ &a_i(t) = \begin{cases} -C_i x(t) & i \in \mathcal{K}_1 \\ 0 & \text{Otherwise} \end{cases} \end{aligned} \tag{8.10}$$

and

$$\begin{aligned} &x'(1) = 0 \\ &w'(t) = 0, t \geq 1 \\ &a_i'(t) = \begin{cases} C_i x(t) & i \in \mathcal{K}_2 \\ 0 & \text{Otherwise,} \end{cases} \end{aligned} \tag{8.11}$$

where C_i denotes the i-th row of sensing matrix C. Using (8.8), we can show that measurement $y(t)$ under (8.10) and $y'(t)$ under (8.11) are identical. However, the state under (8.10) is $x(t) = z^t v$, the state under (8.10) is $x'(t) = 0$, and thus their difference $\|x - x'\|_q$ is unbounded. Consider next when condition (ii) holds. There exists an impulse disturbance $w(0)$ that achieves $x(1) = v + \bar{v}$, so let $x(1) = v + \bar{v}$ replace $x(1)$ in (8.10). Similarly, we can derive from (8.9) that measurements $y(t)$ and $y'(t)$ are identical, but $x(t) = z^t v + \bar{z}^k \bar{v}$ and $x'(t) = 0$, yielding unbounded $\|x - x'\|_q$. Since at least (i) or (ii) holds, we have proved Condition B.

□

Lemma 8.2.2. *If Condition E holds, then a resilient estimator cannot be constructed.*

Proof (Lemma 8.2.2). Let $\hat{x}$ be the state estimation of any estimator when measurement $y = y'$ is observed. From the the triangle inequality, the estimation error

$e = x - \hat{x}$ under (x, w, a, y) and error $e' = x' - \hat{x}$ under (x', w', a', y') satisfies

$$\|x - x'\|_q \leq \|e\|_q + \|e'\|_q \tag{8.12}$$

This suggests that either $\|e\|_q$ or $\|e'\|_q$ are unbounded. Because

$$\sup_{\|w\|_p \leq 1,\, \|a\|_0 \leq r} \|e\|_q \geq \max\{\|e\|_q, \|e'\|_q\}, \tag{8.13}$$

no estimator can achieve bounded worst-case estimation error. □

Proof (Theorem 8.2.1). From Lemma 8.2.1, if $(A, C_{\mathcal{K}})$ being not detectable for some set $\mathcal{K} \subset \mathcal{S}$ with $|\mathcal{K}| = m - 2r$, then Condition B holds. However, due to Lemma 8.2.2, Condition B implies that no resilient estimator can be constructed. □

8.3 The proposed estimator

Assuming condition A, we now propose a resilient state estimator. The proposed estimator constitutes two procedures: 1) local estimation and 2) global fusion. The local estimators are defined by groups of $m - \rho$ sensors for all combinations

$$\mathcal{V} \triangleq \{\mathcal{I} \subset \mathcal{S} : |\mathcal{I}| = m - \rho\}.$$

The number of such groups (local estimators) is $|\mathcal{V}| = \binom{m}{\rho}$. Each local estimator $\mathcal{I}$ generates a state estimation $\hat{x}^{\mathcal{I}}$ separately based on the measurements of its sensors $y_{\mathcal{I}}$. In the global fusion process, the state estimate $\hat{x}$ is generated using the estimates from all local estimators $\mathcal{I} \in \mathcal{V}$. With slight overlap of notation, we use $\mathcal{I} \in \mathcal{V}$ to refer to a set of sensors as well as to the estimator that uses these sensors. Next, we outline these procedures and formally state the estimator in Algorithm 1.

Local estimations

From Assumption A, for any set of sensors $\mathcal{I} \in \mathcal{V}$, there exists a matrix $K^{\mathcal{I}} \in \mathbb{R}^{(m-\rho)\times n}$ such that $A + K^{\mathcal{I}} C_{\mathcal{I}}$ is strictly stable (has all eigenvectors in the open unit circle).[3] Using this matrix $K^{\mathcal{I}}$, we construct a local estimator that only uses measurements from the set of sensors $\mathcal{I}$ to produce a *local state estimate* $\hat{x}^{\mathcal{I}}$:[4]

$$\hat{x}^{\mathcal{I}}(t+1) = A\hat{x}^{\mathcal{I}}(t) - K^{\mathcal{I}}(y_{\mathcal{I}}(t) - C_{\mathcal{I}}\hat{x}^{\mathcal{I}}(t)) \tag{8.14}$$

[3] One way to find the matrix K is via the Riccati equation, *i.e.* $K^{\mathcal{I}} = PC_{\mathcal{I}}^T(C_{\mathcal{I}}PC_{\mathcal{I}}^T + D_{\mathcal{I}}D_{\mathcal{I}}^T)^{-1}$, where P is unique stabilizing solution of the discrete-time algebraic Riccati equation $P = A(P - PC_{\mathcal{I}}^T(C_{\mathcal{I}}PC_{\mathcal{I}}^T + D_{\mathcal{I}}D_{\mathcal{I}}^T)^{-1}C_{\mathcal{I}}P)A^T + BB^T$. Sufficient conditions the existence of solution P is that $(A, C_{\mathcal{I}})$ is detectable and (A, BB^T) is detectable.

[4] We use superscript notations for original vectors and matrices (*e.g.* $K^{\mathcal{I}}$ and $x^{\mathcal{I}}$, respectively) and subscript for vectors and matrices projected by (8.7) (*e.g.* $y_{\mathcal{I}}$ and $C_{\mathcal{I}}$, respectively).

with the initial condition $\hat{x}^{\mathcal{I}}(0) = 0$. The estimation error and residual vector of (8.14) is respectively defined as

$$e^{\mathcal{I}}(t) \triangleq x(t) - \hat{x}^{\mathcal{I}}(t) \tag{8.15}$$

$$r^{\mathcal{I}}(t) \triangleq y_{\mathcal{I}}(t) - C_{\mathcal{I}}\hat{x}^{\mathcal{I}}(t). \tag{8.16}$$

The LTI system from w to $e^{\mathcal{I}}$ is $E^{\mathcal{I}}(K^{\mathcal{I}})$ defined in (1.9), whereas the LTI system from w to $r^{\mathcal{I}}$ is $G^{\mathcal{I}}(K^{\mathcal{I}})$ defined in (1.10).

When the set $\mathcal{I}$ does not contain any compromised sensors, *i.e.* $a_{\mathcal{I}} = 0$, the residual vector $r^{\mathcal{I}}(t)$ is determined by disturbance w alone and is bounded by

$$\|r^{\mathcal{I}}\|_q \leq \|G^{\mathcal{I}}(K^{\mathcal{I}})\|_{p\to q}. \tag{8.17}$$

Condition (8.17) can only be violated when the set $\mathcal{I}$ contains compromised sensors, so (8.17) is a necessary condition for all the sensors in set $\mathcal{I}$ to be benign. The local estimator at time t uses the necessary condition (8.17) to determine the validity of its estimate and label local estimator $\mathcal{I}$ to be *invalid* upon observing $\|r^{\mathcal{I}}(0:t)\|_q > \|G^{\mathcal{I}}(K^{\mathcal{I}})\|_{p\to q}$.

Global fusion

From above, the set of valid local estimators $\mathcal{I} \in \mathcal{V}(t)$ is characterized as

$$\mathcal{V}(t) \triangleq \left\{\mathcal{I} \in \mathcal{S} : \|r^{\mathcal{I}}(0:t)\|_q \leq \|G^{\mathcal{I}}(K^{\mathcal{I}})\|_{p\to q}\right\}. \tag{8.18}$$

Using $\mathcal{V}(t)$, we compute the *global state estimate* as follows: $\hat{x}(t) = [\hat{x}_1(t), \hat{x}_2(t), \cdots, \hat{x}_n(t)]$, where

$$\hat{x}_i(t) = \begin{cases} \dfrac{1}{2}\left(\min\limits_{\mathcal{I}\in\mathcal{V}(t)} \hat{x}_i^{\mathcal{I}}(t) + \max\limits_{\mathcal{J}\in\mathcal{V}(t)} \hat{x}_i^{\mathcal{J}}(t)\right) & q = \infty \\ \dfrac{1}{|\mathcal{V}(t)|}\displaystyle\sum_{\mathcal{I}(t)\in\mathcal{V}(t)} \hat{x}_i^{\mathcal{I}}(t) & q = 2. \end{cases} \tag{8.19}$$

Algorithm 4 The Proposed State Estimator

Initialize $\mathcal{V}(0) \leftarrow \mathcal{V}$ and $\hat{x}^{\mathcal{I}}(0) \leftarrow 0, \mathcal{I} \in \mathcal{V}(0)$
for $t \in \mathbb{N}$ **do**
  for $\mathcal{I} \in \mathcal{V}(t-1)$ (Local Estimation) **do**
    Initialize $\mathcal{V}(t) \leftarrow \emptyset$
    Determine $\hat{x}^{\mathcal{I}}(t)$ from (8.14) and $r^{\mathcal{I}}(t)$ from (8.16)
    if $\|r^{\mathcal{I}}(0:t)\|_q \leq \|G^{\mathcal{I}}(K^{\mathcal{I}})\|_{p\to q}$ **then**
      $\mathcal{V}(t) \leftarrow \{\mathcal{V}(t), \mathcal{I}\}$
    end if
  end for
  Obtain estimate $\hat{x}(t)$ from (8.19) (Global Fusion)
end for

8.4 Resilience of the proposed estimator

Previous works have shown that there exist estimators that can detect the attacks and recover the exact state for noiseless systems if the system is 2ρ-observable [56, Proposition 2][38, Theorem 1][172, Theorem 3.2]. In this section, we show that the proposed estimator is resilient to attack when the system is 2ρ-detectable.

Theorem 8.4.1. *The estimator in Algorithm 1 has a bounded estimation error. In particular, the estimation error is upper-bounded by*

$$\begin{aligned}
&\max_{\mathcal{I}\in\mathcal{V}} \|E^{\mathcal{I}}(K^{\mathcal{I}})\|_\infty + \max_{\mathcal{I},\mathcal{J}\in\mathcal{V}} \sqrt{\tfrac{1}{2}\log|\mathcal{V}|}\, \mathcal{D}^{\mathcal{I},\mathcal{J}}_{2,2} && \text{if } (p,q) = (2,2)\\
&\max_{\mathcal{I},\mathcal{J}\in\mathcal{V}} \left(\|E^{\mathcal{I}}(K^{\mathcal{I}})\|_2 + \tfrac{1}{2}\mathcal{D}^{\mathcal{I},\mathcal{J}}_{2,\infty}\right) && \text{if } (p,q) = (2,\infty)\\
&\max_{\mathcal{I},\mathcal{J}\in\mathcal{V}} \left(\|E^{\mathcal{I}}(K^{\mathcal{I}})\|_1 + \tfrac{1}{2}\mathcal{D}^{\mathcal{I},\mathcal{J}}_{\infty,\infty}\right) && \text{if } (p,q) = (\infty,\infty).
\end{aligned}$$

In the above formula, the term $\mathcal{D}^{\mathcal{I},\mathcal{J}}_{p,q}$ is defined as

$$\begin{aligned}
\mathcal{D}^{\mathcal{I},\mathcal{J}}_{p,q} &= \alpha^{\mathcal{I}\cap\mathcal{J}}_{p,q}\left(\beta^{\mathcal{I},\mathcal{I}\cap\mathcal{J}}_{p,q} + \beta^{\mathcal{J},\mathcal{I}\cap\mathcal{J}}_{p,q}\right)\\
\alpha^{\mathcal{K}}_{p,q} &\triangleq \inf_{K: A+KC_{\mathcal{K}} \text{ strictly stable}} \left\| \left[\begin{array}{c|c} A+KC_{\mathcal{K}} & \begin{bmatrix} I & K \end{bmatrix} \\ \hline I & 0 \end{array}\right] \right\|_{p\to q}\\
\beta^{\mathcal{I},\mathcal{K}}_{p,q} &\triangleq \left\| \begin{bmatrix} -K^{\mathcal{I}} \\ P_{\mathcal{K},\mathcal{I}} \end{bmatrix} \right\|_{p\to q} \|r^{\mathcal{I}}(0:T)\|_p,
\end{aligned}$$

where $P_{\mathcal{K},\mathcal{I}} \in \mathbb{R}^{|\mathcal{K}|\times|\mathcal{I}|}$ is the unique solution of $P_{\mathcal{K}} = P_{\mathcal{K},\mathcal{I}} P_{\mathcal{I}}$, and $\|\cdot\|_{p\to q}$ is an induced norm on matrix.

An immediate consequence of Theorem 8.4.1 is that condition A is a necessary and sufficient condition for the construction of a resilient state estimator, and that

Algorithm 1 resilient to attack. The estimation error upper-bound in Theorem 8.4.1 decomposes into two terms: $\|E^{\mathcal{I}}(K^{\mathcal{I}})\|_{p\to q}$ and the remaining. The first term $\|E^{\mathcal{I}}(K^{\mathcal{I}})\|_{p\to q}$ characterize the error between a local estimator and the true state. That is, if the local estimator $\mathcal{I}$ is used for a system with no attack ($a \equiv 0$), then its estimation error is bounded by $\|E^{\mathcal{I}}(K^{\mathcal{I}})\|_{p\to q}$. The second term exists due to the attack in an unknown set of sensors. When $(p, q) = (2, 2)$, the error upper-bound grows at the order $o(\sqrt{\rho \log m})$ for $m \to \infty$. Therefore, the error can be kept small even for systems with large m. Moreover, it shall be noted that an increase in the tolerable number of compromised sensors ρ may result in an increase in both terms, thus increasing the worst-case estimation error $\sup_{\|w\|_p \le 1, \|a\|_0 = 0} \|e\|_q$.

Corollary 8.4.1. *A necessary and sufficient condition for the existence of an ϵ-resilient estimator for some finite $\epsilon > 0$ is that $(A, C_{\mathcal{K}})$ is detectable for any index set $\mathcal{K} \subset \mathcal{S}$ with cardinality $m - 2\rho$.*

Corollary 8.4.2. *Consider system (8.1) with ρ-sparse attack. The state estimator in Algorithm 1 is ϵ-resilient to attack for some finite $\epsilon > 0$.*

The proof of Theorem 8.4.1 has two procedures: 1) bounding local estimation errors, and 2) bounding global fusion errors. Specifically, from the triangular inequality, at any time $t \in \mathbb{Z}_+$, the estimation error satisfies

$$\begin{aligned} \|e\|_q &= \left\|(x - \hat{x}^{\mathcal{I}}) + (\hat{x}^{\mathcal{I}} - \hat{x})\right\|_q \\ &\le \left\|x - \hat{x}^{\mathcal{I}}\right\|_q + \left\|\hat{x}^{\mathcal{I}} - \hat{x}\right\|_q, \end{aligned} \tag{8.20}$$

where $\mathcal{I} \in \mathcal{B} \subset \mathcal{V}$ is a set that only contains benign sensors (denote $\mathcal{I}$ as the *benign estimator*). The benign estimator $\mathcal{I}$ exists from assumption (8.2). The first term $\|x - \hat{x}^{\mathcal{I}}\|_q$ can be bounded using Lemma 1.5.1 by

$$\|x - \hat{x}^{\mathcal{I}}\|_q \le \|E^{\mathcal{I}}(K^{\mathcal{I}})\|_{p\to q}. \tag{8.21}$$

Now it only remains to show that the second term is bounded.

To bound the second term, we first bound the difference between the estimates of any two valid local estimators $\mathcal{J}_1, \mathcal{J}_2 \in \mathcal{V}(T)$ up to time $T \in \mathbb{Z}_+$, which is given in Lemma 8.4.1. We then use Lemma 8.4.1 to show that the difference between the estimates of the benign estimator $\mathcal{I} \in \mathcal{V}$ and the global estimator is finite. This is shown in Lemma 8.4.3 for $(p, q) = (2, 2)$ and in Lemma 8.4.8 for $(p, q) = (2, \infty), (\infty, \infty)$. In these lemmas, each set of sensors in $\mathcal{V}$ are labeled into

$$\mathcal{J}_1, \mathcal{J}_2, \cdots, \mathcal{J}_{|\mathcal{V}|}. \tag{8.22}$$

Lemma 8.4.1. *Assume that Condition A holds. Let $\mathcal{J}_1$, $\mathcal{J}_2 \in \mathcal{V}(T)$ be two sets of sensors that are valid at time T. The divergence between the local estimator $\mathcal{J}_1$ and $\mathcal{J}_2$ up to time T satisfies*

$$\|\hat{x}^{\mathcal{J}_1}(0:T) - \hat{x}^{\mathcal{J}_2}(0:T)\|_q \leq \mathcal{D}_{p,q}^{\mathcal{J}_1,\mathcal{J}_2}, \tag{8.23}$$

where right hand side is finite, i.e. $\mathcal{D}_{p,q}^{\mathcal{J}_1,\mathcal{J}_2} < \infty$.

Proof (Lemma 8.4.1). Let $\mathcal{J}_1$, $\mathcal{J}_2 \in \mathcal{V}(T)$. We first compute the dynamics of the local estimates $\hat{x}^{\mathcal{J}_i}(t)$, $i = 1, 2$. From (8.14) and (8.16),

$$\begin{aligned} \hat{x}^{\mathcal{J}_i}(t+1) &= A\hat{x}^{\mathcal{J}_i}(t) - K^{\mathcal{J}_i} r^{\mathcal{J}_i}(t), \hat{x}^{\mathcal{J}_i}(0) = 0 \\ y_{\mathcal{J}_i}(t) &= C_{\mathcal{J}_i}\hat{x}^{\mathcal{J}_i}(t) + r^{\mathcal{J}_i}(t) \end{aligned} \tag{8.24}$$

for $t \leq T$. We define the sequences $\phi^{\mathcal{J}_i}(t)$ and $\varphi^{\mathcal{J}_i}(t)$ by

$$\phi^{\mathcal{J}_i}(t) \triangleq -K^{\mathcal{J}_i} r^{\mathcal{J}_i}(t), \qquad \varphi^{\mathcal{J}_i}(t) \triangleq P_{\mathcal{K}_{1,2},\mathcal{J}_i} r^{\mathcal{J}_i}(t),$$

where $P_{\mathcal{K}_{1,2},\mathcal{J}_i} \in \mathbb{R}^{|\mathcal{K}_{1,2}|\times|\mathcal{J}_i|}$ is the unique solution of $P_{\mathcal{K}_{1,2}} = P_{\mathcal{K}_{1,2},\mathcal{J}_i} P_{\mathcal{J}_i}$. Let $\mathcal{K}_{1,2} = \mathcal{J}_1 \cap \mathcal{J}_2$ the intersection between the two sets $\mathcal{J}_1, \mathcal{J}_2$. As the measurements from subset $\mathcal{K}_{1,2} \subset \mathcal{J}_i$ also satisfies $y_{\mathcal{K}_{1,2}}(t) = C_{\mathcal{K}_{1,2}}\hat{x}^{\mathcal{J}_i}(t) + P_{\mathcal{K}_{1,2},\mathcal{J}_i} r^{\mathcal{J}_i}(t)$, combining with (8.24) yields

$$\begin{aligned} \hat{x}^{\mathcal{J}_i}(t+1) &= A\hat{x}^{\mathcal{J}_i}(t) + \begin{bmatrix} I & 0 \end{bmatrix} \begin{bmatrix} \phi^{\mathcal{J}_i}(t) \\ \varphi^{\mathcal{J}_i}(t) \end{bmatrix}, \ \hat{x}^{\mathcal{J}_i}(0) = 0 \\ y_{\mathcal{K}_{1,2}}(t) &= C_{\mathcal{K}_{1,2}}\hat{x}^{\mathcal{J}_i}(t) + \begin{bmatrix} 0 & I \end{bmatrix} \begin{bmatrix} \phi^{\mathcal{J}_i}(t) \\ \varphi^{\mathcal{J}_i}(t) \end{bmatrix}. \end{aligned} \tag{8.25}$$

Now, let $\Delta(t)$ be the difference between the local estimator $\mathcal{J}_1$ and local estimator $\mathcal{J}_2$, *i.e.*

$$\Delta(t) \triangleq \hat{x}^{\mathcal{J}_1}(t) - \hat{x}^{\mathcal{J}_2}(t). \tag{8.26}$$

Subtracting the (8.25) for $\mathcal{J}_1$ from (8.25) for $\mathcal{J}_2$, we obtain the dynamics of Δ as follows:

$$\begin{aligned} \Delta(t+1) &= A\Delta(t) + \begin{bmatrix} I & 0 \end{bmatrix} \begin{bmatrix} \phi^{\mathcal{J}_1}(t) - \phi^{\mathcal{J}_2}(t) \\ \varphi^{\mathcal{J}_1}(t) - \varphi^{\mathcal{J}_2}(t) \end{bmatrix}, \ \Delta(t) = 0, \\ 0 &= C_{\mathcal{K}_{1,2}}\Delta(t) + \begin{bmatrix} 0 & I \end{bmatrix} \begin{bmatrix} \phi^{\mathcal{J}_1}(t) - \phi^{\mathcal{J}_2}(t) \\ \varphi^{\mathcal{J}_1}(t) - \varphi^{\mathcal{J}_2}(t) \end{bmatrix}. \end{aligned}$$

Because a valid set satisfies (8.18), the residual vectors of estimator $\mathcal{J}_i$, $i = 1, 2$, are bounded by $\|r^{\mathcal{J}_i}(0:T)\|_q \le \|G^{\mathcal{J}_i}(K^{\mathcal{J}_i})\|_{p\to q}$, which results in

$$\left\|\begin{bmatrix}\phi^{\mathcal{J}_i}(0:T)\\ \varphi^{\mathcal{J}_i}(0:T)\end{bmatrix}\right\|_p \le \left\|\begin{bmatrix}-K^{\mathcal{J}_i}\\ P_{\mathcal{K}_{1,2},\mathcal{J}_i}\end{bmatrix}\right\|_{p\to p} \|r^{\mathcal{J}_i}(0:T)\|_p = \beta_{p,q}^{\mathcal{J}_i,\mathcal{J}_1\cap\mathcal{J}_2}. \tag{8.27}$$

From the triangle inequality, we obtain

$$\left\|\begin{bmatrix}\phi^{\mathcal{J}_1}(0:T)-\phi^{\mathcal{J}_2}(0:T)\\ \varphi^{\mathcal{J}_1}(0:T)-\varphi^{\mathcal{J}_2}(0:T)\end{bmatrix}\right\|_p \le \beta_{p,q}^{\mathcal{J}_1,\mathcal{J}_1\cap\mathcal{J}_2} + \beta_{p,q}^{\mathcal{J}_2,\mathcal{J}_1\cap\mathcal{J}_2}.$$

Substitute $\phi^{\mathcal{J}_1} - \phi^{\mathcal{J}_2}$ for u in Lemma 8.4.2 and $\Delta(t)$ for x, and we obtain

$$\|\hat{x}^{\mathcal{J}_1}(0:T) - \hat{x}^{\mathcal{J}_2}(0:T)\|_q \le \alpha_{p,q}^{\mathcal{J}_1\cap\mathcal{J}_2}(\beta_{p,q}^{\mathcal{J}_1,\mathcal{J}_1\cap\mathcal{J}_2} + \beta_{p,q}^{\mathcal{J}_1,\mathcal{J}_1\cap\mathcal{J}_2}).$$

□

In the proof of Lemma 8.4.1, we use the following lemma.

Lemma 8.4.2. *Consider system (1.3) where (A, C) is detectable and $\|w\|_p \le 1$. If $y(t) = 0$ for all $t = 0, 1, \cdots, T$, then*

$$\|x(0:T)\|_q \le \inf_{K:A+KC \text{ strictly stable}} \|E(K)\|_{p\to q}, \tag{8.28}$$

where $E(K)$ is given in (1.9).

Proof (Lemma 8.4.2). As (A, C) is detectable, $A + KC$ is strictly stable for some matrix K. For such stabilizing K, we can construct the state estimator (1.8). Since $y(0:T) = 0$, the state estimator (1.8) produces zero estimate $\hat{x}(0:T) = 0$. From Lemma 1.5.1, we obtain

$$\|x(0:T)\|_q = \|e(0:T)\|_q \le \|E(K)\|_{p\to q}.$$

Taking infimum over all K such that $A + KC$ is strictly stable, we obtain (8.28). □

Lemma 8.4.3. *If condition* (8.23) *holds for $(p, q) = (2, 2)$ at all time $T \in \mathbb{Z}_+$, then the divergence between the benign estimator $\mathcal{I}$ and the global estimator satisfies*

$$\|\hat{x}^{\mathcal{I}} - \hat{x}\|_2 \le \max_{\mathcal{J}_1,\mathcal{J}_2\in\mathcal{V}} \sqrt{\frac{1}{2}\log|\mathcal{V}|}\; \mathcal{D}_{p,q}^{\mathcal{J}_1,\mathcal{J}_2}. \tag{8.29}$$

Define the following two optimization problems:

$$\begin{aligned}
\mathcal{P}_\delta(n) := \max_{z_k(i)\geq 0} & \sum_{i=1}^{n} \left(\frac{1}{n-i-1}\right)^2 \left(\sum_{k=i}^{n} z_k(i)\right)^2 \\
\text{s.t.} \quad & \sum_{i=0}^{k} (z_k(i))^2 \leq \delta, \quad k = 1, 2, \ldots, n \\
\mathcal{D}_\delta(n) := \min_{\lambda_i > 0} & \sum_{i=1}^{n} \lambda_i \\
\text{s.t.} \quad & \sum_{i=1}^{j} \frac{1}{\lambda_i} \leq (j+1)^2, \quad j = 1, 2, \ldots, n.
\end{aligned}$$

With the slight abuse of notation, we will also denote $\mathcal{P}_\delta(n)$, $\mathcal{D}_\delta(n)$ as the optimal solutions of the optimization problem $\mathcal{P}_\delta(n)$, $\mathcal{D}_\delta(n)$, respectively. We first show that $\mathcal{P}_\delta(N-1)$ with

$$\delta = \max_{\mathcal{J}_1, \mathcal{J}_2 \in \mathcal{V}} \left(\mathcal{D}_{2,2}^{\mathcal{J}_1, \mathcal{J}_2}\right)^2 \tag{8.30}$$

is an upper-bound of $\|\hat{x}^{\mathcal{I}} - \hat{x}\|_2$ (Lemma 8.4.4). The problem $\mathcal{P}_\delta(n)$ is then converted into its dual problem $\mathcal{D}_\delta(n)$, between which the duality gap is zero (Lemma 8.4.5). The dual problem $\mathcal{D}_\delta(n)$ admits an analytical solution that can be upper-bounded by a simple formula (Lemma 8.4.7).

Lemma 8.4.4. *If condition* (8.23) *holds for* $(p, q) = (2, 2)$*, then the divergence between the benign estimator* $\mathcal{I}$ *and the global estimator satisfies*

$$\|\hat{x}^{\mathcal{I}} - \hat{x}\|_2^2 \leq \mathcal{P}_\delta(N-1), \tag{8.31}$$

where $N = |\mathcal{V}|$ *and* $\delta = \max_{\mathcal{J}_1, \mathcal{J}_2 \in \mathcal{V}} \left(\mathcal{D}_{2,2}^{\mathcal{J}_1, \mathcal{J}_2}\right)^2$.

Proof (Lemma 8.4.4). In order to relate the infinite sequence $\hat{x}^{\mathcal{I}}(t) - \hat{x}(t)$ with the finite-dimensional optimization problems $\mathcal{P}_\delta(n)$, we first divide the infinite time horizon into a finite sequence as below. Let T_i be the time the set $\mathcal{I}_i$ becomes invalid and $T_0 = 0$. Without loss of generality, we assume that

$$T_1 \leq T_2 \leq \cdots \leq T_{N-1} \leq T_N = \infty.$$

The relation $T_N = \infty$ holds because $\mathcal{I}_N$ is a valid from assumption (8.2). We call $\mathcal{I}_N$ the *benign estimator*. If $T_i = \infty$, then we define $\{x^{\mathcal{I}_i}(t)\}_{t \in \mathbb{Z}_+}$ as an infinite sequence

of points in $\mathbb{R}^n$. Otherwise, if T_i is finite, then we define $\{x^{\mathcal{I}_i}(t)\}_{t=0,\ldots,T_i}$ as a finite sequence of length $T_i + 1$.

Recall that $\mathcal{I}_N$ is the benign estimator. Let $\triangle^{\mathcal{I}_k}(t) = \hat{x}^{\mathcal{I}_N}(t) - \hat{x}^{\mathcal{I}_k}(t)$ denote the difference between the benign estimator $\mathcal{I}_N$ and other local estimator $\mathcal{I}_k$. We first define the following variable:

$$z_k(i) = \|\triangle^{\mathcal{I}_k}(T_i + 1 : T_{i+1})\|_2,$$

where $k = 1, \cdots, N-1$ and $i = 0, \cdots, k$.

Using $z_k(i)$, we can bound the estimation error between the local estimator $\mathcal{I}_N$ and the global estimator as follows:

$$\begin{aligned}
&\|\hat{x}^{\mathcal{I}_N} - \hat{x}\|_2^2 \\
&= \sum_{t=0}^{\infty} \|\hat{x}^{\mathcal{I}_N}(t) - \hat{x}(t)\|_2^2 \\
&= \sum_{i=0}^{N-2} \sum_{t=T_i+1}^{T_{i+1}} \left\| \hat{x}^{\mathcal{I}_N}(t) - \frac{1}{|\mathcal{V}(t)|} \sum_{j=i+1}^{N} \hat{x}^{\mathcal{I}_j}(t) \right\|_2^2 \\
&= \sum_{i=0}^{N-2} \sum_{t=T_i+1}^{T_{i+1}} \left\| \frac{1}{N-i} \sum_{k=i+1}^{N-1} \left(\hat{x}^{\mathcal{I}_N}(t) - \hat{x}^{\mathcal{I}_k}(t) \right) \right\|_2^2 \\
&= \sum_{i=0}^{N-2} \left(\frac{1}{N-i} \right)^2 \left\| \sum_{k=i+1}^{N-1} \triangle^{\mathcal{I}_k}(T_i + 1 : T_{i+1}) \right\|_2^2 \\
&\leq \sum_{i=0}^{N-2} \left(\frac{1}{N-i} \right)^2 \left(\sum_{k=i+1}^{N-1} \left\| \triangle^{\mathcal{I}_k}(T_i + 1 : T_{i+1}) \right\|_2 \right)^2 \\
&= \sum_{i=0}^{N-2} \left(\frac{1}{N-i} \right)^2 \left(\sum_{k=i+1}^{N-1} z_k(i) \right)^2 .
\end{aligned}$$

The sum of i and j counts only up to $N-1$ since $\hat{x}(t) = \hat{x}^{\mathcal{I}_N}(t)$ for $t > T_{N-1} + 1$. We also used Cauchy Schwarz inequality in the second to last line. Using the above relation, $\|\hat{x}^{\mathcal{I}_N} - \hat{x}\|_2^2$ is upper-bounded by the optimal value of the following problem:

$$\begin{aligned}
\max_{z_k(i) \geq 0} \quad & \sum_{i=0}^{N-2} \left(\frac{1}{N-i} \right)^2 \left(\sum_{k=i+1}^{N-1} z_k(i) \right)^2 \\
\text{s.t.} \quad & \sum_{i=0}^{k} (z_k(i))^2 \leq \max_{\mathcal{J}_1, \mathcal{J}_2 \in \mathcal{V}} \left(\mathcal{D}_{2,2}^{\mathcal{J}_1, \mathcal{J}_2} \right)^2, k = 1, \ldots, N-1,
\end{aligned} \tag{8.32}$$

which is the optimization problem $\mathcal{P}_\delta(N-1)$ with $\delta = \max_{\mathcal{J}_1,\mathcal{J}_2\in\mathcal{V}} \left(\mathcal{D}_{2,2}^{\mathcal{J}_1,\mathcal{J}_2}\right)^2$. □

Lemma 8.4.5. *The problems $\mathcal{P}_\delta(n)$, $\mathcal{D}_\delta(n)$ have identical optimal values, i.e. $\mathcal{P}_\delta(n) = \mathcal{D}_\delta(n)$.*

We use the following lemma to prove Lemma 8.4.5.

Lemma 8.4.6. *The following two inequalities are equivalent*

$$\Lambda = diag(\lambda_1, \lambda_2, \cdots, \lambda_n) \geq \mathbf{1}\mathbf{1}^T \tag{8.33}$$

$$\sum_{i=1}^{n} \frac{1}{\lambda_i} \leq 1, \text{ and } \lambda_j > 0, \quad j = 1, \ldots, n. \tag{8.34}$$

Lemma 8.4.7. *The solution of the problem $\mathcal{D}_\delta(n)$ satisfies*

$$\mathcal{D}_\delta(n) = \delta \left\{ \frac{1}{4} + \sum_{i=2}^{n} \frac{1}{2i+1} \right\} \leq \frac{1}{2}\delta \log(n+1). \tag{8.35}$$

Proof (Lemma 8.4.5). Let $v \in \mathbb{R}^{n(n-1)/2}$ be a vector that is composed of $z_{i+1:n}(j) = \{z_{i+1}(j), z_{i+2}(j), \cdots, z_n(j)\}$ for all $j = 0, 1, \cdots, p$, *i.e.*

$$v \triangleq \left[z_{1:n}(0), z_{2:n}(1), \cdots, z_n(n) \right].$$

Let the following matrices be defined as

$$\begin{aligned} X &= vv^T \geq 0 \\ F_0 &= \text{diag}\left(\frac{1}{2^2}, \cdots, \frac{\mathbf{1}_{n-1}\mathbf{1}_{n-1}^T}{(n)^2}, \frac{\mathbf{1}_n\mathbf{1}_n^T}{(n+1)^2} \right) \\ F_i &= \text{diag}\left(e_{n,i}, e_{n-1,i}, \cdots, e_{n-i+1,i}, 0_{n-i}, \cdots, 0_1 \right), \end{aligned} \tag{8.36}$$

where 1_k is a k-dimensional vector with all elements being 1; $e_{k,j}$ is a k-dimensional row vector with j-th entry being 1 and other entries being 0; and 0_k is a k-dimensional row vector with all elements being 0. Using SDP relaxation [117], the problem $\mathcal{P}_\delta(n)$ can be converted into

$$\begin{aligned} \mathcal{P}'_\delta(n) = \max_{X\geq 0} \ & tr(F_0 X) \\ \text{s.t.} \quad & tr(F_i X) \leq \delta, \ \forall i = 1, \ldots, n. \end{aligned}$$

Therefore, $\mathcal{P}_\delta(n) \leq \mathcal{P}'_\delta(n)$. This relaxation can be observed from the following relations:

$$\sum_{i=0}^{n-1}\left(\frac{1}{n-i+1}\right)^2\left(\sum_{k=i+1}^{n} z_k(i)\right)^2 = v^T F_0 v = tr(F_0 v v^T)$$
$$\sum_{i=0}^{k}(z_k(i))^2 = v^T F_i v = tr(F_i v v^T).$$

We next show that the relaxation of the problem $\mathcal{P}_\delta(n)$ to the semidefinite problem $\mathcal{P}'_\delta(n)$ is also exact. Assume that $\mathcal{P}_\delta(n)$ is feasible and bounded. Let $X^* = \{x^*_{ij}\}$ be the optimal solution of $\mathcal{P}'_\delta$. Define X as

$$X = \begin{bmatrix}\sqrt{x^*_{11}} & \cdots & \sqrt{x^*_{nn}}\end{bmatrix}^T \begin{bmatrix}\sqrt{x^*_{11}} & \cdots & \sqrt{x^*_{nn}}\end{bmatrix}.$$

From $x_{ii} = x^*_{ii}$ and (8.36), X satisfies the contraints

$$tr(F_i X) = tr(F_i X^*) = \delta. \tag{8.37}$$

Furthermore, because X^* is the optimal solution and $x_{ij} = \sqrt{x^*_{ii}x^*_{jj}} \geq x^*_{ij}$ (due to $X^* \geq 0$),

$$tr(F_0 X^*) \geq tr(F_0 X) \geq tr(F_0 X^*). \tag{8.38}$$

Therefore, (8.37) and (8.38) shows that $\mathcal{P}_\delta(n) = \mathcal{P}'_\delta(n)$.

Next, we consider the following dual problem of $\mathcal{P}'_\delta(n)$:

$$\begin{aligned}\mathcal{D}'_\delta(n) = \min_{\lambda}\ & \delta\sum_{i=1}^{n}\lambda_i \\ \text{s.t.}\ & \sum_{i=1}^{n}\lambda_i F_i \geq F_0.\end{aligned} \tag{8.39}$$

Because there exists an strictly positive definite matrix $X > 0$ such that $tr(F_i X) = \delta$ for all $i = 1, 2, \cdots, n$, from Slater's condition [22], strong duality holds between $\mathcal{P}'_\delta(n)$ and $\mathcal{D}'_\delta(n)$. Let $\Lambda_{1:i} = diag(\lambda_1, \ldots, \lambda_i) \in \mathbb{R}^{i\times i}$, and observe that $\sum_{i=1}^n \lambda_i F_i = diag(\Lambda_{1:1}, \Lambda_{1:2}, \ldots, \Lambda_{1:n})$. Hence, the constraint $\sum_{i=1}^n \lambda_i F_i \geq F_0$ is equivalent to

$$\begin{aligned}& diag(\lambda_1, \ldots, \lambda_j) \geq \frac{1}{(j+1)^2}\mathbf{1}\mathbf{1}^T,\ \forall j = 1, \ldots, n, \\ \iff & \sum_{i=1}^{j}\frac{1}{\lambda_i} \leq (j+1)^2,\quad \lambda_j > 0,\quad j = 1, \ldots, n,\end{aligned}$$

where the second line is due to Lemma 8.4.6. Therefore, the dual problem $\mathcal{D}'_\delta(n)$ can be reformulated into $\mathcal{D}_\delta(n)$. □

Proof (Lemma 8.4.7). We first consider the case when $n \geq 2$. Let us define an auxiliary variable

$$s_k = \sum_{i=1}^{k} \frac{\delta}{\lambda_i}, \qquad k = 1, \cdots, n, \tag{8.40}$$

where $s_0 = 0$, and $s_k = 0$ for $k \geq n+1$. Using the auxiliary variable s_k, we rewrite the optimization problem $\mathcal{D}_\delta(n)$ as

$$\begin{aligned} \min \quad & \sum_{i=1}^{n} \frac{1}{s_i - s_{i-1}} \\ \text{s.t.} \quad & s_i \leq (i+1)^2, \quad s_{i-1} \leq s_i, \quad i = 1, \ldots, n. \end{aligned} \tag{8.41}$$

We define the Lagrangian $L : \mathbb{R}^n \times \mathbb{R}^n \times \mathbb{R}^n \to \mathbb{R}$ of the problem (8.41) as follows:

$$L(s, \mu, \eta) = \sum_{i=1}^{n} \frac{1}{s_i - s_{i-1}} + \mu_i(s_i - (i+1)^2) + \eta_i(s_{i-1} - s_i).$$

Let (s^*, μ^*, η^*) be any optimal primal and dual variables, then (s^*, μ^*, η^*) satisfies the Karush-Kuhn-Tucker (KKT) conditions. Solving the KKT conditions, we obtain that

$$\begin{aligned} s_i^* &= (i+1)^2, && i = 1, \ldots, n \\ \eta_i^* &= 0, && i = 1, \ldots, n \\ \mu_i^* &= \begin{cases} \frac{1}{16} - \frac{1}{25} & \text{if } i = 1 \\ \frac{1}{(2i+1)^2} - \frac{1}{(2i+3)^2} & \text{if } i = 2, \ldots, n-1 \\ \frac{1}{(2n+1)^2} & \text{if } i = n. \end{cases} \end{aligned}$$

To see this, observe that

1. $s_i^* - (i+1)^2 \leq 0$, $\mu_i^*(s_i^* - (i+1)^2) = 0$, $i = 1, \ldots, n$.
2. $s_{i-1}^* - s_i^* \leq 0$, $\eta_i^*(s_{i-1}^* - s_i^*) = 0$, $i = 1, \ldots, n$.
3. $\mu_i^* \geq 0$, $i = 1, \ldots, n$.
4. $\eta_i^* \geq 0$, $i = 1, \ldots, n$.
5. $dL(s^*, \mu^*, \eta^*)/ds_i = 0$.

Since the problem (8.41), which is equivalent with $\mathcal{D}_\delta(n)$, is a convex problem, the KKT conditions are sufficient for optimality [22]. Therefore, the optimal primal and dual variables are (s^*, μ^*, η^*), which result in the optimal value

$$\mathcal{D}_\delta(n) = \frac{1}{4} + \sum_{i=2}^{n} \frac{1}{2i+1}. \tag{8.42}$$

Next, we upper-bound the optimal cost $\mathcal{D}'_\delta(n)$. Since the function $f(i) = (2i + 1)^{-1}$, $i \geq 1$, is convex, from Jensen's inequality, $f(i)$ is upper-bounded by $f(i) \leq \frac{1}{2}\left(f(i - t/2) + f(i + t/2)\right)$, for any $t \in [0, 1]$. Integrating this along $t \in [0, 1]$, we obtain that

$$\begin{aligned} f(i) &\leq \frac{1}{2}\int_{t=0}^{1} f\left(i - \frac{t}{2}\right) + f\left(i + \frac{t}{2}\right) dt \\ &= \frac{1}{2}(\log(i+1) - \log(i)). \end{aligned}$$

Combining above bound with (8.42), we establish a lower-bound of the optimal value

$$\mathcal{D}_\delta(n) = \delta\left\{\frac{1}{4} + \sum_{i=1}^{n} \frac{1}{2i+1} - \frac{1}{3}\right\} \leq \frac{1}{2}\delta\log(n+1).$$

On the other hand, when $n = 1$, the optimal variable is $\lambda_1^* = \delta/4$, which attains the optimal value $\mathcal{D}_\delta(1) = \delta/4 \leq \log(2)/2 \approx \delta 0.346574$. □

Proof. Proof (Lemma 8.4.3) Applying Lemma 8.4.1 and Lemma 8.4.4, Lemma 8.4.5, and then Lemma 8.4.7 consecutively, we obtain

$$\|\hat{x}^{\mathcal{I}} - \hat{x}\|_2^2 \leq \mathcal{P}_\delta = \mathcal{D}_\delta \leq \frac{1}{2}\log(N) \max_{\mathcal{J}_1, \mathcal{J}_2 \in \mathcal{V}} \left(\mathcal{D}_{2,2}^{\mathcal{J}_1, \mathcal{J}_2}\right)^2.$$

□

Lemma 8.4.8. *If condition* (8.23) *holds for* $(p, q) = (2, \infty), (\infty, \infty)$ *at all time* $T \in \mathbb{Z}_+$*, then the divergence between the benign estimator* $\mathcal{I}$ *and the global estimator satisfies*

$$\|\hat{x}^{\mathcal{I}} - \hat{x}\|_\infty \leq \frac{1}{2} \max_{\mathcal{J} \in \mathcal{V}} \mathcal{D}_{p,\infty}^{\mathcal{I}, \mathcal{J}}. \tag{8.43}$$

Lemma 8.4.8 is a trivial extension of the following Proposition. We omit its prove due to space constraints.

Proposition 8.4.1. *Let $z_1, \ldots, z_l$ be real numbers. Define*

$$z = \frac{1}{2}\left(\max_i z_i + \mathcal{J}_1 n_i z_i\right).$$

Then for any i, we have

$$|z - z_i| \leq \frac{1}{2}\max_j |z_j - z_i|. \tag{8.44}$$

Now we are ready to prove Theorem 8.4.1.

Proof. Theorem 8.4.1 Taking supremum over all $t \in \mathbb{Z}_+$ and maximizing over all sensor sets $\mathcal{I}$ in Lemma 8.4.3, we obtain

$$\sup_{\substack{\|w\|_2 \leq 1 \\ \|a\|_0 \leq \rho}} \|e\|_2 \leq \max_{\mathcal{I} \in \mathcal{V}} \|E^{\mathcal{I}}(K^{\mathcal{I}})\|_\infty + \max_{\mathcal{J}_1, \mathcal{J}_2 \in \mathcal{V}} \sqrt{\frac{1}{2}\log|\mathcal{V}|}\, \mathcal{D}_{2,2}^{\mathcal{I},\mathcal{J}}.$$

Applying similar argument for the case of $q = \infty$, we obtain

$$\|e\|_\infty \leq \max_{\mathcal{I},\mathcal{J} \in \mathcal{V}} \left(\|E^{\mathcal{I}}(K^{\mathcal{I}})\|_{p\to\infty} + \frac{1}{2}\mathcal{D}_{p,\infty}^{\mathcal{I},\mathcal{J}} \right),$$

where $p = 2, \infty$. □

8.5 Numerical example

In this section, we study the proposed estimator numerically and compare it with existing algorithms from Shoukry et al. [173], Chong et al. [38], Pajic et al. [147], and Lu et al. [118]. We tested the IEEE 14-Bus system, the Unmanned Ground Vehicle (UGV), and the temperature monitor as follows.

(i) *IEEE 14-Bus system [114, 173, 212]:* The IEEE 14-Bus system is modeled as the system (8.1) with A and C given in [212]. We additionally add process noise and sensor noise by setting $B = \begin{bmatrix} I_{10} & O_{10,35} \end{bmatrix}$ and $D = \begin{bmatrix} O_{10,35} & I_{35} \end{bmatrix}$.

(ii) *Unmanned ground vehicle (UGV) [147, 173]:* A UGV moving in a straight line has the dynamics

$$\begin{bmatrix} \dot{p} \\ \dot{v} \end{bmatrix} = \begin{bmatrix} 0 & 1 \\ 0 & -b/m \end{bmatrix} \begin{bmatrix} \dot{x} \\ \dot{v} \end{bmatrix} + \begin{bmatrix} 0 \\ 1/m \end{bmatrix} u + \begin{bmatrix} I_2 & O_{2,3} \end{bmatrix} w,$$

where p is the position, v is the velocity, u is the force input, w is the disturbance, m is the mechanical mass, b is the translational friction coefficient,

I_n is a n-dimensional identity matrix, and $O_{n,m}$ is a $m \times n$ zero matrix. We assume that the estimator can access the values of u. The UGV is equipped with a sensor measuring x and two sensors measuring v, *i.e.*

$$y = \begin{bmatrix} 1 & 0 \\ 0 & 1 \\ 0 & 1 \end{bmatrix} \begin{bmatrix} p \\ v \end{bmatrix} + \begin{bmatrix} O_{3,2} & I_2 \end{bmatrix} w.$$

The system parameters are the same as [173]: $m = 0.8kg$, $b = 1$, and sampling interval $T_s = 0.1s$.

(iii) *Temperature monitor [131]:* The heat process in a plannar closed region $(z_1, z_2) \in [0, l] \times [0, l]$ can be expressed by

$$\frac{\mathcal{D}ialx}{\mathcal{D}ialt} = \alpha \left(\frac{\mathcal{D}ial^2 x}{\mathcal{D}ialz_1^2} + \frac{\mathcal{D}ial^2 x}{\mathcal{D}ialz_2^2} \right), \tag{8.45}$$

where α is the speed of the diffusion process; and $x(z_1, z_2)$ is the temperature at position (z_1, z_2) subject to the boundary conditions

$$\frac{\mathcal{D}ialx}{\mathcal{D}ialz_1}\Big|_{t,0,z_2} = \frac{\mathcal{D}ialx}{\mathcal{D}ialz_1}\Big|_{t,l,z_2} = \frac{\mathcal{D}ialx}{\mathcal{D}ialz_1}\Big|_{t,z_1,0} = \frac{\mathcal{D}ialx}{\mathcal{D}ialz_1}\Big|_{t,z_1,l} = 0.$$

We discretize the region using a $N \times N$ grid and the continuous-time with sampling interval T_s to model (8.45) into (8.1). We additionally add process noise and sensor noise by setting w, $B = \begin{bmatrix} I_9 & O_{9,20} \end{bmatrix}$ and $D = \begin{bmatrix} O_{9,20} & I_{20} \end{bmatrix}$. We set $\alpha = 0.1m^2/s$, $l = 4m$, and $N = 5$ as in [131].

The noise w is generated from a uniform distribution between $[-1, 1]$. The time horizon is set to be $T = 100$. The number of compromised sensors is set to be 1; the compromised sensor is randomly chosen among non-critical sensors (*i.e.* sensors that can be removed without losing observability). The attack signal is drawn from a Gaussian distribution with mean zero and variance 10^4 and 1. For the proposed algorithm, we used (8.17) with $(p, q) = (2, 2), (2, \infty)$, and (∞, ∞) simultaneously. We ran each example for 100 times and recorded their average estimation errors $\|e\|_2$ and computation times. The code is written in Matlab (Windows) and runs on an Intel Core i5-4690 Processor (4x3.50GHz/6MB L3 Cache). We summarize the estimation errors and computation times in Table S1 and Table S2. Some entries are left as NA (not applicable) because the system (ii) does not satisfy the linear matrix inequality (LMI) assumption required by the algorithm proposed by [118]. The algorithms tested have different relative accuracies and computation times from example to example. Among all examples tested, the proposed algorithm has relatively low estimation errors and average computation times.

	Proposed	[173]	[38]	[149]	[118]
(i)	11.1573	17.2948	13.7927	48.9880	17.5957
(ii)	6.9108	4.7246	7.2937	22.0884	NA
(iii)	6.7833	7.9424	6.8902	8.5448	18.5803

Table S1: Estimation errors in two-norm $\|e(1:100)\|_2$ when the attack variance is 10^4.

	Proposed	[173]	[38]	[149]	[118]
(i)	0.0062	0.0108	0.0045	0.0006	0.0345
(ii)	0.0001	0.0026	0.0002	0.0003	NA
(iii)	0.0023	0.0096	0.0020	0.0005	0.0048

Table S2: Average computation time in second for time horizon 100 when the attack variance is 10^4.

	Proposed	[173]	[38]	[147]	[118]
(i)	6.4653	9.6477	7.4754	9.8822	17.3752
(ii)	6.8500	4.6481	7.2884	23.3668	NA
(iii)	6.7060	8.0070	6.8144	8.6655	NA

Table S3: Estimation errors in two-norm, *i.e.* $\|e(1:100)\|_2$ when the attack variance is 1.

	Proposed	[173]	[38]	[147]	[118]
(i)	0.0062	0.0109	0.0046	0.0005	0.0325
(ii)	0.0001	0.0024	0.0002	0.0003	NA
(iii)	0.0023	0.0093	0.0020	0.0004	NA

Table S4: Average computation time in second for time horizon 100 when the attack variance is 1.

Chapter 9

APPLICATION TO SCHEDULING I: REVERSE ENGINEERING EXISTING SCHEDULING ALGORITHMS

The electrification of transportation provides a great opportunity for energy efficiency and sustainability. There were over a million electric vehicles (EVs) worldwide as of 2015 [4], and accelerated EV proliferation is expected for many years to come. To charge a large number of EVs however presents a tremendous challenge, in terms of both its impact on power grid and management complexity. While the flexibility in charging time and rate can be exploited for coordinated EV charging to control and mitigate the impact on the grid, its efficacy often depends on accurate prediction of EV arrivals and energy demands as well as coordination across time among different EVs. However, the accurate prediction is usually either impossible or very costly (in data collection and computation), and the temporal coordination among a large number of EVs may incur prohibitively large complexity. In view of these limitations, in this chapter we investigate low-complexity EV charging that does not require the prediction of EV arrivals/demands or the temporal coordination.

Specifically, we formulate EV charging as a feasibility problem that meets all EVs' energy demands before departure under individual charging rate constraints and total charging power constraint. We then propose an online algorithm, the smoothed least-laxity-first (sLLF) algorithm, that decides on the current charging rates based on only the information up to the current time. The laxity is defined as an EV's remaining time at the charging station minus the time needed to fully charge it at the maximum rate, and can be seen as the feasibility margin for EV charging. Without information on future EV arrivals, the sLLF algorithm makes best possible decision by maximizing the minimum resulting laxity for the next time among the EVs currently in the system.

As the sLLF algorithm does not take future EV arrivals into consideration, an (offline) feasible EV charging instance may be (online) infeasible under sLLF. We use the resource augmentation framework to study the sLLF algorithm, and characterize the minimum amount of additional resources (total power supply and charging rates) that will allow the algorithm to generate a feasible charging for any offline feasible charging instances. We further carry out numerical experiments

using real-world data, and show that sLLF has significantly higher rate of generating feasible EV charging than several other common EV charging algorithms. This is expected, as the sLLF algorithm tries to leave the largest feasibility margin, so it can best accommodate arbitrary future EV arrivals.

9.1 System model

Consider a system with one charging station that serves a set of EVs, indexed by $i \in \mathcal{V} = \{1,\ 2,\ 3,\ \cdots\}$. We use a discrete-time model where time is divided into slots of equal sampling intervals, indexed by $t \in \mathcal{T} = \{0,\ 1,\ 2,\ \cdots, T\}$. EV i arrives at the charging station with an energy demand e_i at time a_i, and departs from the station at time d_i.[1] During its stay at the station, the EV is charged at a rate (or power) of $r_i(t) \geq 0,\ a_i \leq t < d_i$. For convenience, we extend this definition of $r_i(t)$ to the entire temporal domain. The notations are summarized in Table S1.

To account for limitations in the charger or battery of an EV, each EV i can only be charged up to a peak rate $\bar{r}_i$, *i.e.*

$$\begin{aligned} r_i(t) &\leq \bar{r}_i, \quad t \in [a_i, d_i),\ \ i \in \mathcal{V} \\ r_i(t) &= 0, \quad t \notin [a_i, d_i),\ \ i \in \mathcal{V}. \end{aligned} \tag{9.1}$$

To account for limitations in the grid or power station, the charging station has a (possibly time-varying) power limit $P(t)$ such that[2]

$$\sum_{i \in \mathcal{V}} r_i(t) \leq P(t),\ t \in \mathcal{T}. \tag{9.2}$$

Furthermore, the power limit and maximum charging rates fall within the following nominal ranges:

$$\begin{aligned} &P_{\min} \leq P(t) \leq P_{\max}, \\ &\bar{r}_{\min} \leq \bar{r}_i \leq \bar{r}_{\max},\ i \in \mathcal{V}. \end{aligned}$$

Finally, every EV's energy demands needs to be satisfied, *i.e.*[3]

$$\sum_{t \in \mathcal{T}} r_i(t) = e_i,\ i \in \mathcal{V}. \tag{9.3}$$

[1] Each EV leave at its departure time regardless of its charging conditions. This assumption is applicable for most slow chargers including ACN [102]. Under this assumption, we do need to explicitly model number of stations, as the speed of charging does not affect the availability of chargers for incoming EVs.

[2] All EVs at the charing station can be simultaneously as long as the constraints (9.1)-(9.2) are satisfied.

[3] The actual constraint in ACN is $\sum_{t \in \mathcal{T}} \delta r_i(t) = e_i,\ i \in \mathcal{V}$, where δ (h) is the sojourn time of sampling time intervals, e_i has unit kWh, $r_i(t)$ has unit kW [102]. Since $r_i(t)$ can always be rescaled according to δ, we set $\delta = 1$ without loss of generality.

Table S1: Notation

$\mathcal{I}$	EV charging problem instance
$\mathcal{V}$	set of EVs
$\mathcal{V}_t$	set of EVs remaining in the charging station at time t
$\mathcal{T}$	set of times
e_i	energy demand of EV $i \in \mathcal{V}$
$e_i(t)$	remaining energy demand of EV i at time $t \in \mathcal{T}$
$r_i(t)$	charging rate of EV i at time t
$P(t)$	power limit of the charging station at time t
a_i	arrival time of EV i
d_i	departure time of EV i

Next, we define an EV charging problem instance as a quintuple $\mathcal{I} = \{a_i, d_i, e_i, \bar{r}_i; P(t)\}_{i\in\mathcal{V}, t\in\mathcal{T}}$. The primary goal of EV charging is to satisfy every EV's energy demands under the above power supply and peak rate constraints.

Definition 9.1.1 (Feasible instance)**.** *An EV charging problem instance $\mathcal{I}$ is offline feasible if there exist charging rates $r = \{r_i(t) : i \in \mathcal{V}, t \in \mathcal{T}\}$ that satisfy constraints* (9.1)-(9.3).

Constraints (9.1)-(9.3) are affine. Therefore, verifying the feasibility of an EV charging instance is a linear program (LP) for which many efficient algorithms exist.

In practice, the energy demand and departure time of an EV are only informed after its arrival.[4] Consequently, the charging station must use an *online algorithm* to determine an EV's current charging rate $r_i(t)$ using only information up to the current time t:

$$\mathcal{I}_t = \{a_i, d_i, e_i(\tau), \bar{r}_i; P(\tau)\}_{i\in\mathcal{V}_t, \tau\le t}, \tag{9.4}$$

where $e_i(\tau) = e_i - \sum_{t=0}^{\tau-1} r_i(t)$ is the remaining energy demand of EV i at the beginning of time slot τ.

Definition 9.1.2 (Online algorithm)**.** *An online algorithm is a sequence of functions $\mathcal{A} = \{\mathcal{A}_t\}$ where each function $\mathcal{A}_t : \mathcal{I}_t \to r(t)$ maps the information up to the current time $\mathcal{I}_t$ to the current charging rates $r(t) = \{r_i(t)\}_{i\in\mathcal{V}_t}$.*

[4] In ACN, the energy demand and departure time of EV i is gathered from user inputs upon arrival.

Definition 9.1.3 (Feasibility of the algorithm)**.** *An (online) algorithm $\mathcal{A}$ is feasible (online feasible) on instance $\mathcal{I}$ if it gives charging rates that satisfy constraints* (9.1)-(9.3)*.*[5]

9.2 The proposed algorithm: smoothed least-laxity-first algorithm

Laxity and its properties

A measure for the flexibility (or urgency) in the charging of an EV is its remaining time minus the minimum remaining time needed to fully charge it (time needed to fully charge it at the maximum rate). We refer to this measure as *laxity*.

Definition 9.2.1 (Laxity)**.** *The laxity of an EV $i \in \mathcal{V}$ at time $t \in \mathcal{T}$ is defined as*[6]

$$\ell_i(t) = \begin{cases} [d_i - t]^+ - \dfrac{e_i(t)}{\bar{r}_i}, & t \geq a_i, \\ +\infty, & t < a_i, \end{cases}$$

where "$[\cdot]^+$" denotes the projection onto the set $\mathcal{R}_+$ of non-negative real numbers.

Proposition 9.2.1 (Feasibility condition)**.** *The algorithm $\mathcal{A}$ is feasible on an instance $\mathcal{I}$ if and only if $\mathcal{A}$ gives charging rates that result in non-negative laxities for all EVs, i.e.*

$$\ell_i(t) \geq 0, \quad i \in \mathcal{V}, \ \ t \in \mathcal{T}. \tag{9.5}$$

Proof. (Proposition 9.2.1) Observe that feasibility is equivalent with the condition

$$e_i(d_i) = 0, \qquad i \in \mathcal{V}. \tag{9.6}$$

Condition (9.5) implies that for any EV $i \in \mathcal{V}$, $\ell_i(d_i) = -e_i(d_i)/\bar{r}_i \geq 0$, which yields $e_i(d_i) = 0$. Next, notice that the laxity of EV i is monotonically decreasing at $t < d_i$ and constant at $t \geq d_i$, *i.e.*

$$\ell_i(t) = \ell_i(t+1) + 1 - r_i(t)/\bar{r}_i \geq \ell_i(t+1), \qquad t < d_i \tag{9.7}$$

$$\ell_i(t) = \ell_i(t+1) \qquad t \geq d_i. \tag{9.8}$$

Therefore, condition (9.6) implies that $\ell_i(t) \geq 0$ at any time $t \in \mathcal{T}$. □

[5] The feasibility is defined for an instance $\mathcal{I}$ with respect to an online algorithm $\mathcal{A}$, whereas the offline feasibility is defined for an instance $\mathcal{I}$. Offline feasibility is a necessary condition for an instance $\mathcal{I}$ to be feasible with respect to algorithm $\mathcal{A}$. An instance $\mathcal{I}$ can be online feasible with respect to algorithm $\mathcal{A}$ but infeasible with respect to another algorithm $\mathcal{A}'$.

[6] For convenience, laxity is defined on the whole temporal domain $\mathcal{T}$.

Proposition 9.2.1 suggests that the minimum laxity among all EVs can serve as a measure of the distance from infeasibility. A naive approach—referred to as the least laxity first (LLF) algorithm—is to charge EVs starting from those with the least laxity to those with the most laxity. However, the LLF algorithm may compromise the feasibility of certain offline feasible instances (see Section 9.4) and cause excessive preemptions and oscillations in the charging rate[7], which may reduce the lifetime of certain batteries (*e.g.,* Li-ion) [92]. Alternatively, we consider maximizing the minimum laxity among all EVs in order to maximize the feasibility margin, $\max_r \min_{i\in\mathcal{V}} \ell_i(T)$. Although its solution may be non-unique, for twice continuously differentiable, strictly concave, and strictly increasing f, the following optimization problem produces an unique solution that is also a solution of $\max_r \min_{i\in\mathcal{V}} \ell_i(T)$.[8]

Corollary 9.2.1 (Equivalent problem)**.** *Consider the optimization algorithm*

$$\max_{r} \quad \sum_{i\in\mathcal{V}} \bar{r}_i f(\ell_i(T)) \qquad \text{s.t.} \quad (9.1), (9.2), \sum_{t\in\mathcal{T}} r_i(t) = e_i,\ i \in \mathcal{V}, \tag{9.9}$$

where f is strictly increasing. Algorithm (9.9) *is feasible for any offline feasible instance.*

Proof (Corollary 9.2.1). From constraint $\sum_{t\in\mathcal{T}} r_i(t) \le e_i$ and f strictly increasing, the objective function satisfies

$$\sum_{i\in\mathcal{V}} f(\ell_i(T)) \le \sum_{i\in\mathcal{V}} f(0).$$

If an instance $\mathcal{I}$ is offline feasible, then there exists certain charging rates that achieve $\ell_i(T) = 0, \forall i \in \mathcal{V}$, which yields $\sum_{i\in\mathcal{V}} f(\ell_i(T)) = \sum_{i\in\mathcal{V}} f(0)$. Since the laxity is monotonically decreasing at any $t \in \mathcal{T}$, such charging rates also satisfy condition (9.5). From Proposition 9.2.1, condition (9.5) implies that algorithm (9.9) is feasible on instance $\mathcal{I}$. □

However, we cannot solve (9.9) because of the lack of future information of incoming EVs. Instead, we replace (9.9) with the following online algorithm: at each time

[7]For example, consider a system of two EVs, where $\ell_1(0) = 1.25$, $\ell_2(0) = 0.75$ and $\bar{r}_1 = \bar{r}_2 = P(t) = 1, t \in \mathcal{T}$. EV 1 and EV 2 will be charged according to $(r_1(0), r_2(0)) = (0, 1)$, $(\ell_1(1), \ell_2(1)) = (0.25, 0.75)$; $(r_1(1), r_2(1)) = (1, 0)$, and so on. In this example, both EV switches in-between charging and not charging.

[8]Additionally, we can show the problem (9.9) also has a fairness property.

$t \in \mathcal{T}$, given $\ell_i(t), i \in \mathcal{V}$, compute[9]

$$\max_{r(t)} \sum_{i \in \mathcal{V}_t} \bar{r}_i f(\ell_i(t+1)) \qquad \text{s.t. (9.1), (9.2)}, r_i(t) \le e_i(t),\ i \in \mathcal{V}_t. \tag{9.10}$$

The optimization problem (9.10) also maximizes the minimum laxity $\min_{i \in \mathcal{V}_t} \ell_i(t+1)$, and thus maximizes the feasibility margin at time t.[10] Next, we show the structure of the optimal solution, which will be used to construct a scalable algorithm.

Proposition 9.2.2 (Valley-filling solution)**.** *Assume that f is strictly concave, strictly increasing, and twice continuously differentiable. A solution to the optimization problem* (9.10) *is*

$$r_i^*(t) = [\bar{r}_i(L(t) - \ell_i(t) + 1)]_0^{\min(\bar{r}_i, e_i(t))}, \qquad i \in \mathcal{V}_t, \tag{9.11}$$

where $[x]_a^b$ denotes the projection of the scalar x on interval $[a, b]$, and the value $L(t)$ satisfies

$$\begin{aligned} &\sum_{i \in \mathcal{V}_t} [\bar{r}_i(L(t) - \ell_i(t) + 1)]_0^{\min(\bar{r}_i, e_i(t))} \\ &= \sum_{i \in \mathcal{V}_t} r_i^*(t) = \min\left(P(t), \sum_{i \in \mathcal{V}_t} \min(\bar{r}_i, e_i(t)) \right). \end{aligned} \tag{9.12}$$

Proof. (Proposition 9.2.2)

From the Karush-Kuhn-Tucker (KKT) conditions for the optimization problem (9.10),

$$r_i(t) \ge 0 \qquad i \in \mathcal{V}_t \tag{9.13}$$

$$r_i(t) \le \min(e_i(t), \bar{r}_i) \qquad i \in \mathcal{V}_t \tag{9.14}$$

$$\sum_{i \in \mathcal{V}_t} r_i(t) \le P(t) \qquad i \in \mathcal{V}_t \tag{9.15}$$

$$f'(l_i(t+1)) + \bar{\lambda}_i - \underline{\lambda}_i + \nu = 0 \qquad i \in \mathcal{V}_t \tag{9.16}$$

$$\underline{\lambda}_i \ge 0, \quad \bar{\lambda}_i \ge 0 \qquad i \in \mathcal{V}_t \tag{9.17}$$

$$\underline{\lambda}_i r_i(t) = 0, \quad \bar{\lambda}_i \{r_i(t) - \min(e_i(t), \bar{r}_i)\} = 0 \qquad i \in \mathcal{V}_t, \tag{9.18}$$

where $\underline{\lambda}_i, \bar{\lambda}_i, \nu$ are the dual variables for constraints (9.13), (9.14), (9.15), respectively. We consider three mutually exclusive cases: $r_i(t) = 0, r_i(t) \in (0, \min(e_i(t), \bar{r}_i))$,

[9] For more complex form of power limits, in optimization problems (9.9) and (9.10), the power constraints (9.2) can be replaced by $Ar(t) \le_{e.w.} P(t)$, for element-wise inequality and positive matrix A. The Result in Corollary 9.2.1 also holds for $Ar(t) \le_{e.w.} P(t)$.

[10] The solution of (9.10) is also unique.

or $r_i(t) = \min(e_i(t), \bar{r}_i)$. When $r_i(t) = 0$, $\bar{\lambda}_i = 0$ and

$$r_i(t)/\bar{r}_i = f'^{-1}(-v) - l_i(t) + 1 - \underline{\lambda}_i \leq f'^{-1}(-v) - l_i(t) + 1, \tag{9.19}$$

where the the inverse of f' exists since f' is strictly concave, strictly increasing, and twice continuously differentiable. When $r_i(t) \in (0, \min(e_i(t), \bar{r}_i))$, then from (9.18) (complementary slackness), $\bar{\lambda}_i = \underline{\lambda}_i = 0$. Substituting $\bar{\lambda}_i = \underline{\lambda}_i = 0$ into (9.16), we obtain

$$l_i(t) - 1 + r_i(t)/\bar{r}_i = f'^{-1}(-v). \tag{9.20}$$

When $r_i(t) = \min(e_i(t), \bar{r}_i)$, $\underline{\lambda}_i = 0$ and

$$r_i(t)/\bar{r}_i = f'^{-1}(-v) - l_i(t) + 1 + \hat{\lambda}_i \geq f'^{-1}(-v) - l_i(t) + 1. \tag{9.21}$$

Combining (9.19)-(9.21), we obtain

$$r_i(t) = [\bar{r}_i(f'^{-1}(-v) - l_i(t) + 1)]_0^{\min(\bar{r}_i, e_i(t))}. \tag{9.22}$$

Because the same value of $f'^{-1}(-v)$ is shared for all EVs at the charging station, we can define an variable $L(t) = f'^{-1}(-v)$. Since the optimal solution is attained at the boundary $\sum_{i\in\mathcal{V}_t} r_i^*(t) = \min\left(P(t), \sum_{i\in\mathcal{V}_t} \min(\bar{r}_i, e_i(t))\right)$, we obtain the optimal solution (9.11)-(9.12). □

Observe that for EV $i \in \mathcal{V}_t$ with $\bar{r}_i \leq e_i(t)$, the charging rates (9.11) result in $\ell_i(t+1) = [L(t)]_{\ell_i(t)-1}^{\ell_i(t)}$. Hence, $L(t)$ can be considered as a threshold of $\ell_i(t+1)$, below which the energy is charged to EV i. Since $r_i^*(t)$ in (9.11) is an increasing function of $L(t)$, a binary search can be used to find the threshold $L(t)$ in (9.12). Given $L(t)$, the charging rates $r_i^*(t), i \in \mathcal{V}_t$ is then determined using (9.11). We formally state this procedure in Algorithm 5, and name it as the *smoothed least-laxity-first (sLLF) algorithm*.

Algorithm 5 The Smoothed Least-Laxity-First (sLLF) Algorithm.

for $t \in \mathcal{T}$ **do**
  Update set of EVs $\mathcal{V}_t$ and laxities $\ell_i(t)$, $i \in \mathcal{V}_t$
  Obtain $L(t)$ that solves (9.12) using bisection
  Charge according to rates $r_i(t)$ in (9.11)
end for

The computational complexity of the sLLF algorithm is $O(|\mathcal{V}_t| + \log(1/\delta))$, where δ is the level of tolerable error. Lastly, we note that the sLLF algorithm has other useful properties such as the least-laxity-first property and fairness.

Lemma 9.2.1 (Least-laxity-first property)**.** *Under the sLLF algorithm, if there exist two EVs $i, j \in \mathcal{V}$ such that*

$$\ell_i(t) \le \ell_j(t), \tag{9.23}$$

$$\ell_i(t+1) > \ell_j(t+1), \tag{9.24}$$

then either one of the following holds:

$$t \ge d_i \;\&\; r_i(t) = 0, \tag{9.25}$$

$$t < d_i \;\&\; t < d_j \;\&\; e_j(t+1) = 0 \;\&\; r_i(t) \neq 0. \tag{9.26}$$

Proof. (Lemma 9.2.1) First notice that, by Definition 9.2.1, it satisfies the following relation:

$$\ell_i(t) - 1 \le \ell_i(t+1) \le \ell_i(t),\ i \in \mathcal{V}. \tag{9.27}$$

First, consider the case $r_i(t) = 0$. The evolution of ℓ_i satisfies

$$\ell_i(t+1) = \begin{cases} \ell_i(t) - 1 & t < d_i, \\ \ell_i(t) & t \ge d_i. \end{cases} \tag{9.28}$$

Suppose that $t < d_i$, combining (9.23) and (9.27) gives

$$\ell_j(t+1) \ge \ell_j(t) - 1 \ge \ell_i(t) - 1 = \ell_i(t+1),$$

which contradicts (9.24). Therefore, $t \ge d_i$, and (9.25) follows.

Next, consider the case $r_i(t) \neq 0$. Non-zero $r_i(t)$ implies $t < d_i$. If $t < d_j$, (9.23) and (9.24) jointly implies

$$\frac{r_j(t)}{\bar{r}_j(t)} < \frac{r_i(t)}{\bar{r}_i(t)}. \tag{9.29}$$

Under the sLLF algorithm, (9.29) happens only when $e_j(t) = r_j(t)$, which leads to $e_j(t+1) = 0$. If $t \ge d_j$, then $\ell_j(t+1) = \ell_j(t) \ge \ell_i(t) \ge \ell_i(t+1)$, which contradicts (9.24). Therefore, (9.26) follows. □

Corollary 9.2.2 (Fairness)**.** *Given the past charging rate r^{t-1}, the sLLF algorithm finds a current charging rate $r(t)$ that is both proportionally fair and max-min fair respect to one-step ahead laxity. In other words, let $\ell_i(t+1)$ be the one-step ahead laxity under the sLLF algorithm and $\hat{\ell}_i(t+1)$ be another laxity produced by a charging rate satisfying the constraints of* (9.10)*, and the following two conditions hold:*

- *weighted proportional fairness:*

$$\sum_{i \in \mathcal{V}_t} \bar{r}_i \frac{\hat{\ell}_i(t+1) - \ell_i(t+1)}{\ell_i(t+1)} \leq 0 \tag{9.30}$$

- *max-min fairness: if* $\hat{\ell}_i(t+1) > \ell_i(t+1)$ *for some EV* $i \in V_t$*, then there exits EV* $j \in V_t$ *such that*

$$\ell_j(t+1) \leq \ell_i(t+1), \qquad \hat{\ell}_j(t+1) < \ell_j(t+1). \tag{9.31}$$

For a charging instance $\mathcal{I} = \{a_i, d_i, e_i, \bar{r}_i; P(t)\}_{i \in \mathcal{V}, t \in \mathcal{T}}$ that is not online feasible under the sLLF algorithm, there are times when some EV has negative laxity. Denote by t_- the earliest among such times. Let $\mathcal{F} = \{i \in A_{t_-} : \ell_i(t_-) < 0\}$ denote the set of EVs arriving at the changing station by time t_- that have negative laxity, $\mathcal{S}_1 = \{i \in A_{t_-} : \ell_i(t_-) \geq 0 \ \& \ d_i \leq t_-\}$ the set of EVs with non-negative laxity that depart by time t_-, and $\mathcal{S}_2 = \{i \in A_{t_-} : \ell_i(t_-) \geq 0 \ \& \ d_i > t_-\}$ the set of EVs with non-negative laxity that remain at the charging station at time t_-. The sets $\mathcal{F}$, $\mathcal{S}_1$, and $\mathcal{S}_2$ are mutually exclusive, and $A_{t_-} = \mathcal{F} \cup \mathcal{S}_1 \cup \mathcal{S}_2$.

9.3 Performance analysis

There are two extreme cases, $\bar{r}_i \to \infty$, $i \in \mathcal{V}$ and $P(t) \to \infty$, in which online algorithms can be feasible for any offline feasible instances. When $\bar{r}_i \to \infty$ $i \in \mathcal{V}$, or equivalently $P(t) \leq \min_{i \in \mathcal{V}_t} \bar{r}_i$ for all $t \in \mathcal{T}$, the charging problem is identical to the single processor preemptive scheduling problem where the processing capacity is time-variant. For this case, the earliest-deadline-first (EDF) algorithm is feasible for any offline feasible instances [182]. When $P(t) \to \infty$, or equivalently $P(t) \geq \sum_{i \in V_t} \bar{r}_i(t)$ for all $t \in \mathcal{T}$, the sLLF algorithm is feasible for any offline feasible instances. However, beyond the above two extreme cases, no online algorithm can be feasible on all offline feasible instances [186]. The hardness of finding feasible online algorithms motivates a quantitative measure to evaluate the likelihood of an algorithm being feasible. Observe that if more resources (e.g., $P(t)$, $\bar{r}_i$) are allowed, an otherwise infeasible problem instance may become online feasible under the online algorithm. We use this (minimum) additional resource to analyze the performance of the sLLF algorithm, where either power P or both power P and peak rate $\bar{r}_i$ are augmented. The former allows more EVs to be charged simultaneously, while the latter additionally allows EVs to be charged faster. As we will demonstrate, these two ways of resource augmentation are qualitatively different and provide complementary insights into the behavior of the sLLF algorithm.

Power Augmentation

In the case of power augmentation, the online algorithm is allowed to use more power than the offline algorithm, *i.e.* $P^{on}(t) = (1+\epsilon)P(t)$, $\bar{r}_i^{on} = \bar{r}_i$.

Definition 9.3.1. *[ϵ-power augmented instance] Given an EV charging instance $\mathcal{I} = \{a_i, d_i, e_i, \bar{r}_i; P(t)\}_{i\in\mathcal{V}, t\in\mathcal{T}}$, we define its ϵ-power augmented instance as*

$$\{a_i, d_i, e_i, \bar{r}_i; (1+\epsilon)P(t)\}_{i\in\mathcal{V}, t\in\mathcal{T}} \tag{9.32}$$

Definition 9.3.2. *[ϵ-power feasibility] An online algorithm $\mathcal{A}$ is ϵ-power feasible if $\mathcal{A}$ is feasible on the ϵ-power augmented instances $\mathcal{I}_p(\epsilon)$ generated from any offline feasible instance $\mathcal{I}$.*[11]

Unfortunately, there is no ϵ-power feasible online algorithm for any finite $\epsilon > 0$ [155].[12] However, under a mild assumption, the ϵ-power feasibility condition can be obtained for a finite ϵ. Assume that the energy demand of each EV is bounded by X and that the inter-arrival time between consecutive arrivals is greater than N, *i.e.*

$$e_i \le X, \qquad i \in \mathcal{V}, \tag{9.33}$$

$$|a_i - a_j| > N, \qquad i, j \in \mathcal{V}. \tag{9.34}$$

We can characterize the relation between N and the sufficient amount of resource augmentation ϵ as follows.

Theorem 9.3.1. *If conditions* (9.33) *and* (9.34) *hold, then the sLLF algorithm is ϵ-power feasible with*

$$\epsilon = \frac{P_{\max}}{P_{\min}} \left\{ \log_\varphi \left(\frac{\sqrt{5}X}{NP_{\max}} + \frac{1}{2} \right) + 2 \right\} - 1,$$

where $\varphi = 1.61803$ is the golden ratio.

[11] Alternatively, the (minimum) value of ϵ can also be interpreted as the constraints on instances that are online feasible. That is, given the original resource $P(t), \bar{r}_i(t)$, the algorithm is online feasible for any instances $\mathcal{I} = \{a_i, d_i, e_i, \bar{r}_i; P(t)/(1+\epsilon)\}_{i\in\mathcal{V}, t\in\mathcal{T}}$ that is offline feasible given the reduced resource $P(t)/(1+\epsilon), \bar{r}_i(t)$. Large ϵ restricts possible instances, and are thus less likely to be online infeasible.

[12] It is shown in [155] that the LLF algorithm is not ϵ-power feasible for any $\epsilon > 0$ for uniform processors and time-invariant number of processors. Since their setting is a special case of our setting, the same results extend to our setting.

In particular, for constant power limit $P(t) = P, t \in \mathcal{T}$, if $N \geq X/P$,[13] then we can further simplify the feasibility condition in Theorem 9.3.1.

Corollary 9.3.1. *For constant power limit $P(t) = P, t \in \mathcal{T}$, if $N \geq X/P_{\max}$, then the sLLF algorithm is 3-power feasible.*

Power and rate augmentation

In the case of power and maximum charging rate augmentation, the online algorithm is allowed to use more power and higher maximum rate than the offline algorithm: $P^{on}(t) = (1+\epsilon)P(t)$, $\bar{r}_i^{on} = (1+\epsilon)\bar{r}_i$.

Definition 9.3.3. *[ϵ-augmented instance] Given an EV charging instance $\mathcal{I}\{a_i, d_i, e_i, \bar{r}_i; P(t)\}_{i\in\mathcal{V}, t\in\mathcal{T}}$, we define its ϵ augmented instance as*

$$\{a_i, d_i, e_i, (1+\epsilon)\bar{r}_i; (1+\epsilon)P(t)\}_{i\in\mathcal{V}, t\in\mathcal{T}}. \tag{9.35}$$

Definition 9.3.4. *[ϵ-feasibility] An online algorithm $\mathcal{A}$ is ϵ-feasible if $\mathcal{A}$ is feasible on the ϵ-augmented instances $\mathcal{I}_{pr}(\epsilon)$ generated from any offline feasible instance $\mathcal{I}$.*

Unlike the case of power augmentation, the sLLF algorithm is ϵ-feasible for a finite value of $\epsilon > 0$ without any assumptions of the arrival patterns.

Theorem 9.3.2. *The sLLF algorithm is ϵ-feasible with*

$$\epsilon = \max_{i\in\mathcal{V}} \left\{ \max_{\tau_1,\tau_2\in[a_i,d_i]} \frac{P(\tau_1)}{P(\tau_2)} - \max_{\tau\in[a_i,d_i]} \frac{\bar{r}_i}{P(\tau)} \right\}.$$

As we demonstrate in the next section, actual EV instances in ACN and others require smaller amount of resource augmentation than the worst-case upper bound in practice.

9.4 Performance at Caltech electric vehicle charging testbed

In this section, we show the performance of the sLLF algorithm using trace-base simulation on real EV datasets and compare it to that of several heuristic online EV charging algorithms.

[13] If the inter-arrival time is N, and the power demand is X, the incoming energy demand per unit time is X/N. Since the total power supply is $P_{\max}$ per unit time, N should be at least X/P for offline feasiblity. Therefore, $X/P \leq N$ is a mild assumption.

Experimental setup

Our simulations use datasets from the ACN deployment (CAGarage) and Google's facilities in Mountain View (Google_mtv) and Sunnyvale (Google_svl). They include a total of 52,362 charging sessions over more than 4,000 charging days in 2016 at 104 locations. See Table S1 for a summary of the data. Each instance consists of one day of charging. We can see that there is a large degree of variation in the sojourn time and laxity of the vehicles in the instances.

For each instance, we compute the minimum power capacity in which the instance is feasible by using offline an LP, *i.e.* we minimize $P = P(t)$, subject to (9.1)-(9.3). This corresponds to the minimum power supply in order for the instance to be offline feasible. We use this minimum power supply to generate an offline instance, and tested if the instance is feasible under online algorithms. Besides the sLLF algorithm, we also implemented some common (online) scheduling algorithms: earliest-deadline-first (EDF), least-laxity-first (LLF), equal share (ES), remaining energy proportional (REP) [182], and an online linear program (OLP) [75]:

Earliest Deadline First (EDF) All EVs in $\mathcal{V}_t$ are sorted by their deadlines d_i in an increasing order. The available power $P(t)$ is assigned to EVs in this order up to $\min(\bar{r}_i, e_i(t))$.

Least laxity first algorithms (LLF) All EVs in $\mathcal{V}_t$ are sorted by their laxities $\ell_i(t)$ in an increasing order. The available power $P(t)$ is assigned to EVs in this order up to $\min(\bar{r}_i, e_i(t))$.

Equal Share (ES) The available power supply $P(t)$ is divided equally to all connected EVs able to charge more energy, each EV receives the minimum between their fair share and their maximum charging rate. Repeat until either $P(t)$ power is supplied or no more EV can be charged further.

Remaining Energy Proportional (REP) The available power $P(t)$ is divided to EVs in proportion to their remaining energy demand $e_i(t)$. Each EV receives the minimum between their proportional share and their maximum charging rate. Repeat until either $P(t)$ power is supplied or no more EV can be charged further.

Online Linear Program (OLP) [75] At each time t, the charging rate $r_i(t)$ to EV

$i \in \mathcal{V}_t$ is provided according to the solution of the following LP:

$$\begin{aligned} \min \quad & \sum_{i \in \mathcal{V}_t} \sum_{\tau=t}^{T} \tau r_i(\tau) \\ \text{subject to} \quad & \sum_{\tau=t}^{T} r_i(\tau) = e_i(t), \ \forall i \in U_t \\ & \sum_{i \in U_\tau} r_i(\tau) \leq P(\tau), \ \forall \tau = t, \ldots, T \\ & 0 \leq r_i(t) \leq \bar{r}_i. \end{aligned}$$

The constraints of the online LP to find a feasible schedule for all the currently active EVs assuming no EV arrivals in the future, while objective function encourages the charging station to charge EVs as early as possible.

	Instances	EV sojourn time (m)	Laxity (m)
CAGarage	92	321(11, 720)	231 (0.1, 660)
Google_mtv	3793	149 (10, 720)	35 (0.001, 694)
Google_svl	246	152 (11, 720)	38 (0.02, 676)

Table S2: Statistics of the EV charging instances. Each entry is formated as average (minimum, maximum), unit (m) denotes minutes.

Results without augmented resources

We first evaluate the success rate of the online algorithms without resource augmentation. We define the success rate of an algorithm as the percentage of online feasible instances under the algorithm. The sLLF algorithm achieves uniformly high success rate for all datasets compared to other online algorithms considered. The EDF, ES, and REP algorithms perform much worse in terms of finding feasible schedules (Figure 9.1). This is not surprising as feasibility requires online algorithms to jointly consider deadline, maximum charging rate, and remaining energy of each EV. However, none of these (the EDF, ES and REP algorithms) consider all three factors simultaneously. The low success rate of the LLF algorithm, despite its similarity to the sLLF algorithm, suggests the importance of maximizing minimum laxity (see Section 9.2).

Next, we study what characteristics of the instances affect the success rate. We find that the minimum normalized laxity and the maximum ratio between EV sojourn times have high correlations with the success rate. The maximum ratio between

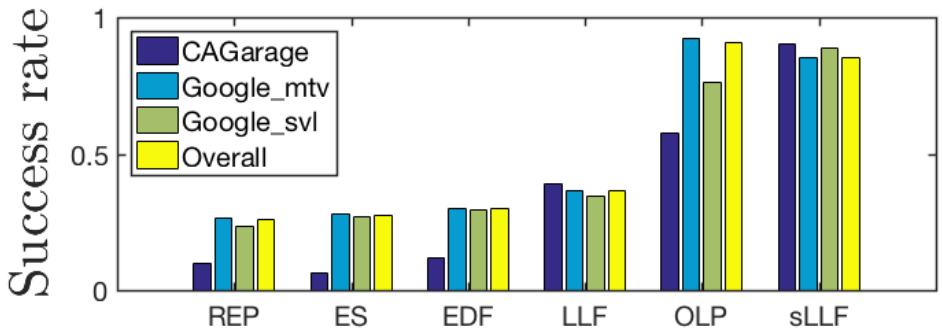

Figure 9.1: Success rates of finding feasible online schedule without resource augmentation.

	REP	ES	EDF	LLF	OLP	sLLF
power	4.61	3.65	1.39	0.07	0.28	0.07
power and rate	4.61	3.24	0.54	0.05	0.28	0.05

Table S3: Minimum resource augmentation for online feasibility for all instances. The LLF and sLLF algorithms have the smallest ϵ among algorithms considered.

EV sojourn times is defined as the maximum ratio between the longest and shortest EV sojourn times in the instances. The minimum normalized laxity of an EV is defined as the laxity divided by the EV sojourn times $\ell_i(a_i)/(d_i - a_i)$. Fig. 9.2 shows that as the minimum normalized laxity increases, all algorithms considered have improved success rates. Among these algorithms, the sLLF algorithm has one of the highest success rate for all minimum normalized laxity. Fig. 9.2b shows that as the maximum ratio between EV sojourn times increases, all algorithms considered have decreased success rates. Among these algorithms, the sLLF algorithm is least sensitive to the maximum ratio between EV sojourn times and maintains highest success rate across all sojourn times. Although instances with urgent schedule (small minimum normalized laxity) and large variety of EV sojourn times tend to have lower success rate, the sLLF algorithm has the best performance in almost all scenarios.

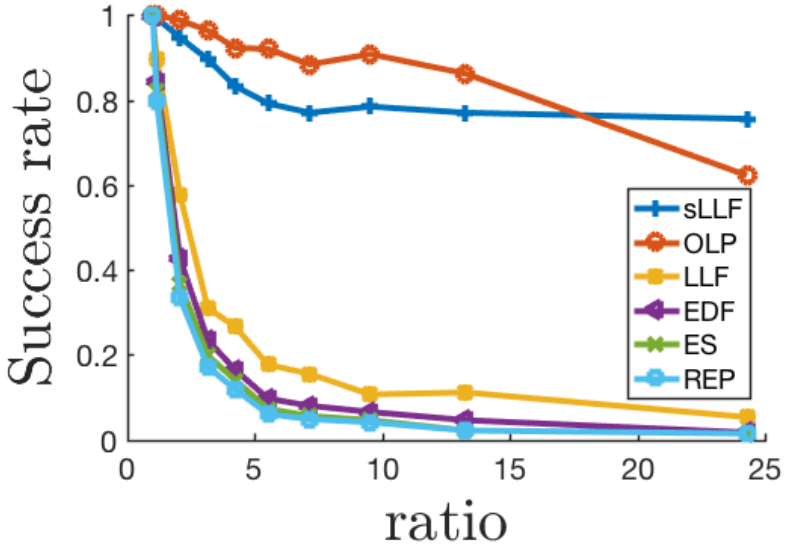

(a)

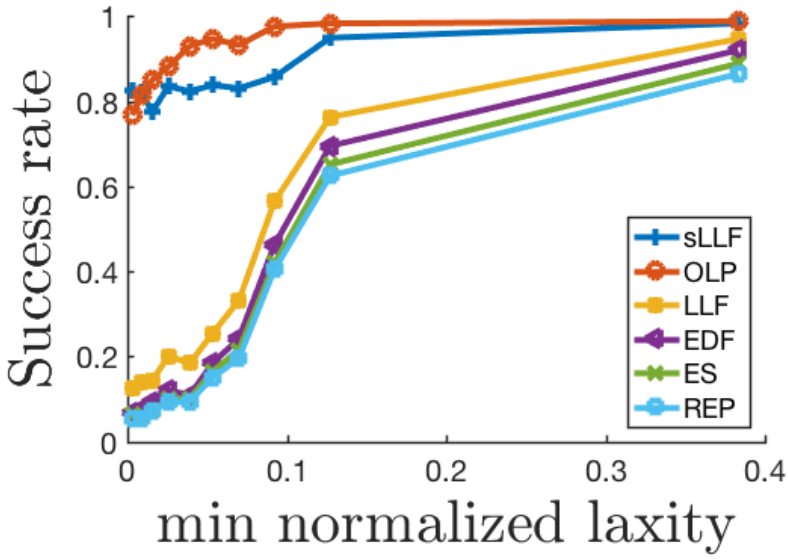

(b)

Figure 9.2: Success rate of finding feasible online schedule without resource augmentation.

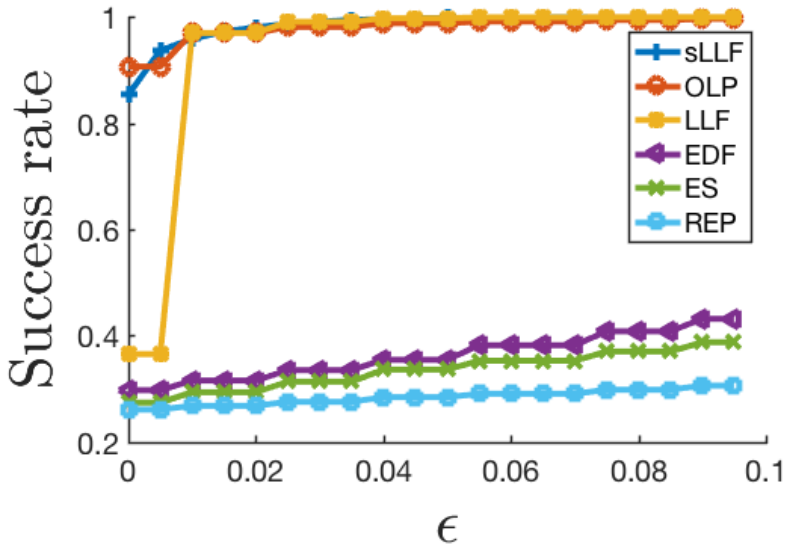

(a) ϵ-power augmentation

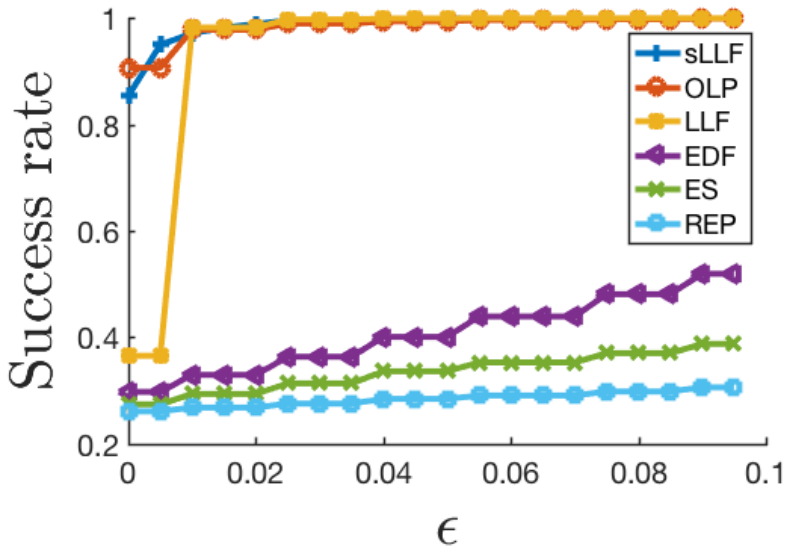

(b) ϵ-power and rate augmentation

Figure 9.3: Success rate of finding feasible online schedule under resource augmentation.

Results with augmented resources

While the sLLF algorithm has shown high success rate in finding feasible online EV charging schedules without resource augmentation, we further analyze the performance of online algorithms with resource augmentation in (a) power, and (b) both power and rate. Fig. 9.3 shows that the sLLF and OLP algorithm have the highest success rate of among other algorithms under various level of resource augmentation. We can see that to achieve 95% success rate for the sLLF algorithm, only 2% increase in resources is required. Table S3 shows that the minimum ϵ resource augmentation required for each algorithm to achieve 100% feasibility for all instances is smallest for the LLF and sLLF algorithms. Other algorithms (EDF, ES, REP and OLP) require significantly larger augmentation compared to the sLLF algorithm. While the OLP algorithm has high success rate without augmentation (Fig. 9.1), it requires much more resource augmentation to achieve 100% success rate (Table S3).

Conclusion

We have formulated EV charging as a feasibility problem that meets all EVs' energy demands before departure under charging rate constraints and total power constraint, and proposed an online algorithm, the sLLF algorithm, that decides on the current charging rates based on only the information up to the current time. We characterize the performance of the sLLF algorithm analytically and numerically. Numerical experiments with real-world data show that it has significantly higher rate of generating feasible EV charging than several other common EV charging algorithms. By finding feasible EV charging schedules using only a small augmentation to the absolute minimum resource needed for offline feasibility, our proposed algorithm (sLLF) can significantly reduce infrastructural cost for EV charging facilities.

Chapter 10

APPLICATION IN SCHEDULING II: OPTIMAL DISTRIBUTED SCHEDULING ALGORITHMS

Traditionally, the scheduling literature has assumed a static or fixed service capacity. However, it is increasingly common for modern applications to have the ability to dynamically adjust their service capacity in order to match the current demand. For example, power distribution networks match the energy supply demand as it changes over time and, when using cloud computing services, one can modify the total computing capacity by changing the number of computing instances and their speeds.

The ability to adapt service capacity dynamically gives rise to challenging new design questions. In particular, how to enhance the predictability and stability of service capacity is of great importance in such applications since peaks and fluctuations often come with significant costs [26, 128, 181]. For example, the emerging load from electric vehicle charging stations leads to new challenges in power distribution networks. Specifically, maintaining stable power consumption is important because fluctuations and large peaks in power use may strain the grid infrastructure and result in a high peak charge for the station operators. The stations also prefer predictable power consumption because purchasing power in real time is typically more expensive than purchasing in advance. Cloud content providers also prefer stable and predictable service capacity because on-demand contracts for compute instances (*e.g.* Amazon EC2 and Microsoft Azure) are typically more expensive than long-term contracts. Additionally, significant fluctuations in service capacity induce unnecessary power consumption and infrastructure strain for computing equipment.

Thus, in situations where service capacity can be dynamically adjusted, an important design goal is to reduce the costs associated with unpredictability and instability in the service capacity while maintaining a high quality of service, *e.g.* meeting job deadlines and satisfying job demands. In this work, we study this problem by minimizing the variance and mean square of the service capacity in systems where jobs arrive with demand and deadline requests. Our model is motivated by power distribution networks, where the size of jobs and (active) service capacity is small

compared to the total energy resources available and where contracts often depend on the mean and variance of service capacity, *e.g.* if a charging station participates in the regulation market, then costs/payments rely explicitly on them [14, 178].

Because of the scale of the service systems considered, we focus on *distributed* scheduling algorithms that use only local information about each job to decide the service rate. For example in power distribution networks and cloud computing, implementing centralized algorithms is likely to be prohibitively slow and costly in large-scale service systems, *i.e.* we are unlikely to be able to access global information about all jobs and servers in the system in real time when deciding the service rate of individual jobs.

In this chapter, we adapt tools from optimization and control theory to characterize in a broad range of settings the optimal distributed policies without any approximation. Further, we provide novel competitive-ratio-like bounds that describes the gap between the performance of optimal distributed policies and the performance of optimal centralized policies. Specifically, we identify the optimal distributed algorithms under strict demand and deadline requirements (Theorem 10.2.1), soft demand requirements (Theorem 10.2.2), soft deadline requirements (Theorem 10.2.3), and soft demand and deadline requirements (Theorem 10.2.4) in settings with stationary Poisson arrivals as well as non-stationary Poisson arrivals (Theorem 10.4.1 and Corollary 10.4.1).

Our first results focus on stationary arrivals. While a considerable amount of work has analyzed the variance of specific policies (see [57] and references therein), little prior work characterizes the optimal policies. In the basic setting of strict service requirements, we show that *Exact Scheduling* is the optimal distributed algorithm, *i.e.* the distributed algorithm that minimizes the stationary service capacity variance. Exact Scheduling is a simple scalable algorithm that works by finishing jobs *exactly* at their deadlines using a constant service rate [26, 57, 111]. Although it has received considerable attention in the existing literature, its optimality conditions have been unknown. In more general settings of soft service requirements, we propose novel generalizations of Exact Scheduling, each of which minimizes a combination of the service capacity variance, the expected penalties for unsatisfied demands, and the expected penalties for deadline extensions. These optimal algorithms all have closed-form expressions and use constant service rates with varying forms of rate and admission control. Due to these properties, they are also easy to implement and highly scalable.

We also extend our results to the case of non-stationary Poisson job arrivals and characterize the policies optimal when the objective is to minimize the time-average of the service capacity variance, the penalties for unsatisfied demands, and the penalties for deadline extensions. Additionally, we consider a more general class of objective functions: the service capacity variance, the mean-squared service capacity, and the weighted sum of the two. The resulting optimal algorithm has a striking analogy to the YDS algorithm [205], which is an offline algorithm that minimizes service capacity peaks in a related, deterministic worst-case version of the problem. This connection suggests the opportunity to transform other deterministic offline algorithms to stochastic online algorithms in related problems.

Given our focus on *distributed* algorithms, an important question is how these distributed algorithms perform compared with the optimal centralized algorithm. However, little work has been done to characterize the performance degradation of distributed algorithms from centralized algorithms in terms of their achievable service capacity variance. A major difficulty comes from that the optimal centralized algorithms are unknown. Leveraging tools from optimal control, we provide closed-form formulas on the performance degradation due to using distributed algorithms in the settings of both strict service requirements (Corollary 10.3.1 and Corollary 10.3.3) and soft service requirements (Corollary 10.3.2). The resulting bounds suggest that, when sojourn times are homogeneous, Exact Scheduling attains the optimal trade-off between service capacity variance and total remaining demand variance achievable by any centralized algorithms. Note that our proof technique (Lemma 10.3.1) is novel in its use of optimal control and has the potential for providing competitive-ratio-like bounds for other scheduling policies. We also compare distributed algorithms with centralized algorithms in our motivating examples of electric vehicle charging. Our test in real Electric Vehicle Charging Testbed [102] shows that the proposed optimal distributed algorithms also achieve comparable performance with existing centralized algorithms in practice.

10.1 System model

The goal of this chapter is to characterize the online scheduling policies that minimize service capacity variance, mean square, and both subject to service quality constraints for systems with the ability to dynamically adjust their service capacity. We use a continuous time model, where $t \in \mathcal{T} = [0, T]$ denotes a point in time and $T \geq 0$ is the (potentially infinite) time horizon. Each job, indexed by $k \in \mathcal{V} = \{1, 2, \cdots\}$, is characterized by an arrival time a_k, a service demand σ_k, a

sojourn time τ_k, a unit cost for unsatisfied demand δ_k, and a unit cost for deadline extension ϵ_k. Given the arrival time a_k and the sojourn time τ_k, the deadline of job k is defined to be $a_k + \tau_k$. Before we formulate the scheduler design problem, we first introduce below the arrival profiles, the service profiles, and the design objectives.

Arrival profiles. We represent the set of jobs as a marked point process $\{(a_k; \sigma_k, \tau_k, \delta_k, \epsilon_k)\}_{k\in\mathcal{V}}$ in space $\mathcal{T}\times S\times C$, where the arrival times $a_k \in \mathcal{T}$ are the set of points, and the service requirements $(\sigma_k, \tau_k) \in S$ and costs for unmet requirements $(\delta_k, \epsilon_k) \in C$ are the set of marks.[1] We assume that the point process is an independently marked Poisson point process, which is defined by an intensity function $\tilde{\Psi}(a)$ on $\mathcal{T}$ and a mark joint density measure $f_a(\sigma, \tau)g_a(\delta)h_a(\epsilon)$ on $S\times C$ [7]. This also implies that $\{(a_k; \sigma_k, \tau_k)\}_{k\in\mathcal{V}}$ is a Poisson point process on $\mathcal{T} \times S$ with the intensity function $\Psi(a, \sigma, \tau) = \tilde{\Psi}(a)f_a(\sigma, \tau)$. Intuitively, the intensity function is the average rate at which jobs with service requirement (σ, τ) arrive at time a. When both $\tilde{\Psi}(a) \equiv \tilde{\Psi}$ and $f_a(\sigma, \tau) \equiv f(\sigma, \tau)$ do not depend on a, we say that the arrival distribution is stationary . For a stationary arrival distribution, the intensity function of the Poisson point process simplifies to $\Psi f(\sigma, \tau)$. We focus on stationary arrival processes in Section 10.2 and then generalize our results to non-stationary arrivals in Section 10.4. Throughout, we assume that the service demand σ and the sojourn time τ has finite first and second moments, S is bounded, and $S \subset \{(\sigma, \tau) : \tau \geq \sigma \text{ and } \sigma \geq 0\}$.[2]

Service profiles. The service system works on each job $k \in \mathcal{V}$ with a *service rate* $r_k(t)$, which is an integrable function of t. The service rate can take any non-negative values that are smaller than the maximum rate $\bar{r}$, and without loss of generality, we assume that $\bar{r} = 1$, *i.e.*

$$r_k(t) \in [0,\ 1]. \tag{10.1}$$

To meet the demand requirements, the service rate must satisfy

$$\int_{a_k}^{\infty} r_k(t)dt = \sigma_k, \qquad k \in \mathcal{V}. \tag{10.2}$$

To meet the deadline requirements, it also need to satisfy

$$r_k(t) \leq \mathbf{1}\{a_k \leq t < a_k + \tau_k\}, \qquad k \in \mathcal{V}, . \tag{10.3}$$

[1] Here, we use $(a; \sigma, \tau, \delta, \epsilon)$ to denote the random variables and $(a_k; \sigma_k, \tau_k.\delta_k, \epsilon_k)$ to denote one realization of them in job k.

[2] The condition $\tau \geq \sigma$ constrains the service demand σ of a job to be no more than the amount of service that can be provided within its sojourn time τ.

where $\mathbf{1}\{A\}$ denotes the indicator function for an event A.

The service rate also determines three important quantities associated with costs: service capacity, the amount of unsatisfied demands, and the amount of deadline extensions. The service capacity is the instantaneous resource consumption of the system, given by

$$P(t) = \sum_{k \in \mathcal{V}} r_k(t). \tag{10.4}$$

We assume that $P(t)$ has no upper bound, implying that there is always enough capacity to serve the jobs. The total penalty for unmet demands of jobs with deadline t is

$$U(t) = \sum_{k \in \mathcal{V}: a_k + \tau_k = t} \delta_k(\sigma_k - \hat{\sigma}_k), \tag{10.5}$$

where $\hat{\sigma}_k = \int_{a_k}^{\infty} r_k(t)dt$ is defined to be the unsatisfied demands of job k. The total penalty for deadline extensions of jobs with deadline t is

$$W(t) = \sum_{k \in \mathcal{V}: a_k + \tau_k = t} \epsilon_k(\hat{\tau}_k - \tau_k), \tag{10.6}$$

where $\hat{\tau}_k = \max\{t - a_k : r_k(t) > 0\}$ is defined to be the actual sojourn time of job k.

Design objectives. We consider designing *online* scheduling algorithms, which decide the service rates in real-time without using the future job arrival information. For scalability, we restrict our attention to *distributed* algorithms which only need the local information about each job to decide its service rate. Examples of online distributed algorithms are *Immediate Scheduling*, *Delayed Schedule*, and *Exact Scheduling* (see Figure 10.1).

Our design objective is to reduce the variance and mean square in service capacity for the settings with strict or soft service constraints. In the case of *strict service constraints*, we consider the optimization problem

$$\text{minimize} \quad \frac{1}{T} \int_0^T \Big(\text{Var}(P(t)) + \alpha \mathbb{E}[P(t)]^2 \Big) dt, \tag{10.7}$$

where the first term quantify the service capacity predictability, the second term quantify the service capacity stability. The coefficient $\alpha (\geq 0)$ balances the predictability and stability of $P(t)$, and at $(\alpha, \beta) = (1, 1)$, the objective function reduces to the time average of $\mathbb{E}[P(t)^2]$. In the case of *soft service constraints*, we consider the optimization problem

$$\text{minimize} \quad \frac{1}{T} \int_0^T \Big(\text{Var}(P(t)) + \mathbb{E}[U(t)] + \mathbb{E}[W(t)] \Big) dt, \tag{10.8}$$

where the unit cost of unmet demands δ_k and the unit cost of deadline extension ϵ_k implicitly balances the cost associated with service capacity variability and the service quality in demand and deadline satisfaction.

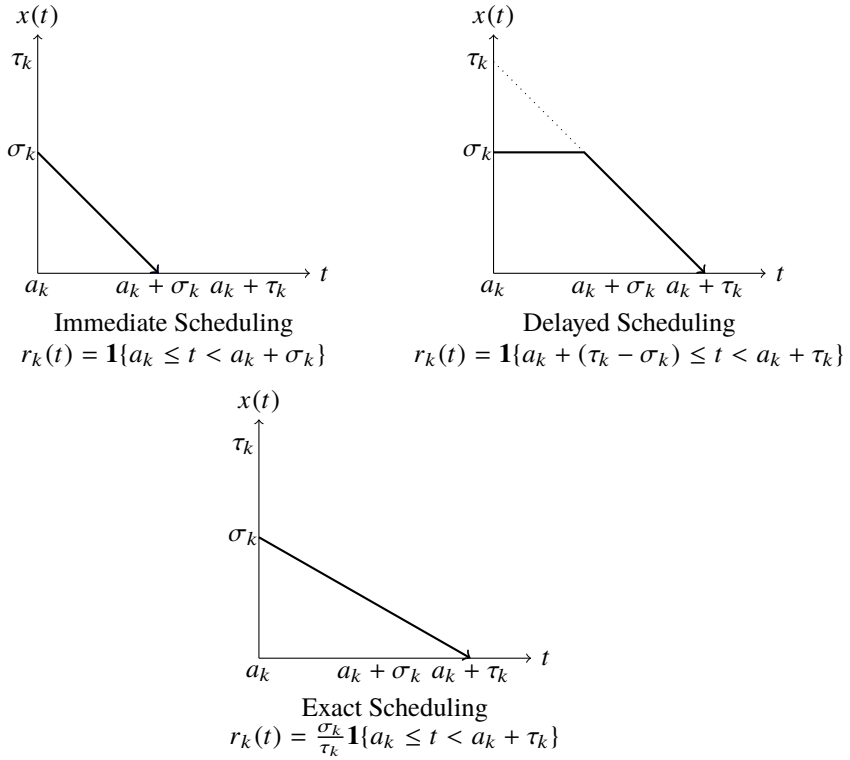

Figure 10.1: Examples of distributed scheduling algorithms. The solid black lines represent the remaining demand $x(t)$ at time t. Immediate Scheduling works by serving jobs at full rate upon arrival. Delayed Scheduling works by serving at full rate with a delay that is equal to its laxity $a + \tau - \sigma$. Exact Scheduling works by throttling service to a constant rate σ/τ so that all jobs are completed exactly at its deadline.

Motivating examples. The general model we have defined is meant to give insight into the design trade-offs that happen in applications with dynamic capacity, *e.g.* electric vehicle charging, cloud content providers, and resource allocations in the Internet of Things. Importantly, in this chapter we are not trying to model a specific application, rather we are exploring design trade-offs using a simple, general model.

However, to highlight the connection to our motivating examples, consider first the case of electric vehicle charging [102]. In this case, each job $k \in \mathcal{V}$ corresponds to an electric vehicle with an arrival time a_k, an energy demand σ_k, and a sojourn time τ_k. At each time t, the charging station draws $P(t) = \sum_{k \in \mathcal{V}} r_k(t)$ amount

of power from the grid to provide each vehicle k with a charging rate of $r_k(t)$. When doing so, stable resource usage is highly desirable because fluctuations and large peaks in $P(t)$ can strain the grid and results in a high peak charge for station operators. Moreover, predictable resource usage is also important when purchasing energy from the day-ahead market, whose price is lower and less volatile than that of the real-time market. Note that our model assumes $P(t)$ is unbounded and, thus, corresponds to a setting where there are more charging stations than arriving cars.

In the case of cloud content providers, each job $k \in \mathcal{V}$ corresponds to a task (requested to the cloud or data centers) with an arrival time a_k, a work requirement σ_k, and an allowable waiting time τ_k. The service system works on job k with speed $r_k(t)$ using $P(t) = \sum_{k\in\mathcal{V}} r_k(t)$ number of computers (or amount of power). Here again, a good estimate of the future resource use enables the cloud users to reserve resources through a long-term contract, whose price is lower and less volatile than that of a short-term contract, suggesting the benefit of having a predictable resource use. Note that our model considers the case where $P(t)$ is unbounded and, thus, the data center has enough capacity to avoid congestion, *i.e.* is in low utilization. Such periods are common, since data centers often operate at utilizations as low as 10% [73]. For future work, it is important to study how to manage congested periods by considering an upper bound on $P(t)$.

10.2 Maximizing predictability under stationary job arrivals

In this section, we characterize optimal distributed scheduling policies in a wide range of objectives when job arrivals are stationary, starting with the simplest and moving toward the most complex. To begin, we define each setting and pose the scheduler design problems as constrained functional optimizations (Section 10.2). Then, we focus on strict service requirements and show that Exact Scheduling minimizes the stationary variance of the service capacity (Section 10.2). Relaxing the demand requirements, we show that a variation of Exact Scheduling minimizes the weighted sum of the stationary variance of service capacity and the penalty for unsatisfied demand (Section 10.2). Relaxing the deadline requirements, we show that a different variation of Exact Scheduling minimizes the weighted sum of both the stationary variance of service capacity and the penalty for demand extension (Section 10.2). Finally, we consider the case when both the demand and deadline requirements are relaxed (Section 10.2) and show that the optimal policy can be constructed from an integration of the above optimal policies. It is interesting that all optimal algorithms admit closed-form expressions, which

provide clear interpretations and insights regarding the optimal trade-offs between reducing service capacity variability, satisfying the demands, and meeting deadlines. Moreover, they are also highly scalable and easy to implement.

Problem formulation

We study the settings when the arrival process is an independently marked *stationary* Poisson point process,

$$\Psi(a, \sigma, \tau) = \Psi f(\sigma, \tau), \qquad a \in \mathcal{T}, (\sigma, \tau) \in S. \tag{10.9}$$

Assuming the unit cost for unsatisfied demands δ_k and that for deadline extensions ϵ_k are homogeneous among different jobs, *i.e.* $\delta_k = \delta$, $\epsilon_k = \epsilon$ for any $k \in \mathcal{V}$, we consider distributed scheduling policies of the form

$$r_k(t) = u(x_k(t), y_k(t)) \geq 0, \tag{10.10}$$

where $u : \mathbb{R}p \times \mathbb{R} \to \mathbb{R}p$ is a non-negative integrable function of the remaining demand $x_k(t)$ and the remaining time $y_k(t)$ of job k. The policy is distributed in the sense that service rate of a job is determined using only its own information. We study policies of the form (10.10) assuming a situation where there is enough capacity available to satisfy the demand, and so the focus is on determining the optimal service rate for the jobs in a distributed manner.

Under any policy of the form (10.10), the process $\{(x_k(t), y_k(t)) : k \in \mathcal{V}, a_k \leq t\}$ for remaining jobs in the system can be represented as a point process in a two-dimensional space of remaining times and remaining demands. Moreover, the set of jobs remaining in the system converges to a stationary distribution. This stationary distribution is a Spatial Poisson Point Process with an intensity function $\lambda(x, y)$ satisfying[3]

$$0 = \frac{\partial}{\partial x}(\lambda(x, y)u(x, y)) + \frac{\partial}{\partial y}\lambda(x, y) + \Psi f(x, y). \tag{10.11}$$

Because the remaining job distribution converges to a stationary distribution, $P(t)$ also converges to a stationary distribution. Moreover, its stationary mean $\mathbb{E}[P]$ is determined only by the total service provided—given the total service, $\mathbb{E}[P]$ does not depend on the specific form of the policy.

[3]We use (x, y) to denote the coordinate in the two dimensional space of remaining demands and remaining times and $(x_k(t), y_k(t))$ to denote a point (job profile) in the space at time t.

Proposition 10.2.1. *Consider a service system with a stationary Poisson arrivals with intensity measure $\Lambda f(\sigma, \tau)$ and a distributed scheduling policy of the form* (10.10)*. Let us define $\hat{\sigma}(\sigma, \tau)$ to be total service provided for a job with demand σ and a sojourn time τ receives. The stationary mean of $P(t)$ is given by*

$$\mathbb{E}[P(t)] = \Psi \mathbb{E}[\hat{\sigma}(\sigma, \tau)]. \tag{10.12}$$

We present a proof of Proposition 10.2.1 in Appendix B.2. Alternatively, it can also be seen from classical queueing results such as Little's Law and the Brumelle's formula [8, Chapter 3, eq. (3.2.1)].

Among policies (10.10) with the same stationary mean (10.12), we consider minimizing the variance of $P(t)$ under strict service constraints, soft demand constraints, soft deadline constraints, and soft demand and deadline constraints. In the case of *strict demand constraints*, we consider the following optimization problem:

$$\underset{u:(10.1)(10.2)(10.3)(10.10)(10.11)}{\text{minimize}} \quad \text{Var}(P), \tag{10.13}$$

where the optimization variable taken over the set of distributed policies (10.10) subject to the service rate constraints (10.1), the demand constraints (10.2), and the deadline constraints (10.3). Here, $\text{Var}(P)$ is a functional of u and $\lambda(\sigma, \tau)$, where $\lambda(\sigma, \tau)$ satisfies from (10.11).

In the case of *soft demand constraints*, we relax the demand constraints (10.2) into paying penalty $\delta_k = \delta$ for each unit of unsatisfied demands and consider balancing the service capacity variance and the penalties due to unsatisfied demands:

$$\underset{u:(10.1)(10.3)(10.10)(10.11)}{\text{minimize}} \quad \text{Var}(P) + \mathbb{E}[U]. \tag{10.14}$$

In the case of *soft deadline constraints*, we relax the deadline constraints (10.3) into paying penality ϵ for each unit of deadlines extensions and consider balancing the service capacity variance and the penalties due to deadline extensions:

$$\underset{u:(10.1)(10.2)(10.10)(10.11)}{\text{minimize}} \quad \text{Var}(P) + \mathbb{E}[W]. \tag{10.15}$$

In the case of *soft demand and deadline constraints*, we relax both the demand and deadline requirements (10.2) and (10.3) into paying δ for each unit of unsatisfied demands and ϵ for each unit of deadline extensions. We consider balancing the

service capacity variance and the penalties due to unsatisfied demands and deadline extensions:

$$\underset{u:(10.1)(10.10)(10.11)}{\text{minimize}} \quad \text{Var}(P) + \mathbb{E}[U] + \mathbb{E}[W]. \tag{10.16}$$

Finally, we consider the most general setting, when the penalties for unsatisfied demands and deadlines are heterogeneous among jobs. To account for this heterogeneity, we consider distributed scheduling policies of the form

$$r_k(t) = \bar{u}(x_k(t), y_k(t), \delta_k, \epsilon_k) \geq 0. \tag{10.17}$$

Under any policy of the form (10.17), the remaining job profiles in the system $\{(x_k(t), y_k(t), \delta_k, \epsilon_k) : k \in \mathcal{V}, a_k \leq t\}$ can be represented as a point process in the 4-dimensional space of remaining times, remaining demands, unit costs for unsatisfied demand, and unit costs for deadline extension. This point process converges to a stationary Spatial Poisson Point Process with an intensity function $\lambda(x, y, \delta, \epsilon)$ satisfying

$$0 = \frac{\partial}{\partial x}(\lambda(x, y, \delta, \epsilon)\bar{u}(x, y, \delta, \epsilon)) + \frac{\partial}{\partial y}\lambda(x, y, \delta, \epsilon) + \Psi f(x, y)g(\delta)h(\epsilon). \tag{10.18}$$

This leads to the following optimization problem:

$$\underset{\bar{u}:(10.1)(10.18)}{\text{minimize}} \quad \text{Var}(P(t)) + \mathbb{E}\left[U(t)\right] + \mathbb{E}\left[W(t)\right]. \tag{10.19}$$

Strict demand and deadline requirements

We first consider the case of strict service requirements and show a closed-form characterization of the optimal algorithm that minimizes the stationary variance $\text{Var}(P)$. To do so, it is worth noticing that peaks in service rate amplifies the uncertainties in the future arrivals, which in turn produces large variance in $P(t) = \sum_k r_k(t) = \sum_k u(x_k(t), y_k(t))$. This observation suggests that having a flat service rate may achieve small variance. One such policy is *Exact Scheduling*,

$$u(x, y) = \begin{cases} \dfrac{x}{y}, & \text{if } y > 0, \\ 0, & \text{otherwise.} \end{cases} \tag{10.20}$$

which works by finishing each jobs *exactly* at its deadline using a constant service rate (Figure 10.2). It is also highly scalable because it is distributed and asynchronous, and it does not require much computation or memory use. Although existing literature has analyzed its performance in various settings [26, 57, 103, 111], no

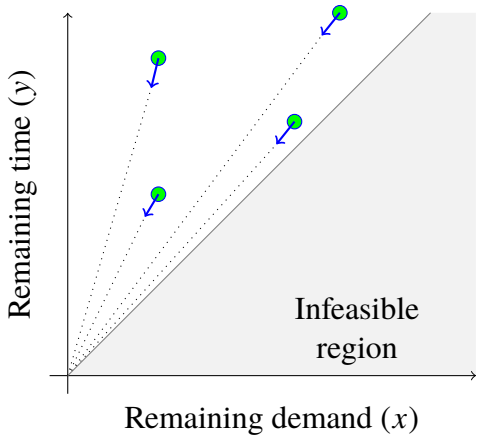

Figure 10.2: *Exact scheduling depicted in the space of remaining demand x and remaining time y.*

work has shown its optimality conditions. In this section, we show that Exact Scheduling minimizes the stationary service capacity variance under strict demand and deadline constraints.

Theorem 10.2.1. *Exact Scheduling* (10.20) *is the optimal solution of* (10.13) *and achieves the optimal value*[4]

$$\mathrm{Var}(P) = \Psi\mathbb{E}\left[\frac{\sigma^2}{\tau}\right]. \tag{10.21}$$

Theorem 10.2.1 shows the achievable performance improvement by controlling the service capacity using distributed algorithms. If no control is applied, then $r_k(t) = \mathbf{1}\{t \in [a_k, a_k + \sigma_k)\}$, and the stationary mean and variance of $P(t)$ is $\mathbb{E}(P) = \mathrm{Var}(P) = \Lambda\mathbb{E}[\sigma]$. By performing a distributed service capacity control, the stationary variance can be reduced by

$$\Lambda\mathbb{E}\left[\frac{\sigma(\tau-\sigma)}{\tau}\right] \in [0, \Lambda\mathbb{E}[\sigma]] \tag{10.22}$$

where $\tau - \sigma$ is a slack time (the amount of time left at job completion if a job is served at its maximum service rate).

Next, we present the proof of Theorem 10.2.1. To circumvent the complex constraints of (10.13), we first provide a lower bound on its optimal solution by relaxing the class of control policies into

$$r_k(t) = v(\sigma_k, \tau_k, y_k(t)) \quad k \in \mathcal{V}, \tag{10.23}$$

[4]Observe that Λ is the cumulative arrival rate.

and solve the optimization problem

$$\underset{v:(10.1)(10.2)(10.3)(10.23)}{\text{minimize}} \quad \text{Var}(P). \tag{10.24}$$

Because the constraint set of (10.13) is contained in the constraint set of (10.24), the optimal value of (10.24) lower-bounds that of (10.13). Therefore, to prove Theorem 10.2.1, it suffices to show that the optimal solution of (10.24) (given in the next lemma) is also achievable by a control policy of the form (10.10).

Lemma 10.2.1. *The optimal solution of* (10.24) *is*

$$v(\sigma, \tau, y) = \frac{\sigma}{\tau}\mathbf{1}\{y > 0\}, \tag{10.25}$$

and it yields the optimal value

$$\text{Var}(P(t)) = \mathbb{E}\left[\frac{\sigma^2}{\tau}\right]. \tag{10.26}$$

To show Lemma 10.2.1, we use the following property of the system: since the control policy only depends on the job parameters, and jobs are served in parallel, the system behaves as an infinite server queue with Poisson arrivals. Therefore the system averages can be computed by integrating along the average trajectory along each job [7].[5] In particular, the following relation holds.

Lemma 10.2.2. *The mean and variance of* $P(t)$ *under the policy* (10.23) *are given by*

$$\mathbb{E}[P] = \int_{(\sigma,\tau)\in S}\int_0^\tau v(\sigma, \tau, y)\Lambda f(\sigma, \tau)dyd\sigma d\tau \tag{10.27}$$

$$\text{Var}(P) = \int_{(\sigma,\tau)\in S}\int_0^\tau v(\sigma, \tau, y)^2\Lambda f(\sigma, \tau)dyd\sigma d\tau. \tag{10.28}$$

Lemma 10.2.2 can be obtained from the Campbell's theorem (see Section B.1). Now we are ready to prove Lemma 10.2.1.

Proof. (Lemma 10.2.1) The demand constraints (10.2) and the deadline constraints (10.3) leads to

$$\int_0^\tau v(\sigma, \tau, y)dy = \sigma, \quad (\sigma, \tau) \in S. \tag{10.29}$$

[5] This is a restatement of Brumelle's formula [24] from queueing theory for the case of an infinite server system with time-varying rates.

The objective function (10.24) satisfies

$$\begin{aligned}\mathrm{Var}(P) &= \int_{(\sigma,\tau)\in S}\int_0^\tau v(\sigma,\tau,y)^2\Lambda f(\sigma,\tau)dyd\sigma d\tau &(10.30)\\ &= \int_{(\sigma,\tau)\in S}\left\{\int_0^\tau v(\sigma,\tau,y)^2dy\right\}\Lambda f(\sigma,\tau)d\sigma d\tau &(10.31)\\ &\geq \int_{(\sigma,\tau)\in S}\left\{\frac{\sigma^2}{\tau}\right\}\Lambda f(\sigma,\tau)d\sigma d\tau. &(10.32)\end{aligned}$$

Here, equality (10.30) is due to Lemma 10.2.2. Inequality (10.32) is due to (10.29) and the Holder's inequality, *i.e.* for any fixed (σ,τ),

$$\left(\int_0^\tau v(\sigma,\tau,y)^2dy\right)^{1/2}\left(\int_0^\tau 1dy\right)^{1/2} \geq \int_0^\tau v(\sigma,\tau,y)dy = \sigma, \tag{10.33}$$

where $v(\sigma,\tau,y)\geq 0$. Alternatively, it can be verified that (10.32) can be attained with equality when v equals (10.25). Therefore, (10.25) is the optimal solution of (10.24).

□

Now, we can prove Theorem 10.2.1 using Lemma 10.2.1.

Proof. (Theorem 10.2.1) Recall that the optimal solution of (10.24) is the policy (10.25). Under the policy (10.25), the ratio between its remaining demand $x(a+t)$ and remaining time $y(a+t)$ are constant for any $t\in[a,a+\tau]$. Therefore, (10.25) can be realized using policies of the form (10.20): Exact Scheduling (10.20). Because the optimal value of (10.24) is a lower bound on that of (10.13), Exact Scheduling is optimal for (10.13). □

Soft demand requirements

The previous section shows the optimal algorithm under strict service requirements. In this section, we relax the assumption of strict service requirements and characterize the optimal algorithm under soft demand constraints. Specifically, the system needs to pay the penalty δ for each unit of unsatisfied demands. The resultant optimal algorithm is a variation of Exact Scheduling with an additional rate upper-bound:

$$u(x,y)=\begin{cases}\dfrac{x}{y}, & \text{if } \dfrac{x}{y}\leq\dfrac{\delta}{2} \text{ and } y>0,\\ \dfrac{\delta}{2}, & \text{if } \dfrac{x}{y}>\dfrac{\delta}{2} \text{ and } y>0,\\ 0, & \text{otherwise.}\end{cases} \tag{10.34}$$

This policy essentially sets a threshold $\delta/2$ on the ratio σ/τ: jobs with the ratio above this threshold is served at a constant rate $\delta/2$ *until its deadline*; jobs with the ratio below this threshold is served according to Exact Scheduling. In other words, a job k receives its full service demand only if $\sigma_k \leq \delta\ \tau_k/2$. The policy (10.34) is extremely simple, and thus similar algorithms may be widely used in practice. However, to the best of our knowledge, their optimality conditions and the optimal thresholds on rate have not been discussed in the existing literature.

Theorem 10.2.2. *The policy* (10.34) *is the optimal solution of* (10.14) *and achieves the optimal value*

$$\mathrm{Var}(P) + \mathbb{E}[\delta U] = \mathbb{E}\left[\frac{\sigma^2}{\tau}\mathbf{1}\left\{\frac{\sigma}{\tau} \leq \frac{\delta}{2}\right\} + \delta\left(\sigma - \frac{\delta\tau}{4}\right)\mathbf{1}\left\{\frac{\sigma}{\tau} > \frac{\delta}{2}\right\}\right]\Lambda. \quad (10.35)$$

Theorem 10.2.2 shows the performance improvement gained by relaxing the demand requirements. If the system is allowed to not satisfy some demand requests, then the cost (objective value of (10.14)) can be reduced from $\mathrm{Var}(P) = \mathbb{E}\left[\sigma^2/\tau\right]$ to (10.35).

Soft deadline requirements

The previous section shows the optimal algorithm under soft demand requirements. In this section, we relax the deadline requirements instead and characterize the optimal distributed algorithm. Specifically, the system needs to pay penalty ϵ for each unit of deadline extensions. The resultant optimal algorithm is another variation of Exact Scheduling and deadline extension:

$$u(x,y) = \begin{cases} \dfrac{x}{y} & \text{if } \dfrac{x}{y} \leq \sqrt{\epsilon} \text{ and } y > 0 \\ \sqrt{\epsilon}\ \mathbf{1}\{x > 0\} & \text{otherwise.} \end{cases} \quad (10.36)$$

Similarly to (10.34), this policy essentially sets a threshold $\sqrt{\epsilon}$ on the ratio σ/τ: jobs with the ratio above this threshold is served according to Equal Service of rate $\sqrt{\epsilon}$ *until it finishes*, jobs with the ratio below this threshold is served according to Exact Scheduling. In other words, the deadline of job k is extended only if $\sigma_k > \sqrt{\epsilon}\tau_k$.

Theorem 10.2.3. *The policy* (10.36) *is the optimal solution of* (10.15) *and achieves the optimal value*

$$\mathrm{Var}(P) + \mathbb{E}[\epsilon W] = \mathbb{E}\left[\frac{\sigma^2}{\tau}\mathbf{1}\left\{\frac{\sigma}{\tau} \leq \sqrt{\epsilon}\right\} + \left(2\sqrt{\epsilon}\sigma - \epsilon\tau\right)\mathbf{1}\left\{\frac{\sigma}{\tau} > \sqrt{\epsilon}\right\}\right]\Lambda. \quad (10.37)$$

Theorem 10.2.3 shows the performance improvement by relaxing the deadline requirements. If all deadline must be satisfied, then $\mathrm{Var}(P) = \mathbb{E}\left[\sigma^2/\tau\right]$ is the minimum stationary variance achievable. If deadline extensions are allowed, then the cost can be further reduced to (10.37), and $\sqrt{\epsilon}$ strikes the optimal balance between minimizing service capacity variance and penalties for deadline extension. Interestingly, the optimal algorithm admits a closed-form solution, despite that scheduling problems with tardiness can sometimes be NP-hard [10, 50].

Soft demand and deadline requirements

The previous sections show the optimal algorithms under soft demand requirements and soft deadline requirements. In this section, we relax both demand and deadline requirements and characterize the optimal distributed algorithm. Specifically, the system needs to pay penalty δ for each unit of unsatisfied demands and penalty ϵ for each unit of deadline extensions. This setting recovers all previous settings as special cases.[6]

Recall from previous sections that, under soft demand requirements, the optimal policy uses a constant service rate and reject partial demand requests only if $\sigma/\tau > \delta/2$. Meanwhile, under soft deadline requirements, the optimal policy uses a constant service rate and extends the deadline only if $\sigma/\tau > \sqrt{\epsilon}$. These two special cases motivate as to combine the policies (10.20), (10.36), and (10.34) as follows:

$$u(x,y) = \begin{cases} \dfrac{x}{y} & \text{if } y > 0 \text{ and } \dfrac{x}{y} \le \min\left\{\dfrac{\delta}{2}, \sqrt{\epsilon}\right\} \\ \dfrac{\delta}{2} & \text{if } y > 0 \text{ and } \dfrac{x}{y} > \dfrac{\delta}{2} \text{ and } \dfrac{\delta}{2} \le \sqrt{\epsilon}\,, \\ \sqrt{\epsilon}\,\mathbf{1}\{x > 0\} & \text{otherwise} \end{cases} \tag{10.38}$$

The policy uses three strategies depending on different regimes of job states and penalties: high penalties regime, low demand penalty regime, and low deadline penalty regime. These regimes are illustrated in Figure 10.3 as the white, light gray, and dark gray regions, respectively.

- *High penalties regime.* When $\min(\delta/2, \sqrt{\epsilon}) > \sigma/\tau$, it is less costly to satisfy the service requirements than paying penalties for unsatisfied demands or deadlines. So, the best strategy is to satisfy both demands and deadlines optimally using Exact Scheduling (10.20).

[6] For sufficiently large δ, this setting recovers the case of strict demand requirements. For sufficiently large ϵ, this setting recovers the case of strict deadline requirements. For sufficiently large δ and ϵ, this setting recovers the case of strict demand and deadline requirements.

- *Low demand penalty regime.* When $\delta/2 \le \sqrt{\epsilon}$, the penalties for unsatisfied demands is smaller than that of deadline extensions, so the best strategy is to meet all deadlines optimally with potentially unsatisfied demands using the policy (10.34).

- *Low deadline penalty regime.* When $\delta/2 > \sqrt{\epsilon}$, the penalties for deadline extension is smaller than that of unsatisfied demands, so the best strategy is to satisfy demands optimally with potential deadline extensions using the policy (10.36).

From above, the policy (10.38) generalizes the optimal algorithms in Section 10.2-10.2, and we term it *Generalized Exact Scheduling*. The following theorem states its optimality condition.

Theorem 10.2.4. *The policy* (10.38) *is the optimal solution of* (10.16) *and achieves the optimal value*

$$\begin{aligned}&\mathrm{Var}(P) + \mathbb{E}[\delta U] + \mathbb{E}[\epsilon W] = \\ &\mathbb{E}\Bigg[\frac{\sigma^2}{\tau}\mathbf{1}\left\{\frac{\sigma}{\tau} \le \min\left\{\frac{\delta}{2}, \sqrt{\epsilon}\right\}\right\} \\ &+ \delta\left(\sigma - \frac{\delta\tau}{4}\right)\mathbf{1}\left\{\frac{\sigma}{\tau} > \frac{\delta}{2} \ge \sqrt{\epsilon}\right\} + \left(2\sqrt{\epsilon}\sigma - \epsilon\tau\right)\mathbf{1}\left\{\frac{\sigma}{\tau} > \sqrt{\epsilon} > \frac{\delta}{2}\right\}\Bigg]\Lambda.\end{aligned} \tag{10.39}$$

Theorem 10.2.4 shows when one should extend the deadline to satisfy the demand or let the job depart at its deadline with unsatisfied demands. Moreover, Generalized Exact Scheduling is also optimal for a more general problem (10.19), when the unit costs for unsatisfied demands and deadline extensions are allowed to be heterogeneous.

Corollary 10.2.1. *The optimal solution of* (10.19) *is*

$$\bar{u}(x, y, \delta, \epsilon) = \begin{cases} \dfrac{x}{y} & \text{if } y > 0 \text{ and } \dfrac{x}{y} \le \min\left\{\dfrac{\delta}{2}, \sqrt{\epsilon}\right\} \\ \dfrac{\delta}{2} & \text{if } y > 0 \text{ and } \dfrac{x}{y} > \dfrac{\delta}{2} \text{ and } \dfrac{\delta}{2} \le \sqrt{\epsilon} \\ \sqrt{\epsilon}\,\mathbf{1}\{x > 0\} & \text{otherwise} \end{cases}. \tag{10.40}$$

The proof of Corollary 10.2.1 is an immediate consequence of Theorem 10.2.4.

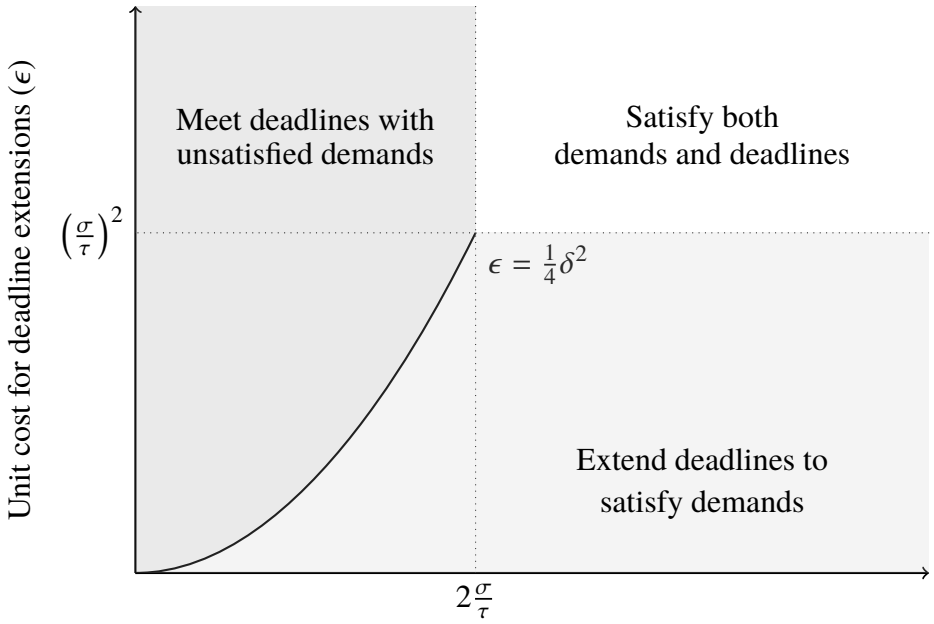

Figure 10.3: The decision space of the optimal policy for (10.16). For job profiles with a service demand σ, a sojourn time τ, and costs (δ, ϵ), the optimal policy performs either one of the following using constant service rates: satisfy both demands and deadlines (white region), meet deadlines with unsatisfied demand (dark gray region), or satisfy the demand by extending the deadline (light gray region).

10.3 Performance degradation inherent to distributed algorithms

Given our focus on distributed algorithms, it is important to understand how much performance degradation is incurred in comparison to centralized algorithms. In this section, we characterize this performance degradation at stationarity. Specifically, we first provide the upper bounds on the performance degradation (Section 10.3). We present the proof of the upper bound, which are potentially useful for analyzing other policies (Section 10.3).

Theoretical performance

In this section, we compare the performance of distributed policies and that of centralized policies. To this end, we first define centralized (online) policies and then bound their achievable performance. Centralized policies are the class of algorithms of the form

$$r_k(t) = w(k, t, A_t), \quad \forall k \in \mathcal{V}, \tag{10.41}$$

where $A_t = \{(a_k, \sigma_k, \tau_k, y_k(t)) : a_k \leq t\}$ is the set that contains the information of jobs arriving before t, and $w(k, t.\cdot)$ is a deterministic mapping from A_t to a service rate $r_k(t)$.

Lemma 10.3.1. *Under any centralized policy of the form* (10.41)*, the stationary variance of $P(t)$ is lower-bounded by*

$$\mathrm{Var}(P) \geq \frac{\Lambda^2 \mathbb{E}[\sigma^2]^2}{4\mathrm{Var}(X)}, \tag{10.42}$$

where $X(t)$ is the total remaining demands of jobs arriving before t, and $\mathrm{Var}(X)$ is the stationary variance of $X(t)$.

Lemma 10.3.1 characterizes the tradeoff between achieving a small variance of $X(t)$ and achieving a small variance of $P(t)$. Plugging in Exact Scheduling's stationary variance of X,

$$\mathrm{Var}(X) = \Lambda \mathbb{E}\left[\frac{1}{3}\sigma^2 \tau\right], \tag{10.43}$$

we obtain a competitive-ratio like bound for Exact Scheduling (10.20).

Corollary 10.3.1. *Let $\mathrm{Var}(P)$ be the stationary variance of $P(t)$ that is attained by Exact Scheduling* (10.20)*. Let $\mathrm{Var}(P^*)$ be the minimum stationary variance attainable by any centralized algorithm* (10.41) *with the same level of $\mathrm{Var}(X)$ as Exact Scheduling. Then, the following condition holds:*

$$\mathrm{Var}(P) \leq \frac{\mathbb{E}[\sigma^2/\tau]\mathbb{E}[\sigma^2\tau]}{\mathbb{E}[\sigma^2]^2}\mathrm{Var}(P^*), \tag{10.44}$$

where the expectations on the right hand side are taken over the arrival distribution.

Corollary 10.3.1 bounds the ratio of $\mathrm{Var}(P)$, achievable by Exact Scheduling (the optimal distributed algorithm), and $\mathrm{Var}(P^*)$, achievable by any centralized algorithms. When the sojourn time τ is a deterministic random variable, (10.44) reduces to $\mathrm{Var}(P) \leq \mathrm{Var}(P^*)$, implying that distributed algorithms can perform equally well compared to the centralized algorithms of the same $\mathrm{Var}(X)$. One such case is when both demands and sojourn times are deterministic, and the service demand of each job equals its sojourn time (here, the arrival time is still random). In this case, due to the rate limit (10.1), the demand constraints (10.2), and the deadline constraints (10.3), both the optimal centralized policy and the optimal distributed policy are

identical, *i.e.* $r_k(t) = \mathbf{1}\{t \in [a_k, a_k + \tau_k)\}$. In the setting of soft service requirements, Generalized Exact Scheduling attains

$$\begin{aligned}\mathrm{Var}(X) =& \mathbb{E}\left[\frac{\sigma^2\tau}{3}\mathbf{1}\left\{\frac{\sigma}{\tau} \le \min\left\{\frac{\delta}{2}, \sqrt{\epsilon}\right\}\right\}\right]\Lambda \\ &+ \mathbb{E}\left[\left(\frac{\delta^2\tau^3}{12} - \frac{1}{2}\delta\sigma\tau^2 + \sigma^2\tau\right)\mathbf{1}\left\{\frac{\sigma}{\tau} > \frac{\delta}{2} \ge \sqrt{\epsilon}\right\} + \left(\frac{\sigma^3}{3\sqrt{\epsilon}}\right)\mathbf{1}\left\{\frac{\sigma}{\tau} > \sqrt{\epsilon} > \frac{\delta}{2}\right\}\right]\Lambda.\end{aligned} \tag{10.45}$$

Combining above and Lemma 10.3.1, we obtain the following corollary.

Corollary 10.3.2. *Let* $\mathrm{Var}(P)$ *be the stationary variance of* $P(t)$ *that is attained by Generalized Exact Scheduling* (10.38) . *Let* $\mathrm{Var}(P^*)$ *be the minimum stationary variance attainable by any centralized algorithm of the form* (10.41) *with the same level of* $\mathrm{Var}(X)$ *as Generalized Exact Scheduling. Then, the following condition holds:*

$$\mathrm{Var}(P) \le \frac{\alpha\beta}{\mathbb{E}[\sigma^2]^2}\mathrm{Var}(P^*), \tag{10.46}$$

where

$$\begin{aligned}\alpha =& \mathbb{E}\Bigg[\frac{\sigma^2}{\tau}\mathbf{1}\left\{\frac{\sigma}{\tau} \le \min\left\{\frac{\delta}{2}, \sqrt{\epsilon}\right\}\right\} + \delta\left(\sqrt{\epsilon} - \frac{\delta\tau}{4}\right)\mathbf{1}\left\{\frac{\sigma}{\tau} > \frac{\delta}{2} \ge \sqrt{\epsilon}\right\} \\ &+ \left(2\sqrt{\epsilon}\sigma - \epsilon\tau\right)\mathbf{1}\left\{\frac{\sigma}{\tau} > \sqrt{\epsilon} > \frac{\delta}{2}\right\}\Bigg] \\ \beta =& \mathbb{E}\Bigg[\frac{\sigma^2\tau}{3}\mathbf{1}\left\{\frac{\sigma}{\tau} \le \min\left\{\frac{\delta}{2}, \sqrt{\epsilon}\right\}\right\} + \left(\frac{\delta^2\tau^3}{12} - \frac{1}{2}\delta\sigma\tau^2 + \sigma^2\tau\right)\mathbf{1}\left\{\frac{\sigma}{\tau} > \frac{\delta}{2} \ge \sqrt{\epsilon}\right\} \\ &+ \left(\frac{\sigma^3}{3\sqrt{\epsilon}}\right)\mathbf{1}\left\{\frac{\sigma}{\tau} > \sqrt{\epsilon} > \frac{\delta}{2}\right\}\Bigg].\end{aligned}$$

Corollary 10.3.2 bounds the ratio of $\mathrm{Var}(P)$ achievable by Generalized Exact Scheduling (the optimal distributed algorithm) to $\mathrm{Var}(P^*)$ achievable by any centralized algorithms. Here, the optimal distributed algorithm is subject to soft service constraints (10.2)–(10.3), while the optimal centralized algorithm is subject to the same $\mathrm{Var}(X)$ with Generalized Exact Scheduling.

Corollary 10.3.3. *Let* $\mathrm{Var}(P)$ *be the stationary variance of* $P(t)$ *attained by Exact Scheduling* (10.20). *Let* $\mathrm{Var}(P^\dagger)$ *be the optimal performance among the centralized scheduling policies that satisfy the demand and deadline constraints* (10.2)–(10.3). *Then, the following condition holds:*

$$\mathrm{Var}(P) \le \frac{1}{12}\frac{\Lambda\mathbb{E}[\sigma^2]^2\mathbb{E}\left[\sigma^2\tau\right]}{\mathbb{E}[\tau\sigma^2] + \Lambda\mathbb{E}\left[\tau\sigma\right]^2}\mathrm{Var}(P^\dagger). \tag{10.47}$$

Corollary 10.3.3 bounds the ratio of $\mathrm{Var}(P)$ achievable by the optimal distributed algorithm to $\mathrm{Var}(P^*)$ achievable by any centralized algorithms. Here, both the optimal distributed algorithm and the optimal centralized algorithm are subject to strict service constraints (10.2)–(10.3). The bound (10.47) may not be tight because the relationship between $\mathrm{Var}(X)$ and the service constraints are hard to characterize precisely.

Proof of Lemma 10.3.1

Let

$$\mathrm{Var}(X) \leq D \tag{10.48}$$

for some $D > 0$. We consider the following problem:

$$Q_{\mathrm{on}} = \underset{w:(10.48)}{\text{minimize}} \lim_{T\to\infty} \frac{1}{T} \int_0^T \mathrm{Var}(P(t))dt,$$

where the optimization is taken over all centralized policies of the form (10.41). The Lagrangian of Q_{on} is

$$L(w; r) = \lim_{T\to\infty} \frac{1}{T} \int_0^T \mathrm{Var}(P(t)) + \gamma(\mathrm{Var}(X(t)) - D)dt, \tag{10.49}$$

where $\gamma \geq 0$ is the Lagrangian multiplier associated with the constraint (10.48). Due to

$$\inf_w L(w; \gamma) \leq Q_{\mathrm{on}} \leq \mathrm{Var}(P), \tag{10.50}$$

we can derive a lower bound of $\mathrm{Var}(P)$ via solving $\inf_w L(w; \gamma)$ as follows.

Lemma 10.3.2. *The minimum value of $L(w; r)$ is*

$$\mathrm{Var}(P(t)) + \gamma(\mathrm{Var}(X(t)) - D) = \sqrt{\gamma}\Lambda\mathbb{E}[\sigma^2] - \gamma D, \tag{10.51}$$

which is achieved by

$$P(t) = \sqrt{\gamma}(X(t) - \bar{X}(t)) + \bar{P}. \tag{10.52}$$

Lemma 10.3.2 is proven in Appendix B.6. From Lemma 10.3.2, the optimal solution of (10.50) attains

$$\mathrm{Var}(P(t)) + \gamma\mathrm{Var}(X(t)) = 2\gamma\mathrm{Var}(X(t)). \tag{10.53}$$

Combining (10.48), (10.51), and (10.53) leads to

$$\mathrm{Var}(X(t)) = \frac{1}{2\sqrt{\gamma}}\Lambda\mathbb{E}[\sigma^2]. \tag{10.54}$$

Since $X(t)$ also satisfies the constraint (10.48), the Lagrangian multiplier γ is lower-bounded by

$$\frac{1}{2D}\Lambda\mathbb{E}[\sigma^2] \leq \sqrt{\gamma}. \tag{10.55}$$

Therefore, we obtain

$$\begin{aligned}
\mathrm{Var}(P(t)) &\geq \inf_{w} L(u;\gamma) && (10.56)\\
&\geq \frac{\sqrt{\gamma}}{2}\Lambda\mathbb{E}[\sigma^2] && (10.57)\\
&\geq \frac{1}{4D}\Lambda^2\mathbb{E}[\sigma^2]^2. && (10.58)
\end{aligned}$$

where (10.56) is due to (10.50); (10.57) is due to (10.51) and (10.52); and (10.58) is due to (10.55).

10.4 Balancing predictability and stability under non-stationary job arrivals

Building upon the results of stationary job arrivals, we consider a more general setting of non-stationary job arrivals in this section. The non-stationary setting is particularly appealing for practical applications since dynamic capacity management is crucial when the workload is not stationary. In contrast to the stationary setting, there exists a trade-off between maximizing the stability and predictability of the service capacity in the non-stationary setting. We characterize such tradeoffs and the Pareto-optimal distributed algorithm that balances stability and predictability. Below, we first formally define the notion of Pareto-optimality, which recovers maximum predictability and maximum stability as two special cases (Section 10.4). Then, at one extreme case of maximizing predictability, we show that Generalized Exact Scheduling is the optimal algorithm (Section 10.4). At the other extreme case of maximizing stability, we characterize the optimal algorithm and notice an interesting connection to the well-known YDS algorithm [205], which is optimal in a related, deterministic worst-case setting. Generalizing the two extreme cases, we describe the Pareto-optimal algorithm that balances predictability and stability (Section 10.5).

Problem formulation

In this section, we relax our previous stationary assumptions on the arrival process. We assume that the arrival distribution is a non-stationary independently marked

Poisson process with the intensity function $\tilde{\Psi}(a)$ and a mark joint density measure $f_a(\sigma,\tau)g_a(\delta)h_a(\epsilon)$ (see Section 10.1). To cope with the non-stationary arrivals, we allow the scheduling policies to change over time as follows:

$$r_k(t) = u(a_k, x_k(t), y_k(t)) \geq 0 \quad k \in \mathcal{V} \tag{10.59}$$

$$r_k(t) = \bar{u}(a_k, x_k(t), y_k(t), \delta_k, \epsilon_k) \geq 0 \quad k \in \mathcal{V} \tag{10.60}$$

$$r_k(t) = v(a_k, \sigma_k, \tau_k, y_k(t)) \geq 0 \quad k \in \mathcal{V}, \tag{10.61}$$

The policies of the form (10.59), (10.60), and (10.61) are all online and distributed in the sense that the service rate of job k only depends on the information of itself.

We seek to design policies that balance three important performance criteria: the quality of service, the service capacity variance associated with the predictability, and its mean square associated with the stability. In the most basic settings involving the first two criteria, we consider

$$\underset{u:(10.1)(10.2)(10.3)(10.59)}{\text{minimize}} \quad \lim_{T\to\infty} \frac{1}{T}\int_0^T \text{Var}(P(t))dt \tag{10.62}$$

$$\underset{\bar{u}:(10.1)(10.60)}{\text{minimize}} \quad \lim_{T\to\infty} \frac{1}{T}\int_0^T \Big(\text{Var}(P(t)) + \mathbb{E}[U(t)] + \mathbb{E}[W(t)]\Big)dt. \tag{10.63}$$

In a more advanced settings involving all three criteria, we consider

$$\underset{v:(10.2)(10.3)(10.61)}{\text{minimize}} \quad \lim_{T\to\infty} \frac{1}{T}\int_0^T \alpha\mathbb{E}[P(t)]^2 + \beta\text{Var}(P(t))dt, \tag{10.64}$$

which includes an important special case of maximizing stability via

$$\underset{v:(10.2)(10.3)(10.61)}{\text{minimize}} \quad \lim_{T\to\infty} \frac{1}{T}\int_0^T \mathbb{E}[P(t)]^2 dt. \tag{10.65}$$

One can formulate other optimization problems by combining (10.62)–(10.65). Although those problems are beyond the scope of this chapter, our techniques can be used to analyze these problems as well.

Maximizing predictability

In this section, we show the optimal algorithms that balance the service quality and service capacity variance. Recall from Section 10.2 that $\text{Var}(P(t))$ is minimized at a flat service rate because peaks in service rate amplifies the uncertainties of the future arrivals to cause large $\text{Var}(P(t))$. In fact, this intuition holds beyond stationary arrivals, and so does the optimal algorithm.

Theorem 10.4.1. *The optimal solution of* (10.62) *is Exact Scheduling, defined by*

$$u(a, x, y) = \begin{cases} \dfrac{x}{y} & y > 0 \\ 0 & \textit{otherwise} \end{cases}. \tag{10.66}$$

The proof of Theorem 10.4.1 is given in Appendix B.8. Moreover, Generalized Exact Scheduling is also optimal under soft demand and deadline constraints.

Corollary 10.4.1. *The optimal solution of* (10.63) *is*

$$\bar{u}(a, x, y, \delta, \epsilon) = \begin{cases} \dfrac{x}{y} & \textit{if } y > 0 \textit{ and } \dfrac{x}{y} \leq \min\left\{\dfrac{\delta}{2}, \sqrt{\epsilon}\right\} \\ \dfrac{\delta}{2} & \textit{if } y > 0 \textit{ and } \dfrac{x}{y} > \dfrac{\delta}{2} \textit{ and } \dfrac{\delta}{2} \leq \sqrt{\epsilon} \\ \sqrt{\epsilon}\ 1\{x > 0\} & \textit{otherwise} \end{cases}, \tag{10.67}$$

As the unit costs for unmet demands and deadlines (δ_k, ϵ_k) increase, Corollary 10.4.1 recovers Theorem 10.4.1 as a special case. When the job arrivals are stationary, Corollary 10.4.1 recovers Corollary 10.2.1 as a special case.

Maximizing stability

In this section, we show the optimal algorithms that minimizes mean squared service capacity. Let us first understand why Exact Scheduling is not optimal by considering an example instance shown in Figure 10.4. In this instance, the arrival rate increases over time, and Exact Scheduling is likely to incur a substantial cost in later time. Meanwhile, an ideal algorithm should account for the increment in future arrivals by serving previous jobs more aggressively than Exact Scheduling. We formalize this intuition below.

Corollary 10.4.2. *The optimal solution of* (10.65) *has the following properties: for each job profiles* $(a, \sigma, \tau) \in (\mathcal{T}, S)$*,*

(i) $\mathbb{E}[P(h)]$ *takes a constant value for any time* h *at which* $v(a, \sigma, \tau, a+\tau-h) > 0$*,*

(ii) $\mathbb{E}[P(h')] \geq \mathbb{E}[P(h)]$ *for any time* $h' \in [a, a+\tau]$ *at which* $v(a, \sigma, \tau, a+\tau-h') = 0$*.*

Corollary 10.4.2 is a special case of Theorem 10.5.1 in the next section. Intuitively, condition (i) avoids oscillations in $\mathbb{E}[P(h)]$, while condition (ii) evens up the service

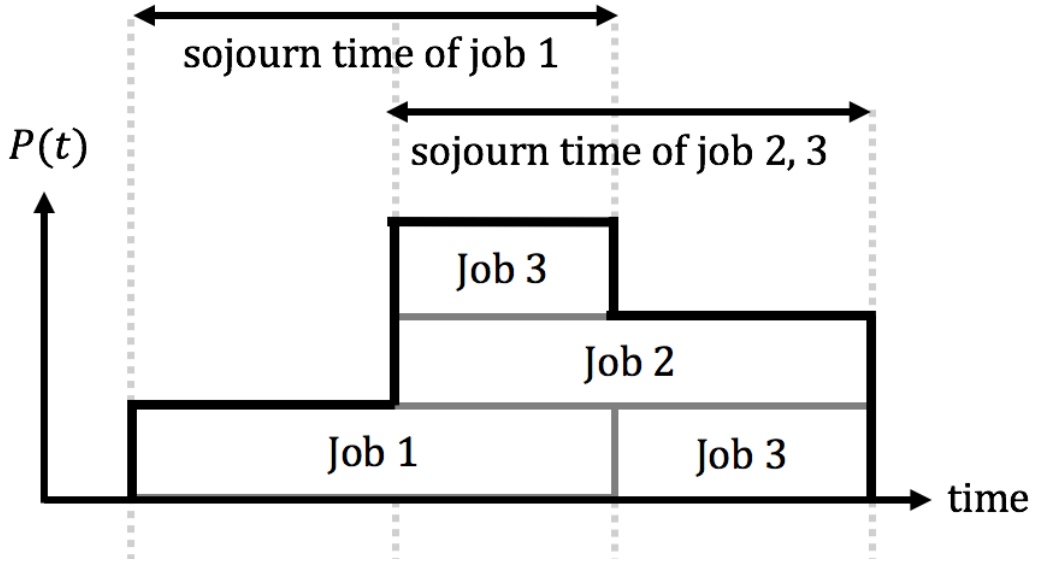

(a) The behavior of Exact Scheduling. If the arrival rate is higher at a later time, Exact Scheduling is likely to incur a substantial cost at the later time.

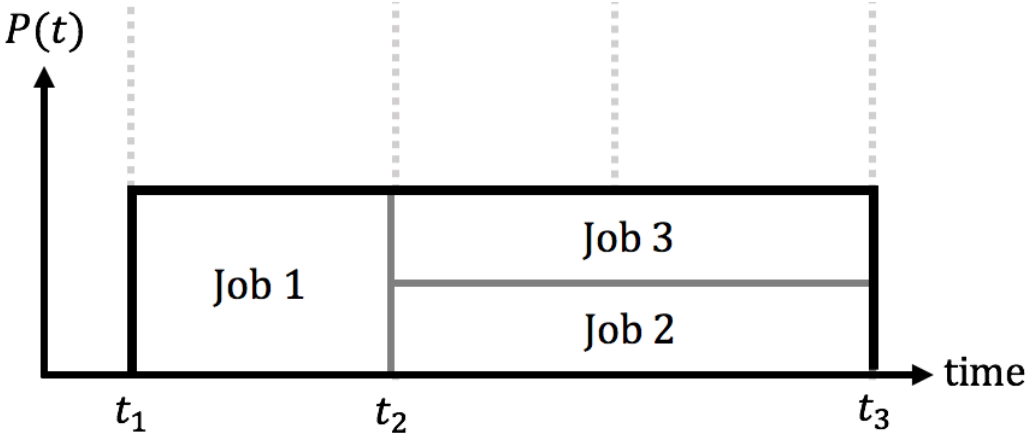

(b) Ideal behavior. The service rate of job 1 is increased to account for potentially large arrivals in the future.

Figure 10.4: This example demonstrates why Exact Scheduling does not maximize stability.

capacity over time. In the example, condition (i) forces $P(t)$ to be constant during the time intervals $[t_1, t_2]$ and $[t_2, t_3]$ because fluctuations of $\mathbb{E}[P(h)]$ during these intervals compromise stability. Condition (ii) constrains $\mathbb{E}[P(h')] \geq \mathbb{E}[P(h)]$ for any $h \in [t_1, t_2)$, $h' \in [t_2, t_3)$ because, during the uncrowded time $[t_1, t_2]$, job 1 does not need to be served beyond an extent required to account for the crowded time $[t_2, t_3]$. Consequently, the resulting service capacity has less fluctuations (Figure 10.4b).

The optimal policy in Corollary 10.4.2 also has an interesting similarity to the YDS algorithm, the centralized offline algorithm that minimizes CPU energy [11, 205]. Specifically, the YDS algorithm is the solution of

$$\underset{r \geq 0:(10.2)(10.3)}{\text{minimize}} \quad \frac{1}{T} \sum_{t=0}^{T} P(t)^{\alpha} \tag{10.68}$$

where $\alpha > 1$ is some constant. The optimal solution of (10.68) satisfies the following conditions: for any job $k \in \mathcal{V}$,

(iii) $P(h)$ takes a constant value at any time h at which $r_k(h) > 0$,

(iv) $P(h') \geq P(h)$ for any time $h' \in [a_k, a_k + \tau_k]$ at which $r_k(h') = 0$.

When we replace $\mathbb{E}[P(t)]$ with $P(t)$ and u with r, condition (i)–(ii) in Corollary 10.4.2 become condition (iii)–(iv) above. This relationship allows us to adapt the computational tool of the YDS algorithm to find the optimal distributed policy in our setting.

Algorithm 6 finds the optimal distributed policy that maximizes stability. Let $\mathcal{V}(t_1, t_2) = \{(a, \sigma, \tau) : a \geq t_1, a + \tau \leq t_2, (\sigma, \tau) \in S\}$ be the set of job profiles that have an arrive time after t_1 and a deadline before t_2. When $(a, \sigma, \tau) \in \mathcal{V}(t_1, t_2)$, we say that jobs with (a, σ, τ) present in the interval $[t_1, t_2]$. Let $w(t_1, t_2)$ denote the expected cumulative demand of jobs satisfying $\mathcal{V}(t_1, t_2)$, *i.e.*

$$w(t_1, t_2) = \int_{a \geq t_1} \int_{(\sigma,\tau) \in S, a+\tau \leq t_2} \sigma \Psi(a, \sigma, \tau) d\sigma d\tau da. \tag{10.69}$$

Intuitively, $w(t_1, t_2)$ is the minimum expected demand that must be supplied during a time interval $[t_1, t_2]$ to satisfy the demand requirements. We further define the intensity of an interval $[t_1, t_2]$ as

$$I(t_1, t_2) = \frac{w(t_1, t_2)}{t_2 - t_1}. \tag{10.70}$$

The algorithm finds the service rate $v^*(a, \sigma, \tau, y)$ in descending order of the intensity $I(t_1, t_2)$ in which a job present. Specifically, it iterates the following procedures. After initialization (line 1), the maximum intensity interval $[t_1, t_2]$ is computed (line 4). Jobs present in this interval are served in ascending order of their deadlines subject to

$$\mathbb{E}[P(h)] = \frac{I(t_1, t_2)}{t_2 - t_1} \qquad h \in [t_1, t_2). \tag{10.71}$$

As jobs not present in $\mathcal{V}(t_1, t_2)$ are assigned zero service capacity during $[t_1, t_2]$, the maximum service rates of jobs present in $\mathcal{V}(t_1, t_2)^c$ are set to be zero during $[t_1, t_2]$ (line 6). Because jobs in $\mathcal{V}(t_1, t_2)$ are already scheduled, before the next iteration, they are removed from the arrival statistics $\Psi(a, \sigma, \tau)$ as if the arrival probability of jobs present in $\mathcal{V}(t_1, t_2)$ is zero (line 7). Using the modified arrival statistics, the algorithm repeats the same process of finding a new maximum intensity interval, computing the service rates of jobs present during this interval, and modifying job statistics. We can observe that Algorithm 1 also minimizes $\max_{t \in \mathcal{T}} \mathbb{E}[P(t)]$. Because the interval $[t_1, t_2]$ found by the first iteration is the most intensive interval of an instance, the value of $\max_{t \in \mathcal{T}} \mathbb{E}[P(t)]$ cannot be smaller than what is required to schedule jobs present in $\mathcal{V}(t_1, t_2)$ in the first iteration.

Algorithm 6 Computing he optimal distributed policy that maximizes stability. The input of the algorithm is $\Psi(a, \sigma, \tau)$, and the output of the algorithm is $v^*(a, \sigma, \tau, y)$.

Initialize $\bar{v}(a, \sigma, \tau, y) \leftarrow \infty$
while $\Psi(a, \sigma, \tau) > 0$ for some (a, σ, τ) **do**
  Identify the maximum intensity interval $[t_1, t_2]$ by solve $\max_{t_1, t_2} I(t_1, t_2)$
  Compute $v^*(a, \sigma, \tau, y)$ for job profiles $\mathcal{V}(t_1, t_2)$ s.t. (10.71) and $v^*(a, \sigma, \tau, y) \leq \bar{v}(a, \sigma, \tau, y)$
end while
for $(a, \sigma, \tau) \notin \mathcal{V}(t_1, t_2)$ **do**
  Set $\bar{v}(a, \sigma, \tau, y) \leftarrow 0$ for any $a + \tau - y \in [t_1, t_2]$
  Set $\Psi(a, \sigma, \tau) \leftarrow 0$
end for

10.5 Balancing stability and predictability

Previous sections show the optimal policy of maximum predictability and that of maximum stability. Beyond the two special cases, however, balancing stability and predictability is a much more complex problem, and it is too ambitious to seek a purely analytic solution. In this section, we characterize the the Pareto-optimality condition for the distributed algorithm that balances predictability and stability.

Recall that, with regard to maximizing predictability, it is favorable to have a fixed service rate $r_k(t)$ over time. Meanwhile, with regard to maximizing stability, it is desirable to have a fixed service capacity $\mathbb{E}[P(t)]$ over time. These special cases provide us with the intuition that the evenness of $r_k(t)$ and $\mathbb{E}[P(t)]$ may be used to balance predictability and stability. This intuition can be formalized in the following theorem.

Theorem 10.5.1. *The optimal solution of* (10.64) *has the following properties: for each job profiles* $(a, \sigma, \tau) \in (\mathcal{T}, S)$*,*

(i) $\alpha\mathbb{E}[P(h)] + \beta v(a, \sigma, \tau, a + \tau - h)$ *takes a constant value for any time* h *at which* $v(a, \sigma, \tau, a + \tau - h) > 0$*,*

(ii) $\alpha\mathbb{E}[P(h')] \geq \alpha\mathbb{E}[P(h)] + \beta v(a, \sigma, \tau, a + \tau - h)$ *for any time* $h' \in [a, a + \tau]$ *at which* $v(a, \sigma, \tau, a + \tau - h') = 0$*.*

When $\alpha = 0$, Theorem 10.5.1 essentially states that Exact Scheduling maximizes predictability. This is because condition (ii) cannot happen when $\alpha = 0$, so the optimality condition reduces to the case when $v(a, \sigma, \tau, y)$ is constant at all $y \in [0, \tau]$. When $\beta = 0$, Theorem 10.5.1 recovers Corollary 10.4.2. Next, we overview the proof of Theorem 10.5.1.

Proof. (Theorem 10.5.1) From Lemma 10.2.2, the objective function of (10.65) is equivalent to

$$\begin{aligned}
&\int_0^T \alpha\mathbb{E}[P(t)]^2 + \beta\mathrm{Var}(P(t))dt \qquad (10.72)\\
&= \alpha \int_0^T \left\{ \int_{(\sigma,\tau)\in S} \int_{y=0}^{\tau} v(t + y - \tau, \sigma, \tau, y)\Psi(t + y - \tau, \sigma, \tau)dyd\sigma d\tau \right\}^2 dt \\
&\quad + \beta \int_0^T \int_{(\sigma,\tau)\in S} \int_{y=0}^{\tau} v(t + y - \tau, \sigma, \tau, y)^2\Psi(t + y - \tau, \sigma, \tau)dyd\sigma d\tau dt
\end{aligned}$$

Moreover, the constraints of (10.64) are equivalent to

$$\int_{y=0}^{\tau} v(a, \sigma, \tau, y)dy = \sigma, \qquad (\sigma, \tau) \in S, \quad a \in \mathcal{T} \qquad (10.73)$$

$$v(a, \sigma, \tau, y) \geq 0, \qquad (\sigma, \tau) \in S, \quad a \in \mathcal{T}, \quad y \in [0, \tau]. \qquad (10.74)$$

The Lagrangian associated with problem (10.65) is

$$\begin{aligned} L(v;\mu,\nu) =& \alpha \int_0^T \left\{ \int_{(\sigma,\tau)\in S} \int_{y=0}^{\tau} v(t+y-\tau,\sigma,\tau,y)\Psi(t+y-\tau,\sigma,\tau)dyd\sigma d\tau \right\}^2 dt \\ &+ \beta \int_{(\sigma,\tau)\in S} \int_{y=0}^{\tau} \int_{a=0}^{T} v(a,\sigma,\tau,y)^2\Psi(a,\sigma,\tau)dadyd\sigma d\tau \\ &- \int_{a=0}^{T} \int_{(\sigma,\tau)\in S} \mu(\sigma,\tau,a) \int_{y=0}^{\tau} v(y,\sigma,\tau,a)dyd\sigma d\tau da \\ &- \int_{a=0}^{T} \int_{(\sigma,\tau)\in S} \int_{y=0}^{\tau} \nu(a,\sigma,\tau,y)v(y,\sigma,\tau,a)dyd\sigma d\tau da, \end{aligned}$$

where $\mu(\sigma,\tau,a)$ is the Lagrange multiplier associated with (10.73), and $\nu(a,\sigma,\tau,y) \geq 0$ is the Lagrange multiplier associated with (10.74). We can alternatively consider $L : U \to \mathbb{R}$ as a functional defined on the function space U of policies. Let $U_f \subset U$ be the space of feasible scheduling policies, *i.e.*

$$U_f = \{v : v \text{ satisfies (10.73)\&(10.74)}\}. \tag{10.75}$$

Now we consider perturbing v' using the original v as

$$v' = v + \epsilon\lambda \tag{10.76}$$

where $\epsilon\lambda$ satisfies the constraint $v' \in U_f$.

Let $G : (\mathcal{T}, U) \to \mathbb{R}$ be the following functional:

$$G(t;v) = \mathbb{E}[P(t)] = \int_{(\sigma,\tau)\in S} \int_{a=t-\tau}^{t} v(\sigma,\tau,a,y)\Psi(a,\sigma,\tau)dad\sigma d\tau. \tag{10.77}$$

The difference in Lagrangian can be written as

$$L(v';\mu,\nu) - L(v;\mu,\nu) \tag{10.78}$$

$$=\alpha \int_0^T 2\ G(t;u) \left\{ \int_{(\sigma,\tau)\in S} \int_{a=t-\tau}^{t} \epsilon\lambda(a,\sigma,\tau,y)\Psi(a,\sigma,\tau)dad\sigma d\tau \right\} dt \tag{10.79}$$

$$+ \beta \int_{(\sigma,\tau)\in S} \int_{y=0}^{\tau} \int_{a=0}^{T} 2\epsilon\lambda(a,\sigma,\tau,y)v(a,\sigma,\tau,y)\Psi(a,\sigma,\tau)dady d\sigma d\tau$$

$$- \int_{(\sigma,\tau)\in S} \int_{a=0}^{T} \mu(\sigma,\tau,a) \int_{y=0}^{\tau} \epsilon\lambda(a,\sigma,\tau,y)dydad\sigma d\tau$$

$$- \int_{y=0}^{\tau} \nu(\sigma,\tau,a,y)\epsilon\lambda(\sigma,\tau,a,y)dydad\sigma d\tau + O(\epsilon^2)$$

$$=\alpha \int_{(\sigma,\tau)\in S} \int_{y=0}^{\tau} \int_{a=0}^{T} 2\epsilon G(t;u)\lambda(a,\sigma,\tau,y)\Psi(a,e,\tau)dady d\sigma d\tau \tag{10.80}$$

$$+ \beta \int_{(\sigma,\tau)\in S} \int_{y=0}^{\tau} \int_{a=0}^{T} 2\epsilon\lambda(a,\sigma,\tau,y)v(a,\sigma,\tau,y)\Psi(a,\sigma,\tau)dady d\sigma d\tau$$

$$- \int_{(\sigma,\tau)\in S} \int_{a=0}^{T} \int_{y=0}^{\tau} \epsilon(\mu(\sigma,\tau,a)\lambda(a,\sigma,\tau,y) + \nu(\sigma,\tau,a,y)\lambda(\sigma,\tau,a,y))dydad\sigma d\tau$$

$$+ O(\epsilon^2) \tag{10.81}$$

$$=\epsilon \int_{(\sigma,\tau)\in S} \int_{y=0}^{\tau} \int_{a=0}^{T} \{2(\alpha G(t;u) + \beta v(a,\sigma,\tau,y))\Psi(a,\sigma,\tau) - \mu(\sigma,\tau,a)$$

$$- \nu(\sigma,\tau,a,y)\}\lambda(a,\sigma,\tau,y)dady d\sigma d\tau + O(\epsilon^2), \tag{10.82}$$

where (10.80) is obtained using integration by substitution. For a functional L to be stationary at some $v \in U_f$, the first term should be zero for any $\lambda(a,\sigma,\tau,y)$ satisfying the constraint $v' \in U_f$. From (10.82), the stationary point of L satisfies

$$\alpha\mathbb{E}[P(t)] + \beta v(a,\sigma,\tau,a+\tau-h_1) = \alpha G(t;u) + \beta v(a,\sigma,\tau,a+\tau-h_1) \tag{10.83}$$

$$= \frac{\mu(\sigma,\tau,a) + \nu(\sigma,\tau,a,y)}{2\Psi(a,\sigma,\tau)} \tag{10.84}$$

for any $y \in [0,\tau]$, $(\sigma,\tau) \in S$, $a \in \mathcal{T}$. Since the optimal solution of (10.65) is a stationary point of L, (10.83) is the necessary condition for optimality:

(i) For any job profiles (a,σ,τ), if the service rate is strictly positive at h_1, h_2 such that $h_1 \neq h_1$ and $h_1, h_1 \in [a, a+\tau]$, then

$$v(a-h_1+\tau,\sigma,\tau,a) = v(a-h_2+\tau,\sigma,\tau,a) = 0. \tag{10.85}$$

Combining (10.83) and (10.85) leads to

$$\alpha\mathbb{E}[P(h_1)] + \beta v(a, \sigma, \tau, a + \tau - h_1) \tag{10.86}$$
$$= \frac{\mu(\sigma, \tau, a)}{2\Psi(a, \sigma, \tau)} \tag{10.87}$$
$$= \alpha\mathbb{E}[P(h_2)] + \beta v(a, \sigma, \tau, a + \tau - h_2). \tag{10.88}$$

(ii) For any job profiles (a, σ, τ), if its service rate is strictly positive at $h \in [a, a + \tau]$ and zero at $h' \in [a, a + \tau]$, then

$$\alpha\mathbb{E}[P(h)] + \beta v(a, \sigma, \tau, a + \tau - h_1) = \frac{\mu(\sigma, \tau, a)}{2\Psi(a, \sigma, \tau)} \tag{10.89}$$
$$\leq \frac{\mu(\sigma, \tau, a) + \nu(\sigma, \tau, a, y)}{2\Psi(a, \sigma, \tau)} \tag{10.90}$$
$$= \alpha\mathbb{E}[P(h')]. \tag{10.91}$$

□

10.6 Performance at Caltech electrical vehicle charging testbed

To further evaluate the performance of distributed algorithms, we compare their performance with existing scheduling algorithms in the Caltech Electric Vehicle Charging Testbed [102]. We employ a trace-driven simulation on a total of 92 charging instances in the testbed. Each instance contains a set of requested jobs within a day, whose statistics are summarized in Table S1. Using these instances, we compare the following algorithms.

Distributed algorithms:

- Generalized Exact Scheduling (10.38), which recovers Exact Scheduling (10.20) under strict service requirements, the policy (10.34) under soft demands, and the policy (10.36) under soft deadlines.
- Immediate Scheduling, *i.e.* $r_k(t) = \mathbf{1}\{x_k(t) > 0\}$.
- Equal Service, which offers a homogeneous service rate to all unfinished jobs. Under strict service requirements, it serves jobs with positive laxity at a homogeneous service rate c_{ES} and jobs with zero laxity at its maximum rate, *i.e.* $r_k(t) = c_{\text{ES}}\mathbf{1}\{(x/\bar{r}_k) - y > 0 \text{ and } x > 0\} + \mathbf{1}\{(x/\bar{r}_k) - y \leq 0 \text{ and } x > 0\}$. Under soft demand constraints, it serves jobs at a homogeneous service rate c'_{ES} before its deadline, *i.e.* $r_k(t) = c'_{\text{ES}}\mathbf{1}\{x_k(t) > 0\}$. Under soft deadline

constraints, it serves jobs at a homogeneous service rate until its completion, *i.e.* $r_k(t) = c''_{\text{ES}}\mathbf{1}\{x_k(t) > 0\}$. Here, the parameters $c_{\text{ES}}, c'_{\text{ES}}, c''_{\text{ES}}$ are chosen to be the optimal offline values.[7]

Centralized algorithms:

- Earliest Deadline First (EDF), which allocates a fixed capacity p_{EDF} to jobs in ascending order of their deadlines. Under soft demand constraints, jobs are served until their deadline. Under soft deadline constraints, jobs are served until completion.

- Least Laxity First (LLF), which allocates a fixed capacity p_{LLF} to jobs in ascending order of their laxity.[8] Under soft demand constraints, jobs are served until their deadlines. Under soft deadline constraints, jobs are served until completion.

- Fair Sharing (FS), which equally distributes a fixed capacity among jobs. Under soft demand constraints, jobs are served until their deadlines according to $r_k(t) = \min\{p_{\text{FS}}/n(t), \bar{r}_k\}\mathbf{1}\{y_k(t) > 0\}$, where $n(t)$ the is number of unfinished jobs at time t. Under soft deadline constraints, jobs are served to their completion according to $r_k(t) = \min\{p'_{\text{FS}}/n(t), \bar{r}_k\}\mathbf{1}\{x_k(t) > 0\}$. Here p_{FS} and p'_{FS} are chosen to be the optimal offline values.[9]

In the case of strict demand and deadline constraints, Figure 10.5 shows that Exact Scheduling has significant performance gains compared to other algorithms that can guarantee demand and deadline satisfaction (Immediate Scheduling and Equal Service). Although we show the optimality of Exact Scheduling under Poisson arrivals, Figure 10.5 suggests that Exact Scheduling can also perform better than other distributed algorithms in settings with non-Poisson arrivals.

In the case of soft demand constraints, Figure 10.7 (a) shows the average cost of an instance for each algorithm as a function of the unit penalty for unsatisfied demands δ. As δ grows, all algorithms inevitably suffer from increased costs as well. However, the cost of Generalized Exact Scheduling plateau out at relatively

[7] Since the offline optimal parameters is unknown in practice, the obtained performance in this chapter is optimistic.

[8] The laxity of job k at time t is defined to be $y_k(t) - x_k(t)$.

[9] The offline optimal parameters can be unknown in an online setting.

(a) Job profiles

	Demand σ_k (kW × m)	Sojourn time τ_k (m)	Rate limit $\bar{r}_k$ (kW)
Mean	$5.1 \cdot 10^2$	$4.5 \cdot 10^3$	6.37
Variance	$3.1 \cdot 10^5$	$7.7 \cdot 10^6$	12.7

(b) Instance profiles

	Total demand $\sum_{k \in \mathcal{V}} e_k$ (kW × m)	Time horizon T (m)	Number of jobs $\lvert\mathcal{V}\rvert$
Mean	$8.4 \cdot 10^3$	$6.5 \cdot 10^2$	14.2
Variance	$2.0 \cdot 10^7$	$1.4 \cdot 10^4$	48.2

Table S1: Statistics of the EV charging instances at Caltech testbed.

small δ, which results in lower cost compared with other algorithms. Figure 10.7 (b) suggests that the quick plateau is achieved by a highly adaptive reduction in the total amount of unsatisfied demands: it is among the algorithms with the largest amount of unmet demands at small δ and, at the same time, the ones with the smallest amount of unmet demands at large ϵ. This property suggests the importance of systematically optimizing and adjusting the level of unmet demands.

In the case of soft deadline constraints, Figure 10.6 (a) shows that Generalized Exact Scheduling achieves lower cost than other distributed algorithms. It also has a comparable performance with the centralized algorithms when the unit penalty for unsatisfied deadline ϵ is large. Figure 10.6 (b) suggests that such performance is achieved by drastically reducing the total amount of unsatisfied deadline as ϵ increases.

Generalized Exact Scheduling demonstrates the power of systematically optimizing service capacity to find the right balance between service capacity variance and the penalties for unsatisfied demands or deadlines. The resulting performance is not surprising because existing algorithms are not designed or optimized for dynamic service capacity, and existing algorithms do not have a systematic way to optimally trade-off service capacity variance and unmet demands or deadlines.

Conclusion

As it becomes more common for service systems to have a dynamic capacity that instantaneously adapts to demand, the goal of providing a high quality of service

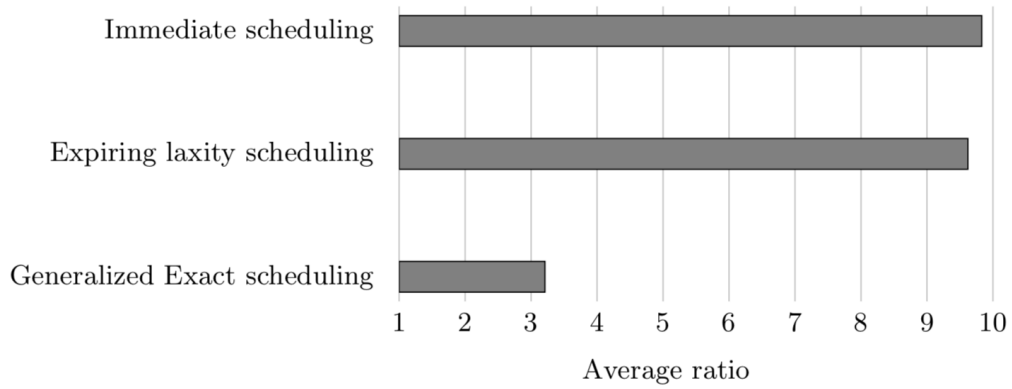

Figure 10.5: Performance comparison of algorithms under strict demand constraints. The ratio of each algorithm's empirical variance to the offline optimal algorithm's empirical variance is averaged over all scheduling instances. The parameters c_{ES} are set to be the offline optimal.[9]

(*e.g.* meeting deadlines) while minimizing the variance of service capacity has received increasing attention. While there exists an extensive literature analyzing existing algorithms, little analytic results were known for the optimal policies in such settings. In this chapter, we characterize the optimal policies in many common scenarios, stationary and non-stationary arrivals, strict or soft demands, with or without deadline extensions, and a variety of objective functions.

The results highlight that novel generalizations of Exact Scheduling are optimal under both stationary and non-stationary Poisson arrival processes. For more complex objective functions, more complex policies turn out to be optimal, specifically a novel variation of the YDS algorithm. This connection and the proof of optimality highlight new bridges between the stochastic and worst-case scheduling communities will be interesting to explore in future work. In addition to characterizing optimal distributed policies, our results also bound the gap between the performance of distributed policies and centralized policies – showing that distributed policies can nearly match the performance of centralized policies.

Typically, the analysis of scheduling policies for non-stationary settings with deadlines has been done using asymptotic regimes, *e.g.* heavy-traffic regimes; however, the techniques we develop in this chapter do not require passing into these asymptotic regimes. Thus, in addition to the results we have proven, our techniques are also an important contribution. We hope they these techniques will inspire the discovery of other optimality results in the context of deadline scheduling in the coming years. app-

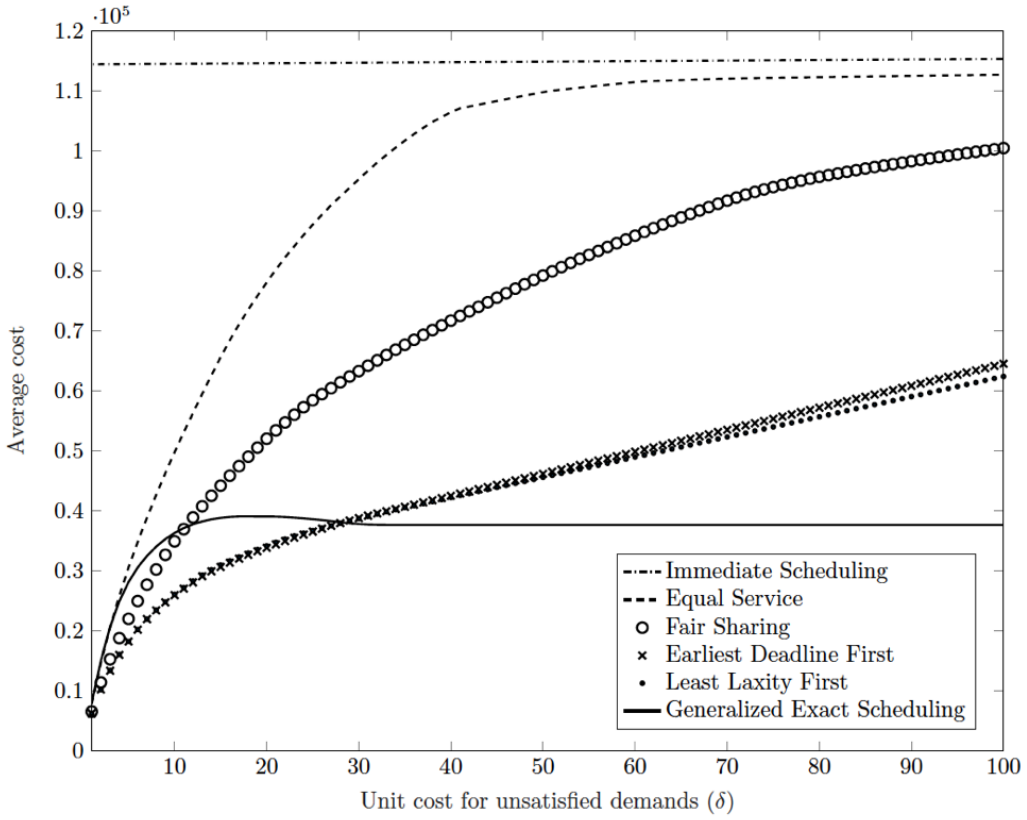

(a) Average total costs (10.15) for varying ϵ.

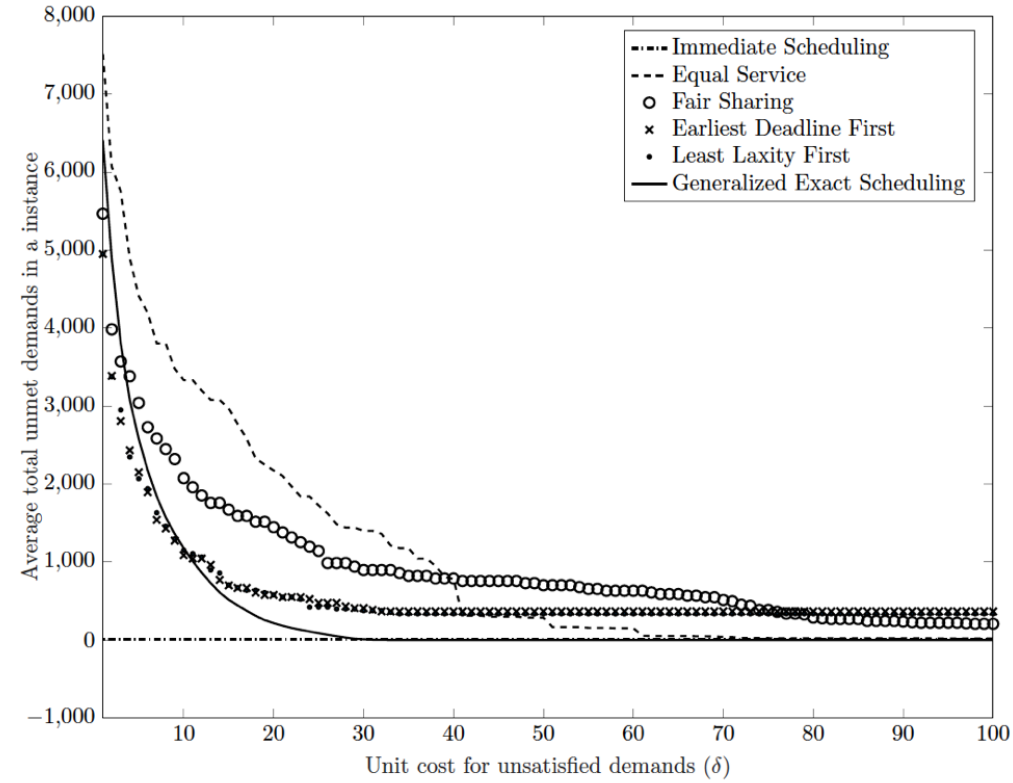

(b) Average of the total deadline extension in an instance for varying ϵ.

Figure 10.6: Performance of algorithms under soft deadline constraints.[9]

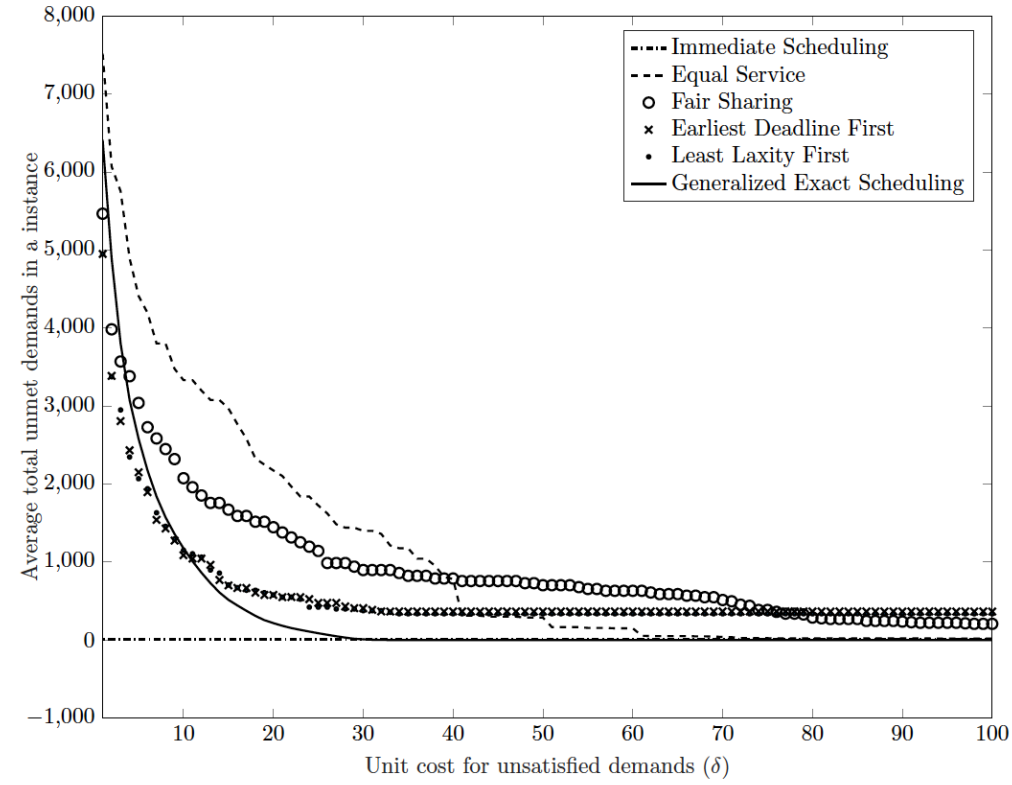

(a) Average total costs (10.14) for varying δ.

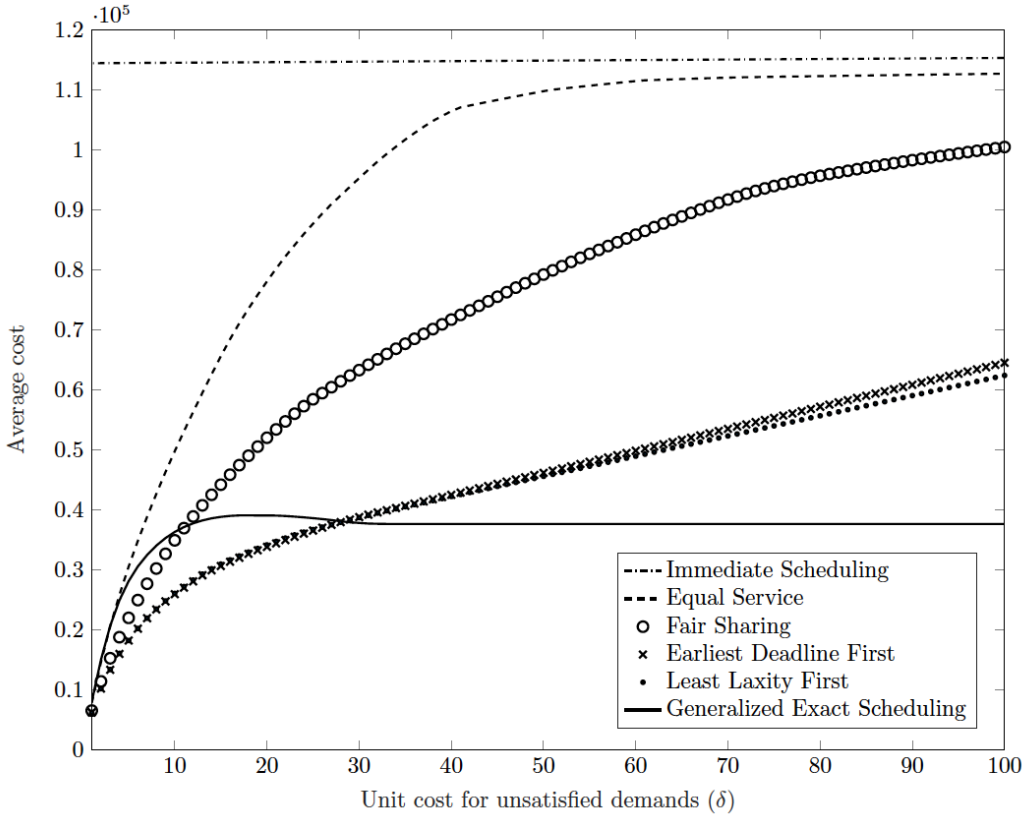

(b) Average of the total unsatisfied demands in an instance for varying δ.

Figure 10.7: Performance of algorithms under soft demand constraints. The parameters c'_{ES}, p_{EDF}, p_{LLF}, and p_{FS} are set to be the offline optimal ones.[9]

BIBLIOGRAPHY

[1] Abul K Abbas, Andrew HH Lichtman, and Shiv Pillai. *Basic Immunology E-Book: Functions and Disorders of the Immune System*. Elsevier Health Sciences, 2015.

[2] Muhammad A. Adnan and Rajesh K. Gupta. Workload shaping to mitigate variability in renewable power use by data centers. In *2014 IEEE 7th International Conference on Cloud Computing*, pages 96–103, 2014.

[3] Muhammad A. Adnan, Ryo Sugihara, and Rajesh K. Gupta. Energy efficient geographical load balancing via dynamic deferral of workload. In *2012 IEEE 5th International Conference on Cloud Computing (CLOUD)*, pages 188–195, 2012.

[4] International Energy Agency. Global ev outlook 2016. `https://www.iea.org/publications/freepublications/publication/Global_EV_Outlook_2016.pdf`, 2016.

[5] Boris Rostislavovich Andrievsky, Aleksei Serafimovich Matveev, and Aleksandr L?vovich Fradkov. Control and estimation under information constraints: Toward a unified theory of control, computation and communications. *Automation and Remote Control*, 71(4):572–633, 2010.

[6] Tuncer Can Aysal, Mark J Coates, and Michael G Rabbat. Distributed average consensus with dithered quantization. *IEEE Transactions on Signal Processing*, 56(10):4905–4918, 2008.

[7] François Baccelli and Bartlomiej Błaszczyszyn. *Stochastic Geometry and Wireless Networks, Volume I - Theory*. Now Publishers, 2009.

[8] Francois Baccelli and Pierre Brémaud. *Elements of queueing theory: Palm Martingale calculus and stochastic recurrences*, volume 26. Springer Science & Business Media, 2013.

[9] John Baillieul and Panos J Antsaklis. Control and communication challenges in networked real-time systems. *Proceedings of the IEEE*, 95(1):9–28, 2007.

[10] Kenneth R Baker and Gary D Scudder. Sequencing with earliness and tardiness penalties: a review. *Operations research*, 38(1):22–36, 1990.

[11] Nikhil Bansal, Tracy Kimbrel, and Kirk Pruhs. Speed scaling to manage energy and temperature. *Journal of the ACM (JACM)*, 54(1):3, 2007.

[12] Lei Bao, Mikael Skoglund, and Karl Henrik Johansson. Iterative encoder-controller design for feedback control over noisy channels. *IEEE Transactions on Automatic Control*, 56(2):265–278, 2011.

[13] Yaakov Bar-Shalom and Edison Tse. Dual effect, certainty equivalence, and separation in stochastic control. *IEEE Transactions on Automatic Control*, 19(5):494–500, 1974.

[14] Mahdi Behrangrad. A review of demand side management business models in the electricity market. *Renewable and Sustainable Energy Reviews*, 47: 270–283, 2015.

[15] Dimitri P Bertsekas, Dimitri P Bertsekas, Dimitri P Bertsekas, and Dimitri P Bertsekas. *Dynamic programming and optimal control*, volume 2. Athena scientific Belmont, MA, 1995.

[16] J Gordon Betts, Peter DeSaix, Eddie Johnson, Jody E Johnson, Oksana Korol, Dean H Kruse, Brandon Poe, James A Wise, Kelly A Young, et al. *Anatomy and physiology*. Rice university, 2014.

[17] Partha P Bhattacharya and Anthony Ephremides. Optimal scheduling with strict deadlines. *IEEE Transactions on Automatic Control*, 34(7):721–728, 1989.

[18] Giulio Binetti, Ali Davoudi, David Naso, Biagio Turchiano, and Frank L Lewis. Scalable real-time electric vehicles charging with discrete charging rates. *IEEE Transactions on Smart Grid*, 6(5):2211–2220, 2015.

[19] Clara Bodelon, Mazyar Fallah, and John H Reynolds. Temporal resolution of the human visual system for processing color, orientation, and color/orientation conjunctions. *Journal of Vision*, 5(8):758–758, 2005.

[20] Simon Bouisset and Manh-Cuong Do. Posture, dynamic stability, and voluntary movement. *Neurophysiologie Clinique/Clinical Neurophysiology*, 38 (6):345–362, 2008.

[21] Eric Boutin, Jaliya Ekanayake, Wei Lin, Bing Shi, Jingren Zhou, Zhengping Qian, Ming Wu, and Lidong Zhou. Apollo: Scalable and coordinated scheduling for cloud-scale computing. In *OSDI*, volume 14, pages 285–300, 2014.

[22] Stephen Boyd and Lieven Vandenberghe. *Convex Optimization*. Cambridge University Press, 2004.

[23] Vladimir Brezina, Irina V Orekhova, and Klaudiusz R Weiss. The neuromuscular transform: the dynamic, nonlinear link between motor neuron firing patterns and muscle contraction in rhythmic behaviors. *Journal of neurophysiology*, 83(1):207–231, 2000.

[24] Shelby L Brumelle. On the relation between customer and time averages in queues. *Journal of Applied Probability*, 8(3):508–520, 1971.

[25] RS Bucy. Distortion-rate theory and filtering. In *Advances in Communications*, pages 11–15. Springer, 1980.

[26] Giorgio C Buttazzo. *Hard real-time computing systems: predictable scheduling algorithms and applications*, volume 24. Springer Science & Business Media, 2011.

[27] Alvaro Cardenas, Saurabh Amin, Bruno Sinopoli, Annarita Giani, Adrian Perrig, and Shankar Sastry. Challenges for securing cyber physical systems. In *Workshop on future directions in cyber-physical systems security*, volume 5, 2009.

[28] Alvaro A Cardenas, Saurabh Amin, and Shankar Sastry. Secure control: towards survivable cyber-physical systems. In *IEEE 28th International Conference on Distributed Computing Systems Workshops (ICDCS)*, pages 495–500. IEEE, 2008.

[29] Rui Carvalho, Lubos Buzna, Richard Gibbens, and Frank Kelly. Congestion control in charging of electric vehicles. *arXiv preprint arXiv:1501.06957*, 2015.

[30] Sabri Çelik and Constantinos Maglaras. Dynamic pricing and lead-time quotation for a multiclass make-to-order queue. *Management Science*, 54(6): 1132–1146, 2008.

[31] Charalambos D Charalambous and Alireza Farhadi. LQG optimality and separation principle for general discrete time partially observed stochastic systems over finite capacity communication channels. *Automatica*, 44(12): 3181–3188, 2008.

[32] Charalambos D Charalambous, Photios A Stavrou, and Nasir U Ahmed. Nonanticipative rate distortion function and relations to filtering theory. *IEEE Transactions on Automatic Control*, 59(4):937–952, 2014.

[33] Jie Chen and Ron J Patton. *Robust model-based fault diagnosis for dynamic systems*, volume 3. Springer Science & Business Media, 2012.

[34] Niangjun Chen, Lingwen Gan, Steven H Low, and Adam Wierman. Distributional analysis for model predictive deferrable load control. In *Proc. of the IEEE 53rd annual Conference on Decision and Control*, 2014.

[35] Niangjun Chen, Chee Wei Tan, and Tony QS Quek. Electric vehicle charging in smart grid: Optimality and valley-filling algorithms. *IEEE Journal of Selected Topics in Signal Processing*, 8(6):1073–1083, 2014.

[36] Shiyao Chen, Yuting Ji, and Lang Tong. Large scale charging of electric vehicles. In *2012 IEEE Power and Energy Society General Meeting*, pages 1–9. IEEE, 2012.

[37] Yiyu Chen, Amitayu Das, Wubi Qin, Anand Sivasubramaniam, Qian Wang, and Natarajan Gautam. Managing server energy and operational costs in hosting centers. In *ACM SIGMETRICS Performance Evaluation Review*, volume 33 (1), pages 303–314. ACM, 2005.

[38] Michelle S Chong, Masashi Wakaiki, and Joao P Hespanha. Observability of linear systems under adversarial attacks. In *American Control Conference (ACC)*, pages 2439–2444. IEEE, 2015.

[39] Thomas M Cover and Joy A Thomas. *Elements of information theory*. John Wiley & Sons, 2012.

[40] Munther A Dahleh and Ignacio J Diaz-Bobillo. *Control of uncertain systems: a linear programming approach*. Prentice-Hall, Inc., 1994.

[41] Anupam Datta, Soummya Kar, Bruno Sinopoli, and Sean Weerakkody. Accountability in cyber-physical systems. In *Science of Security for Cyber-Physical Systems Workshop (SOSCYPS)*, pages 1–3. IEEE, 2016.

[42] M Davis. Capacity and cutoff rate for Poisson-type channels. *IEEE Transactions on Information Theory*, 26(6):710–715, 1980.

[43] Robert I Davis and Alan Burns. A survey of hard real-time scheduling for multiprocessor systems. *ACM Computing Surveys (CSUR)*, 43(4):35, 2011.

[44] Jeffrey Dean and Luiz André Barroso. The tail at scale. *Communications of the ACM*, 56(2):74–80, 2013.

[45] Milan S Derpich and Jan Ostergaard. Improved upper bounds to the causal quadratic rate-distortion function for Gaussian stationary sources. *IEEE Transactions on Information Theory*, 58(5):3131–3152, 2012.

[46] Michael L. Dertouzos and Aloysius K. Mok. Multiprocessor online scheduling of hard-real-time tasks. *IEEE Transactions on software engineering*, 15 (12):1497–1506, 1989.

[47] John Doyle. Robust and optimal control. In *Proceedings of the 35th IEEE Conference on Decision and Control*, volume 2, pages 1595–1598, 1996.

[48] John Doyle, Yorie Nakahira, Yoke Peng Leong, Emily Jenson, Adam Dai, Dimitar Ho, and Nikolai Matni. Teaching control theory in high school. In *Decision and Control (CDC), 2016 IEEE 55th Conference on*, pages 5925–5949. IEEE, 2016.

[49] John C. Doyle and Marie Csete. Architecture, constraints, and behavior. *Proceedings of National Academy of Science*, 108(s3), 2011.

[50] Jianzhong Du and Joseph Y-T Leung. Minimizing total tardiness on one machine is np-hard. *Mathematics of operations research*, 15(3):483–495, 1990.

[51] Qiang Du, Vance Faber, and Max Gunzburger. Centroidal voronoi tessellations: Applications and algorithms. *SIAM review*, 41(4):637–676, 1999.

[52] D. Marigold et al. Exercise leads to faster postural reflexes, improved balance and mobility, and fewer falls in older persons with chronic stroke. *JAGS*, 53: 416–?423, 2005.

[53] Fabio Fagnani and Sandro Zampieri. Quantized stabilization of linear systems: complexity versus performance. *IEEE Transactions on Automatic Control*, 49(9):1534–1548, 2004.

[54] Song Fang, Jie Chen, and I Hideaki. *Towards integrating control and information theories*. Springer, 2017.

[55] James P Farwell and Rafal Rohozinski. Stuxnet and the future of cyber war. *Survival*, 53(1):23–40, 2011.

[56] Hamza Fawzi, Paulo Tabuada, and Suhas Diggavi. Secure estimation and control for cyber-physical systems under adversarial attacks. *IEEE Transactions on Automatic Control*, 59(6):1454–1467, 2014.

[57] Andres Ferragut, Fernando Paganini, and Adam Wierman. Controlling the variability of capacity allocations using service deferrals. *ACM Transactions on Modeling and Performance Evaluation of Computing Systems (TOMPECS)*, 2(3):15, 2017.

[58] Thomas R. Fischer. Optimal quantized control. *IEEE Transactions on Automatic Control*, 27(4):996–998, 1982.

[59] Paul M Fitts. The information capacity of the human motor system in controlling the amplitude of movement. *Journal of experimental psychology*, 47 (6):381, 1954.

[60] Paul M Fitts and James R Peterson. Information capacity of discrete motor responses. *Journal of experimental psychology*, 67(2):103, 1964.

[61] Jessica L Fox, Adrienne L Fairhall, and Thomas L Daniel. Encoding properties of haltere neurons enable motion feature detection in a biological gyroscope. *Proceedings of the National Academy of Sciences*, page 200912548, 2010.

[62] David W Franklin and Daniel M Wolpert. Computational mechanisms of sensorimotor control. *Neuron*, 72(3):425–442, 2011.

[63] James S Freudenberg, Richard H Middleton, and Victor Solo. Stabilization and disturbance attenuation over a Gaussian communication channel. *IEEE Transactions on Automatic Control*, 55(3):795–799, 2010.

[64] Emilia Fridman and Michel Dambrine. Control under quantization, saturation and delay: An lmi approach. *Automatica*, 45(10):2258–2264, 2009.

[65] Minyue Fu. Lack of separation principle for quantized linear quadratic Gaussian control. *IEEE Transactions on Automatic Control*, 57(9):2385–2390, 2012.

[66] Lingwen Gan, Ufuk Topcu, and Steven H Low. Optimal decentralized protocol for electric vehicle charging. *IEEE Transactions on Power Systems*, 28 (2):940–951, 2013.

[67] Lingwen Gan, Adam Wierman, Ufuk Topcu, Niangjun Chen, and Steven H Low. Real-time deferrable load control: handling the uncertainties of renewable generation. In *Proceedings of eEnergy*, 2013.

[68] Anshul Gandhi. *Dynamic server provisioning for data center power management*. PhD thesis, Carnegie Mellon University, 2013.

[69] Anshul Gandhi, Mor Harchol-Balter, Rajarshi Das, and Charles Lefurgy. Optimal power allocation in server farms. In *ACM SIGMETRICS Performance Evaluation Review*, volume 37(1), pages 157–168. ACM, 2009.

[70] Janos Gertler. *Fault detection and diagnosis in engineering systems*. CRC press, 1998.

[71] Geoffrey Goldspink. Malleability of the motor system: a comparative approach. *Journal of experimental biology*, 115(1):375–391, 1985.

[72] AK Gorbunov and Marks Shlemovich Pinsker. Nonanticipatory and prognostic epsilon entropies and message generation rates. *Problemy Peredachi Informatsii*, 9(3):12–21, 1973.

[73] Albert Greenberg, James Hamilton, David A Maltz, and Parveen Patel. The cost of a cloud: research problems in data center networks. *ACM SIGCOMM computer communication review*, 39(1):68–73, 2008.

[74] H Christian Gromoll and Łukasz Kruk. Heavy traffic limit for a processor sharing queue with soft deadlines. *The Annals of Applied Probability*, 17(3): 1049–1101, 2007.

[75] Linqi Guo, Karl F Erliksson, and Steven H Low. Optimal online adaptive electric vehicle charging. In *2017 IEEE Power & Energy Society General Meeting*, pages 1–5. IEEE, 2017.

[76] Herbert Hatze. A teleological explanation of weber's law and the motor unit size law. *Bulletin of mathematical biology*, 41(3):407–425, 1979.

[77] WP Maurice H Heemels, Andrew R Teel, Nathan Van de Wouw, and Dragan Nešić. Networked control systems with communication constraints: Tradeoffs between transmission intervals, delays and performance. *IEEE Transactions on Automatic Control*, 55(8):1781–1796, 2010.

[78] Elwood Henneman, George Somjen, and David O Carpenter. Functional significance of cell size in spinal motoneurons. *Journal of neurophysiology*, 28(3):560–580, 1965.

[79] Joao P Hespanha, Payam Naghshtabrizi, and Yonggang Xu. A survey of recent results in networked control systems. *Proceedings of the IEEE*, 95(1): 138, 2007.

[80] Jiawei Hong, Xiaonan Tan, and Don Towsley. A performance analysis of minimum laxity and earliest deadline scheduling in a real-time system. *IEEE Transactions on Computers*, 38(12):1736–1744, 1989.

[81] Peter J. Huber and Elvezio M. Ronchetti. *Robust Statistics*. Wiely, 2009.

[82] Sungjin Im, Janardhan Kulkarni, and Kamesh Munagala. Competitive algorithms from competitive equilibria: non-clairvoyant scheduling under polyhedral constraints. In *Proceedings of the 46th Annual ACM Symposium on Theory of Computing*, pages 313–322. ACM, 2014.

[83] Sungjin Im, Janardhan Kulkarni, Kamesh Munagala, and Kirk Pruhs. Selfishmigrate: A scalable algorithm for non-clairvoyantly scheduling heterogeneous processors. In *Foundations of Computer Science (FOCS), 2014 IEEE 55th Annual Symposium on*, pages 531–540. IEEE, 2014.

[84] Rolf Isermann. *Fault-diagnosis systems: an introduction from fault detection to fault tolerance*. Springer Science & Business Media, 2006.

[85] Daniel Kahneman and Patrick Egan. *Thinking, fast and slow*, volume 1. Farrar, Straus and Giroux New York, 2011.

[86] Bala Kalyanasundaram and Kirk Pruhs. Speed is as powerful as clairvoyance. *Journal of the ACM (JACM)*, 47(4):617–643, 2000.

[87] Saleem A Kassam and H Vincent Poor. Robust techniques for signal processing: A survey. *Proceedings of the IEEE*, 73(3):433–481, 1985.

[88] Anatoly Khina, Gustav M Pettersson, Victoria Kostina, and Babak Hassibi. Multi-rate control over AWGN channels via analog joint source-channel coding. In *Proceedings of the 55th IEEE Conference on Decision and Control (CDC)*, pages 5968–5973, 2016.

[89] John FC Kingman. *Poisson Processes (Oxford studies in probability; 3)*. Clarendon Press, 1993.

[90] Leonard Kleinrock. *Queueing systems, volume I: Theory*. Wiley Interscience, 1975.

[91] Christof Koch and Naotsugu Tsuchiya. Attention and consciousness: two distinct brain processes. *Trends in cognitive sciences*, 11(1):16–22, 2007.

[92] Fanxin Kong, Qiao Xiang, Linghe Kong, and Xue Liu. On-line event-driven scheduling for electric vehicle charging via park-and-charge. In *2016 IEEE Real-Time Systems Symposium (RTSS)2016 IEEE*, pages 69–78. IEEE, 2016.

[93] Victoria Kostina and Babak Hassibi. Rate-cost tradeoffs in control. In *arXiv:1612.02126*, 2016.

[94] Łukasz Kruk, John Lehoczky, Kavita Ramanan, Steven Shreve, et al. Heavy traffic analysis for edf queues with reneging. *The Annals of Applied Probability*, 21(2):484–545, 2011.

[95] Dara Kusic, Jeffrey O Kephart, James E Hanson, Nagarajan Kandasamy, and Guofei Jiang. Power and performance management of virtualized computing environments via lookahead control. *Cluster computing*, 12(1):1–15, 2009.

[96] Tarald O Kvåiseth. Note on information capacity of discrete motor responses. *Perceptual and Motor Skills*, 49(1):291–296, 1979.

[97] S Lac, Jennifer L Raymond, Terrence J Sejnowski, and Stephen G Lisberger. Learning and memory in the vestibulo-ocular reflex. *Annual review of neuroscience*, 18(1):409–441, 1995.

[98] Andrew Lamperski and John C Doyle. Dynamic programming solutions for decentralized state-feedback lqg problems with communication delays. In *ACC*, pages 6322–6327, 2012.

[99] Andrew Lamperski and John C Doyle. Output feedback h_2 model matching for decentralized systems with delays. *arXiv preprint arXiv:1209.3600*, 2012.

[100] Andrew Lamperski and Laurent Lessard. Optimal decentralized state-feedback control with sparsity and delays. *arXiv preprint arXiv:1306.0036*, 2013.

[101] T. Le and J. Dorsey. Patellar tendon refles time in psychiatric and in neurologic cases. *Arch NeurPsych*, 22:99–104, 1929.

[102] George Lee, Ted Lee, Zhi Low, Steven H. Low, and Christine Ortega. Adaptive charging network for electric vehicles. In *Proceedings of the IEEE Global Conference on Signal and Information Processing (GlobalSIP)*, Washington, DC, December 2016.

[103] John Lehoczky, Lui Sha, and Ye Ding. The rate monotonic scheduling algorithm: Exact characterization and average case behavior. In *Real Time Systems Symposium, 1989., Proceedings.*, pages 166–171. IEEE, 1989.

[104] John P Lehoczky. Real-time queueing network theory. In *Proc of the 18th IEEE Real-Time Systems Symposium*, pages 58–67, 1997.

[105] John P Lehoczky. Using real-time queueing theory to control lateness in real-time systems. *ACM SIGMETRICS Performance Evaluation Review*, 25 (1):158–168, 1997.

[106] Yoke Peng Leong and John C Doyle. Understanding robust control theory via stick balancing. In *Decision and Control (CDC), 2016 IEEE 55th Conference on*, pages 1508–1514. IEEE, 2016.

[107] Laurent Lessard and Sanjay Lall. Optimal controller synthesis for the decentralized two-player problem with output feedback. In *ACC*, pages 6314–6321. IEEE, 2012.

[108] Ioannis Lestas, Glenn Vinnicombe, and Johan Paulsson. Fundamental limits on the suppression of molecular fluctuations. *Nature*, 467(7312):174, 2010.

[109] Minghong Lin, Adam Wierman, Lachlan LH Andrew, and Eno Thereska. Dynamic right-sizing for power-proportional data centers. *IEEE/ACM Transactions on Networking*, 21(5):1378–1391, 2013.

[110] Stephen G Lisberger. Visual guidance of smooth-pursuit eye movements: sensation, action, and what happens in between. *Neuron*, 66(4):477–491, 2010.

[111] Chung Laung Liu and James W Layland. Scheduling algorithms for multiprogramming in a hard-real-time environment. *Journal of the ACM (JACM)*, 20(1):46–61, 1973.

[112] Quangying Liu, Yorie Nakahira, Ahkeel Mohideen, Sunghoon Choi, and John C. Doyle. Wheelcon: A wheel control-based gaming platform for studying human sensorimotor control. https://arxiv.org/abs/1811.00738, 2018.

[113] Shuai Liu, Tao Li, and Lihua Xie. Distributed consensus for multiagent systems with communication delays and limited data rate. *SIAM Journal on Control and Optimization*, 49(6):2239–2262, 2011.

[114] Yao Liu, Michael Reiter, and Peng Ning. False data injection attacks against state estimation in electric power grids. In *Proceedings of the 16th ACM conference on Computer and communications security*, 2009.

[115] Zhenhua Liu, Minghong Lin, Adam Wierman, Steven H Low, and Lachlan LH Andrew. Greening geographical load balancing. In *Proceedings of the ACM SIGMETRICS joint international conference on Measurement and modeling of computer systems*, pages 233–244. ACM, 2011.

[116] Stuart Lloyd. Least squares quantization in pcm. *IEEE transactions on information theory*, 28(2):129–137, 1982.

[117] Steven H Low. Convex relaxation of optimal power flow: A tutorial. In *Bulk Power System Dynamics and Control-IX Optimization, Security and Control of the Emerging Power Grid (IREP), 2013 IREP Symposium*, pages 1–15. IEEE, 2013.

[118] An-Yang Lu and Guang-Hong Yang. Secure state estimation for cyber-physical systems under sparse sensor attacks via a switched luenberger observer. *Information sciences*, 417:454–464, 2017.

[119] Zhongjing Ma, Duncan Callaway, and Ian Hiskens. Decentralized charging control for large populations of plug-in electric vehicles. In *49th IEEE conference on decision and control (CDC)*, pages 206–212. IEEE, 2010.

[120] I Scott MacKenzie. A note on the information-theoretic basis for fitts' law. *Journal of motor behavior*, 21(3):323–330, 1989.

[121] Constantinos Maglaras and Jan A. Van Mieghem. Queueing systems with leadtime constraints: A fluid-model approach for admission and sequencing control. *European journal of operational research*, 167(1):179–207, 2005.

[122] Zachary F Mainen and Terrence J Sejnowski. Reliability of spike timing in neocortical neurons. *Science*, 268(5216):1503–1506, 1995.

[123] Ricardo A. Maronna, Douglas R. Martin, and Victor J. Yohai. *Robust Statistics: Theory and Methods*. Wiley, 2006.

[124] James Massey. Causality, feedback and directed information. In *Proceedings of the International Symposium on Information Theory and Applications (ISITA-90)*, pages 303–305, 1990.

[125] Jean Massion. Movement, posture and equilibrium: interaction and coordination. *Progress in neurobiology*, 38(1):35–56, 1992.

[126] Peter BC Matthews. The human stretch reflex and the motor cortex. *Trends in neurosciences*, 14(3):87–91, 1991.

[127] Markus Maurer, J Christian Gerdes, Barbara Lenz, and Hermann Winner. *Autonomous driving: technical, legal and social aspects*. Springer, 2016.

[128] Sergey Melnik, Andrey Gubarev, Jing Jing Long, Geoffrey Romer, Shiva Shivakumar, Matt Tolton, and Theo Vassilakis. Dremel: interactive analysis of web-scale datasets. *Proceedings of the VLDB Endowment*, 3(1-2):330–339, 2010.

[129] Yilin Mo and Emanuele Garone. Secure dynamic state estimation via local estimators. In *Decision and Control (CDC), 2016 IEEE 55th Conference on*, pages 5073–5078. IEEE, 2016.

[130] Yilin Mo and Bruno Sinopoli. Secure estimation in the presence of integrity attacks. *IEEE Transactions on Automatic Control*, 60(4):1145–1151, 2015.

[131] Yilin Mo, Roberto Ambrosino, and Bruno Sinopoli. Sensor selection strategies for state estimation in energy constrained wireless sensor networks. *Automatica*, 47(7):1330–1338, 2011.

[132] Pascal Moyal. On queues with impatience: stability, and the optimality of earliest deadline first. *Queueing Systems*, 75(2-4):211–242, 2013.

[133] Tridib Mukherjee, Ayan Banerjee, Georgios Varsamopoulos, Sandeep KS Gupta, and Sanjay Rungta. Spatio-temporal thermal-aware job scheduling to minimize energy consumption in virtualized heterogeneous data centers. *Computer Networks*, 53(17):2888–2904, 2009.

[134] Hideo Nagai. Bellman equations of risk-sensitive control. *SIAM journal on control and optimization*, 34(1):74–101, 1996.

[135] Arne J Nagengast, Daniel A Braun, and Daniel M Wolpert. Risk sensitivity in a motor task with speed-accuracy trade-off. *Journal of neurophysiology*, 105(6):2668–2674, 2011.

[136] Girish N Nair and Robin J Evans. Stabilization with data-rate-limited feedback: Tightest attainable bounds. *Systems & Control Letters*, 41(1):49–56, 2000.

[137] Girish N Nair and Robin J Evans. Stabilizability of stochastic linear systems with finite feedback data rates. *SIAM Journal on Control and Optimization*, 43(2):413–436, 2004.

[138] Girish N Nair, Fabio Fagnani, Sandro Zampieri, and Robin J Evans. Feedback control under data rate constraints: An overview. *Proceedings of the IEEE*, 95(1):108–137, 2007.

[139] Yorie Nakahira and Yilin Mo. Dynamic state estimation in the presence of compromised sensory data. In *IEEE 54th Annual Conference on Decision and Control (CDC)*, pages 5808–5813. IEEE, 2015.

[140] Yorie Nakahira, Nikolai Matni, and John C Doyle. Hard limits on robust control over delayed and quantized communication channels with applications to sensorimotor control. In *Decision and Control (CDC), 2015 IEEE 54th Annual Conference on*, pages 7522–7529. IEEE, 2015.

[141] Yorie Nakahira, Fangzhou Xiao, Victoria Kostina, and John C Doyle. Fundamental limits and achievable performance in biomolecular control. In *2018 Annual American Control Conference (ACC)*, pages 2707–2714. IEEE, 2018.

[142] Yorie Nakahira, Quangying Liu, Terry Sejnowski, and John C. Doyle. Diversity sweet spots in layered architectures and speed-accuracy trade-offs in sensorimotor control. Draft, 2019.

[143] Ashutosh Nayyar, Josh Taylor, Anand Subramanian, Kameshwar Poolla, and Pravin Varaiya. Aggregate flexibility of a collection of loadsπ. In *Decision and Control (CDC), 2013 IEEE 52nd Annual Conference on*, pages 5600–5607. IEEE, 2013.

[144] Dragan Nesic and Daniel Liberzon. A unified framework for design and analysis of networked and quantized control systems. *IEEE Transactions on Automatic Control*, 54(4):732–747, 2009.

[145] Calvin Nobles. Cyber threats in civil aviation. *Security Solutions for Hyperconnectivity and the Internet of Things*, page 272, 2016.

[146] Krishnan Padmanabhan and Nathaniel N Urban. Intrinsic biophysical diversity decorrelates neuronal firing while increasing information content. *Nature neuroscience*, 13(10):1276, 2010.

[147] Miroslav Pajic, James Weimer, Nicola Bezzo, Paulo Tabuada, Oleg Sokolsky, Insup Lee, and George J Pappas. Robustness of attack-resilient state estimators. In *ACM/IEEE International Conference on Cyber-Physical Systems (ICCPS)*, pages 163–174. IEEE, 2014.

[148] Miroslav Pajic, Insup Lee, and George J Pappas. Attack-resilient state estimation for noisy dynamical systems. *IEEE Transactions on Control of Network Systems*, 4(1):82–92, 2017.

[149] Miroslav Pajic, James Weimer, Nicola Bezzo, Oleg Sokolsky, George J Pappas, and Insup Lee. Design and implementation of attack-resilient cyberphysical systems: With a focus on attack-resilient state estimators. *IEEE Control Systems*, 37(2):66–81, 2017.

[150] Shivendra S Panwar and Don Towsley. On the optimality of the ste rule for multiple server queues that serve customers with deadlines. Technical report, University of Massachusetts, 1988.

[151] Shivendra S Panwar, Don Towsley, and Jack K Wolf. Optimal scheduling policies for a class of queues with customer deadlines to the beginning of service. *Journal of the ACM (JACM)*, 35(4):832–844, 1988.

[152] Ron J Patton, Paul M Frank, and Robert N Clark. *Issues of fault diagnosis for dynamic systems*. Springer Science & Business Media, 2013.

[153] János A Perge, Kristin Koch, Robert Miller, Peter Sterling, and Vijay Balasubramanian. How the optic nerve allocates space, energy capacity, and information. *Journal of Neuroscience*, 29(24):7917–7928, 2009.

[154] János A Perge, Jeremy E Niven, Enrico Mugnaini, Vijay Balasubramanian, and Peter Sterling. Why do axons differ in caliber? *Journal of Neuroscience*, 32(2):626–638, 2012.

[155] Cynthia A Phillips, Cliff Stein, Eric Torng, and Joel Wein. Optimal time-critical scheduling via resource augmentation. In *Proceedings of the twenty-ninth annual ACM symposium on Theory of computing*, pages 140–149. ACM, 1997.

[156] Michael Pinedo. Stochastic scheduling with release dates and due dates. *Operations Research*, 31(3):559–572, 1983.

[157] Erica Plambeck, Sunil Kumar, and Michael J. Harrison. A multiclass queue in heavy traffic with throughput time constraints: Asymptotically optimal dynamic controls. *Queueing Systems*, 39(1):23–54, 2001.

[158] Ragunathan Raj Rajkumar, Insup Lee, Lui Sha, and John Stankovic. Cyber-physical systems: the next computing revolution. In *Proceedings of the 47th Design Automation Conference*, pages 731–736. ACM, 2010.

[159] Farzad Rezaei, NU Ahmed, and Charalambos D Charalambous. Rate distortion theory for general sources with potential application to image compression. *International Journal of Applied Mathematical Sciences*, 3(2):141–165, 2006.

[160] Peter Richardson, Damian Flynn, and Andrew Keane. Local versus centralized charging strategies for electric vehicles in low voltage distribution systems. *IEEE Transactions on Smart Grid*, 3(2):1020–1028, 2012.

[161] Per E Roland, Akitoshi Hanazawa, Calle Undeman, David Eriksson, Tamas Tompa, Hiroyuki Nakamura, Sonata Valentiniene, and Bashir Ahmed. Cortical feedback depolarization waves: a mechanism of top-down influence on early visual areas. *Proceedings of the National Academy of Sciences*, 103 (33):12586–12591, 2006.

[162] Michael Rotkowitz and Sanjay Lall. A characterization of convex problems in decentralized control. *IEEE Transactions on Automatic Control*, 51(2): 274–286, 2006.

[163] A. Sahai and S. Mitter. The necessity and sufficiency of anytime capacity for stabilization of a linear system over a noisy communication link—part i: Scalar systems. *IEEE Transactions on Information Theory*, 52(8):3369–3395, Aug 2006. ISSN 0018-9448. doi: 10.1109/TIT.2006.878169.

[164] Emilio Salinas and Terrence J Sejnowski. Correlated neuronal activity and the flow of neural information. *Nature reviews neuroscience*, 2(8):539, 2001.

[165] Henrik Sandberg, Andre Teixeira, and Karl H. Johansson. On security indices for state estimators in power networks. In *First Workshop on Secure Control Systems*, 2010.

[166] Terence D Sanger. Neuro-mechanical control using differential stochastic operators. In *Engineering in Medicine and Biology Society (EMBC), 2010 Annual International Conference of the IEEE*, pages 4494–4497. IEEE, 2010.

[167] Terence D Sanger. Risk-aware control. *Neural computation*, 26(12):2669–2691, 2014.

[168] Luca Schenato, Bruno Sinopoli, Massimo Franceschetti, Kameshwar Poolla, and S Shankar Sastry. Foundations of control and estimation over lossy networks. *Proceedings of the IEEE*, 95(1):163–187, 2007.

[169] Lui Sha, Tarek Abdelzaher, Karl-Erik Årzén, Anton Cervin, Theodore Baker, Alan Burns, Giorgio Buttazzo, Marco Caccamo, John Lehoczky, and Aloysius K Mok. Real time scheduling theory: A historical perspective. *Real-time systems*, 28(2-3):101–155, 2004.

[170] Parikshit Shah, Pablo Parrilo, et al. An optimal controller architecture for poset-causal systems. In *CDC-ECC*, pages 5522–5528. IEEE, 2011.

[171] Claude E Shannon. A mathematical theory of communication. *ACM SIGMOBILE Mobile Computing and Communications Review*, 5(1):3–55, 2001.

[172] Yasser Shoukry and Paulo Tabuada. Event-triggered state observers for sparse sensor noise/attacks. *IEEE Transactions on Automatic Control*, 61(8):2079–2091, 2016.

[173] Yasser Shoukry, Pierluigi Nuzzo, Alberto Puggelli, Alberto L Sangiovanni-Vincentelli, Sanjit A Seshia, and Paulo Tabuada. Secure state estimation for cyber physical systems under sensor attacks: a satisfiability modulo theory approach. *IEEE Transactions on Automatic Control*, 2017.

[174] Eduardo I Silva, Milan S Derpich, and Jan Ostergaard. A framework for control system design subject to average data-rate constraints. *IEEE Transactions on Automatic Control*, 56(8):1886–1899, 2011.

[175] Eduardo I Silva, Milan S Derpich, Jan Østergaard, and Marco A Encina. A characterization of the minimal average data rate that guarantees a given closed-loop performance level. *IEEE Transactions on Automatic Control*, 61 (8):2171–2186, 2016.

[176] William R Softky and Christof Koch. The highly irregular firing of cortical cells is inconsistent with temporal integration of random epsps. *Journal of Neuroscience*, 13(1):334–350, 1993.

[177] Lauren M Sompayrac. *How the immune system works*. Wiley-Blackwell, 2019.

[178] Kathleen Spees and Lester B Lave. Demand response and electricity market efficiency. *The Electricity Journal*, 20(3):69–85, 2007.

[179] Siddharth Sridhar, Adam Hahn, and Manimaran Govindarasu. Cyber–physical system security for the electric power grid. *Proceedings of the IEEE*, 100(1):210–224, 2012.

[180] Kyle H Srivastava, Caroline M Holmes, Michiel Vellema, Andrea R Pack, Coen PH Elemans, Ilya Nemenman, and Samuel J Sober. Motor control by precisely timed spike patterns. *Proceedings of the National Academy of Sciences*, 114(5):1171–1176, 2017.

[181] John A Stankovic and Krithi Ramamritham. What is predictability for real-time systems? *Real-Time Systems*, 2(4):247–254, 1990.

[182] John A. Stankovic, Krithi Ramamritham, and Marco Spuri. *Deadline Scheduling for Real-Time Systems: EDF and Related Algorithms*. Kluwer Academic Publishers, Norwell, MA, USA, 1998. ISBN 0792382692.

[183] Richard B Stein, E Roderich Gossen, and Kelvin E Jones. Neuronal variability: noise or part of the signal? *Nature Reviews Neuroscience*, 6(5):389, 2005.

[184] Sebastian Stein, Enrico Gerding, Valentin Robu, and Nicholas R. Jennings. A model-based online mechanism with pre-commitment and its application to electric vehicle charging. In *Proceedings of the 11th International Conference on Autonomous Agents and Multiagent Systems - Volume 2*, AAMAS '12, pages 669–676, Richland, SC, 2012. International Foundation for Autonomous Agents and Multiagent Systems. ISBN 0-9817381-2-5, 978-0-9817381-2-3. URL `http://dl.acm.org/citation.cfm?id=2343776.2343792`.

[185] Peter Sterling and Simon Laughlin. *Principles of neural design*. MIT Press, 2015.

[186] Anand Subramanian, Manuel J Garcia, Duncan S Callaway, Kameshwar Poolla, and Pravin Varaiya. Real-time scheduling of distributed resources. *IEEE Transactions on Smart Grid*, 4(4):2122–2130, 2013.

[187] Olle Sundström and Carl Binding. Planning electric-drive vehicle charging under constrained grid conditions. In *Power System Technology (POWERCON), 2010 International Conference on*, pages 1–6. IEEE, 2010.

[188] Takashi Tanaka, Peyman Mohajerin Esfahani, and Sanjoy K Mitter. Lqg control with minimum directed information: Semidefinite programming approach. *IEEE Transactions on Automatic Control*, 63(1):37–52, 2018.

[189] Sekhar Tatikonda and Sanjoy Mitter. Control under communication constraints. *IEEE Transactions on Automatic Control*, 49(7):1056–1068, 2004.

[190] Sekhar Tatikonda, Anant Sahai, and Sanjoy Mitter. Stochastic linear control over a communication channel. *IEEE Transactions on Automatic Control*, 49 (9):1549–1561, 2004.

[191] Emanuel Todorov and Michael I Jordan. Optimal feedback control as a theory of motor coordination. *Nature neuroscience*, 5(11):1226–1235, 2002.

[192] Robert J van Beers, Pierre Baraduc, and Daniel M Wolpert. Role of uncertainty in sensorimotor control. *Phil. Trans. of the Royal Society B: Bio. Sciences*, 357(1424):1137–1145, 2002.

[193] Luis M Vaquero, Luis Rodero-Merino, and Rajkumar Buyya. Dynamically scaling applications in the cloud. *ACM SIGCOMM Computer Communication Review*, 41(1):45–52, 2011.

[194] Domitilla Del Vecchio and Richard M. Murray. *Biomolecular Feedback Systems*. Princeton University Press, 2014.

[195] Venkat Venkatasubramanian, Raghunathan Rengaswamy, Kewen Yin, and Surya N Kavuri. A review of process fault detection and diagnosis: Part i: Quantitative model-based methods. *Computers & chemical engineering*, 27 (3):293–311, 2003.

[196] Sergio Verdu. The exponential distribution in information theory. *Problemy peredachi informatsii*, 32(1):100–111, 1996.

[197] Xiaorui Wang and Ming Chen. Cluster-level feedback power control for performance optimization. In *High Performance Computer Architecture, 2008. HPCA 2008. IEEE 14th International Symposium on*, pages 101–110. IEEE, 2008.

[198] Yuh-Shyang Wang and Nikolai Matni. Localized distributed optimal control with output feedback and communication delays. In *Annual Allerton Conference on Communication, Control, and Computing*, pages 605–612. IEEE, 2014.

[199] Yuh-Shyang Wang, Nikolai Matni, and John C Doyle. Localized lqr optimal control. In *CDC*, pages 1661–1668. IEEE, 2014.

[200] Peter Whittle. Restless bandits: Activity allocation in a changing world. *Journal of applied probability*, 25(A):287–298, 1988.

[201] Peter Whittle. *Risk-sensitive optimal control*. Wiley, 1990.

[202] Wikipedia. Fitts's law (wikipedia). `https://en.wikipedia.org/wiki/Fitts\%27s_law`, 2019.

[203] Wing Shing Wong and Roger W Brockett. Systems with finite communication bandwidth constraints. ii. stabilization with limited information feedback. *IEEE Transactions on Automatic Control*, 44(5):1049–1053, 1999.

[204] Le Xie, Yilin Mo, and B. Sinopoli. Integrity data attacks in power market operations. *IEEE Transactions on Smart Grid*, 2(4):659–666, 2011. doi: 10.1109/TSG.2011.2161892.

[205] Frances Yao, Alan Demers, and Scott Shenker. A scheduling model for reduced cpu energy. In *Foundations of Computer Science, 1995. Proceedings., 36th Annual Symposium on*, pages 374–382. IEEE, 1995.

[206] Zhe Yu, Yunjian Xu, and Lang Tong. Deadline scheduling as restless bandits. *arXiv preprint arXiv:1610.00399*, 2016.

[207] Serdar Yuksel. Stochastic stabilization of noisy linear systems with fixed-rate limited feedback. *IEEE Transactions on Automatic Control*, 55(12): 2847–2853, 2010.

[208] Serdar Yuksel. Jointly optimal LQG quantization and control policies for multi-dimensional systems. *IEEE Transactions on Automatic Control*, 59(6): 1612–1617, 2014.

[209] Serdar Yüksel and T Basar. Stochastic networked control systems. *AMC*, 10: 12, 2013.

[210] Li Zhaoping. *Understanding vision: theory, models, and data*. Oxford University Press, 2014.

[211] Qian Zhu and Gagan Agrawal. Resource provisioning with budget constraints for adaptive applications in cloud environments. In *Proc. of the 19th ACM International Symposium on High Performance Distributed Computing*, pages 304–307. ACM, 2010.

[212] Ray Daniel Zimmerman, Carlos Edmundo Murillo-Sánchez, and Robert John Thomas. Matpower: Steady-state operations, planning, and analysis tools for power systems research and education. *IEEE Transactions on power systems*, 26(1):12–19, 2011.

Appendix A

ADDITIONAL PROOFS FOR SECTION VIII

A.1 Additional proofs

We first introduce some notation that will be used later. Denote by $A_t = \{i \in \mathcal{V} : a_i \leq t\}$ the set of EVs that have arrived by time t, $D_t = \{i \in A_t : d_i \leq t \text{ or } e_i(t) = 0\}$ the set of EVs that have either departed or finished charging by time t, $V_t = \{i \in A_t : a_i \leq t < d_i\}$ the set of EVs remaining in the charging station at time t, and $U_t = \{i \in V_t : e_i(t) > 0\}$ the set of EVs with unfulfilled energy demand at the beginning of time slot t, where we reload the notation and use $e_i(t)$ to denote the remaining energy demand of EV i at the beginning of time slot t. In addition, denote by $A_{[t_1,t_2]} = \{i \in \mathcal{V} : a_i \in [t_1, t_2]\}$ the set of EVs that arrive during time interval $[t_1, t_2]$, $t_1, t_2 \in \mathcal{T}$. See Table S1 for a summary of notation.

Denote the total energy supply to EVs in set $\mathcal{S} \subseteq \mathcal{V}$ during the interval $[t_1, t_2]$ under the (feasible) offline algorithm by

$$\Psi^*_{[t_1:t_2]}(\mathcal{S}; \mathcal{I}) := \sum_{i \in \mathcal{S}} \sum_{\tau=t_1}^{t_2} r_i(\tau),$$

and the total energy supply to EVs in set $\mathcal{S} \subseteq \mathcal{V}$ during the interval $[t_1, t_2]$ under the ϵ-power augmentation (or ϵ-augmentation) by

$$\Psi^\epsilon_{[t_1:t_2]}(\mathcal{S}; \mathcal{I}) := \sum_{i \in \mathcal{S}} \sum_{\tau=t_1}^{t_2} r_i(\tau).$$

We use superscript * to indicate variables under an (feasible) offline algorithm with original power limit $P(t)$ and maximum charging rates $\bar{r}_i$, and use superscript $^\epsilon$ to indicate variables under the augmented resources.

Lemma A.1.1. *When the sLLF algorithm is used on instance $\mathcal{I}$, for any EV $i \in \mathcal{S}_2$ and $j \in \mathcal{F}$, their laxities satisfy*

$$\ell_i(t) > \ell_j(t),\ t \in [\max(a_i, a_j),\ t_-]. \tag{A.1}$$

Proof (Lemma A.1.1). By the construction of $\mathcal{S}_2$, relation (A.1) holds at time $t = t_-$. By Lemma 9.2.1, a necessary condition for the inequality in (A.1) to flip at some time $t + 1 \leq t_-$ is for (9.26) to hold for EV i. We show below that this condition

Table S1: Additional Notation

A_t	set of EVs arriving by time t
$A_{[t_1,t_2]}$	set of EVs arriving during interval $[t_1, t_2]$
D_t	set of EVs either departed or finished by time t
V_t	set of EVs at the charging station at time t
U_t	set of EVs unfinished charging at time t
$\Psi_{[t_1:t_2]}(\mathcal{S}; \mathcal{I})$	total energy supplied to the set of EVs $\mathcal{S}$ during the interval $[t_1, t_2]$ under instance $\mathcal{I}$
$\Psi^{\epsilon}_{[t_1:t_2]}(\mathcal{S}; \mathcal{I})$	total energy supplied to $\mathcal{S}$ during $[t_1, t_2]$ under instance $\mathcal{I}$ with ϵ augmented resources

cannot hold for any EV in $\mathcal{F}$ or $\mathcal{S}_1$. For EVs in $\mathcal{F}$, condition $e_j(t+1) = 0$ in (9.26) cannot happen because negative laxity at some time implies the energy demand will not be fulfilled. For EVs in $\mathcal{S}_1$, (A.1) holds only after $e_j(t+1) = 0$ when they have energy demand fulfilled at time $t+1$. Consequently, condition (A.1) holds for all $t \in [\max(a_i, a_j), t_-]$. □

Notice that the sLLF algorithm prioritizes EVs with smaller laxity so the presence of EVs with strictly greater laxity will not impact the charging of the EVs with smaller laxity. Let $\tilde{\mathcal{V}} = \mathcal{F} \cup \mathcal{S}_1$, and use it to define another instance that does not contain the EVs in S_2: $\tilde{\mathcal{I}} = \{a_i, d_i, e_i, \bar{r}_i; P(t)\}_{i \in \tilde{\mathcal{V}}, t \in \mathcal{T}}$. The following Corollary can be obtained as a consequence of Lemma A.1.1.

Corollary A.1.1. *Regardless of the actual instance being $\mathcal{I}$ or $\tilde{\mathcal{I}}$, the EVs in $\tilde{\mathcal{F}}$ are charged in exactly the same way under the sLLF algorithm by time t_-.*

Let $\mathcal{I}$ be an EV charging instances that are offline feasible. Consider using the sLLF algorithm with the ϵ augmented resources (either power augmentation $P^{on}(t) = \epsilon P(t)$, or power and rate augmentation $P^{on}(t) = \epsilon P(t), \bar{r}^{on}_i(t) = \bar{r}_i(t)$). Now, the above result from previous section, we derive a condition for the sLLF algorithm being infeasible on some online feasible instance, which holds for both power augmentation and power and rate augmentation.

Since the EVs in $\mathcal{S}_1$ are fully charged by time t_- under both the sLLF algorithm and the offline algorithm, we have

$$\Psi^{\epsilon}_{[0:t_-]}(\mathcal{S}_1; \mathcal{I}) = \Psi^{*}_{[0:t_-]}(\mathcal{S}_1; \mathcal{I}), \tag{A.2}$$

where $\mathcal{S}_1, \mathcal{F}$ are the sets defined above under the sLLF algorithm using augmented resources. Notice that $\ell_i(t) \geq 0,\ \forall t \in \mathcal{T}$ is a necessary condition for EV i to be feasible. Thus, for EV $i \in \mathcal{F}$, the offline algorithm must maintain $\ell_i(t_-) \geq 0$. Given that laxity $\ell_i(t)$ is strictly decreasing in the remaining energy demand $e_i(t)$, the total energy fulfilled by t_- under the offline algorithm must be strictly greater than that with the sLLF algorithm, *i.e.*

$$\Psi^{\epsilon}_{[0:t_-]}(\{i\}; \mathcal{I}) < \Psi^{*}_{[0:t_-]}(\{i\}; \mathcal{I}),\ i \in \mathcal{F} \tag{A.3}$$

from which

$$\Psi^{\epsilon}_{[0:t_-]}(\mathcal{F}; \mathcal{I}) < \Psi^{*}_{[0:t_-]}(\mathcal{F}; \mathcal{I}). \tag{A.4}$$

Recall that $\tilde{\mathcal{V}} = \mathcal{V} \backslash S_2$. Combining (A.2) and (A.4), we have

$$\Psi^{\epsilon}_{[0:t_-]}(\tilde{\mathcal{V}}; \mathcal{I}) < \Psi^{*}_{[0:t_-]}(\tilde{\mathcal{V}}; \mathcal{I}). \tag{A.5}$$

Corollary A.1.1 implies

$$\Psi^{\epsilon}_{[0:t_-]}(i; \mathcal{I}) = \Psi^{\epsilon}_{[0:t_-]}(i; \tilde{\mathcal{I}}),\ i \in \tilde{\mathcal{V}}, \tag{A.6}$$

$$\Psi^{\epsilon}_{[0:t_-]}(\tilde{\mathcal{V}}; \mathcal{I}) = \Psi^{\epsilon}_{[0:t_-]}(\tilde{\mathcal{V}}; \tilde{\mathcal{I}}). \tag{A.7}$$

Further, since the charging instance $\mathcal{I}$ is offline feasible, its sub-instance $\tilde{\mathcal{I}}$ is offline feasible too. Similar to equations (A.2)-(A.5), we can show that

$$\Psi^{\epsilon}_{[0:t_-]}(\mathcal{S}_1; \tilde{\mathcal{I}}) = \Psi^{*}_{[0:t_-]}(\mathcal{S}_1; \tilde{\mathcal{I}}), \tag{A.8}$$

$$\Psi^{\epsilon}_{[0:t_-]}(\{i\}; \tilde{\mathcal{I}}) < \Psi^{*}_{[0:t_-]}(\{i\}; \tilde{\mathcal{I}}),\ i \in \mathcal{F}, \tag{A.9}$$

$$\Psi^{\epsilon}_{[0:t_-]}(\mathcal{F}; \tilde{\mathcal{I}}) < \Psi^{*}_{[0:t_-]}(\mathcal{F}; \tilde{\mathcal{I}}), \tag{A.10}$$

$$\Psi^{\epsilon}_{[0:t_-]}(\tilde{\mathcal{V}}; \tilde{\mathcal{I}}) < \Psi^{*}_{[0:t_-]}(\tilde{\mathcal{V}}; \tilde{\mathcal{I}}). \tag{A.11}$$

A.2 Proof of Theorem 9.3.1

Consider the use of the sLLF algorithm on an offline feasible instance $\mathcal{I} = \{a_i, d_i, e_i, \bar{r}_i; P(t)\}_{i \in \mathcal{V}, t \in \mathcal{T}}$ under ϵ-power augmented resources. Let

$$n = (1 + \epsilon)\frac{P_{\min}}{P_{\max}}. \tag{A.12}$$

For $m \leq n$, we define the earliest time to charge at a power greater than $mP_{\max}$ for the rest of the time until t_- as

$$t_m = \min\left\{ t \in \mathcal{T} : \sum_{j \in V_t} \min(\bar{r}_j, e_j(\tau)) \geq mP_{\max}, \tau \in [t, t_-] \right\}. \tag{A.13}$$

Let $T_m = [t_{m-1}, t_m)$ and $\hat{T}_m = [t_m, t_-]$ and denote their lengths by $|T_m|$ and $|\hat{T}_m|$.

We first present a lemma that is used in the proof of Theorem 9.3.1.

Lemma A.2.1. *For any integer $i \leq n-1$, the following two relations hold:*

$$\Psi^*_{[0:t_i]}(A_{T_i}; \tilde{\mathcal{I}}) - \Psi^{\epsilon}_{[0:t_i]}(A_{T_i}; \tilde{\mathcal{I}}) > P_{\max}|\hat{T}_{i+1}|, \tag{A.14}$$

$$|T_i| > |\hat{T}_{i+1}|. \tag{A.15}$$

Proof (Lemma A.2.1). On one hand, from definition (A.13),

$$\sum_{j \in V_{(t_{i-1})-1}} \min(\bar{r}_j, e_j(t_{i-1}-1)) < (i-1)P_{\max}.$$

This implies that the EVs that have arrived before t_{i-1} are charged at a total power of at most $(i-1)P_{\max}$ at t_{i-1} and after. On the other hand, from definition (A.13), the total power supply is at least $iP_{\max}$ during the interval $T_{i+1} = [t_i, t_{i+1}]$. Therefore, the total charing power to the EVs that arrive after t_{i-1} is at least $P_{\max}$ during T_{i+1}. Since the offline algorithm can only use a power of at most $P_{\max}$, for the EVs that arrive after t_{i-1} we obtain

$$\begin{aligned} &\Psi^*_{[0;t_{i+1}]}(A_{\hat{T}_{i-1}}; \tilde{\mathcal{I}}) - \Psi^{\epsilon}_{[0;t_{i+1}]}(A_{\hat{T}_{i-1}}; \tilde{\mathcal{I}}) \\ &< \Psi^*_{[0;t_i]}(A_{\hat{T}_{i-1}}; \tilde{\mathcal{I}}) - \Psi^{\epsilon}_{[0;t_i]}(A_{\hat{T}_{i-1}}; \tilde{\mathcal{I}}). \end{aligned} \tag{A.16}$$

The same argument can be applied to the interval $\hat{T}_{i+1} = [t_{i+1}, t_-]$. From definition (A.13), the total charging power is at least $(i+1)P_{\max}$ during $\hat{T}_{i+1}$. Therefore, during $\hat{T}_{i+1}$, the total charing power to the EVs that arrive after t_{i-1} is at least $2P_{\max}$. Since the offline algorithm can only use a power of at most $P_{\max}$, the total energy supply to EVs in $\hat{T}_{i-1}$ under the augmented resources is greater than that without augmented resources, *i.e.*

$$\begin{aligned} 0 &< \Psi^*_{[0;t_-]}(A_{\hat{T}_{i-1}}; \tilde{\mathcal{I}}) - \Psi^{\epsilon}_{[0;t_-]}(A_{\hat{T}_{i-1}}; \tilde{\mathcal{I}}) \\ &< \Psi^*_{[0;t_{i+1}]}(A_{\hat{T}_{i-1}}; \tilde{\mathcal{I}}) - \Psi^{\epsilon}_{[0;t_{i+1}]}(A_{\hat{T}_{i-1}}; \tilde{\mathcal{I}}) - P_{\max}|\hat{T}_{i+1}|. \end{aligned} \tag{A.17}$$

Combining (A.16)-(A.17), we have

$$\Psi^*_{[0;t_i]}(A_{\hat{T}_{i-1}}; \tilde{\mathcal{I}}) - \Psi^{\epsilon}_{[0;t_i]}(A_{\hat{T}_{i-1}}; \tilde{\mathcal{I}}) > P_{\max}|\hat{T}_{i+1}|. \tag{A.18}$$

Since the set A_{T_i} is identical to the subset of $A_{\hat{T}_{i-1}}$ that contains only the EVs that have arrived by t_i,

$$\begin{aligned} &\Psi^*_{[0;t_i]}(A_{T_i}; \tilde{\mathcal{I}}) - \Psi^{\epsilon}_{[0;t_i]}(A_{T_i}; \tilde{\mathcal{I}}) \\ &= \Psi^*_{[0;t_i]}(A_{\hat{T}_{i-1}}; \tilde{\mathcal{I}}) - \Psi^{\epsilon}_{[0;t_i]}(A_{\hat{T}_{i-1}}; \tilde{\mathcal{I}}). \end{aligned} \tag{A.19}$$

Combining (A.18) and (A.19) leads to relation (A.14).

Finally, as all EVs in A_{T_i} arrives after t_{i-1}, during T_i the offline algorithm can charge a total energy of at most $|T_i|P_{\max}$, we obtain

$$\Psi^*_{[0:t_i]}(A_{T_i};\tilde{\mathcal{I}}) - \Psi^{\epsilon}_{[0:t_i]}(A_{T_i};\tilde{\mathcal{I}}) \leq |T_i|P_{\max},$$

which together with (A.14) leads to (A.15). □

Proof. (Theorem 9.3.1)

Suppose that there exists an offline feasible instance $\mathcal{I} = \{a_i, d_i, e_i, \bar{r}_i; P(t)\}_{i\in\mathcal{V},t\in\mathcal{T}}$ such that the sLLF algorithm is not feasible with ϵ-power augmented resources. Then, from Section A.1, there exists another offline feasible instance $\tilde{\mathcal{I}} = \{a_i, d_i, e_i, \bar{r}_i; P(t)\}_{i\in\tilde{\mathcal{V}},t\in\mathcal{T}}$ such that

$$\Psi^{\epsilon}_{[0:t_-]}(\{i\};\tilde{\mathcal{I}}) < \Psi^*_{[0:t_-]}(\{i\};\tilde{\mathcal{I}}),\ i \in \mathcal{V}. \tag{A.20}$$

When $m = 1$, we obtain $\sum_{j\in V_{t_1-1}} \min(\bar{r}_j, e_j(t_1-1)) < P_{\max}$. Let $\mathcal{S} = \{i \in A_{T_1} : e_i(t_1) > 0\} \subset A_{T_1}$ denote the set of EVs that arrive during T_1 and have not yet been fully charged by t_1. Because the number of EVs is upper bounded by $P_{\max}/\bar{r}_{\min}$ (from (A.13)), and the EVs in $A_{T_1}\backslash S$ are all fully charged,

$$\begin{aligned} P_{\max}|\hat{T}_2| &\leq \Psi^*_{[0:t_-]}(A_{T_1};\tilde{\mathcal{I}}) - \Psi^{\epsilon}_{[0:t_-]}(A_{T_1};\tilde{\mathcal{I}}) \\ &= \Psi^*_{[0:t_-]}(\mathcal{S};\tilde{\mathcal{I}}) - \Psi^{\epsilon}_{[0:t_-]}(\mathcal{S};\tilde{\mathcal{I}}) \\ &\leq X P_{\max}/\bar{r}_{\min}. \end{aligned}$$

This leads to

$$|\hat{T}_2| < \frac{X}{\bar{r}_{\min}}. \tag{A.21}$$

At time $t < t_{m-1}$, we have

$$\sum_{j\in V_{t_{m-1}-1}} \min(\bar{r}_j, e_j(t_{m-1}-1)) < (m-1)P_{\max},$$

which implies that there are at most $(m-1)P_{\max}/\bar{r}_{\min}$ EVs with unfulfilled energy demand by time t_f. Meanwhile, at time $t \geq t_m$, we have

$$\sum_{j\in V_{t_m}} \min(\bar{r}_j, e_j(t_m)) \geq mP_{\max},$$

which implies that there are at least $mP_{\max}/\bar{r}_{\max}$ EVs with unfulfilled energy demand during T_{m-1}. Therefore, the number of EVs that arrive during $[t_{m-1}, t_m]$ is greater than the following:

$$\frac{mP_{\max}}{\bar{r}_{\max}} - \frac{(m-1)P_{\max}}{\bar{r}_{\min}} \geq \frac{P_{\max}}{\bar{r}_{\min}}. \tag{A.22}$$

Since the inter-arrival periods of EVs are at least N, the length of $\hat{T}_{m-1}$ satisfies

$$|\hat{T}_{m-1}| \geq \frac{P_{\max}N}{\bar{r}_{\min}}. \tag{A.23}$$

Now, consider the following recursion:

$$\begin{aligned}
|\hat{T}_2| &= |\hat{T}_3| + |T_3| \\
&\geq |\hat{T}_3| + |\hat{T}_4| \geq 2|\hat{T}_4| + |\hat{T}_5| \\
&\geq 3|\hat{T}_5| + 2|\hat{T}_6| \geq 5|\hat{T}_6| + 3|\hat{T}_7| \\
&\geq \cdots \geq f_{k-2}|\hat{T}_{m-1}| + f_{k-3}|\hat{T}_m|,
\end{aligned}$$

where f_k is the Fibonacci sequence defined by $f_1 = 1$, $f_2 = 1$ and $f_k = f_{k-1} + f_{k-2}$ for $k \geq 3$. From the above, we have

$$|\hat{T}_2| > f_{m-2}|\hat{T}_{m-1}|.$$

Combining equations (A.21)-(A.23) gives

$$\frac{X}{\bar{r}_{\min}} > |T_2| > f_{m-2}|\hat{T}_{m-1}| > f_{m-2}\frac{P_{\max}N}{\bar{r}_{\min}}. \tag{A.24}$$

From $m \leq n$ for n defined in (A.12), we obtain

$$\begin{aligned}
\left\lfloor (1+\epsilon)\frac{P_{\min}}{P_{\max}} \right\rfloor - 2 = m - 2 \\
&= \log_\varphi \left(\sqrt{5} f_{n-2} + \frac{1}{2} \right) \\
&< \log_\varphi \left(\frac{\sqrt{5}X}{NP_{\max}} + \frac{1}{2} \right),
\end{aligned}$$

which gives $(1+\epsilon)P_{\min}/P_{\max} < \log_\varphi \left(\sqrt{5}X/NP_{\max} + 1/2 \right) + 2$.

□

Corollary 9.3.1. Suppose there exists an offline feasible instance $\mathcal{I}$ that is not feasible under the sLLF algorithm with 3-power augmentation. Using the same argument

of the proof for Theorem 9.3.1, we obtain inequality (A.24). However, from assumption

$$f_1 \frac{P_{\max} N}{\bar{r}_{\min}} \leq \frac{X}{\bar{r}_{\min}},$$

which contradicts (A.24). □

A.3 Proof of Theorem 9.3.2

Proof (Theorem 9.3.1). Suppose that there exists an instance $\mathcal{I} = \{a_i, d_i, e_i, \bar{r}_i; P(t)\}_{i\in\mathcal{V}, t\in\mathcal{T}}$ such that the sLLF algorithm is not feasible with ϵ-augmented resources. We then have (A.11), repeated here for convenience:

$$\Psi^{\epsilon}_{[0:t_-]}(\tilde{\mathcal{V}}; \tilde{\mathcal{I}}) < \Psi^{*}_{[0:t_-]}(\tilde{\mathcal{V}}; \tilde{\mathcal{I}})$$

for another instance $\tilde{\mathcal{I}} = \{a_i, d_i, e_i, \bar{r}_i; P(t)\}_{i\in\tilde{\mathcal{V}}, t\in\mathcal{T}}$.

Let $\mathcal{S}(\tilde{\mathcal{V}})$ be the set of EVs in the instance $\tilde{\mathcal{I}}$ that receive strictly less energy under the online algorithm than under the offline algorithm by some time t at which $\Psi^{\epsilon}_{[0:t]}(\tilde{\mathcal{V}}; \tilde{\mathcal{I}}) < \Psi^{*}_{[0:t]}(\tilde{\mathcal{V}}; \tilde{\mathcal{I}})$:

$$\begin{aligned} S(\tilde{\mathcal{V}}) = \{i \in \tilde{\mathcal{V}} : \exists t \in \mathcal{T} \text{ s.t. } & \Psi^{\epsilon}_{[0:t]}(\{i\}; \tilde{\mathcal{I}}) < \Psi^{*}_{[0:t]}(\{i\}; \tilde{\mathcal{I}}) \\ & \& \ \Psi^{\epsilon}_{[0:t]}(\tilde{\mathcal{V}}; \tilde{\mathcal{I}}) < \Psi^{*}_{[0:t]}(\tilde{\mathcal{V}}; \tilde{\mathcal{I}})\}. \end{aligned}$$

In view of (A.11), $\mathcal{S}(\tilde{\mathcal{V}}) \neq \emptyset$. Consider EV $j = \arg\min_{i\in\mathcal{S}(\tilde{\mathcal{V}})} a_i$ that arrives the earliest among those in $\mathcal{S}(\tilde{\mathcal{V}})$. There exists a time $t \in [a_j, d_j]$ such that

$$\Psi^{\epsilon}_{[0:t]}(\{j\}; \tilde{\mathcal{I}}) < \Psi^{*}_{[0:t]}(\{j\}; \tilde{\mathcal{I}}), \tag{A.25}$$

$$\Psi^{\epsilon}_{[0:t]}(\tilde{\mathcal{V}}; \tilde{\mathcal{I}}) < \Psi^{*}_{[0:t]}(\tilde{\mathcal{V}}; \tilde{\mathcal{I}}). \tag{A.26}$$

Notice that $\Psi^{\epsilon}_{[0:a_j-1]}(\tilde{\mathcal{V}}; \tilde{\mathcal{I}}) < \Psi^{*}_{[0:a_j-1]}(\tilde{\mathcal{V}}; \tilde{\mathcal{I}})$ can only happen when there is another EV in $\mathcal{S}(\tilde{\mathcal{V}})$ that arrives before EV j, which however contradicts the definitions of $\mathcal{S}(\tilde{\mathcal{V}})$ and j. So,

$$\Psi^{\epsilon}_{[0:a_j-1]}(\tilde{\mathcal{V}}; \tilde{\mathcal{I}}) \geq \Psi^{*}_{[0:a_j-1]}(\tilde{\mathcal{V}}; \tilde{\mathcal{I}}),$$

which implies

$$\Psi^{\epsilon}_{[a_j:t]}(\tilde{\mathcal{V}}; \tilde{\mathcal{I}}) < \Psi^{*}_{[a_j:t]}(\tilde{\mathcal{V}}; \tilde{\mathcal{I}}). \tag{A.27}$$

Now, let us take a look at the energy demand fulfilled during the interval $[a_j, t]$ under the sLLF algorithm with ϵ-augmented resources. Define the overloaded times

$$T_o = \left\{ t \in [a_j, t] : \sum_{i\in\tilde{\mathcal{V}}} r_i(t) = (1+\epsilon)P(t) \right\}$$

and underloaded times

$$T_u = \left\{ t \in [a_j, t] : \sum_{i \in \tilde{\mathcal{V}}} r_i(t) < (1+\epsilon) P(t) \right\},$$

we have $|T_o| + |T_u| = t + 1 - a_j$. The total energy demand fulfilled during the overloaded period is lower bounded by $|T_o|(1+\epsilon) \min_{\tau \in [a_j, d_j]} P(\tau)$, while that during the underloaded period is at least $|T_u|(1+\epsilon)\bar{r}_j$. Hence, the total and individual energy demands fulfilled during $[a_j, t]$ are lower bounded by

$$(1+\epsilon)\left(|T_u|\bar{r}_j + |T_o| \min_{\tau \in [a_j, d_j]} P(\tau) \right) \leq \Psi^{\epsilon}_{[a_j:t]}(\tilde{\mathcal{V}}; \tilde{\mathcal{I}}), \tag{A.28}$$

$$(1+\epsilon)|T_u|\bar{r}_j \leq \Psi^{\epsilon}_{[a_j:t]}(\{j\}; \tilde{\mathcal{I}}). \tag{A.29}$$

Next, let us take a look at the energy demand fulfilled during the interval $[a_j, t+1]$ by the offline algorithm without resource augmentation. The total energy fulfilled is upper bounded by

$$\Psi^{*}_{[a_j:t]}(\tilde{\mathcal{V}}; \tilde{\mathcal{I}}) \leq (t + 1 - a_j) \max_{\tau \in [a_j, d_j]} P(\tau), \tag{A.30}$$

and the energy fulfilled to EV j is upper bounded by

$$\Psi^{*}_{a_j:t}(j) \leq (t + 1 - a_j)\bar{r}_j. \tag{A.31}$$

By equations (A.25), (A.29) and (A.31), we have

$$|T_u|(1+\epsilon) < (t - a_j + 1). \tag{A.32}$$

By equations (A.27) (A.28) and (A.30), we have

$$\begin{aligned} &(1+\epsilon)(|T_u|\bar{r}_j + |T_o| \min_{\tau \in [a_j, d_j]} P(\tau)) \\ &< (t + 1 - a_j) \max_{\tau \in [a_j, d_j]} P(\tau). \end{aligned}$$

Combining (A.32) becomes

$$\begin{aligned} &(|T_u| + |T_o|)(1+\epsilon) \min_{\tau \in [a_j, d_j]} P(\tau) \\ &< (t - a_j + 1)\left(\max_{\tau \in [a_j, d_j]} P(\tau) + \min_{\tau \in [a_j, d_j]} P(\tau) - \bar{r}_j \right). \end{aligned}$$

Notice that $|T_o| + |T_u| = t + 1 - a_j$, the above inequality leads to

$$\epsilon < \max_{\tau_1, \tau_2 \in [a_j, d_j]} \frac{P(\tau_1)}{P(\tau_2)} - \min_{i \in \mathcal{V}} \max_{\tau \in [a_i, d_i]} \frac{\bar{r}_i}{P(\tau)}.$$

□

Appendix B

ADDITIONAL PROOFS FOR SECTION XII

B.1 Proof of Lemma 10.2.2

In this section, we present results that are useful for proving our main theorems. First, we restate one part of the Campbell's theorem, which is relevant to our proofs.

Theorem B.1.1 (Campbell [89])**.** *Consider a Poisson point process* $\{x_k \in \mathbb{R}^d\}_k$ *with intensity measure* $\Lambda : \mathbb{R}^d \to \mathbb{R}_+$*. Let* $g : \mathbb{R}^d \to \mathbb{R}$ *be a measurable function satisfying*

$$\int_{\mathbb{R}^d} \min(|g(x)|, 1)\Lambda(x)dx \leq \infty. \tag{B.1}$$

Then, the random sum

$$G = \sum_k g(x) \tag{B.2}$$

is absolutely convergent with probability one and satisfies

$$\mathbb{E}[G] = \int_{\mathbb{R}^d} g(x)\Lambda(x)dx \tag{B.3}$$

$$\mathrm{Var}(G) = \int_{\mathbb{R}^d} g(x)^2\Lambda(x)dx. \tag{B.4}$$

Throughout, we consider a scheduling policy (10.23), which is defined by a function $v : S \times \mathbb{R} \to \mathbb{R}_+$ as follows:

$$r_k(t) = v(\sigma_k, \tau_k, y_k(t)) \qquad\qquad k \in \mathcal{V}. \tag{B.5}$$

The function v satisfies

$$\int_{(\sigma,\tau)\in S} \int_{\mathbb{R}_+} \min(|v(\sigma, \tau, a + \tau - t)|, 1)\Lambda f(\sigma, \tau)dad\sigma d\tau \tag{B.6}$$

$$= \int_{(\sigma,\tau)\in S} \int_{\mathbb{R}_+} \min(|v(\sigma, \tau, a + \tau - t)|, 1)\Lambda f(\sigma, \tau)dad\sigma d\tau \tag{B.7}$$

$$= \int_{(\sigma,\tau)\in S} \int_{\mathbb{R}} v(\sigma, \tau, y)dy\Lambda f(\sigma, \tau)d\sigma d\tau \tag{B.8}$$

$$\leq \Lambda \int_{(\sigma,\tau)\in S} e f(\sigma, \tau)d\sigma d\tau \tag{B.9}$$

$$= \mathbb{E}[e]\Lambda \leq \infty. \tag{B.10}$$

The inequality in (B.9) holds because $\int_{a_k}^{\infty} r_k(t)dt = \int_{a_k}^{\infty} v(\sigma_k, \tau_k, a_k+\tau_k-t)dt \leq \sigma_k$. Combining (B.6)–(B.9) and Theorem B.1.1, we obtain

$$\mathbb{E}[P(t)] = \int_{(\sigma,\tau)\in S} \int_0^{\tau} v(\sigma, \tau, y)\Lambda f(\sigma, \tau)dyd\sigma d\tau \tag{B.11}$$

$$\mathrm{Var}(P(t)) = \int_{(\sigma,\tau)\in S} \int_0^{\tau} v(\sigma, \tau, y)^2\Lambda f(\sigma, \tau)dyd\sigma d\tau, \tag{B.12}$$

which yields Lemma 10.2.2.

Below we explain the intuitions behind Lemma 10.2.2. Consider a discretized space of $S \times \mathbb{R}$ and define disjoint sets A_{hij} for $h, i, j \in \mathbb{Q}$ such that

$$A_{hij} = \{(\sigma, \tau, a) : \bar{\sigma}_h < \sigma \leq \bar{\sigma}_{h+1}, \bar{\tau}_i < \tau \leq \bar{\tau}_{i+1}, \bar{a}_j < a \leq \bar{a}_{j+1}\}. \tag{B.13}$$

Here, we assume a uniform discretization of internal δ, so $\bar{\sigma}_h = h\delta$, $\bar{\tau}_i = h\delta$, and $\bar{a}_j = j\delta$. Let $N(A_{hij})$ denote the number of jobs satisfying $(\sigma_k, \tau_k, a_k) \in A_{hij}$. From [7, Definition 1.1.1], $N(A_{hij})$ is a scalar Poisson random variable, and $N(A_{hij})$ and $N(A_{h'i'j'})$ are independent if $(h, i, j) \neq (h', i', j')$. Similarly, we also approximate v using some function $v_\delta(h, i, j)$ that only depends on (h, i, j) and satisfies

$$\lim_{\delta\to 0} v_\delta = v. \tag{B.14}$$

Let us define

$$P_\delta(t) = \sum_{h,i,j} \sum_{k\in A_{hij}} v_\delta(h, i, j). \tag{B.15}$$

The function v_δ is constructed so that it approximates v to an arbitrary precision. So we can also expect the mean and variance of $P_\delta(t)$ to approximate $P(t)$ to an arbitrary precision.

$$\mathbb{E}[P(t)] = \lim_{\delta\to\infty} \mathbb{E}[P_\delta(t)] \tag{B.16}$$

$$\mathrm{Var}(P(t)) = \lim_{\delta\to\infty} \mathrm{Var}(P_\delta(t)). \tag{B.17}$$

The proof of (B.16) and (B.17) is fairly technical and is beyond the scope of this chapter. However, given (B.16) and (B.17), we can intuitively see (B.116) and

(B.117) by taking $\delta \to 0$ in $P_\delta(t)$:

$$\lim_{\delta\to\infty} \mathbb{E}[P_\delta(t)] = \lim_{\delta\to\infty} \mathbb{E}\left[\sum_{h,i,j}\sum_{k\in A_{hij}} v_\delta(h,i,j)\right] \tag{B.18}$$

$$= \lim_{\delta\to\infty} \sum_{h,i,j} v_\delta(h,i,j)\mathbb{E}[N(A_{hij})] \tag{B.19}$$

$$= \lim_{\delta\to\infty} \sum_{h,i,j} v_\delta(h,i,j) \int_{A_{hij}} \Lambda f(\sigma,\tau)dyd\sigma d\tau \tag{B.20}$$

$$= \int_{(\sigma,\tau)\in S}\int_0^\tau \lim_{\delta\to\infty} v_\delta(h,i,j)\Lambda f(\sigma,\tau)dyd\sigma d\tau \tag{B.21}$$

$$= \int_{(\sigma,\tau)\in S}\int_0^\tau v(\sigma,\tau,y)\Lambda f(\sigma,\tau)dyd\sigma d\tau. \tag{B.22}$$

The variance of $P_\delta(t)$ as $\delta \to 0$ can be computed by

$$\lim_{\delta\to\infty} \mathrm{Var}(P_\delta(t)) \tag{B.23}$$

$$= \lim_{\delta\to\infty} \mathbb{E}\left[\left(\sum_{h,i,j}\sum_{k\in A_{hij}} v_\delta(h,i,j) - \mathbb{E}\left[\sum_{h,i,j}\sum_{k\in A_{hij}} v_\delta(h,i,j)\right]\right)^2\right] \tag{B.24}$$

$$= \lim_{\delta\to\infty} \mathbb{E}\left[\left(\sum_{h,i,j} v_\delta(h,i,j)\left\{N(A_{hij}) - \mathbb{E}[N(A_{hij})]\right\}\right)^2\right] \tag{B.25}$$

$$= \lim_{\delta\to\infty} \sum_{h,i,j} \mathbb{E}\left[\left(v_\delta(h,i,j)\left\{N(A_{hij}) - \mathbb{E}[N(A_{hij})]\right\}\right)^2\right] \tag{B.26}$$

$$= \lim_{\delta\to\infty} \sum_{h,i,j} \left[v_\delta(h,i,j)^2\mathbb{E}\left[\left(N(A_{hij}) - \mathbb{E}[N(A_{hij})]\right)^2\right]\right] \tag{B.27}$$

$$= \lim_{\delta\to\infty} \sum_{h,i,j} \left[v_\delta(h,i,j)^2 \int_{A_{hij}} \Lambda f(\sigma,\tau)dyd\sigma d\tau\right] \tag{B.28}$$

$$= \int_{(\sigma,\tau)\in S}\int_0^\tau \lim_{\delta\to\infty} v_\delta(h,i,j)^2\Lambda f(\sigma,\tau)dyd\sigma d\tau \tag{B.29}$$

$$= \int_{(\sigma,\tau)\in S}\int_0^\tau v(\sigma,\tau,y)^2\Lambda f(\sigma,\tau)dyd\sigma d\tau. \tag{B.30}$$

Here, (B.26) holds because $N(A_{hij}) - \mathbb{E}[N(A_{hij})]$ has mean zero, and $N(A_{hij})$ and $N(A_{h'i'j'})$, $(h,i,j) \neq (h',i',j')$, are independent.

B.2 Proof of Proposition 10.2.1

We observe that

$$\int_{-\infty}^{\infty}\int_{0}^{\infty}\frac{\partial}{dy}\lambda(x,y)xdxdy = \int_{0}^{\infty}x\left\{\int_{-\infty}^{\infty}\frac{\partial}{dy}\lambda(x,y)dy\right\}dx \tag{B.31}$$

$$= -\int_{0}^{\infty}x\lim_{L\to\infty}\lambda(x,L)dx \tag{B.32}$$

$$= -\Psi\mathbb{E}[\sigma-\hat{\sigma}(\sigma,\tau)], \tag{B.33}$$

where (B.31) holds because bounded S implies that $\lambda(x,\infty)=0$. Therefore, the stationary mean of the service capacity satisfies

$$\mathbb{E}[P(t)] = \mathbb{E}\left[\sum_{k\in\mathcal{V}}u(x_k(t),y_k(t))\right] \tag{B.34}$$

$$= \int_{-\infty}^{\infty}\int_{0}^{\infty}\lambda(x,y)u(x,y)dxdy \tag{B.35}$$

$$= -\int_{-\infty}^{\infty}\int_{0}^{\infty}\frac{d}{dx}\left(\lambda(x,y)u(x,y)\right)xdxdy \tag{B.36}$$

$$= \int_{-\infty}^{\infty}\int_{0}^{\infty}\left(\frac{\partial}{dy}\lambda(x,y)+\Lambda f(x,y)\right)xdxdy \tag{B.37}$$

$$= -\Psi\mathbb{E}[\sigma-\hat{\sigma}(\sigma,\tau)]+\Psi\mathbb{E}[\sigma] \tag{B.38}$$

$$= \Psi\mathbb{E}[\hat{\sigma}(\sigma,\tau)]. \tag{B.39}$$

Here, (B.36) is due to Integration by Parts, (B.37) is due to (10.11), (B.38) is due to (B.31)–(B.33).

B.3 Proof of Theorem 10.2.2

Since the constraints of (10.14) is hard to solve, we first consider providing a lower bound on its optimal solution. Again, we consider the class of control policies representable by (10.23) and the optimization problem

$$\underset{v:(10.1)(10.3)(10.23)}{\text{minimize}} \quad \mathrm{Var}(P)+\mathbb{E}[U]. \tag{B.40}$$

Because the constraint set of (B.40) contains that of (10.14), the optimal value of (B.40) lower-bounds that of (10.14). Therefore, to prove Theorem 10.2.2, it suffices to solve (B.40) (in the next lemma) and observe that its optimal solution is representable by a control policy of the form (10.10).

Lemma B.3.1. *The optimal solution of* (B.40) *is*

$$v(\sigma,\tau,y) = \min\left\{\frac{\delta}{2},\ \frac{\sigma}{\tau}\right\}1\{y>0\}, \tag{B.41}$$

and it achieves the optimal value (10.35).

Proof. First, we derive an analytical formula for $\mathbb{E}[U]$ as a function of the scheduling policy v. A job with a service demand σ and a sojourn time τ receives the following amount of service at its deadline:

$$\hat{\sigma}(\sigma, \tau) = \int_0^\tau v(\sigma, \tau, y)dy, \tag{B.42}$$

resulting in an unsatisfied demand $\sigma - \hat{\sigma}(\sigma, \tau)$. Additionally, $\hat{\sigma}(\sigma, \tau)$ satisfies

$$0 \le \hat{\sigma}(\sigma, \tau) \le \sigma, \qquad \forall (\sigma, \tau) \in S. \tag{B.43}$$

Consequently, the stationary mean of U satisfies

$$\mathbb{E}[U] = \lim_{t\to\infty} \mathbb{E}\left[\sum_{k\in\mathcal{V}:d_k=t} (\sigma_k - \hat{\sigma}(\sigma_k, \tau_k))\right] \tag{B.44}$$

$$= \int_{(\sigma,\tau)\in S} (\sigma - \hat{\sigma}(\sigma, \tau))\Lambda f(\sigma, \tau)d\sigma d\tau. \tag{B.45}$$

Then, we use (B.45) to rewrite (B.40) as follows:

$$\inf_{v:(10.1)(10.3)(10.23)} \mathrm{Var}(P) + \mathbb{E}[U] \tag{B.46}$$

$$= \inf_{\hat{\sigma}:(B.43)} \left[\inf_{v:(10.1)(10.3)(10.23)} \mathrm{Var}(P) + \delta \int_{(\sigma,\tau)\in S} (\sigma - \hat{\sigma}(\sigma, \tau))\Lambda f(\sigma, \tau)d\sigma d\tau\right] \tag{B.47}$$

$$= \inf_{\hat{\sigma}:(B.43)} \left[\left\{\inf_{v:(10.1)(10.3)(10.23)} \mathrm{Var}(P)\right\} + \delta \int_{(\sigma,\tau)\in S} (\sigma - \hat{\sigma}(\sigma, \tau))\Lambda f(\sigma, \tau)d\sigma d\tau\right]. \tag{B.48}$$

Equality (B.48) holds because, constrained on $\hat{\sigma}(\sigma, \tau) = \int_0^\tau v(\sigma, y, \tau)dy$ for some fixed $\hat{\sigma}$, the second term of (B.47) is not a function of v. From Lemma 10.2.1, the first term of (B.48) admits the closed-form expression

$$\inf_{v:(10.1)(10.3)(10.23)} \mathrm{Var}(P) = \int_{(\sigma,s)\in S} \frac{\hat{\sigma}'(\sigma, \tau)^2}{\tau} \Lambda f(\sigma, \tau)d\sigma d\tau, \tag{B.49}$$

which is attained by

$$v(\sigma, \tau, y) = \frac{\hat{\sigma}}{\tau}. \tag{B.50}$$

Substituting (B.49) into (B.48) yields

$$\inf_{\hat{\sigma}:(B.43)} \int_{(\sigma,\tau)\in S} \left\{\frac{\hat{\sigma}'(\sigma, \tau)^2}{\tau} + \delta(\sigma - \hat{\sigma}'(\sigma, \tau))\right\} \Lambda f(\sigma, \tau)d\sigma d\tau, \tag{B.51}$$

where the optimization variable is now $\hat{\sigma}'$ instead of v. To derive a closed-form solution of (B.40), we can minimize the integrand of (B.51) point-wisely. By doing so, we observe that, for each $(\sigma, \tau) \in S$, a necessary and sufficient condition for optimality is

$$\hat{\sigma}(\sigma, \tau) = \arg \inf_{\hat{\sigma}:(\text{B.43})} \frac{\hat{\sigma}(\sigma, \tau)^2}{\tau} + \delta(\sigma - \hat{\sigma}(\sigma, \tau)) = \left\{ \frac{\delta\tau}{2}, \sigma \right\}. \tag{B.52}$$

Combining (B.50) and (B.52), we obtain that (B.41) is the optimal solution of (B.40). Substituting (B.41) into (B.51) gives its optimal value (10.35).

□

Given Lemma B.3.1, Theorem 10.2.2 can be derived as follows. It can be verified that (B.41) can be realized using (10.34). This implies that the optimal solution of (B.40) lies within the constraint set of (10.14). Because the cost attained by (B.41) is a lower bound on the optimal value of (10.14), the optimal solution of (10.14) is (B.41).

B.4 Proof of Theorem 10.2.3

Since the constraints of (10.15) is hard to solve, we first consider providing a lower bound on its optimal solution. Again, we consider the class of control policies representable by (10.23) and the optimization problem

$$\underset{v:(10.1)(10.2)(10.23)}{\text{minimize}} \quad \text{Var}(P) + \mathbb{E}[W]. \tag{B.53}$$

Because the optimal value of (B.53) lower-bounds that of (10.14), to prove Theorem 10.2.3, we can solve (B.53) (in the next lemma) and observe that its optimal solution is representable by a control policy of the form (10.10).

Lemma B.4.1. *The optimal solution of* (B.53) *is*

$$v(\sigma, \tau, y) = \begin{cases} \dfrac{\sigma}{\tau}\, 1\{y > 0\} & \text{if } \dfrac{\sigma}{\tau} \le \sqrt{\epsilon} \\ \sqrt{\epsilon}\, 1\left\{ y > \tau - \dfrac{\sigma}{\sqrt{\epsilon}} \right\} & \text{otherwise} \end{cases} \tag{B.54}$$

and it achieves the optimal value (10.37)*.*

Proof. With a slight abuse of notation, let $\hat{\tau}(\sigma, \tau) \ge \tau$ denote the actual sojourn time for jobs having a service demand σ and a sojourn time τ. Then, the stationary

mean of W satisfies

$$\mathbb{E}[W] = \epsilon \int_{(\sigma,\tau)\in S} (\hat{\tau}(\sigma,\tau) - \tau)\Lambda f(\sigma,\tau) d\sigma d\tau. \tag{B.55}$$

The optimization problem (B.53) can then be written into

$$\inf_{v:(10.1)(10.2)(10.23)} \mathrm{Var}(P) + \mathbb{E}[\epsilon W] \tag{B.56}$$

$$= \inf_{\hat{\tau}\geq\tau} \left[\left\{ \inf_{v:(10.1)(10.2)(10.23)} \mathrm{Var}(P) \right\} \right. \tag{B.57}$$

$$\left. + \epsilon \int_{(\sigma,\tau)\in S} (\hat{\tau}(\sigma,\tau) - \tau)\Lambda f(\sigma,\tau) d\sigma d\tau \right] \tag{B.58}$$

$$= \inf_{\hat{\tau}\geq\tau} \int_{(\sigma,\tau)\in S} \left\{ \frac{\sigma^2}{\hat{\tau}} + \epsilon(\hat{\tau}(\sigma,\tau) - \tau) \right\} \Lambda f(\sigma,\tau) d\sigma d\tau, \tag{B.59}$$

where $\inf_{v:(10.1)(10.2)(10.23)} \mathrm{Var}(P)$ in (B.57) is attained by

$$v(\sigma,\tau,y) = \frac{\sigma}{\hat{\tau}(\sigma,\tau)}. \tag{B.60}$$

The optimal choice of deadline extensions $\hat{\tau}^\star(\sigma,\tau)$ is the point-wise maximum of the integrand of (B.59), *i.e.*

$$\hat{\tau}^\star(\sigma,\tau) = \arg \inf_{\hat{\sigma}:(B.43)} \frac{\sigma^2}{\hat{\tau}} + \epsilon(\hat{\tau}(\sigma,\tau) - \tau) = \left\{ \frac{\sigma}{\sqrt{\epsilon}}, \tau \right\}. \tag{B.61}$$

Combining (B.60) and (B.61), we obtain (B.54) as the closed-form solution of (B.53).

□

Given Lemma B.4.1, we are now ready to prove Theorem 10.2.3.

Proof. (Theorem 10.2.3)

Recall that the optimal value of (B.53) lower-bounds that of (10.15). Therefore, if there is a policy of the form (10.10) that produces identical service rates to (B.54), it is also optimal for (10.15). Next, we show that the policy (10.36) satisfies the above description.

Given any job $k \in \mathcal{V}$ with $\sigma \leq \tau\sqrt{\epsilon}$, both (10.10) and (B.54) produce the service rates $r_k(t) = \sigma_k/\tau_k$ if $t \in [a_k, a_k+\tau_k]$ and $r_k(t) = 0$ otherwise. Given any job $k \in \mathcal{V}$ with $\sigma < \sqrt{\epsilon}\tau$, (10.10) produces the service rates $r_k(t) = \sqrt{\epsilon}$ if $t \in [a_k, a_k + \sigma/\sqrt{\epsilon}\ ]$

and $r_k(t) = 0$ otherwise. Observe that under the policy (B.54), for any $y(t) > 0$, we have

$$\frac{x(t)}{y(t)} - \frac{\sigma}{\tau} = \frac{\sigma - \sqrt{\epsilon}(t-a)}{\tau - (t-a)} - \frac{\sigma}{\tau} \geq \frac{(-\sqrt{\epsilon}+1)(t-a)}{\tau-(t-a)} \geq \frac{(-\sigma/\tau+1)(t-a)}{\tau-(t-a)} \geq 0, \tag{B.62}$$

where the third inequality is due to $-\sqrt{\epsilon} \geq \sigma/\tau$. Thus, the policy (B.54) also produce the service rates $r_k(t) = \sqrt{\epsilon}$ if $t \in [a_k, a_k + \sigma/\sqrt{\epsilon}\,]$ and $r_k(t) = 0$ otherwise.

□

B.5 Proof of Theorem 10.2.4

We first consider providing a lower bound of (10.16) by solving the optimization problem

$$\underset{v:(10.1)(10.23)}{\text{minimize}} \quad \text{Var}(P) + \mathbb{E}[U] + \mathbb{E}[W]. \tag{B.63}$$

The solution of (B.63) is given in the next lemma, which is also a feasible policy for the constraint set of (10.16).

Lemma B.5.1. *The optimal solution of* (B.63) *is*

$$v(\sigma,\tau,y) = \begin{cases} \dfrac{\sigma}{\tau} 1\{y>0\} & \text{if } \dfrac{\sigma}{\tau} \leq \min\left\{\dfrac{\delta}{2}, \sqrt{\epsilon}\right\} \\ \dfrac{\delta}{2} 1\{y>0\} & \text{if } \dfrac{\sigma}{\tau} > \dfrac{\delta}{2} \text{ and } \dfrac{\delta}{2} \leq \sqrt{\epsilon}\,. \\ \sqrt{\epsilon} 1\left\{y > \tau - \dfrac{\sigma}{\sqrt{\epsilon}}\right\} & \text{otherwise} \end{cases} \tag{B.64}$$

and it achieves the optimal value (10.39).

Proof. Let $\hat{\sigma}(\sigma,\tau)$ denote the actual service supply for jobs having a service demand σ and a sojourn time τ, and let $\hat{\tau}(\sigma,\tau)$ denote the actual sojourn time for such jobs.

The optimization problem (B.63) can be written into

$$\inf_{v:(10.1)(10.23)} \quad \mathrm{Var}(P(t)) + \mathbb{E}[\delta U] + \mathbb{E}[\epsilon W] \tag{B.65}$$

$$= \inf_{\substack{\hat{\sigma}(\sigma,\tau)\geq\sigma \\ \hat{\tau}(\sigma,\tau)\geq\tau}} \left[\inf_{v:(10.1)(10.23)} \mathrm{Var}(P) + \int_{(\sigma,\tau)\in S} \{\delta(\sigma - \hat{\sigma}(\sigma,\tau)) + \epsilon(\hat{\tau}(\sigma,\tau) - \tau)\} \Lambda f(\sigma,\tau) d\sigma d\tau \right] \tag{B.66}$$

$$= \inf_{\substack{\hat{\sigma}(\sigma,\tau)\geq\sigma \\ \hat{\tau}(\sigma,\tau)\geq\tau}} \int_{(\sigma,\tau)\in S} \left[\frac{\hat{\sigma}(\sigma,\tau)^2}{\hat{\tau}(\sigma,\tau)} + \delta(\sigma - \hat{\sigma}(\sigma,\tau)) + \epsilon(\hat{\tau}(\sigma,\tau) - \tau) \right] \Lambda f(\sigma,\tau) d\sigma d\tau \tag{B.67}$$

$$= \inf_{\substack{\hat{\sigma}(\sigma,\tau)\geq\sigma \\ \hat{\tau}(\sigma,\tau)\geq\tau}} \int_{(\sigma,\tau)\in S} C(\sigma,\hat{\tau}) \Lambda f(\sigma,\tau) d\sigma d\tau, \tag{B.68}$$

where $C(\sigma,\hat{\tau})$ is defined to be

$$C(\sigma,\hat{\tau}) := \frac{\hat{\sigma}(\sigma,\tau)^2}{\hat{\tau}(\sigma,\tau)} + \delta(\sigma - \hat{\sigma}(\sigma,\tau)) + \epsilon(\hat{\tau}(\sigma,\tau) - \tau) \tag{B.69}$$

$$= \begin{cases} \dfrac{\sigma^2}{\tau} & \text{if } \hat{\tau} = \tau \text{ and } \dfrac{\sigma}{\tau} \leq \dfrac{\delta}{2} \\ \delta\left(\sigma - \dfrac{\delta\tau}{4}\right) & \text{if } \hat{\tau} = \tau \text{ and } \dfrac{\sigma}{\tau} > \dfrac{\delta}{2} \\ \dfrac{\sigma^2}{\hat{\tau}} + \epsilon(\hat{\tau} - \tau) & \text{if } \hat{\tau} > \tau \text{ and } \dfrac{\sigma}{\hat{\tau}} \leq \dfrac{\delta}{2} \\ \delta\left(\sigma - \dfrac{\delta\hat{\tau}}{4}\right) + \epsilon(\hat{\tau} - \tau) & \text{if } \hat{\tau} > \tau \text{ and } \dfrac{\sigma}{\hat{\tau}} > \dfrac{\delta}{2} \end{cases}. \tag{B.70}$$

Relation (B.67) holds because $\inf_{v:(10.1)(10.23)} \mathrm{Var}(P)$ is attained by

$$v(\sigma,\tau,y) = \frac{\hat{\sigma}(\sigma,\tau)}{\hat{\tau}(\sigma,\tau)}. \tag{B.71}$$

The optimal $\hat{\sigma}^*(\sigma,\tau)$ and $\hat{\tau}^*(\sigma,\tau)$ is the point-wise maximum of the integrand of (B.67).

To derive a closed form expression for $\hat{\sigma}^*(\sigma,\tau)$ and $\hat{\tau}^*(\sigma,\tau)$, we first show that in the case of $\delta^2/4 \leq \epsilon$, we have $\hat{\tau}^*(\sigma,\tau) = \tau$. Suppose not and $\hat{\tau}(\sigma,\tau) = \hat{\tau} \geq \tau$.

Then, if $\sigma \leq \delta\tau/2$, we have

$$C(\hat{\tau}) - C(\tau) = \frac{\sigma^2}{\hat{\tau}} + \epsilon(\hat{\tau} - \tau) - \frac{\sigma^2}{\tau} \tag{B.72}$$

$$= (\hat{\tau} - \tau)\left(\epsilon - \frac{\sigma^2}{\tau\hat{\tau}}\right) \tag{B.73}$$

$$\geq (\hat{\tau} - \tau)\left\{\epsilon - \left(\frac{\delta\tau}{2}\right)^2 \frac{1}{\tau\hat{\tau}}\right\} \tag{B.74}$$

$$\geq (\hat{\tau} - \tau)\left\{\epsilon - \frac{\delta^2}{4}\right\} \tag{B.75}$$

$$\geq 0, \tag{B.76}$$

where (B.74) is due to $\sigma \leq \delta\tau/2$; (B.75) is due to $\hat{\tau} > \tau$; and (B.76) is due to $\delta^2/4 \leq \epsilon$. When $\sigma \in (\delta\tau/2, \delta\hat{\tau}/2]$, we have

$$C(\hat{\tau}) - C(\tau) = \frac{\sigma^2}{\hat{\tau}} + \epsilon(\hat{\tau} - \tau) - \delta\left(\sigma - \frac{\delta\tau}{4}\right) \tag{B.77}$$

$$\geq \epsilon(\hat{\tau} - \tau) + \left(\frac{\delta\tau}{2}\right)^2 \frac{1}{\hat{\tau}} - \delta\frac{\delta\hat{\tau}}{2} + \frac{\delta^2\hat{\tau}}{4} \tag{B.78}$$

$$\geq \epsilon(\hat{\tau} - \tau) + \frac{1}{2}\delta^2(\tau - \hat{\tau}) \tag{B.79}$$

$$= (\hat{\tau} - \tau)\left\{\epsilon - \frac{\delta^2}{4}\right\} \tag{B.80}$$

$$\geq 0, \tag{B.81}$$

where (B.78) is due to $\sigma \leq \delta\tau/2$; (B.79) is due to $\hat{\tau} > \tau$; and (B.81) is due to $\delta^2/4 \leq \epsilon$. When $\sigma > \delta\hat{\tau}/2$, we have

$$C(\hat{\tau}) - C(\tau) = \delta\left(\sigma - \frac{\delta\hat{\tau}}{4}\right) + \epsilon(\hat{\tau} - \tau) - \delta\left(\sigma - \frac{\delta\tau}{4}\right) \tag{B.82}$$

$$= (\hat{\tau} - \tau)\left(\epsilon - \frac{\delta^2}{4}\right) \tag{B.83}$$

$$\geq 0, \tag{B.84}$$

where (B.84) is due to $\delta^2/4 \leq \epsilon$. Since (B.76), (B.81), and (B.84) contradict with the supposition that $\hat{\tau}(\sigma, \tau) = \hat{\tau} > \tau$ is optimal, we have $\hat{\tau}^*(\sigma, \tau) = \tau$. Then, given $\hat{\tau}^*(\sigma, \tau) = \tau$, the optimal $\hat{\sigma}^*(\sigma, \tau)$ follows from Lemma B.3.1. In a similar manner, we can show that, in the case of $\delta^2/4 > \epsilon$, the optimal service supply is $\hat{\sigma}^*(\sigma, \tau) = \sigma$. Then, given $\hat{\sigma}^*(\sigma, \tau) = \sigma$, the optimal $\tau^*(\sigma, \tau)$ follows from Lemma B.4.1. Finally, combining above, we obtain (B.64) as the closed-form solution of (B.63).

□

Theorem 10.2.4 is an immediate consequence of Lemma B.5.1. To see it, recall that the optimal value of (B.63) lower-bounds that of (10.16). Moreover, a policy of the form (10.10) can produce identical service rates to (B.64), so it is also optimal for (10.16).

B.6 Proof of Lemma 10.3.2

To solve $\inf_w L(w;\gamma)$, we first observe that

$$\inf_w L(w;\gamma) = \inf_w \lim_{T\to\infty} \frac{1}{T}\int_0^T \mathrm{Var}(P(t)) + \gamma(\mathrm{Var}(X(t)) - D)dt \tag{B.85}$$

$$\geq \inf_w \lim_{T\to\infty} \inf_w \frac{1}{T}\int_0^T \mathbb{E}[(P(t)-\bar{P})^2 + \gamma((X(t)-\bar{X})^2 - D)]dt \tag{B.86}$$

$$= \lim_{T\to\infty} \inf_w \frac{1}{T}\int_0^T \mathbb{E}[(P(t)-\bar{P})^2 + \gamma((X(t)-\bar{X})^2 - D)]dt, \tag{B.87}$$

where $\bar{P}$ and $\bar{X}$ are the stationary variance of $P(t)$ and $X(t)$ respectively. Now we consider representing the integral of (B.87) as the sum of $\mathbb{E}[(P(t_n) - \bar{P})^2 + \gamma(X(t_n) - \bar{X})^2$ at discrete points in time, where $\{t_n\}$ have a fixed sampling interval $h = t_{n+1} - t_n, \forall n \in \mathbb{Z}_+$. So, the dynamics of $X(t_n)$ satisfies

$$X(t_{n+1}) = X(t_n) + A(t_n, h) - hP(t_n), \tag{B.88}$$

where u is assumed to be constant during each sampling intervals. Then, (B.87) satisfies

$$\lim_{T\to\infty} \inf_w \frac{1}{T}\int_0^T \mathbb{E}[(P(t)-\bar{P})^2 + \gamma((X(t)-\bar{X})^2 - D)]dt \tag{B.89}$$

$$= \lim_{T\to\infty} \inf_w \lim_{h\to 0} \frac{1}{T} L_{h,\lceil T/h\rceil}(u;r)h - \gamma D \tag{B.90}$$

$$= \lim_{T\to\infty} \lim_{h\to 0} \inf_w \frac{1}{T} L_{h,\lceil T/h\rceil}(u;r)h - \gamma D, \tag{B.91}$$

where $L_{h,N}(u;\gamma)$ is defined by

$$L_{h,N}(u;\gamma) := \mathbb{E}\left[\gamma(X(t_N) - \bar{X})^2\right] + \sum_{k=0}^{N-1} \mathbb{E}\left[(P(t_k)-\bar{P})^2 + \gamma(X(t_k)-\bar{X})^2\right].$$

To solve (B.91), we first consider the cost-to-go $J_n(X(t_n))$ for some $h > 0$ and $N \in \mathbb{Z}_+$, *i.e.*

$$J_n(X(t_n)) := \mathbb{E}\left[\gamma(X(t_N) - \bar{X})^2\right] + \sum_{k=n}^{N-1} \mathbb{E}\left[(P(t_k)-\bar{P})^2 + \gamma(X(t_k)-\bar{X})^2\right]. \tag{B.92}$$

Using mathematical induction, we show below that, at the optimal solution w^*, the cost-to-go takes the form

$$J_n(X(t_n)) = \mathbb{E}[p_n(X(t_n) - \bar{X})^2 + \sum_{k=n}^{N-1} \mathbb{E}[p_{k+1}(A(t_n, h) - \bar{A})^2], \tag{B.93}$$

where $\{p_k\}$ satisfyes the Riccati difference equation

$$p_k = p_{k+1} - \frac{h^2 p_{k+1}^2}{h^2 p_{k+1} + 1} + \gamma, \qquad p_N = \gamma. \tag{B.94}$$

First, condition (B.93) holds for $n = N$. Second, if condition (B.93) holds for $n + 1$, then

$$J_n(X(t_n)) = \inf_{P(t_n,h)} \mathbb{E}[(P(t_n) - \bar{P})^2 + \gamma(X(t_n) - \bar{X})^2 + J_{n+1}(X(t_{n+1}))] \tag{B.95}$$

$$\begin{aligned} &= \inf_{P(t_n,h)} \mathbb{E}[(P(t_n) - \bar{P})^2 + \\ &\quad \gamma(X(t_n) - \bar{X})^2 + p_{n+1}(X(t_n) + (A(t_n, h) - \bar{A}) - h(P(t_n) - \bar{P}))^2], \end{aligned} \tag{B.96}$$

where $\bar{A}_h$ are the stationary mean of $A(t_n, h)$, and $\bar{A}_h = h\bar{P}$ from Brumelle's formula. Expanding the last quadratic term in (B.95) and applying $\mathbb{E}[(A(t, h) - \bar{A})X(t_n)] = 0$, (B.95) can be written into

$$\begin{aligned} J_n(X(t_n)) =& (p_{n+1} + \gamma)(X(t_n) - \bar{X})^2 + \sum_{k=n}^{N} p_{k+1}\mathbb{E}(A(t_k, h) - \bar{A})^2] \\ &+ \inf_{P(t_n)} \{(1 + h^2 p_{n+1})(P(t_n, h) - \bar{P}_h)^2 - 2h\gamma p_{n+1}(X(t_n) - \bar{X})(P(t_n) - \bar{P})]. \end{aligned} \tag{B.97}$$

The minimum value of (B.97) is attained by

$$P(t_n, h) - \bar{P}_h = \frac{h p_n}{1 + h^2 p_n}(X(t_n) - \bar{X}), \tag{B.98}$$

and the optimal cost-to-go becomes (B.93), where p_n is defined by (B.94). As $N \to \infty$, p_k converges to a unique positive scalar

$$p := \lim_{N\to\infty} p_k = \frac{h^2\gamma + h\sqrt{\gamma}\sqrt{h^2\gamma + 4}}{2h^2}, \tag{B.99}$$

which is also a fixed point of (B.94) [15]. Taking the limit of $N \to \infty$ and $h \to 0$ for (B.98) and (B.99), the infimum of (B.91) is attained by

$$P(t) - \bar{P} = \sqrt{\gamma}\ (X(t) - \bar{X}). \tag{B.100}$$

From (B.92), we obtain

$$\mathrm{Var}(P(t)) + \gamma \mathrm{Var}(X(t)) = p\mathbb{E}[(A(t_k, h) - \bar{A})^2] \tag{B.101}$$

$$= ph\Lambda\mathbb{E}[\sigma_0^2] \tag{B.102}$$

$$= \sqrt{\gamma}\Lambda\mathbb{E}[\sigma_0^2]. \tag{B.103}$$

B.7 Proof of Corollary 10.3.3

For any time interval $h > 0$, $X(t)$ satisfies the following dynamics:

$$X(t + h) = X(t) + A(t, h) - P(t, h), \tag{B.104}$$

where $A(t, h)$ is the arriving demands during the time interval $[t, t + h]$, and $P(t, h)$ is the amount of service during this interval, *i.e.*

$$A(t, h) := \sum_{i \text{ s.t. } a_k \in [t, t+h)} \sigma_k, \tag{B.105}$$

$$P(t, h) := \int_t^{t+h} P(\tau) d\tau. \tag{B.106}$$

From the demand requirement (10.2), $X(t)$ is bounded from above by

$$X(t) = \sum_{k \in A_t} \sigma_k - \int_{t \le \tau} P(t) dt \tag{B.107}$$

$$\le \sum_{k \in A_t} \sigma_k - \sum_{i \in D_t} \sigma_k \tag{B.108}$$

$$\le \sum_{k \in A_t \setminus D_t} \sigma_k, \tag{B.109}$$

where $D_t = \{k \in \mathcal{V} : d_k \le t\}$ is the set of jobs that departs by time t. From (B.109) and $X(t) \ge 0$, the variance of $X(t)$ is upper-bounded by

$$\mathrm{Var}(X(t)) \le \mathbb{E}[X(t)^2] \tag{B.110}$$

$$\le \mathbb{E}\left[\left(\sum_{k \in A_t \setminus D_t} \sigma_k\right)^2\right] \tag{B.111}$$

$$= \mathrm{Var}\left(\sum_{k \in A_t \setminus D_t} \sigma_k\right) + \mathbb{E}\left[\sum_{k \in A_t \setminus D_t} \sigma_k\right]^2 \tag{B.112}$$

$$= \int_{(\sigma,\tau) \in S} \tau\sigma^2 \Lambda f(\sigma, \tau) d\sigma d\tau + \left(\int_{(\sigma,\tau) \in S} \tau\sigma\Psi(\sigma, \tau) d\sigma d\tau\right)^2 \tag{B.113}$$

$$= \Lambda\mathbb{E}\left(\tau\sigma^2\right) + (\Lambda\mathbb{E}\left[\tau\sigma\right])^2 \tag{B.114}$$

Applying $D = \Lambda\mathbb{E}\left(\tau\sigma^2\right) + (\Lambda\mathbb{E}\left[\tau\sigma\right])^2$ to Lemma 10.3.1, we obtain (10.47).

B.8 Proof of Theorem 10.4.1.

To prove Theorem 10.4.1, it suffices to derive the optimal solution of a relaxation of (10.62) and observe that the resultant optimal solution lies in the constraint set of (10.62).

Lemma B.8.1. *Exact Scheduling* $v(a, \sigma, \tau, y) = (\sigma/\tau)1\{y > 0\}$ *is the optimal solution of*

$$\underset{v:(10.2)(10.3)(10.61)}{\text{minimize}} \quad \int_0^T \text{Var}(P(t))dt. \tag{B.115}$$

The proof of Lemma B.8.1 uses the following lemma.

Lemma B.8.2. *The mean and variance of* $P(t)$ *under the policy* (10.61) *is given by*

$$\mathbb{E}[P(t)] = \int_{(\sigma,\tau)\in S} \int_0^\tau v(t+y-\tau, \sigma, \tau, y)\Lambda(t+y-\tau, \sigma, \tau)dyd\sigma d\tau \tag{B.116}$$

$$\text{Var}(P(t)) = \int_{(\sigma,\tau)\in S} \int_0^\tau v(t+y-\tau, \sigma, \tau, y)^2\Lambda(t+y-\tau, \sigma, \tau)dyd\sigma d\tau, \tag{B.117}$$

The proof of Lemma B.8.2 is a trivial extension of that of Lemma 10.2.2 (see Appendix B.1). Now we are ready to prove Lemma B.8.1.

Proof. (Lemma B.8.1)

From Lemma B.8.2, the objective function of (B.115) satisfies

$$\int_0^T \text{Var}(P(t))dt$$

$$= \int_0^T \int_{(\sigma,\tau)\in S} \int_{y=0}^\tau v(t+y-\tau, \sigma, \tau, y)^2\Psi(t+y-\tau, \sigma, \tau)dyd\sigma d\tau dt \tag{B.118}$$

$$= \int_{(\sigma,\tau)\in S} \left\{ \int_{y=0}^\tau \int_0^T v(t+y-\tau, \sigma, \tau, y)^2\Psi(t+y-\tau, \sigma, \tau)dtdy \right\} d\sigma d\tau. \tag{B.119}$$

Moreover, the constraints of (B.115) can be rewritten into

$$\int_{y=0}^\tau v(a, \sigma, \tau, y)dy = \sigma \qquad a \in \mathcal{T}, (\sigma, \tau) \in S \tag{B.120}$$

$$0 \le v(a, \sigma, \tau, y) \le 1 \qquad a \in \mathcal{T}, (\sigma, \tau) \in S, y \in [0, \tau]. \tag{B.121}$$

For any $(\sigma, \tau) \in S$, the optimal solution of (B.115) is attained at the minimum of the following optimization problem:

$$\underset{v:(B.120)(B.121)}{\text{minimize}} \quad \int_{y=0}^{\tau} \int_{t=0}^{T} v(t+y-\tau, \sigma, \tau, y)^2 \Psi(t+y-\tau, \sigma, \tau) dt dy. \tag{B.122}$$

From integration by substitution, the objection function of (B.122) satisfies

$$\int_{y=0}^{\tau} \int_{t=0}^{T} v(t+y-\tau, \sigma, \tau, y)^2 \Psi(t+y-\tau, \sigma, \tau) dt dy \tag{B.123}$$

$$= \int_{y=0}^{\tau} \int_{a=y-\tau}^{T+y-\tau} v(a, \sigma, \tau, y)^2 \Psi(a, \sigma, \tau) da dy \tag{B.124}$$

$$= \int_{y=0}^{\tau} \int_{a=0}^{T} v(a, \sigma, \tau, y)^2 \Psi(a, \sigma, \tau) da dy, \tag{B.125}$$

where the last equality is due to the assumption that $\Psi(a, \sigma, \tau) = 0$ if $a \notin [0, T-\tau]$. The Lagrangian of (B.122) is

$$L(v; \mu, \nu) = \int_{y=0}^{\tau} \int_{a=y-\tau}^{T+y-\tau} v(a, \sigma, \tau, y)^2 \Psi(a, \sigma, \tau) da dy - \int_{a=0}^{T} \mu_{\sigma,\tau}(a) \int_{y=0}^{\tau} v(a, \sigma, \tau, y) dy da \tag{B.126}$$

$$\int_{a=0}^{T} \int_{y=0}^{\tau} (\bar{\nu}_{\sigma,\tau}(a, y) - \underline{\nu}_{\sigma,\tau}(a, y)) v(a, \sigma, \tau, y) dy da, \tag{B.127}$$

where $\mu_{\sigma,\tau}(a)$ is the Lagrange multiplier associated with constraint (B.120); $\underline{\nu}_{\sigma,\tau}(a, y) \geq 0$ is the Lagrange multiplier associated with the constraint $v(a, \sigma, \tau, y) \geq 0$, and $\underline{\nu}_{\sigma,\tau}(a, y)$ is the Lagrange multiplier associated with the constraint $\bar{v}(a, \sigma, \tau, y) \leq 1$. A necessary condition for v^* to be the optimal scheduling policy is that $L(v; \mu, \nu)$ is stationary at $v = v^*$. After some tedious manipulation, the stationary condition can be computed as follows:

$$v^*(a, \sigma, \tau, y) = \frac{\mu_{\sigma,\tau}(a) + \underline{\nu}_{\sigma,\tau}(a, y) - \bar{\nu}_{\sigma,\tau}(a, y)}{\Psi(a, \sigma, \tau)}. \tag{B.128}$$

We observe that $\underline{\nu}_{\sigma,\tau}(a, y) = 0$ when $v^*(a, \sigma, \tau, y) > 0$. Combining this condition with (B.120) and (B.121) leads to

$$\frac{\mu_{\sigma,\tau}(a) - \bar{\nu}_{\sigma,\tau}(a, y)}{\Psi(a, \sigma, \tau)} > 0. \tag{B.129}$$

We first suppose $v^*(a, \sigma, \tau, y) = 0$ at some $y \in [0, \tau)$, then for that y,

$$v^*(a, \sigma, \tau, y) = 0 = \frac{\mu_{\sigma,\tau}(a) - \bar{\nu}_{\sigma,\tau}(a, y)}{\Psi(a, \sigma, \tau)} + \frac{\underline{\nu}_{\sigma,\tau}(a, y)}{\Psi(a, \sigma, \tau)} > \frac{\mu_{\sigma,\tau}(a) - \bar{\nu}_{\sigma,\tau}(a, y)}{\Psi(a, \sigma, \tau)}. \tag{B.130}$$

This is a contradiction, so $v^*(a, \sigma, \tau, y) \neq 0$ at all $y \in [0, \tau)$. We then suppose that $v^*(a, \sigma, \tau, y_1) < v^*(a, \sigma, \tau, y_2) = 1$ for some $y_1, y_2 \in [0, \tau)$. Then

$$v^*(a, \sigma, \tau, y_1) = \frac{\mu_{\sigma,\tau}(a)}{\Psi(a, \sigma, \tau)} > \frac{\mu_{\sigma,\tau}(a) - \bar{v}_{\sigma,\tau}(a, y)}{\Psi(a, \sigma, \tau)} = v^*(a, \sigma, \tau, y_2). \quad \text{(B.131)}$$

This is also a contradiction, so $v^*(a, \sigma, \tau, y_1)$ takes a constant value at all $y \in [0, \tau)$. Therefore, the optimal solution of (B.115) is Exact Scheduling. □

Next we consider the optimization problem (10.62). From the proof of Lemma B.8.1, we can observe that the optimal solution of (10.62) is also the point-wise minimum of

$$\int_{a=0}^{T} \int_{\mathbb{R}_+} \int_{\mathbb{R}_+} \left\{ \int_{y=0}^{\tau} v(a, \sigma, \tau, y)^2 + \delta v(a, \sigma, \tau, y) dy + \epsilon(\hat{\tau}(a, \sigma, \tau) - \tau) \right\}$$
$$\Psi(a, \sigma, \tau) f(\delta) f(\epsilon) d\delta d\epsilon da. \quad \text{(B.132)}$$

This observation yields Theorem 10.4.1.